Development and control of a novel-structure two-wheeled robotic vehicle manoeuvrable in different terrains

by

Abdullah M. Almeshal

A thesis submitted to The University of Sheffield
for the fulfilment of the degree of

DOCTOR OF PHILOSOPHY

Department of Automatic Control and Systems Engineering
The University of Sheffield
Mappin Street
Sheffield S1 3JD
UK

December 2013

Abstract

This thesis presents the development of a novel two-wheeled robotic vehicle with a movable payload and able to manoeuvre in different environments and terrains. The vehicle structure is based on the double inverted pendulum on cart mechanism. The system has five degrees of freedom that allow the vehicle to serve as a basis for new mobility solution applications. In this study, the vehicle model is derived mathematically using the Euler-Lagrange approach to describe the system dynamics. A hybrid fuzzy logic control approach is designed to stabilise and drive the vehicle on different terrains with different inclination angles. The Matlab Simulink environment is used to simulate the vehicle system. A hybrid spiral dynamic bacteria chemotaxis optimisation algorithm is used to optimise the control parameters to achieve the least mean square error of system response and to reduce the amount of exerted control effort. Various simulation scenarios are considered to demonstrate the vehicle's ability to work on smooth and frictional surfaces.

Disturbances are applied to the vehicle to evaluate the performance of the developed control system in coping with disturbances of variable amplitudes and durations. It is shown that the vehicle exhibits a stable response and a high degree of control robustness. A steering mechanism is implemented to drive the vehicle in different environments and terrains encountered in real life. Environment modelling has been incorporated into the vehicle system to simulate various ground types and levels of frictional forces.

It is demonstrated that the vehicle is able to successfully manoeuvre in indoor and outdoor environments and on flat and sloped surfaces fulfilling the aims and objectives of the research.

Acknowledgements

I would like to express my appreciation to my supervisor Dr. M. O. Tokhi for his continuous support. It would have not been possible for me to conclude this research without his guidance and motivation. His time, patience and efforts in helping me throughout the research are very much appreciated.

Thanks to my country, Kuwait, the government of Kuwait and my employers who funded my scholarship and gave me the chance to be here.

A warm and special thanks to my beloved parents and family for their endless support and patience.

Thanks to Dr. Khaled Goher for his support and advices, thanks to all my friends who have always supported and motivated me during this research.

List of figures

List of tables

Nomenclature

Variable	***Description***	***Unit***
$L_{M(t)}$	Distance to the COM of the payload	*m*
$L_{2u(t)}$	Distance to the COM of the upper part of second link	*m*
L_a	Position of the linear actuator	*m*
L_l	Half length of the first link	*m*
$2L_1$	Length of the first link	*m*
H	Distance between wheels along X axis	*m*
Q	Displacement of the linear actuator	*m*
M_1	Mass of the first link	*kg*
M_m	Mass of motor driving the second link	*kg*
M_{2l}	Mass of the lower part of the second link	*kg*
M_a	Mass of the linear actuator	*kg*
M_{2u}	Mass of the upper part of the second link	*kg*
M	Payload mass	*kg*
T_R,T_L	Right and left wheels driving torques	*N.m*
T_m	Motor torque	*N.m*
F_a	Linear actuator force	*N*
F_f	Frictional force in the linear actuator	*N*

F_d	External disturbance force	N
θ_1	Angular position of the first link to the positive Z axis	rad
θ_2	Angular position of the second link to the positive Z axis	rad
ϕ	Yaw angle of the vehicle around the Z axis	rad
δ_R, δ_L	Displacements of right and left wheels	m
J_l	Mass moment of inertia of first link	$kg.m^2$
J_{2u}	Mass moment of inertia of the upper rod of the second link	$kg.m^2$
J_a	Mass moment of inertia of the actuator	$kg.m^2$
J_M	Mass moment of inertia of the payload	$kg.m^2$
J_w	Mass moment of inertia of the wheels	$kg.m^2$
J_{IB}	Mass moment of inertia of the intermediate body	$kg.m^2$
J_{2L}	Mass moment of inertia of the lower rod of the second link	$kg.m^2$
α	Surface inclination angle	Rad
θ_{tumble}	Bacteria angular displacement on $x_i - x_j$ plane around the origin for tumbling	rad
θ_{swim}	Bacteria angular displacement on $x_i - x_j$ plane around the origin for swimming	rad
S	Total number of the bacteria in the population. S must be even.	
p	The dimension of the search space	

N_c	Number of chemotactic steps of the bacterium lifetime between reproduction steps
N_s	Number of the swims of the bacterium in the same direction
N_{re}	Number of reproduction steps
p_{ed}	Probability of bacterium to be eliminated or dispersed
J	The cost function value
C	Step size of the tumble of the bacterium
C_i	Constant values
$k_{\max}$	Maximum iteration number.
r	Convergence rate of distance between a point and the origin $0 \le r \le 1$
$R_{i,j}$	Rotation matrix between xi – xj planes
m	Dimension of the search space
r_{tumble}	Spiral radius from bacteria tumble
r_{swim}	Spiral radius for bacteria swim
m	Number of search points
$k_{\max}$	Maximum iteration number
N_{sw}	Maximum number of swim
$x_i(k)$	Bacteria position.

R^n	*n x n* rotational matrix
$K_{\eta F}$	Linear stiffness factor
$B'_{\eta F}$	Nonlinear damping factor
η	Directions in x and y
x_{if0}, y_{if0}	Coordinates of the wheel-ground touchdown
v_η	A parameter dependent on ground characteristics with $0.9 < v_\eta < 1.0$
Δ_{iyFMax}	Maximum penetration depth of wheel into ground
L_{c1}	Half length of the first link
Lc2	Half length of the lower part of the second link

Abbreviations

MIMO	Multi-input-multi-output system
IP	Inverted pendulum
MSE	Mean square error
NB	Negative big
NS	Negative small
PB	Positive big
PS	Positive small
Z	Zero

COM	Centre of mass
DOF	Degrees of freedom
PD	Proportional-derivative control
PID	Proportional-integral-derivative control
FLC	Fuzzy logic control
BFA	Bacterial foraging algorithm
SDA	Spiral dynamics algorithm
HSDBC	Hybrid spiral dynamic bacterial chemotaxis algorithm

Table of contents

Chapter 1
Introduction and literature review

1.1 Introduction

The inverted pendulum (IP) system has always been of interest to control system engineers and researchers due to its nonlinear and under-actuated nature. Many variations of the IP system exists such as linear IP system (Ban et al., 2004), the mobile IP on a cart (Asa et al., 2008), and the rotational IP (Benjanarasuth & Nundrakwang, 2008). The variations of the IP system have facilitated the researchers to develop a variety of applications based on the IP system including the gaits of humanoid robots such as ASIMO (Honda motor Co., 2000), personal transporters such as Segway (Segway Inc., 2001), and self-balancing wheelchairs such as iBot by the (Independence technology, 2001). In recent years, variations of the structure of the classical IP system have been observed to include multiple links such as triple IP systems (Yang et al., 2010). This extension has increased the degrees of freedom and complexity of the system; thus allowing more complex applications to be developed applications (Ahmad et al., 2009; Aoi et al., 2005).

In this research, a new structure of a two-wheeled robotic vehicle based on a double IP with a moving payload system and five degrees of freedom is developed. Equations of motion describing system dynamics are derived and presented. The model developed will contribute to serve as basis for new applications and mobility solutions such as self-balancing wheelchairs with the ability to manoeuvre on irregular and uneven surfaces and environments. The research investigates the development and implementation of various control strategies on the system. The model is simulated and analysed using the Matlab Simulink© software package.

1.2 Literature review

Reviewing past and ongoing studies that are relevant to this area and with focuses on the IP system is an important phase for this research. This helps identify the gaps of the field and the existing problems, as well helping develop new approaches to solving existing problems. The IP system is a highly unstable and non-linear system with coupled dynamics.

Some of the researches have focused on designing swing-up controllers for the IP system (Bugeja, 2003; Chung and Hauser, 1995; Yi et al., 1999). Other research has examined the design of a stabilisation controller (Angeli, 2001; Ban et al., 2004; Goher et al., 2010). Whilst most of the developed controllers combine both the control of the swing-up process and stabilisation of the pendulum, various control techniques have been developed and implemented on the IP system. Such techniques include, but are not limited to: linear quadratic controllers (Lingyan et al, 2009; Wongsathan and Sirima, 2009; Xiong and Wan, 2010); non-linear controllers (Mills et al., 2009; Wang et al., 1996); fuzzy logic controllers (Liu et al., 2009; Wang et al., 1996); embedding neural networks (Chen et al., 2010; Jung and Kim, 2008) and embedding different optimisation algorithms with various controllers (Wang and Fan, 2009; Xiong and Wan, 2010; Yang et al., 2007).

The literature review is categorised based on the type of the controllers applied on the system. Moreover, applications based on the IP systems are presented with their various structures and control approaches.

Lin et al. (1996) have designed state feedback controller to balance an IP on a cart system with limited travel distance. The authors have utilised high gain low gain state feedback control strategy to balance the system. The reported results show that the pendulum was stabilised with an infinite amount of gain margin.

Fiacchini et al. (2006) have presented a personal pendulum-based vehicle with a steering mechanism. Various linear and non-linear controller types have been presented, such as partial linearisation, velocity stabilisation, non-linear controller tuning and energy shaping. Experiments a comparison of the behaviour of the linear quadratic regulator (LQR) and energy-shaping controllers were presented.

Li et al. (2007) have developed a two-wheeled mobile robot based on IP system with high manoeuvrability allowing it to work on inclined surfaces and narrow spaces. The design has advantages of being a low power, lightweight and compact. It can be used to transport goods as well as humans. The authors have derived the model of the robot and have presented the equations of motion in a linearised form. The vehicle is equipped with a gyroscope and an accelerometer for the tilt angle estimation. Experiments were carried out on the robot to test its ability in climbing on an inclined plane and avoiding obstacles. The robot has moved successfully on a slope with an angle of elevation of 15^{o} and avoided obstacles.

Further work was carried out by the same authors, (Li et al., 2008) to design a control system for the developed two-wheeled robot. The authors have modelled the system with a human rider standing on the cart. This is to mimic the real scenario and to drive the system in a forward and backward motion by using the applied force from the rider. A pole placement control strategy has been implemented and yielded to a good transiet response. The system has been built and simulated in the Matlab using the virtual reality model (VRM) and then tested experimentally. The results show that the robot was stabilised and the controller has a good response in achieving the desired response.

Lingyan et al. (2009) demonstrated a simulation and presented an experimental work on stabilising an IP system using LQR. The simulation shows that the pendulum angle stabilise after 2.5 seconds whilst the position of the cart stabilise after 3 seconds. The experimental work shows some delay in stabilising the system because of the neglected terms in the simulation, such as friction, thus idealising the system.

Xiong et al. (2010) have used LQR control to stabilise a double IP system. The authors have developed a new method to find the optimal LQR control parameters. A comparison of the response with heuristically tuned parameters and the optimised parameters has been presented. The optimal selection of the LQR controller parameters was superior and reached the equilibrium point faster than the heuristic selection of the parameters.

A series of studies have been carried out to design and control a two-wheeled wheelchair. Takahashi et al. (1999) have designed and presented a mechanism for a wheelchair to be able to climb over stairs and ramps. They have designed a lifting mechanism to raise the front wheels of the robot when climbing a step without loosing the postural balance. The presented wheelchair has a steering mechanism to drive forward and backward by the force applied from the rider and the rider's posture. The authors have used a simple PI controller to control the wheelchair. Further work by Takahashi et al. (2000; 2001a; 2001b) has been presented to analyse the lifting of the wheelchair wheels. Soft lifting and lowering of the wheels have been utilised to solve the overshoot and speed of the wheel lifting problems as reported by Takahashi et al. (2003). Takahashi et al. (2005) have reported a new control approach for the robotic wheelchair where they have used Linear Quadratic Gaussian (LQG) controller with added integral action to improve the system response. Experiments have been carried out and simulations have been presented that show the response improvement.

Chung et al. (1995) have reported a non-linear controller to swing up and regulate the cart position of an IP system. Bugeja (2003) developed a swing up and stabilisation non-linear control method for the IP system. A cascaded state feedback pole placement control strategy has been used to control the system. The controller successfully stabilised the system and have shown a good performance in coping with external disturbances.

Lee et al. (2009) have completed a hill-climbing algorithm of an IP. Mathematical models were presented for the situations of the IP robot climbing up and down the hill. The paper has considered modelling friction force and the effect of horizontal and vertical forces applied on the cart of the IP. Experiments have been carried out to provide a comparison of the controller effort for various angles. It is shown that the pendulum stays in the upright position in small angles. Increasing the inclination angle increases the disturbances and, therefore, decreases the controllability of the pendulum.

Some researchers have have utilised energy-shaping controllers to control IP systems. Angeli (2001) have used energy-shaping controller for an almost global stabilisation of an IP system. Smooth switching feedback control between positive and negative feedback signals has been used to stabilise the IP system.

Zhong et al. (2001) have energy shaping to swing up and balance a double IP system. The authors have shown simulation results where the controller can swing up and balance the pendulum from any initial condition.

Ashrafiuon et al. (2010) have utilised sliding mode control strategy to control a rotary IP system. Simulations were carried out and the developed controller has successfully stabilised the system. A comparison between analytical solution and simulations has been presented.

1.2.1 Intelligent controllers

Intelligent control approaches have been implemented to control a variety of IP-based systems. Kiankhah et al. (2009) have reported a feedback-error-learning (FEL) controller for stabilising a double IP system. The control system is composed of two types of controllers, a state feedback controller to provide the stability and a neuro-fuzzy controller to learn the weights and provide more control and to converge faster to the desired values. The system has been simulated, and results show that the developed control strategy successfully stabilise the system with a fast settling time to the desired values.

Noh et al. (2009) have designed a radial basis function (RBF) neural network to provide a robust control of a mobile IP robot. A Proportional-Derivative-Integral (PID) controller has been used as a primary controller of the system with the RBF network as an auxiliary controller to assist the PID controller to achieve a better response. The use of the RBF network is to compensate for the uncertainties of the system that cannot be controlled by the PID controller. Experiments have been carried out to demonstrate the balancing control of the robot on flat and inclined surfaces.

The results show that the robot was successfully balanced in both standing state and moving state.

Tinkir et al. (2010) introduced a comparative study in controlling a double IP system between a PID and interval type-2 fuzzy logic controller (IT2FL). The Matlab SimMechanics toolbox was used to simulate the system. Simulation results showed a stable and fast convergence response of the system with IT2FL controller.

Liu et al. (2009) presented an Adaptive Neuro-Fuzzy Inference System (ANFIS) controller on an IP system. The system was simulated using the Matlab Simulink environment with the real-time workshop toolbox connected to the IP system. Experiments were carried out to demonstrate the controller ability to balance the system and control the position of the IP.

Wang et al. (2010) developed an adaptive dynamic programming method design for angle bracket IP. The angle bracket IP is simply an IP system on a cart placed over an inclined surface. The pendulum undergoes an inertia weight caused by gravity downward along the inclined surface. In this situation, the control of the IP is a more challenging problem. The authors presented Action-Dependent Adaptive Dynamic Programming (ADADP). ADADP is an approximate optimal control that has a utility function representing the local cost of the system. A kind of utility function composed of an inertial weight compensation part was designed. Two neural networks were utilised to achieve the function estimation and control action through a continuous learning process. The authors carried out simulations that showed the balancing of the pendulum after a few trials of learning with less oscillation. The results proved the feasibility of the control method in compensating for the inertia problems and in the ability to move on inclined surfaces.

Zhang et al. (2010) developed a new fuzzy control approach based on the fusion function to control a double IP system. The authors implemented the fusion function to reduce the large number of the fired fuzzy rules. The reduction has been achieved by dividing the number of inputs into two main types, the comprehensive error and the comprehensive rate of change of error. Simulations have proved the feasibility of the control approach in stabilising the system with different initial values within a fast convergence time of five seconds. The authors reported that the developed controller is robust and has anti-interference ability. Wang et al. (2010) presented a similar fuzzy control of a double IP based on information fusion. They designed a state fusion function to reduce the system dimensionality and to simplify the controller design. Simulations were carried out with two different initial values. The results show the feasibility and good response of the system with such a controller.

Tatikonda et al. (2010) applied an ANFIS controller on an IP system. A comparison between a PID controller and ANFIS was presented. The system has been simulated with various values of pendulum mass and the control balanced the system successfully in the upright position.

Jung et al. (2008) carried out experiments in controlling a wheel-driven IP system. Neural networks combined with a PID controller have been used to stabilise the system and drive on the predefined path. Disturbnaces were applied on the system to test the robustness of the controller. The controller has shown a robust performance and successfully stabilised the perturbed IP system.

Shimizu et al. (2010) developed a direct tilt angle control (DTAC) for an IP-based mobile robot. The control system is composed of a DTAC control with a disturbance observer using a Kalman filter. The authors reported that the DTAC is suitable for high-speed movements of the IP system. Simulations have been presented showing the successful control and feasibility of the approach.

An adaptive neuro sliding mode control for IP system has been presented by Wu (2010). The author has used RBF neural networks to control the position of the IP. Simulations show a robust performance of the control and a good convergence to the desired values.

Han et al. (2010) developed a self-adaptive fuzzy PID with fuzzy controller for the IP system. The controller consists of three double-input single-output fuzzy controllers to tune the parameters of a PID controller by measuring the error and the rate of change of error. Experiments show that the controller was able to stabilise the system within 2 seconds but with some minor oscillations that need further improvments.

Yi et al. (1999) developed a fuzzy controller based on Single Input Rule Modules (SIRMs) to swing up and balance an IP on a cart system. A single controller was used to swing up and stabilise the system. Results show a successful control with a fast convergence time to the desired values within 2 seconds.

Chen et al. (2010) investigated chaos optimisation neural network control of a double IP system. Simulation results show a stable response. Azizan et al. (2010) have developed a novel intelligent fuzzy control scheme for a two-wheeled human transporter. The human body inclination drives the transporter forward and backward movements, much like the Segway, with a lighter weight and ability to control the velocity of the vehicle. The authors used the Linear Matrix Inequalities (LMI) method to find the optimal controller gains. The control scheme was applied to a sample two-wheeled transporter and has shown the effectiveness of the controller with high robustness against the change of rider's mass.

Xu et al. (2002) have developed a fuzzy logic controller that obtains fuzzy rules from a simplified look-up table (LUT). The simulation results show a good response of the system and with stable balancing.

Muskinja and Tovornik (2006) have developed a swing up and stabilisation controller for the IP on a cart system. Two types of controllers have been utilised to swing up the system, a fuzzy logic control and an energy-based control. A comparison between the two controllers has been presented showing the superior performance of the FLC controller. While for the stabilisation of the IP system, an adaptive state controller has been used to balance and drive the system.

Bogdanov (2004) has implemented various optimal controllers on a double IP system. A state-dependent Riccati equation (SDRE), LQR and optimal neural network controllers have been implemented and reported. Simulations show that SDRE controllers combined with optimal neural network controller achieved optimal response.

Qiang et al. (2008) have presented an ANFIS controller for double IP system. The approach utilises the use of least square estimator hybrid-training algorithm to adjust the membership function and optimise the fuzzy rules. The presented controller has successfully balanced both pendulums.

1.2.2 Predictive controllers

Predictive control approaches to control the IP system have been presented in the literature. Balan et al. (2005) have utilised predictive control to stabilise an IP system.

The controller predicts a suitable control signal for the future behaviour of the system by analysing the signals through a set of rules and find the optimal signal. The approach has been proven to be efficient, with the presented simulations, in stabilising the system. Similarly, Chalupa et al. (2008) implemented a predictive controller for the IP system. The system has been simulated using The Matlab Simulink with real-time toolbox. Experiments show a successful control with a good response of the system. Mills et al. (2009) applied a Non-linear Model Predictive Control (NMPC) on an IP system. The authors have demonstrated that the controller was able to balance the IP at approximately 1.5 seconds. Askari et al. (2009) presented a similar approach with small variation in the parameters of the IP system. Lu et al. (2007) investigated swing up and stabilisation control of the parallel type double IP system via a model predictive control method. The authors utilised a cascade controller with an energy-based controller for swinging up the pendulums. The cascaded controller consists of an inner state-feedback controller and a model predictive controller forming the outer loop. The approach has proven good system response with the unconstrained model predictive controller.

1.2.3 Hybrid controllers

Hybrid controllers have been reported and developed for various IP-based systems and applications. Some hybrid type controllers have combined FLC with neural networks, as mentioned earlier, whilst some have combined energy-shaping controllers with sliding mode controllers, etc. Nundrakwang et al. (2006) presented a hybrid control strategy to swing up and stabilise an IP on a cart system. A proportional-derivative (PD) controller was used to swing up the pendulum with a fast convergence to the upright position. A switching mechanism was implemented to switch to the stabilisation controller once the pendulum is at the upright position. A state feedback controller was used to balance the pendulum at the upright position. Simulations were carried out with various pendulum lengths. Despite negligible oscillations around the zero-degree tilt angle, results have shown a superior performance of the hybrid controller.

A hybrid swing up and stabilisation control has been developed by Amir and Chevranov (2010) for the IP on cart system. They have presented a swing up controller, a fuzzy switching controller and a fuzzy stabilisation controller. The developed controller is self-adaptive and can swing up and stabilise the system from arbitrary initial values with a fast convergence time. They have compared their developed control strategy with the aforementioned fuzzy SIRMs control method reported by Yi et al. (1999). The authors have presented the comparison showing an improvement of 150% and a better system response.

Benjanarasuth and Nundrakwang (2008) have utilised energy-based controller on a rotary IP system. While for stabilisation of the system, the authors have utilised a state feedback with a minimum-order observer controller. The developed control has been able to swing up the control the system with a good performance. Similarly, Asa et al. (2008) applied the same approach on an IP a on cart system. Panya et al. (2008) developed a hybrid controller to swing up and stabilse an IP on cart system. The hybrid controller presented consists of a PD controller to swing the pendulum cascaded by a sliding mode controller to keep the pendulum in an upright position.

Ban et al. (2004) presented a hybrid fuzzy PD controller to balance an IP on a cart system. Simulations were carried out in real-time to balance and track the cart position and have shown the efficiency of the developed controller.

A combination of fuzzy controllers and model predictive controllers has been investigated by Wang et al. (2006). The authors tested the controller on the IP system and results proved the efficiency and feasibility of the approach.

1.2.4 Evolutionary optimisation algorithms

Evolutionary optimisation algorithms have been reported in literature to optimise various controllers of the IP systems. A genetic optimisation algorithm (GA) has been implemented by Ha et al. (1997) to optimise the weights of an LQR controller for an IP system. Similarly, Wongsathan and Sirima (2008) have applied a GA to find optimal values of weight matrices of an LQR controller for an IP system. A significant improvement of the system response with the optimised LQR has been illustrated via comparative simulations.

Ahmad et al. (2009) applied a genetic optimisation algorithm on a fuzzy logic controller for lifting and balancing a two-wheeled wheelchair. The genetic algorithm was used to tune the input output scaling factors of the fuzzy logic controller. Simulation results show the effectiveness of the approach. Similarly, Cheng-jun et al. (2009) have used GA to optimise the weighting coefficients of a fuzzy logic controller of a double IP system. It has been shown that the approach achieve better stability than the conventional FLC with high-speed response.

Nakayama et al. (2010) combined GA with the Robust Solution Searching Scheme (GA/RS^3) for choosing the controller parameters. The approach was applied to a double IP system on a cart. The authors have demonstrated numerical and simulation results that prove the robustness and effectiveness of the approach. Wei et al. (2008) have optimised a sliding mode controller using a GA for a double IP system. The GA has been used to find the optimal sliding surface for the controller.

Particle swarm optimisation (PSO) algorithm has been utilised for optimising IP controllers. Wang et al. (2008) have used an improved PSO algorithm to find the optimal parameters of an FLC applied to a double IP system on an inclined rail. The system has stabilised within two seconds. Results have proven the effectiveness and robustness of the controller with the improved PSO algorithm. Wang and Fan (2009) have applied an improved PSO algorithm on a fuzzy PID controller for a rotated IP system. The approach has successfully balanced the pendulum within 1.5 seconds, showing its feasibility and effectiveness. Solihin et al. (2009) optimised a state feedback control to swing up a single link IP using PSO algorithm. The optimisation was carried out using a huge number of iterations of six-figures. Authors claimed that smaller number of iterations might not find the optimal parameters of the controller. With this constraint, the approach would become more time consuming and not suitable for a more complex IP system.

1.3 Applications of IP systems

The IP system, with its existing design variations, has enabled researchers to develop various applications, like the personal transporter (Azizan et al., 2010; Fiacchini et al., 2006), develop gaits for humanoid robots (Huang et al., 2008; Kajita and Tani, 1996a,b; Liu et al., 2012;) and autonomous two-wheeled vehicles for transporting goods as well as balancing wheelchairs (Ahmad et al., 2009; Goher et al., 2010).

Furuta et al. (1980) have presented an optimal control scheme of a double IP moving on an inclined rail. The authors have presented successful experimental results within an inclination range of $\pm 5^{o}$. However, the configuration is limited to move on the rail and limited to three degrees of freedom

Recently, newly developed applications based on IP systems have been introduced in the literature. A new patent for video conferencing, based on a remotely-controlled self-balancing robot, has been developed by Blackwell et al. (2012). The patent was enhanced and introduced commercially as the Anybots system by the Anybots company. Anybots is a telepresence and video conferencing solution for corporates and individuals. It is a self-balancing vehicle based on a simple IP on a cart system with an attached video camera on top of the link. With the absence of the rider, Anybots is a remotely-controlled vehicle that works in indoor areas and is equipped with speakers, a microphone and a Wifi connection to enable video conferencing.

Furthermore, a recent mobility solution named Solowheel, based on the IP system, has been developed by the Solowheel company (2011). Solowheel is a single wheel with foldable foot supports on the sides that allow the rider to stand and balance. The Solowheel system has a gyroscope that measures the tilt angle of the rider to balance and to drive. It is a portable and lightweight mobility solution. Solowheel was tested to work on different environments such as beach sands, parks and urban areas. It has a maximum allowable rider mass of 99 kg and a limited travel time, when fully charged, to 16 km. In addition, Solowheel is limited to working on a maximum inclination angle of 15 degrees.

A recent patent of an IP-type vehicle was presented by Shirokura et al. (2013) and invented for the Honda motor company. The vehicle is a self-balancing based on an IP system with an attached auxiliary driving unit at the rear with a smaller wheel for turning the vehicle in all directions. The inventors claim that the second unit allows better manoeuvrability when attached to the self-balancing vehicle. The vehicle is equipped for a rider seat with hand supports on the sides to enable convenient ride.

Miki et al. (2011) have invented a two-wheeled balancing wheelchair for the Equos company. The wheelchair design consists of an occupant seat, two large wheels, control unit and a balancer system. The balancer system employs the weight and counterweight to maintain the balance of the vehicle in the upright position. The design utilises the centre of gravity (COG) of the vehicle in balancing the vehicle and driving it forward. This is achieved by the mechanical gear system attached underneath the occupant seat. This allows the balancer system to move the counterweight to an appropriate point to maintain the overall balance of the vehicle and the occupant. The vehicle had some limitations, as reported by Doi (2012). The vehicle design was assumed to be functional for a limited ratio of weight of an occupant to the weight of the vehicle. Problems occur when this ratio is larger than one. Such problems were reported by Doi (2012) as difficulties in turning performance, due to the narrow space between the two wheels, as well as the slipping of the inner wheels. These problems cause the vehicle to deviate from its steering path and collapse and lose its balance. Doi (2012) has enhanced the design by modifying the structure by increasing the space between the wheels. Moreover, the vehicle was equipped by a limiting mechanism for the speed and turning radius that is dependent on the weight of the occupant and the COG.

Further work was carried out by Doi (2013) to test the vehicle's ability to balance on a sloped surface. The vehicle was equipped with a control unit that estimates the road inclination angle by measuring the tilt angle and COG of the occupant and thus providing an appropriate driving torque to balance the vehicle on the slope. The author claims that by measuring the tilt angle of the occupant and the vehicle, the road slope can be estimated with high accuracy and, therefore, the control unit provides sufficient amount of torque to maintain the vehicle balance.

1.4 Statement of the problem

Previous studies on double IP based vehicles have presented many important modelling and control schemes and roused researchers interest in IP systems due to their nature. In two-wheeled balancing vehicles, the majority of the presented literature assumed a load-free model of the vehicle, except for the human transporter vehicles presented by Li et al. (2008), Takahashi et al. (1999) and Azizan et al. (2010). This observation raises questions as to how the payload mass affects the overall vehicle response whilst manoeuvring or steering on inclined surfaces of various grades. Moreover, questions are also asked as to what extent these types of vehicles are able to cope with the change of environment, in terms of different ground types, as well as dynamic change of surface inclination.

Moreover, and to the best of the author's knowledge, no research has been found that discusses a balancing vehicle structure, based on double IP, with a movable payload to a demanded height and moving in different environments with irregular terrains. The objective of this thesis is to develop a balancing two-wheeled robotic vehicle that will balance on inclined surfaces and terrains with a dynamic payload.

In the literature, none of the researchers has presented a double IP system moving on an inclined surface except Furuta et al. (1980). However, the double IP system they used was a laboratory apparatus with the system fixed on a conveyer belt and a monorail. With the limitation of the apparatus, the tilt angle of each of the pendulum links was constrained to within a range of $\pm 5^{o}$. Despite previous studies on double IP-based robotic vehicles, there is still a need for mobile IP vehicles that are capable of moving in different environments and that can cope with different types of surfaces.

Relevant designs, such as the iBot by the Independence Technology Company, have had production discontinued because of a high selling price. With continued demand from disabled and elderly people for this type of product, new designs should be within affordable production and selling price range to fulfil the large demand. Moreover, designs are needed with capabilities for the robot to move on irregular and inclined terrains found in real life such as parks, golf courses, confined areas and country pathways.

This research presents a novel design of a two-wheeled robotic vehicle with a movable payload that is capable of manoeuvring in different environments and terrains. The model will form a basis for more applications to be developed, such as advanced human transporters and wheelchairs for elderly and disabled persons. These types of wheelchairs that reach extended heights can help a person with everyday activities such as reaching higher shelves and eye-to-eye contact, in addition to moving on uneven surfaces such as rough and sloping terrains in indoor and outdoor areas.

1.5 Objectives of the research

- To develop a balancing two-wheeled robotic vehicle that will manoeuvre on inclined surfaces and terrains with a dynamic payload.
- To derive the mathematical model of new type of two-wheeled robotic vehicle with a moving payload that can extend to a demanded height based on a double IP system.

- To provide a non-linear model that includes the uncertainties to mimic as close to real-life design as possible.
- To design a robotic vehicle that is capable of moving on flat and sloped surfaces and on different environments and grounds.
- To study the behaviour of the system whilst undergoing external disturbance forces of various types.
- To develop a steering strategy for manoeuvring on flat and sloped terrains of different grounds and in various environments.
- To design an intelligent robust controller to stabilise the system and reject disturbances that may affect the system response.

1.6 Contributions

- Mathematical model of a novel two-wheeled robotic vehicle with an extendable upper link that is able to lift the payload to a demanded height with five degrees of freedom. The Euler-Lagrange modelling approach is used to derive the mathematical model of the system.
- Incorporating a linear actuator to lift the payload to an extended height and to have a movable payload whilst maintaining stability.
- A balancing robotic two-wheeled vehicle with the capability of steering and manoeuvring on inclined and irregular surfaces and terrains whilst carrying a payload.
- A robust intelligent control strategy that is able to stabilise the vehicle and move it in different environments with various frictional and disturbance forces.

- Optimising the vehicle control system with hybrid spiral dynamic bacterial chemotaxis algorithm (HSDBC) to improve the system response, within the stability region, with minimal control effort.

1.7 Thesis outline

Chapter 1: The study begins by presenting relevant literature in the field of IP systems and mobile vehicle designs based on the IP systems. Different control strategies that have been adopted by researchers are discussed and reviewed. The novelty of the proposed design is presented later in the chapter with the targeted aims and objectives of the study.

Chapter 2: This chapter describes the design of the vehicle and the modelling approach of the vehicle's initial design on flat surfaces. Furthermore, initial control strategies are implemented and presented in this chapter to validate the model and demonstrate the controllability of the non-linear model. Moreover, the development of two control strategies is presented along with initial simulation results.

Chapter 3: In this chapter, a general model of the vehicle that is able to work on irregular surfaces and inclinations is derived and presented. The Euler-Lagrange modelling approach is described and utilised to derive the vehicle dynamics presented by the system equations of motion. A hybrid fuzzy logic controller is developed and implemented to control the vehicle whilst moving on surfaces with various inclination angles. The vehicle's ability to work on inclined surfaces is illustrated through simulation results.

Chapter 4: This chapter presents the implementation of the hybrid spiral dynamic bacterial chemotaxis (HSDBC) optimisation algorithm to optimise the control parameters of the hybrid FLC controller. The HSDBC algorithm is described and implemented to achieve the minimum mean square error (MSE) of the vehicle system and minimise the exerted control effort. A comparative assessment of the HSDBC algorithm's performance with other optimisation algorithms is presented to obtain the best control parameters for the system.

Chapter 5: This chapter illustrates the vehicle's robustness and its ability to overcome disturbance forces. The vehicle is perturbed using various disturbance signals that vary in amplitude and duration of application. Rigorous analyses are presented to evaluate the vehicle's performance in the presence of disturbance signals in challenging movement scenarios.

Chapter 6: This chapter lays out challenging movement scenarios that mimic real-life situations. A differential steering mechanism is adopted and implemented to allow the manoeuvrability and track predefined trajectories. Moreover, environment modelling is implemented into the vehicle system to simulate the vehicle response in working on different frictional environments with various degrees of friction profiles. Steering in indoor and outdoor environments is presented in this chapter to prove the robustness and capabilities of the vehicle working in different environments.

Chapter 7: This chapter summarises and assesses the results of the study in meeting the aimed objectives of the research. Recommendations for future work to further enhance the system and extend its capabilities are presented.

1.8 Publications

Journals

1. **Almeshal, A. M.,** Goher, K. M., & Tokhi, M. O. (2013). Dynamic modelling and stabilization of a new configuration of two-wheeled machines. *Robotics and Autonomous Systems*, 61(5), 443-472. doi: 10.1016/j.robot.2013.01.006
2. **Almeshal, A. M.**, Goher K M and Tokhi M O and Agouri S A, (2013), Mathematical modelling of a new configuration of a two-wheeled vehicle with an extendible intermediate body on an inclined surface, *Journal of Applied mathematical modelling*. **[SUBMITTED]**
3. Agouri S. A., Nasir A. N. K., **Almeshal A**., Goher K. M., Tokhi M. O. and Alzanki T. (2013), Hybrid spiral-dynamic bacteria-chemotaxis algorithm with application to a new configuration two-wheeled robotic vehicle. Integrated Computer-Aided Engineering. **[SUBMITTED]**

Conferences

3. **A M Almeshal**, K M Goher, A N K Nasir, M O Tokhi, Steering and dynamic performance of a new configuration of a wheelchair on two wheels in various indoor and outdoor environments, *Proceedings of 18th International Conference on Methods and Models in Automation and Robotics (MMAR),* Miedzyzdroje, Poland, 26-29 Aug. 2013.
4. **A M Almeshal**, K M Goher, A N K Nasir, M O Tokhi, S A Agouri, Fuzzy logic optimized control of a novel structure two-wheeled robotic vehicle using HSDBC, SDA and BFA: a comparative study, *Proceedings of 18th International Conference on Methods and Models in Automation and Robotics (MMAR),* Miedzyzdroje, Poland, 26-29 Aug. 2013.

5. **A M Almeshal,** K M Goher, A N K Nasir M O Tokhi, S A Agouri, Hybrid spiral dynamic bacterial chemotaxis optimisation for hybrid fuzzy logic control of a novel two wheeled robotic vehicle, *Proceeedings of 16th International Conference on Climbing and Walking Robots (CLAWAR 2013),* Sydney, Australia, 14-17 Jul. 2013, pp 179-188.
6. S. A. Agouri, M O Tokhi, **A M Almeshal**, K M Goher , Control of a two wheeled robot with extendable intermediate body on an inclined surface using bacterial foraging algorithm, *Proceeedings of 16th International Conference on Climbing and Walking Robots (CLAWAR 2013),* Sydney, Australia, 14-17 Jul. 2013, pp 189-196.
7. S A Agouri, M O Tokhi, **A Almeshal**, K M Goher (2013), Modeling and robust analysis control of a two wheeled vehicle with an extendable intermediate body on an inclined surface, *Proceedings of the the 1st International Conference on Electrical and Computer Engineering (ICECE 2013)*, Benghazi, Libya, 26-28 Mar. 2013. pp 161-166.
8. S A Agouri, M O Tokhi, **A Almeshal**, O Sayidmarie, K M Goher (2013), Modelling And Control Of A Two-Wheeled Vehicle With Extendable Intermediate Body On An Inclined Surface, *Proceedings of the 32nd IASTED International Conference on Modelling, Identification and Control*, Innsbruck, Austria, 11-12 Feb. 2013. pp 383-393.
9. **A M Almeshal**, K M Goher M O Tokhi and S A Agouri, A new configuration of a two-wheeled double inverted pendulum-like robotic vehicle with movable payload on an inclined plane, *Proceedings of the 1st International Conference on Innovative Engineering (ICIES 2012)*, Alexandria, Egypt, 7-9 Dec. 2012. pp 97-102

10. **A M Almeshal,** M O Tokhi and K M Goher, Stabilization of a new configurable two-wheeled machine using a PD-PID and a hybrid FL control strategies: a comparative study, *Proceedings of the 32nd International Conference on Control, Automation and Robotics (ICCAR 2012)*, Dubai, UAE, 8-9 Oct. 2012. pp 65-72
11. S. Agouri, O. Tokhi, **A. M. Almeshal**, O. Sayidmarie and K M Goher, Dynamic modelling of a new configuration of two wheeled robotic machine on an inclined surface, *Proceedings of the 17th International Conference on Methods and Models in Automation and Robotics (MMAR)*, Międzyzdroje, Poland, 27-30 Aug. 2012. pp 315-318
12. K Sayidmarie, M O Tokhi, **A M Almeshal**, S A Agouri, Design and real-time implementation of a fuzzy logic control system for a two-wheeled robot, *Proceedings of 17th International Conference on Methods and Models in Automation and Robotics (MMAR)*, Miedzyzdroje, Poland, 27-30 Aug. 2012. pp 569-572
13. **A M Almeshal**, M O Tokhi, K M Goher, Robust hybrid fuzzy logic control of a novel two-wheeled robotic vehicle with a movable payload under various operating conditions, *Proceedings of the United Kingdom Automatic Control Council International Conference on Control (UKAAC 2012),* University of Glamorgan, Cardiff, UK, 3-5 Sept 2012. pp 747-752
14. **A M Almeshal**, K M Goher, M O Tokhi, O Sayidmarie, S A Agouri, Hybrid fuzzy logic control of a two wheeled double inverted pendulum-like robotic vehicle, *Proceedings of 15th International Conference on Climbing and Walking Robots and the Support Technologies for Mobile Machines (CLAWAR 2012),* Baltimore, USA, 23-26 Jul. 2012. pp 681-688

15. **A M Almeshal**, K M Goher, M O Tokhi, O Sayidmarie, S A Agouri, Robust PD-PID control of a new configuration of two-wheeled machines under various operating conditions, *Proceedings of 15th International Conference on Climbing and Walking Robots and the Support Technologies for Mobile Machines (CLAWAR 2012),* Baltimore, USA, 23-26 Jul. 2012. pp 673-680
16. K M Goher, A Al-Harrasi, S Al-Abdali, J Al-Abri, A Al-Siyabi, M O Tokhi, **A M Almeshal**, O Sayidmarie and S A Agouri, State space modelling and control of squ-two-wheeled mobility vehicle (SQU-TWMV): an energy analysis approach, *Proceedings of 15th International Conference on Climbing and Walking Robots and the Support Technologies for Mobile Machines (CLAWAR 2012),* Baltimore, USA, 23-26 Jul. 2012. pp 55-62
17. K M Goher, A Al-Harrasi, S Al-Abdali, J Al-Abri, A Al-Siyabi, M O Tokhi, **A M Almeshal**, O Sayidmarie and S A Agouri, Mathematical modelling and pid control of squ-two-wheeled mobility vehicle (SQU-TWMV), *Proceedings of 15th International Conference on Climbing and Walking Robots and the Support Technologies for Mobile Machines (CLAWAR 2012),* Baltimore, USA, 23-26 Jul. 2012. pp 137-144
18. K M Goher, M O Tokhi, **A M Almeshal**, O Sayidmarie and S A Agouri, Impact of payload inertia on the system damping characteristics of a two-wheeled robotic machine, *Proceedings of 15th International Conference on Climbing and Walking Robots and the Support Technologies for Mobile Machines (CLAWAR 2012),* Baltimore, USA, 23-26 Jul. 2012. pp 113-120
19. R. Short, O. K. Sayidmarie, S. A. Agouri, M. O. Tokhi, K. M. Goher, And **A. M. Almeshal**, Real time PID control of a two-wheeled robot, *Proceedings of 15th International Conference on Climbing and Walking Robots and the Support*

Technologies for Mobile Machines (CLAWAR 2012), Baltimore, USA, 23-26 Jul. 2012. pp 73-80

20. **Abdullah M. Al-Meshal**, K. M. Goher and M.O. Tokhi, Modelling of two-wheeled robotic wheelchair with moving payload. *Proceedings of the 14th International Conference on Climbing and Walking Robots and the Support Technologies for Mobile Machines (CLAWAR 2011)*, Paris, France, 8-10 Sept. 2011. pp 731-741

1.9 Summary

A review of different types of IP systems has been presented. Previous studies have reported different designs of IP systems incorporating different structures and applications. In addition, a considerable amount of different control schemes has been found in the literature that swings up and stabilises the IP system, as well as using it as a basis for different applications. It has been shown that the literature lacks studies concerned with double IP-based robotic vehicles that have multiple degrees of freedom (DOF) and are able to move on inclined and irregular surfaces of different environments.

Chapter 2
Mathematical modelling of the vehicle on flat surface

2.1 Introduction

In this chapter, mathematical model of a two-wheeled robotic vehicle with a movable payload moving on flat surfaces is presented. The Euler-Lagrange modelling approach is used to produce the proposed vehicle model. For modelling complex and coupled systems, the Euler-Lagrange method utilises the kinetic and potential energies to describe system dynamics. This model is the basic model of the proposed vehicle design that is able to move on flat surfaces. In later chapters, this model will be used as a building block to derive a more general model of the vehicle that allows moving on irregular and uneven terrains with different slopes.

2.2 System description and mathematical modelling

The vehicle proposed design is illustrated in Figures 2.1 and 2.2, with the corresponding parameters of the system given in Table 2.1. The vehicle consists of two wheels driven by two motors, an intermediate body (IB) that is composed of two rods representing the first and second links, a motor driving the second link and a linear actuator on the second link to lift up the payload. The second link consists of two coaxial-parts to be able to extend and lift the payload to further levels of height. Hence, the vehicle design possesses a total of five degrees of freedom (DOF) to provide more flexibility. The vehicle's flexible structure allows it to manoeuvre on irregular terrains and follow more complex steering trajectories.

In Figure 2.2, the tilt angles of the first and second links are measured from the positive vertical Z axis. In order to keep the tilt angles in the upright position, the vehicle is allowed to move in a planar motion along the XY plane. The movement of the vehicle depends on the received signals from the system controllers in order to stabilise the vehicle. The wheels respond, independently, with the appropriate speed and direction based on the received control signal.

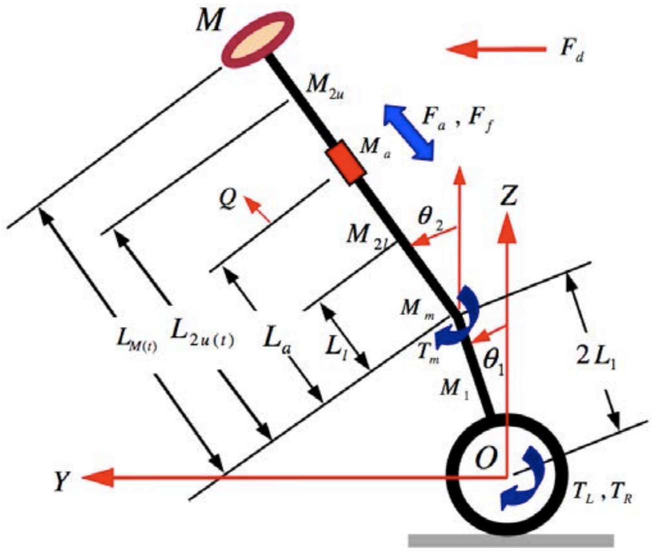

Figure 2.1: Schematic diagram of the vehicle

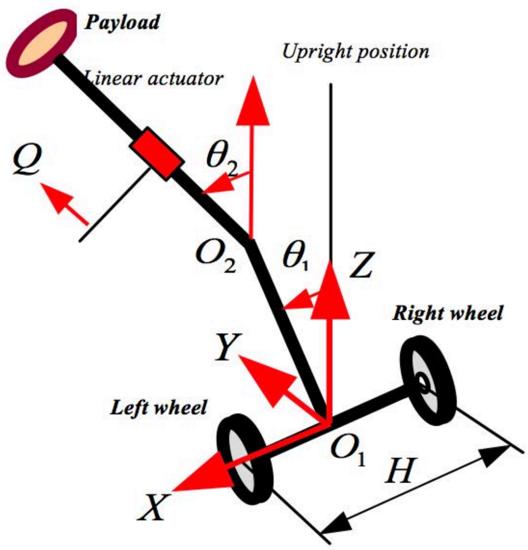

Figure 2.2: vehicle schematic diagram

Table 2.1: Nomenclature

Variable	***Description***	***Unit***
$L_{M(t)}$	Distance to the payload from centre of mass	m
$L_{2u(t)}$	Distance to the centre of upper part of second link	m
L_a	Position of the linear actuator	m
L_l	Half length of the first link	m
H	Distance between vehicle wheels – x axis	m
Q	Displacement of the linear actuator	m
M_1	Mass of the first link	kg
M_m	Mass of the connecting motor driving the second link	kg
M_{2l}	Mass of the lower part of second	kg
M_a	Mass of the linear actuator	kg
M_{2u}	Mass of the upper part of the second link	kg
M	Payload mass	kg
T_R, T_L	Right and left wheels driving torques	N.m
T_m	Motor torque	N.m
F_a	Linear actuator force	N
F_f	Frictional force in the linear actuator	N
F_d	External disturbance force	N
θ_1	Tilt angle of the first link	rad
θ_2	Tilt angle of the second link	rad
ϕ	Vehicle yaw angle measured from the z axis	rad
δ_R , δ_L	Displacement of the right and left wheels	m
J_l	Mass moment of inertia of first link	$kg.m^2$
J_{2u}	Mass moment of inertia of the upper part of second link	$kg.m^2$
J_a	Mass moment of inertia of the linear actuator	$kg.m^2$
J_M	Mass moment of inertia of the payload	$kg.m^2$
J_w	Mass moment of inertia of the wheels	$kg.m^2$
J_{IB}	Mass moment of inertia of the intermediate body	$kg.m^2$
J_{2L}	Mass moment of inertia of the lower rod of the second link	$kg.m^2$

2.3 System dynamic model and equations of motion

Due to the complexity of coupling between different vehicle components, the Euler-Lagrange approach is used to derive equations of motion of the vehicle system. With this approach, the system kinetic and potential energies are utilised to derive the dynamic model of the system. The Lagrange equation is defined as:

$$\frac{d}{dt}\left(\frac{\partial L}{\partial \dot{q}_i}\right) - \frac{\partial L}{\partial q_i} = Q_i \tag{2.1}$$

where:

$L = T_T - V_T$ *Lagrangian function*

Q_i = *Generalized force vector*

q_i = *Generalized coordinate vector*

T_T = *Total kinetic energy of the system*

V_T = *Total potential energy of the system*

Since the system has five DOF, the coordinates of the system are selected as:

$$q_i = \begin{bmatrix} \delta_L & \delta_R & \theta_1 & \theta_2 & Q \end{bmatrix}^T \tag{2.2}$$

The force vector is defined as:

$$Q_i = \begin{bmatrix} T_{LT} & T_{RT} & 0.5(T_{LT} + T_{RT}) & T_{MT} & F_{aT} \end{bmatrix}^T \tag{2.3}$$

where:

$$T_{LT} = T_L - T_{fL} \tag{2.4}$$

$$T_{RT} = T_R - T_{fR} \tag{2.5}$$

$$T_{MT} = T_M - T_{fM} \tag{2.6}$$

$$F_{aT} = F_a - F_{fa} \tag{2.7}$$

T_{fL}, T_{fR}, are the frictional moments of the left and right wheels respectively. Where T_{fM}, F_{fa} are the frictional moments of the intermediate joint connecting the first and second links and the frictional force in the actuator. These frictional moments are based on Coulomb friction model.

The total kinetic energy and the total potential energy of the vehicle system can be expressed as:

$$T_T = T_1 + T_{2l} + T_{2u} + T_m + T_a + T_M + T_c + T_\phi \tag{2.8}$$

$$V_T = V_1 + V_{2l} + V_{2u} + V_m + V_M + V_a \tag{2.9}$$

The kinetic energies of system components are derived as follows:

$$T_1 = \frac{1}{2} M_1 \left(\left(\frac{R_w}{2} (\dot{\delta}_L + \dot{\delta}_R) + L_1 \dot{\theta}_1 \cos\theta_1 \right)^2 + \left(L_1 \dot{\theta}_1 \sin\theta_1 \right)^2 \right) + \frac{1}{2} J_1 \dot{\theta}_1^2 \tag{2.10}$$

$$T_m = \frac{1}{2} M_M \left(\left(\frac{R_w}{2} (\dot{\delta}_L + \dot{\delta}_R) + 2L_1 \dot{\theta}_1 \cos\theta_1 \right)^2 + \left(2L_1 \dot{\theta}_1 \sin\theta_1 \right)^2 \right) + \frac{1}{2} J_m \dot{\theta}_1^2 \tag{2.11}$$

$$T_{2l} = \frac{1}{2} M_{2l} \left(\begin{array}{l} \left(\frac{R_w}{2} (\dot{\delta}_L + \dot{\delta}_R) + 2L_1 \dot{\theta}_1 \cos\theta_1 + L_{2l} \dot{\theta}_2 \cos\theta_2 \right)^2 \\ + \left(2L_1 \dot{\theta}_1 \sin\theta_1 + L_{2l} \dot{\theta}_2 \sin\theta_2 \right) \end{array} \right) + \frac{1}{2} J_{2l} \dot{\theta}_2^2 \tag{2.12}$$

$$T_a = \frac{1}{2} M_a \left(\begin{array}{l} \left(\frac{R_w}{2} (\dot{\delta}_L + \dot{\delta}_R) + 2L_1 \dot{\theta}_1 \cos\theta_1 + 2L_{2l} \dot{\theta}_2 \cos\theta_2 \right)^2 \\ + \left(2L_1 \dot{\theta}_1 \sin\theta_1 + 2L_{2l} \dot{\theta}_2 \sin\theta_2 \right)^2 \end{array} \right) + \frac{1}{2} J_a \dot{\theta}_2^2 \tag{2.13}$$

$$T_{2u} = \frac{1}{2} M_{2u} \left(\begin{array}{l} \dot{Q}^2 + \left(\frac{R_w}{2} (\dot{\delta}_L + \dot{\delta}_R) + 2L_1 \dot{\theta}_1 \cos\theta_1 + 2L_{u(t)} \dot{\theta}_2 \cos\theta_2 \right)^2 \\ + \left(2L_1 \dot{\theta}_1 \sin\theta_1 + L_{2u(t)} \dot{\theta}_2 \sin\theta_2 \right)^2 \end{array} \right) + \frac{1}{2} J_{2u} \dot{\theta}_2^2 \tag{2.14}$$

$$T_M = \frac{1}{2}M\left(\begin{array}{l}\dot{Q}^2+\left(\frac{R_w}{2}(\dot{\delta}_L+\dot{\delta}_R)+2L_1\dot{\theta}_1\cos\theta_1+2L_{M(t)}\dot{\theta}_2\cos\theta_2\right)^2\\+\left(2L_1\dot{\theta}_1\sin\theta_1+L_{2M(t)}\dot{\theta}_2\sin\theta_2\right)^2\end{array}\right)+\frac{1}{2}J_M\dot{\theta}_2^2 \tag{2.15}$$

$$T_c = (M_wR_w^2+J_w)(\dot{\delta}_L^2+\dot{\delta}_R^2) \tag{2.16}$$

$$T_\phi = \frac{1}{2}(2J_w+J_{IB})\dot{\phi}^2 \tag{2.17}$$

Substituting for kinetic energies from equations (2.10)-(2.17) into equation (2.8) and simplifying yields the total kinetic energy of the system expressed as:

$$\begin{aligned}T_T &= C_{21}(\dot{\delta}_L^2+\dot{\delta}_R^2)+C_{22}\dot{\delta}_L\dot{\delta}_R+\frac{1}{2}C_8\dot{Q}^2+\frac{1}{2}C_{16}\dot{\phi}_2+C_{18}\dot{\theta}_1^2\\&+\frac{1}{2}(C_{20}+C_{12}Q+C_8Q^2)\dot{\theta}_2^2+C_9\frac{R_w}{2}L_1\dot{\theta}_1(\dot{\delta}_L+\dot{\delta}_R)\cos\theta_1\\&+\frac{R_w}{2}(C_{10}+C_8Q)(\dot{\delta}_L+\dot{\delta}_R)\dot{\theta}_2\cos\theta_2+2L_1(C_{10}+C_8Q)\dot{\theta}_1\dot{\theta}_2\cos(\theta_1-\theta_2)\end{aligned} \tag{2.18}$$

The potential energies for each vehicle component are expressed as:

$$V_1 = M_1gL_1\cos\theta_1 \tag{2.19}$$

$$V_m = 2M_{m1}gL_1\cos\theta_1 \tag{2.20}$$

$$V_{2l} = M_{2l}g(2L_1\cos\theta_1+L_{2l}\cos\theta_2) \tag{2.21}$$

$$V_{2u} = M_{2u}g(2L_1\cos\theta_1+2L_{2u(t)}\cos\theta_2) \tag{2.22}$$

$$V_a = M_ag(2L_1\cos\theta_1+2L_{2l}\cos\theta_2) \tag{2.23}$$

$$V_M = Mg(2L_1\cos\theta_1+2L_{2M(t)}\cos\theta_2) \tag{2.24}$$

where

$$L_{2u(t)} = 2L_{2l}+L_{2u}+Q \tag{2.25}$$

$$L_{M(t)} = 2L_{2l}+2L_{2u}+Q \tag{2.26}$$

Similarly, substituting for potential energies from equations (2.19)-(2.24) into equation (2.9) and simplifying yields the total potential energy of the system as:

$$V_T = C_3 g\cos\theta_1 + (C_{15} + C_8 Q) g\cos\theta_2 \tag{2.27}$$

The Lagrangian function is defined as

$$L = T_T - V_T \tag{2.28}$$

Substituting for T_T and V_T from equations (2.18) and (2.27) into equation (2.28) yields the Lagrangian of the system as

$$\begin{aligned} L &= C_{21}(\dot{\delta}_L^2 + \dot{\delta}_R^2) + C_{22}\dot{\delta}_L\dot{\delta}_R + \frac{1}{2}C_8\dot{Q}^2 + \frac{1}{2}C_{16}\dot{\phi}_2 + C_{18}\dot{\theta}_1^2 \\ &+ \frac{1}{2}(C_{20} + C_{12}Q + C_8 Q^2)\dot{\theta}_2^2 + C_9\frac{R_w}{2}L_1\dot{\theta}_1(\dot{\delta}_L + \dot{\delta}_R)\cos\theta_1 \\ &+ \frac{R_w}{2}(C_{10} + C_8 Q)(\dot{\delta}_L + \dot{\delta}_R)\dot{\theta}_2\cos\theta_2 + 2L_1(C_{10} + C_8 Q)\dot{\theta}_1\dot{\theta}_2\cos(\theta_1 - \theta_2) \\ &- (C_3 g\cos\theta_1 + (C_{15} + C_8 Q) g\cos\theta_2) \end{aligned} \tag{2.29}$$

System equations of motion can be derived by solving equation (2.1) for each system coordinate defined in the coordinate vector of equation (2.2) as follows

$$\frac{d}{dt}\left(\frac{\partial L}{\partial\dot{\delta}_L}\right) - \frac{\partial L}{\partial\delta_L} = T_L - T_{fL} \tag{2.30}$$

$$\frac{d}{dt}\left(\frac{\partial L}{\partial\dot{\delta}_R}\right) - \frac{\partial L}{\partial\delta_R} = T_R - T_{fR} \tag{2.31}$$

$$\frac{d}{dt}\left(\frac{\partial L}{\partial\dot{\theta}_1}\right) - \frac{\partial L}{\partial\theta_1} = 0.5(T_{LT} + T_{RT}) \tag{2.32}$$

$$\frac{d}{dt}\left(\frac{\partial L}{\partial\dot{\theta}_2}\right) - \frac{\partial L}{\partial\theta_2} = T_M - T_{FM} - L_d F_d \tag{2.33}$$

$$\frac{d}{dt}\left(\frac{\partial L}{\partial\dot{Q}}\right) - \frac{\partial L}{\partial Q} = F_a - F_{fa} \tag{2.34}$$

Solving equations (2.30) to (2.34) yields the following five non-linear differential equations describing the system dynamics

$$
\begin{aligned}
&2C_{21}\ddot{\delta}_L + C_{22}\ddot{\delta}_R + C_9\frac{R_w}{2}L_1\ddot{\theta}_1\cos\theta_1 - C_9\frac{R_w}{2}L_1\dot{\theta}_1^2\sin\theta_1 \\
&+\frac{R_w}{2}(C_{10}+C_8Q)\ddot{\theta}_2\cos\theta_2 - \frac{R_w}{2}(C_{10}+C_8Q)\dot{\theta}_2^2\sin\theta_2 \\
&+\frac{R_w}{2}C_8\dot{Q}\dot{\theta}_2\cos\theta_2 = T_L - T_{fL}
\end{aligned}
\tag{2.35}
$$

$$
\begin{aligned}
&2C_{21}\ddot{\delta}_R + C_{22}\ddot{\delta}_L + C_9\frac{R_w}{2}L_1\ddot{\theta}_1\cos\theta_1 - C_9\frac{R_w}{2}L_1\dot{\theta}_1^2\sin\theta_1 \\
&+\frac{R_w}{2}(C_{10}+C_8Q)\ddot{\theta}_2\cos\theta_2 - \frac{R_w}{2}(C_{10}+C_8Q)\dot{\theta}_2^2\sin\theta_2 \\
&+\frac{R_w}{2}C_8\dot{Q}\dot{\theta}_2\cos\theta_2 = T_R - T_{fR}
\end{aligned}
\tag{2.36}
$$

$$
\begin{aligned}
&2C_{18}\ddot{\theta}_1 + C_9\frac{R_w}{2}L_1(\ddot{\delta}_L + \ddot{\delta}_R)\cos\theta_1 - C_9\frac{R_w}{2}L_1(\dot{\delta}_L + \dot{\delta}_R)\dot{\theta}_1\sin\theta_1 \\
&+2L_1(C_{10}+C_8Q)\ddot{\theta}_2\cos(\theta_1-\theta_2) - 2L_1(C_{10}+C_8Q)\dot{\theta}_1\dot{\theta}_2\sin(\theta_1-\theta_2) \\
&+2L_1(C_{10}+C_8Q)\dot{\theta}_2^2\sin(\theta_1-\theta_2) + 2L_1C_8\dot{Q}\dot{\theta}_2\cos(\theta_1-\theta_2) \\
&+C_9\frac{R_w}{2}L_1\dot{\theta}_1^2(\dot{\delta}_L + \dot{\delta}_R)\sin\theta_1 + 2L_1(C_{10}+C_8Q)\dot{\theta}_1^2\dot{\theta}_2\sin(\theta_1-\theta_2) \\
&-C_3g\dot{\theta}_1\sin\theta_1 = 0.5(T_{LT}+T_{RT})
\end{aligned}
\tag{2.37}
$$

$$
\begin{aligned}
& C_{20}\ddot{\theta}_2 + (C_{12}\dot{Q} + 2C_8 Q)\dot{\theta}_2 + (C_{12}Q + C_8 Q^2)\ddot{\theta}_2 \\
& + \frac{R_w}{2}(C_{10} + C_8 Q)(\ddot{\delta}_L + \ddot{\delta}_R)\cos\theta_2 - \frac{R_w}{2}(C_{10} + C_8 Q)(\dot{\delta}_L + \dot{\delta}_R)\dot{\theta}_2 \sin(\theta_2) \\
& + C_8 \frac{R_w}{2}\dot{Q}(\dot{\delta}_L + \dot{\delta}_R)\cos\theta_2 + 2L_1(C_{10} + C_8 Q)\ddot{\theta}_1 \cos(\theta_1 - \theta_2) \\
& - 2L_1(C_{10} + C_8 Q)\dot{\theta}_1^2 \sin(\theta_1 - \theta_2) + 2L_1(C_{10} + C_8 Q)\dot{\theta}_1 \dot{\theta}_2 \sin(\theta_1 - \theta_2) \\
& + 2C_8 L_1 \dot{\theta}_1 \dot{\theta}_2 \cos(\theta_1 - \theta_2) + \frac{R_w}{2}(C_{10} + C_8 Q)(\dot{\delta}_L + \dot{\delta}_R)\dot{\theta}_2^2 \sin\theta_2 \\
& - (C_{15} + C_8 Q) g \dot{\theta}_2 \sin\theta_2 - 2L_1(C_{10} + C_8 Q)\dot{\theta}_1 \dot{\theta}_2^2 \sin(\theta_1 - \theta_2) = T_M - T_{FM} - L_d F_d
\end{aligned}
\tag{2.38}
$$

$$
\begin{aligned}
& C_8 \ddot{Q} - \frac{1}{2}(C_{12} + 2C_8 Q)\dot{\theta}_2^2 - C_8 \frac{R_w}{2}\dot{\theta}_2(\dot{\delta}_L + \dot{\delta}_R)\cos\theta_2 \\
& - 2L_1 C_8 \dot{\theta}_1 \dot{\theta}_2 \cos(\theta_1 - \theta_2) + C_8 g \cos\theta_2 = F_a - F_{fa}
\end{aligned}
\tag{2.39}
$$

Detailed descriptions of constant parameters C_i featured in equations (2.35)-(2.39) are given in Appendix A.

2.4 System open loop response

To analyse and study the behaviour of the presented model, open loop system response has to be investigated. The presented model was implemented and simulated in the Matlab Simulink environment using the simulation parameters shown in Table 2.2. The selection of these simulation parameters is based on standard wheelchair dimensions reported by Ahmad (2010) with modifications. The vehicle was simulated using step response to study the behaviour of the system. In addition, the payload actuator was set to follow the predefined input signal shown in Figure 2.3. The system open loop response is shown in Figure 2.4. It is noted that the system was clearly unstable, with outputs reaching infinity.

Table 2.2 Simulation parameters

Variable	***Value***	***Unit***
L_{2l}, L_{2u}	0.25	m
L_l	0.11	m
M_1	3	kg
M_m	0.3	kg
M_{2l}	1.5	kg
M_a	0.8	kg
M_{2u}	1.5	kg
M	70	kg

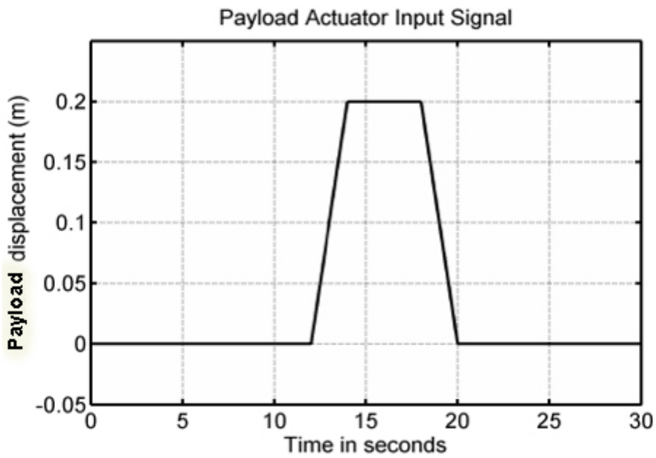

Figure 2.3: Input signal for the payload linear actuator

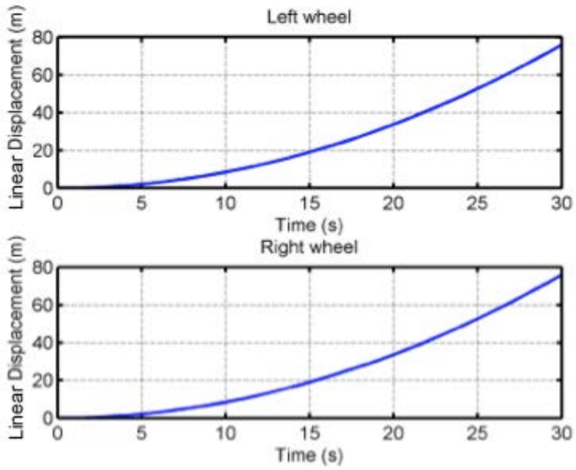

(a) Linear displacements of left and right wheels.

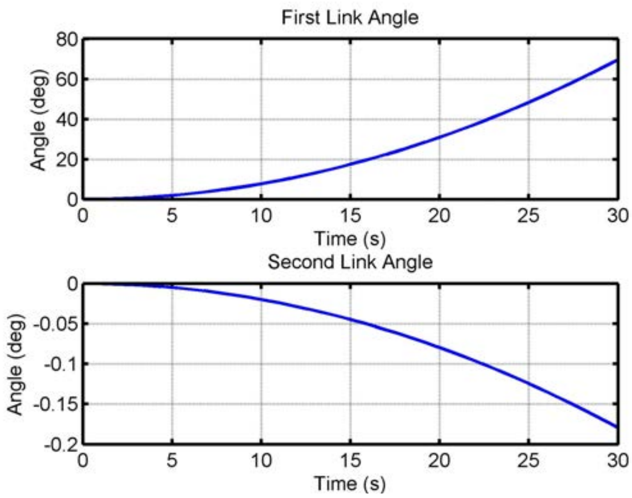

(b) Tilt angles of the first and second pendulums

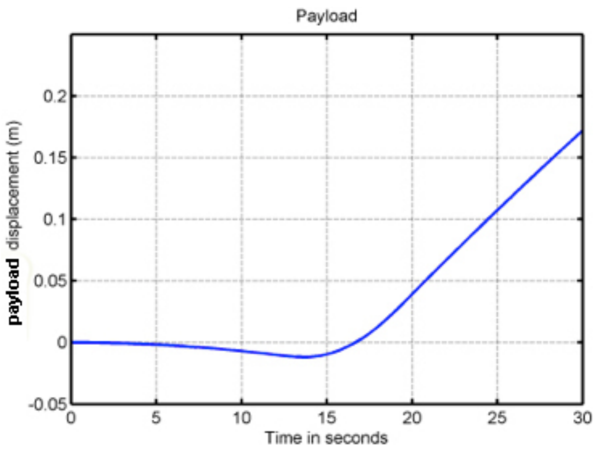

(c) Displacement of payload linear actuator

Figure 2.4: System open loop response.

2.5 Initial control design using Proportional-Integral-Derivative control

In order to test the system controllability, an initial control strategy is realised using a PID controller. For the system to be stabilised, both tilt angles must be at the upright position and stabilised at an angle of zero degrees. The vehicle wheels will be limited to move within a limited displacement of 0.8 meters. A combination of proportional-integral-derivative (PID) and proportional-derivative (PD) controllers is used as initial control attempt to study the system response. Analysis of the vehicle response and dynamic behaviour while moving on a flat surface are presented in the upcoming sections.

The vehicle system is a multi-input multi-output (MIMO) system. To stabilise and control the system, five control loops are used in which two loops are used for the control for each wheel, two loops for the first and second link tilt angles and one loop to control the payload linear actuator displacement. For the initial control of the system and to verify the model, a simple PID control strategy is used. A combination of PD and PID controllers is utilised to control the vehicle components. A PD controller is used to control the wheel motors, to achieve the desired displacement, and to control the first link tilt angle. While PID controllers are used to control the second link's tilt angle and the payload linear actuator displacement.

2.6 The Matlab Simulink© model simulation results

A system model was built in the Matlab Simulink simulation environment using the derived equations (2.35)-(2.39). With the large number of constants and due to the complexity of the equations, the system was divided into sub systems in which each each subsystem corresponds to an equation for simplification. Figure 2.5 shows the block diagram of the control system.

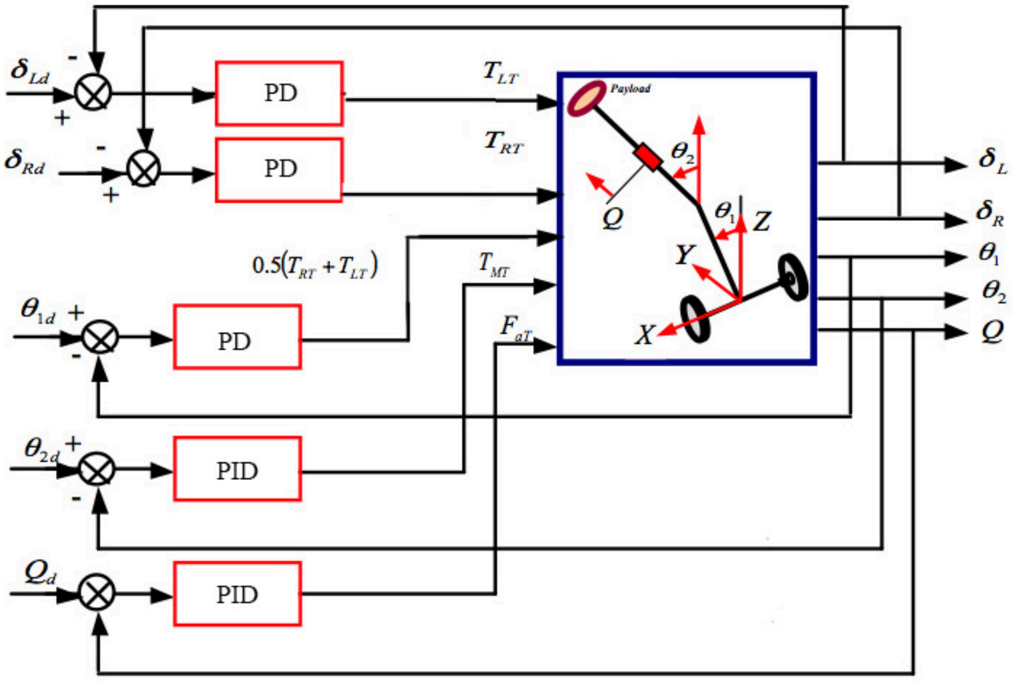

Figure 2.5: Block diagram of the control system

As an initial control test, linear displacement of the wheels will be limited to 0.8 m in order to simulate the system within the approximate linear region. The system is simulated with the initial conditions $\delta_L = \delta_R = 0$, $\theta_1 = \theta_1 = 0$, $Q_d = 0$. For the payload linear actuator input, a predefined signal will be fed into the input to simulate the actuator movement. The payload linear actuator signal used is shown earlier in Figure 2.3

At this stage of verification and initial control of the model, the control parameters were tuned heuristically with the gains in Table 2.3.

Table 2.3 : PID / PD controller gains

Loop	***PID controller Gains***		
	K		
Left / right wheels	1000	-	600
First pendulum link	50	-	50
Second pendulum link	80	30	60
Payload linear actuator	6000	100	1200

The interaction among the control loops is a sign of the strong coupling between the system parameters. The interaction, depending on how strong it is, may affect the system stability.

In the vehicle system, the loop interaction is demonstrated by detuning one of the control loops and simulating the system. Figure 2.6 demonstrates the effect of detuning the left wheel PID controller on the system stability. The impact of the improper tuning of one of the controllers has resulted in an unstable response due to the strong coupling and loop interaction of the system.

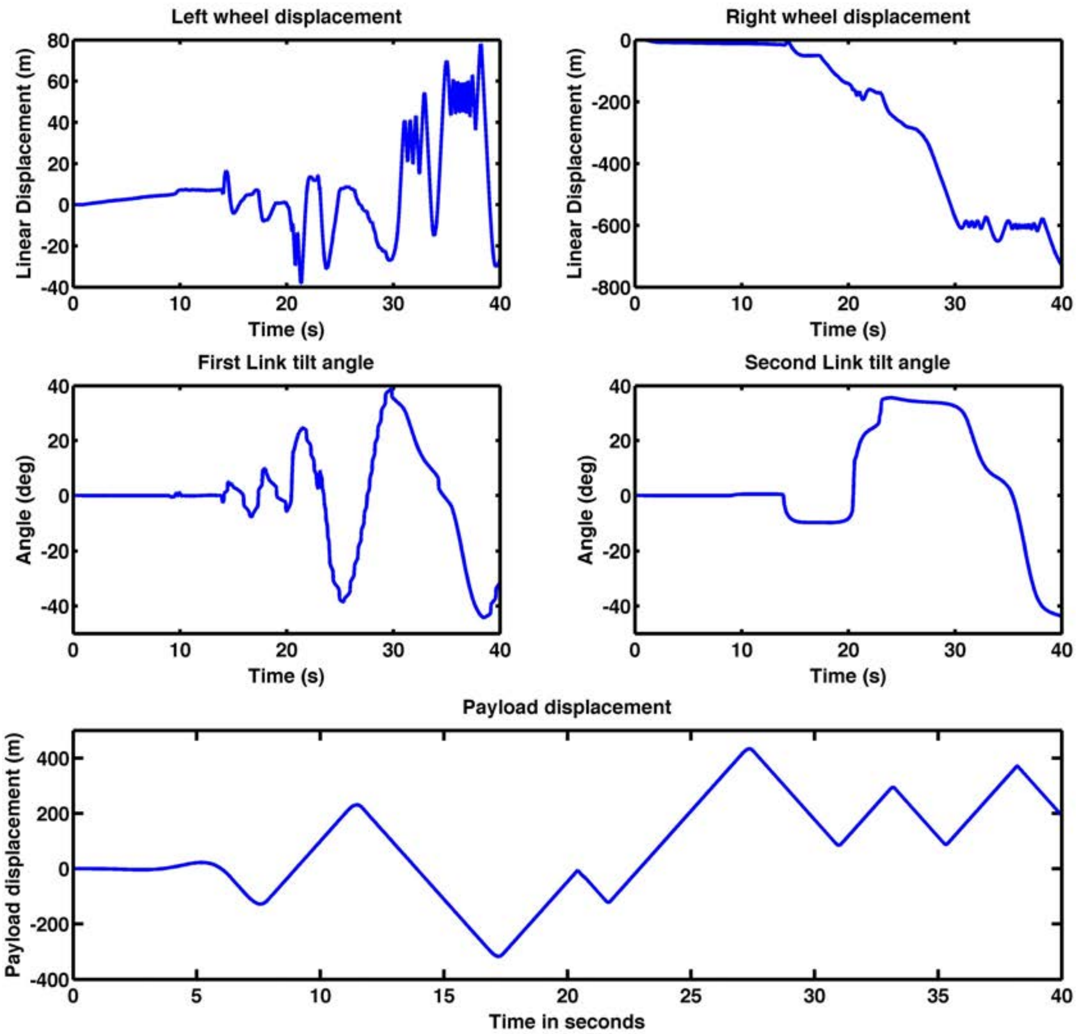

Figure 2.6 The interaction among the loops with improper tuning of the PID control parameters

Figure 2.7 illustrates the controlled system response. With the developed control strategy, the system was stabilised and converged to the set values. Figure 2.8 illustrates the system control effort used to stabilise the system.

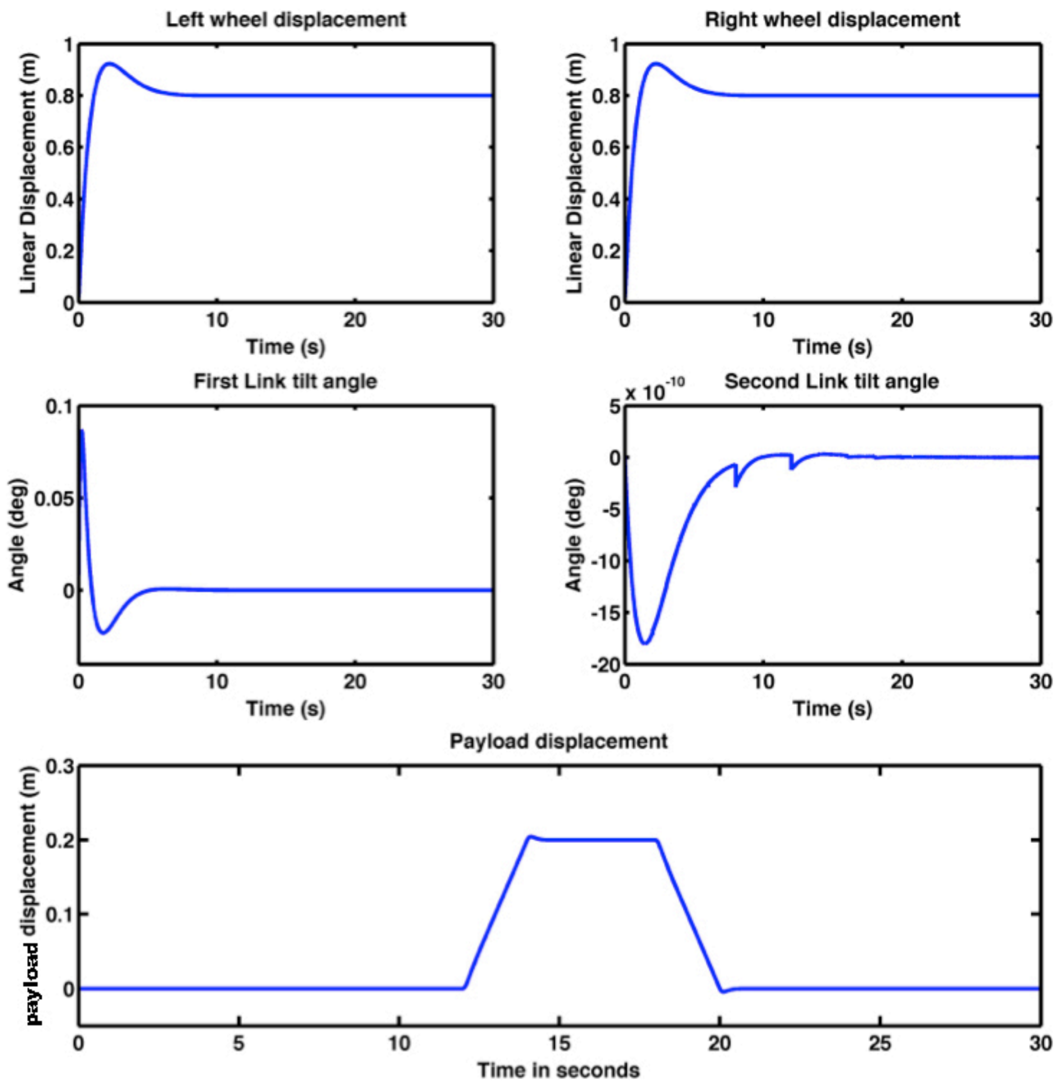

Figure 2.7 System response with PID controller

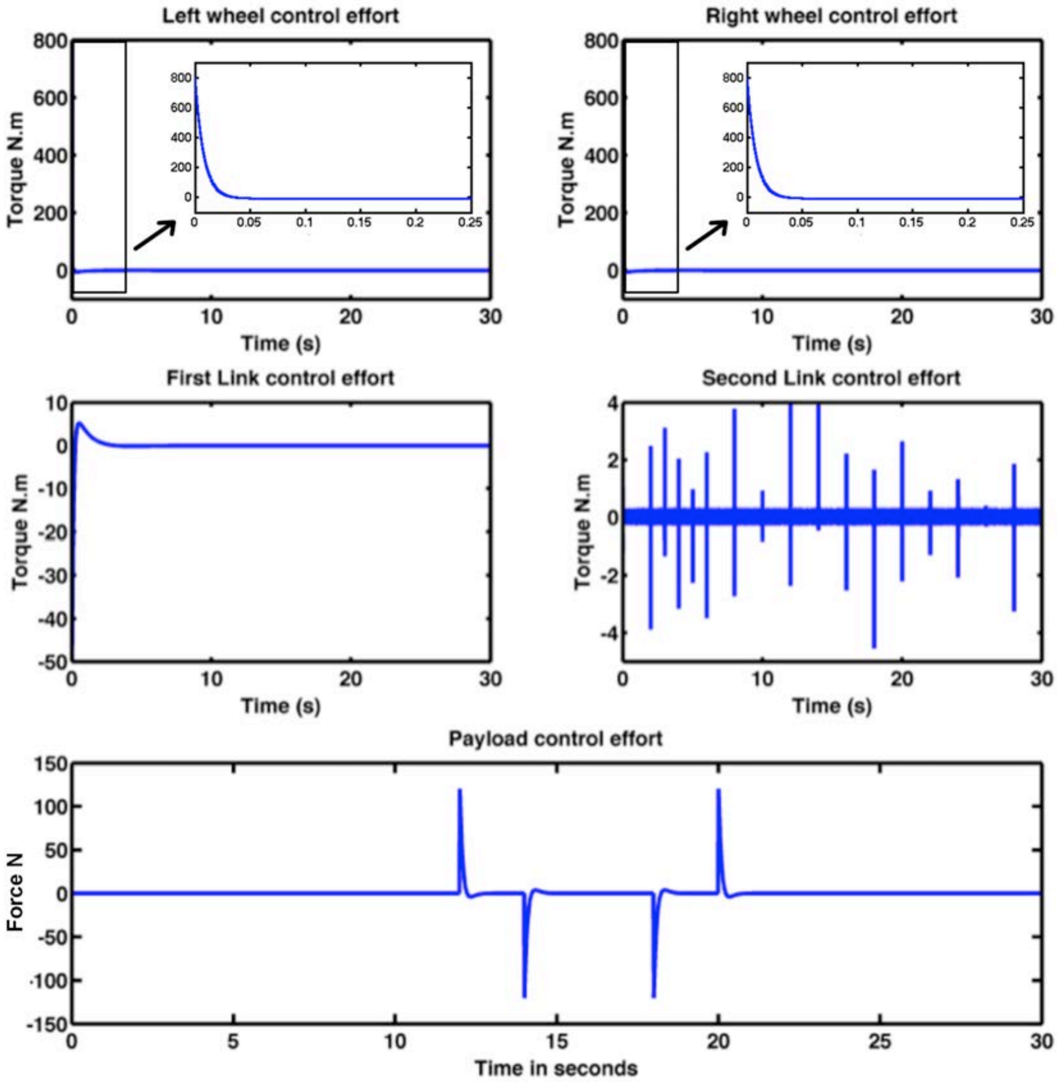

Figure 2.8 PID controller efforts exerted o stabilise the system

It can be clearly observed that the controller has exerted high torque values to stabilise the system. This can be explained due to the high control gain parameters used. A further investigation to control the system while minimising the control effort is needed in order to save energy. One solution is to integrate a fuzzy logic controller (FLC) with the current PID to form a hybrid fuzzy logic control system. The following section presents the design of the hybrid FLC system.

2.7 Hybrid fuzzy logic control strategy

Fuzzy logic controllers are intelligent controllers that have been proven to be powerful in controlling nonlinear system. This is due to the fact that FLC is a model-free control for complex systems that are difficult to be modelled mathematically. The hybrid FLC approach will be utilised to control the non-linear vehicle system. The hybrid FLC mechanism is implemented to control the non-linear vehicle model. Two types of hybrid FLC are designed and implemented. Proportional-Derivative-like fuzzy logic control (PD-like FLC) is used to control the displacement of the left and right wheels of the vehicle, the tilt angle of the first link and the payload linear actuator displacement. While for the second link tilt angle, a PD plus integral fuzzy logic control (PD+I FLC) is used to stabilise the link and to overcome the steady-state error.

Inputs to the PD-like FLC are the error and change of error signals. While the inputs for the PD+I FLC are the error, change of error and the sum of previous errors. Figures 2.9 and 2.10 illustrate PD-like FLC and PD+I FLC respectively. Figure 2.11 presents the block diagram of the controlled system.

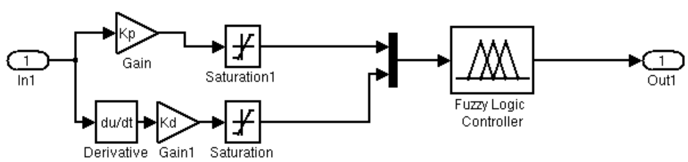

Figure 2.9 PD-Like Fuzzy logic control

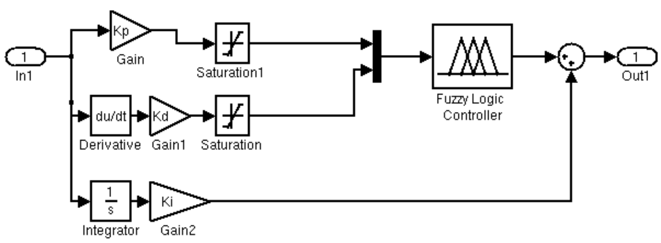

Figure 2.10 PD+I fuzzy logic control

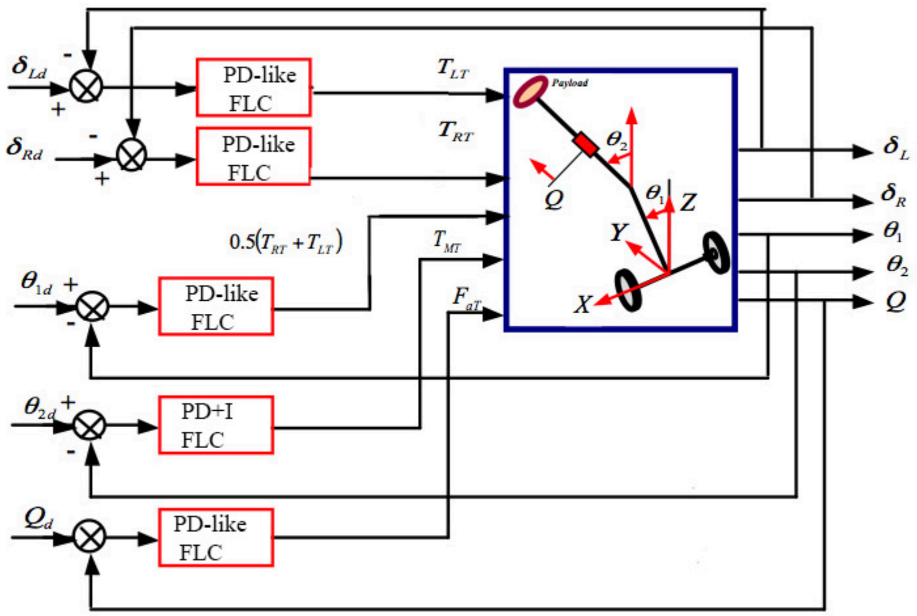

Figure 2.11 System block diagram

The FLC fuzzy inference engine is based on Mamdani-type of the form:

If (*error*) is *x* **and** (*change of error*) is *y* **then** the (*output)* is *z*

where: x, y and z are linguistic variables describing the input and output levels. The Mamdani-type fuzzy inference engine has a sufficient description of input and output values and has a simple formulation. The membership functions are of a Gaussain type. The Gaussain membership functions are selected to provide smooth inputs and outputs of the system. The membership functions are illustrated in Figure 2.11. The linguistic variables describing the inputs and outputs were chosen as Positive Big (PB), Positive Small (PS), Zero (Z), Negative Big (NB) and Negative Small (NS).

The interaction of the loops with the hybrid FLC control strategy is demonstrated by detuning one of the control loops and observing the affect on the stability of the system as shown in Figure 2.12. The interaction among the system control loops, due to the improper tuning of the right wheel controller gain, has resulted in an unstable response.

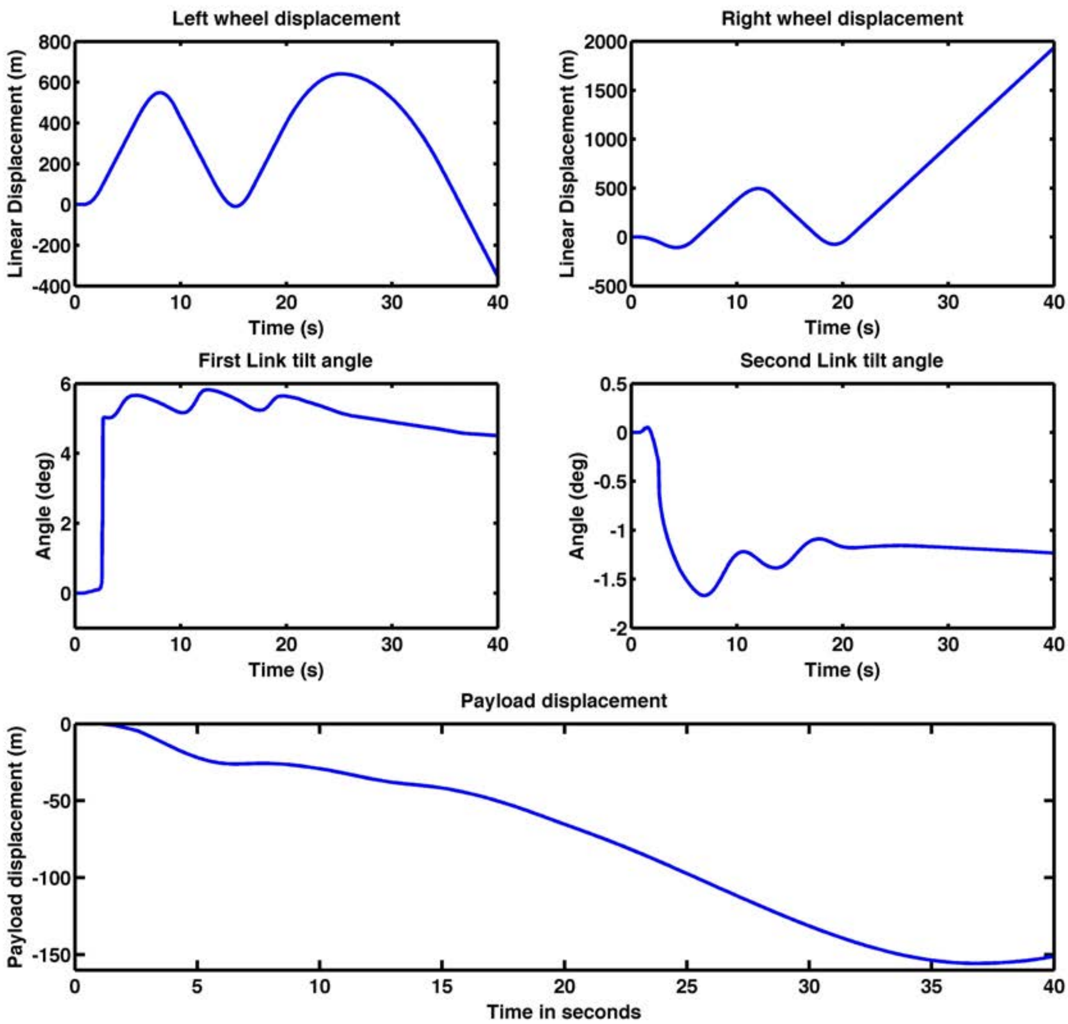

Figure 2.12 The interaction among the loops with improper tuning of the FLC c1ontrol parameters

2.8 Simulation and results

The fuzzy rules in the fuzzy-rules base are generated to control the system and minimise the error between the desired values and the actual output of the system. Table 2.4 presents the 25 fuzzy rule-base for the hybrid FLC. At this stage, the FLC gains were tuned manually and are presented in Table 2.5. A proper tuning of the FLC gains would be more beneficial in terms of minimising the energy consumption and to lead to an optimal control performance. This will be demonstrated in the upcoming chapters of this work. Figure 2.13 illustrates the Gaussain membership functions used.

Table 2.4 Fuzzy rules base

e \ ê	NB	NS	Z	PS	PB
NB	NB	NB	NB	NS	Z
NS	NB	NB	NS	Z	PS
Z	NB	NS	Z	PS	PB
PS	NS	Z	PS	PB	PB
PB	Z	PS	PB	PB	PB

Table 2.5 PD and PID controllers gains

Loop	***PID gains***		
	$\boldsymbol{K_P}$	$\boldsymbol{K_I}$	$\boldsymbol{K_D}$
Left wheel	2	-	2
Right wheel	2	-	2
First pendulum link	10	0.01	10
Second pendulum link	150	200	100
Payload linear actuator	10	-	2

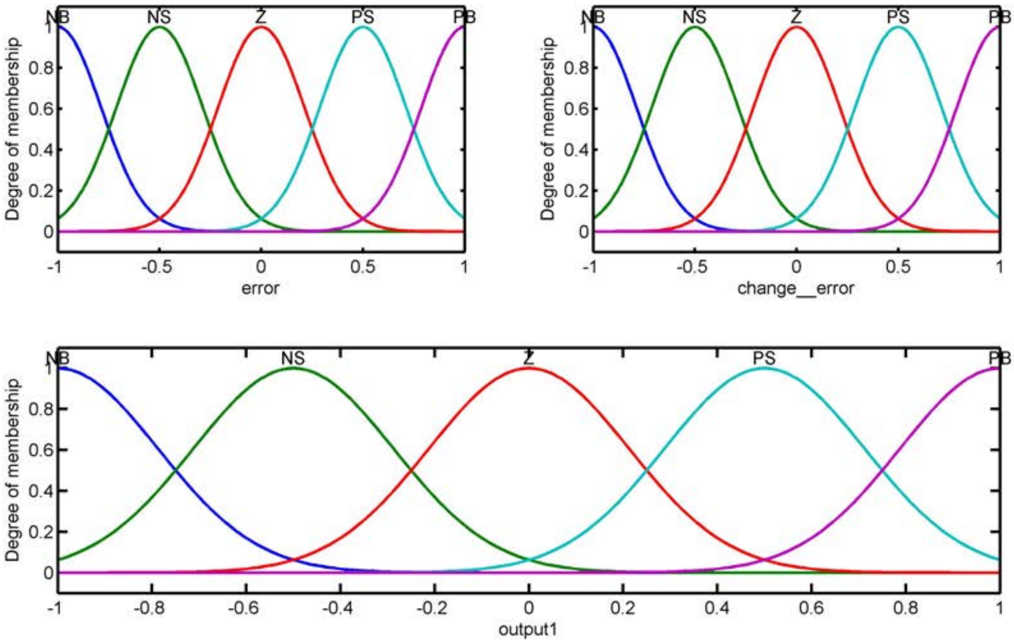

Figure 2.13: Gaussian fuzzy membership functions

Figure 2.14 shows the controlled system response. It can be noticed that the wheels linear displacement had a stable response without an overshoot, while the first and second link tilt angles had an improved overshoot when compared to the PID controller response. On the payload actuator response, it is clear that the controller forced the system to follow the desired input signal but with a slight steady state error that will need a further integral action to be eliminated. The overall response of the system was improved with the implemented hybrid FLC.

Figure 2.15 illustrates the control effort exerted to stabilise the system with the hybrid FLC. The integration of FLC has resulted in a significant reduction of the exerted torques, when compared to the PID control strategy, without affecting the system stability. The promising results of the system behaviour can be improved further by properly tuning the control parameters using optimisation algorithms; this process will be demonstrated in the upcoming chapters.

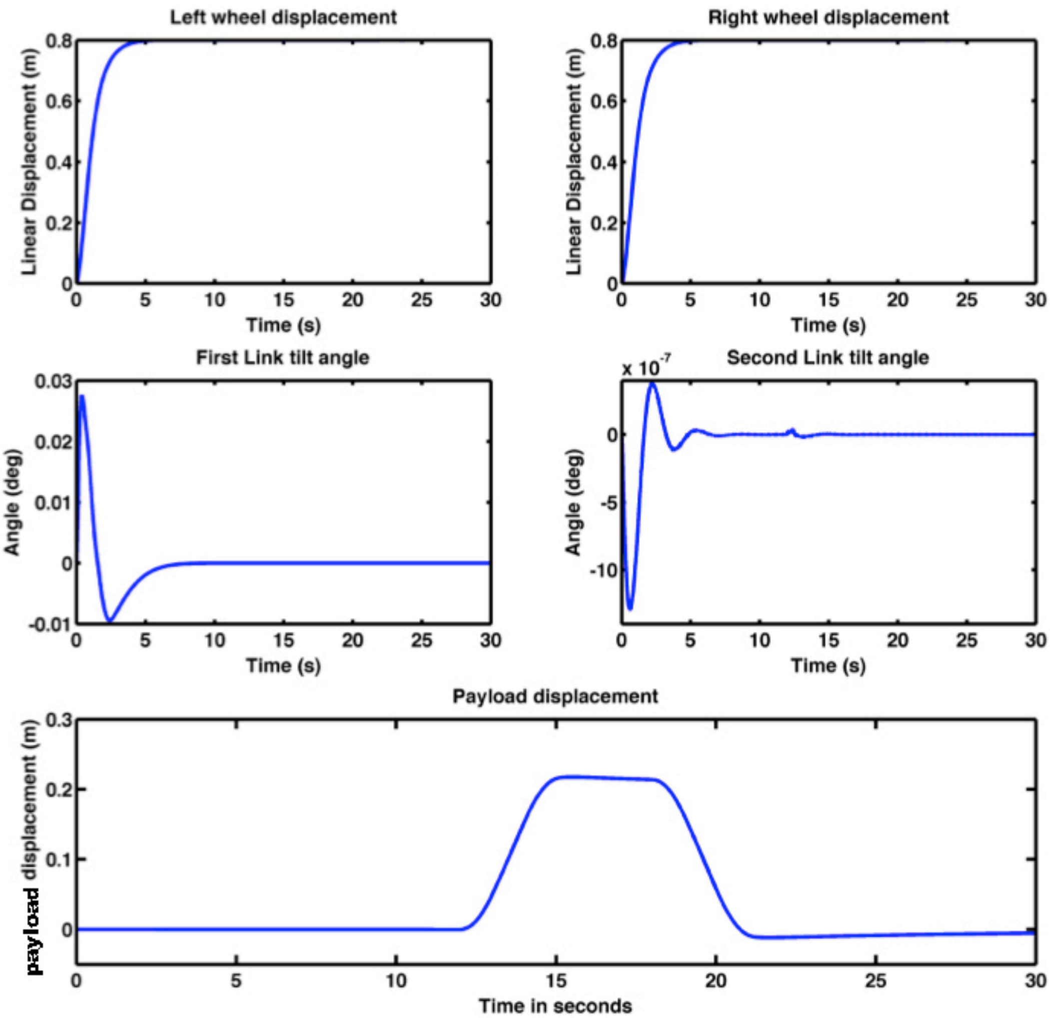

Figure 2.14 Closed system response with hybrid FLC controller

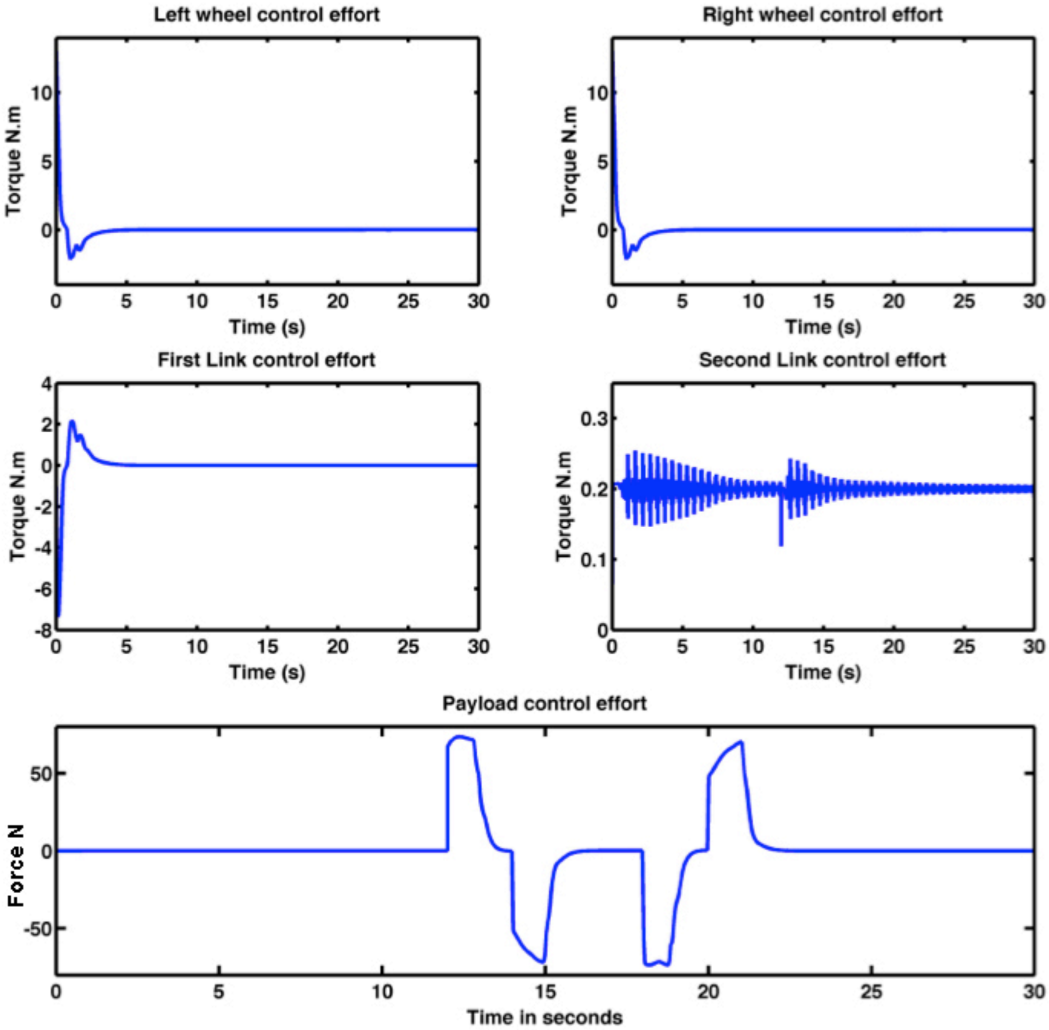

Figure 2.15 Hybrid FLC control effort to stabilise the system

2.9 Summary

The research objective is to develop a novel design of two-wheeled robotic vehicle with an extended height and moving payload that is able to manoeuvre in different environments and on uneven surfaces. A mathematical model of the vehicle on flat surfaces has been derived based on the Euler-Lagrange approach to describe the system dynamics. The model has been tested and simulated in the Matlab Simulink© environment and it confirmed that the system was unstable. As a first step to control the system, a combination of PID and PD controllers have been used to stabilise the system within the linear operating region to test the system controllability.

Further work carried out to design a hybrid fuzzy logic controller. While the PID control resulted in a stable response of the system, the hybrid FLC resulted in a significantly decreased amount of the exerted control effort. The hybrid FLC controller combined both PD-like FLC and PD+I FLC together to stabilise the system. Simulations have shown a successful stable response. A more general model of the vehicle is needed in order to test its ability in moving on different terrains and various sloped surfaces with nonlinear frictional elements. The next chapter will demonstrate the derivation of the general model of the vehicle.

Chapter 3
System description and mathematical modelling

3.1 Introduction

In this chapter, a general mathematical model of the vehicle incorporating a surface inclination angle is presented. The system model is derived using the Euler-Lagrange approach. The general model obtained is simulated, validated and tested on different inclined surfaces. The mathematical model is derived in a general nonlinear form, including the joint frictions, to allow the study of system dynamics with different movement scenarios in later chapters. A detailed modelling process is presented and discussed in this chapter. To control the general model of the vehicle, a hybrid FLC is designed using the same strategy that was detailed in chapter 2.

3.2 General mathematical model of the vehicle moving on an inclined surface

Using the Euler-Lagrange approach to derive the system mathematical model yields to a set of coupled differential equations that describe the system. These equations are the equations of motion of the system and describe the dynamics of the system. The Lagrangian approach is advantageous for complex systems such as the vehicle structure.

As previously mentioned the derivation is based on energy calculations of the physical system. As energy calculations are independent of vector representation, the derivation process would be simplified for such complex models when compared to Newton-Euler formulation. One of the most imperative reasons of adopting the Euler-

Lagrange approach in modelling is that it utilises the generalised coordinates of the system to describe the system degrees of freedom in a general representation.

Referring to Figure 3.1, a vehicle model on an inclined plane is illustrated. Table 3.1 presents the nomenclature of variables used in the derivation of the general vehicle model.

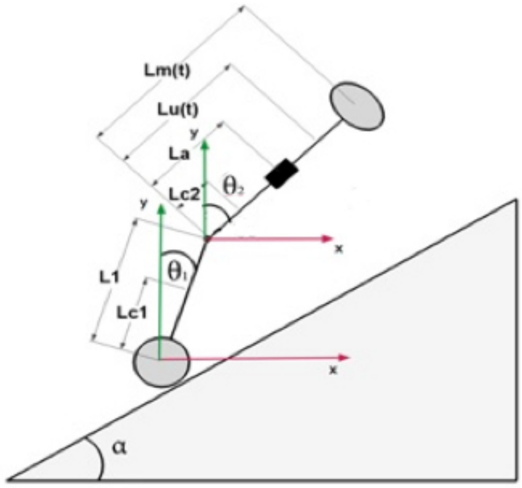

Figure 3.1: Schematic diagram of the vehicle on an inclined surface

Table 3.1 Parameters and description

Terminology	Description	Units
$L_{M(t)}$	Distance to payload from the centre of mass	m
$L_{2u(t)}$	Distance to the upper part of second link from the centre of mass	m
L_a	Position of the linear actuator	m
L_{c1}	Half length of the first link	m
L_{c2}	Half length of the lower part of second link	m
H	Distance between the wheels along the x axis	m
Q	Displacement of the linear actuator	m
M_1	Mass of the first link	kg
M_m	Mass of motor of the second link	kg
M_{2l}	Mass of the lower part of the second link	kg
M_a	Mass of the linear actuator	kg
M_{2u}	Mass of the upper part of the second link	kg
M	Payload mass	kg
T_R, T_L	Wheels driving torques	N.m
T_m	Motor torque	N.m
θ_1	Angular position of link 1 to the positive Z axis	rad
θ_2	Angular position of link 2 to the positive Z axis	rad
α	Surface inclination angle	rad

Using the Lagrange formulation for the system dynamics, the following dynamic equation can be expressed for an *n* degrees of freedom (DOF) system

$$\frac{dq}{dt}\left(\frac{\partial L}{\partial \dot{q}_i}\right)-\frac{\partial L}{\partial q_i}=Q_i \tag{3.1}$$

where

$L=T-V$, is the Lagrangian function

$Q_i=$ Generalized force associated with a generalized coordinate q_i

$q_i=$ Generalized coordinate

$n=$ Number of degrees of freedom of the system

$T=$ System kinetic energy

$V=$ System potential energy.

3.3 System energy requirements

Lagrangian technique considers the system energy, consisting of kinetic energy and potential energy. The total energy, U , of the two-wheeled robot can be described as the sum of the kinetic energy, T , and the potential energy, V , of each of the system components. These can be expressed as:

$$U=T+V \tag{3.2}$$

$$T=T_c+T_\phi+T_1+T_m+T_{2l}+T_a+T_{2u}+T_M \tag{3.3}$$

$$V = V_1 + V_m + V_{2l} + V_a + V_{2u} + V_M \tag{3.4}$$

$$T_c = \left(M_W R_W^2 + J_W\right)\left(\dot{\delta}_L^2 + \dot{\delta}_R^2\right) \tag{3.5}$$

$$T_\phi = \frac{1}{2}\left(2J_W + J_{IB}\right)\dot{\varphi}^2 \tag{3.6}$$

The links kinetic energies can be expressed as the sum of their translational energy and rotational energy;

$$T_1 = 0.5M_1 \left\{ \begin{array}{l} \left[\frac{d}{dt}\left(L_{c1}\sin\theta_1 + \frac{R_w}{2}(\delta_L + \delta_R)\cos\alpha\right)\right]^2 \\ + \left[\frac{d}{dt}\left(L_{c1}\cos\theta_1 + \frac{R_w}{2}(\delta_L + \delta_R)\sin\alpha\right)\right]^2 \end{array} \right\} \tag{3.7}$$

$$T_m = 0.5M_m \left\{ \begin{array}{l} \left[\frac{d}{dt}\left(L_1\sin\theta_1 + \frac{R_w}{2}(\delta_L + \delta_R)\cos\alpha\right)\right]^2 \\ + \left[\frac{d}{dt}\left(L_1\cos\theta_1 + \frac{R_w}{2}(\delta_L + \delta_R)\sin\alpha\right)\right]^2 \end{array} \right\} \tag{3.8}$$

$$T_{2l} = 0.5M_{2l} \left\{ \begin{array}{l} \left[\frac{d}{dt}\left(L_1\sin\theta_1 + L_{c2}\sin\theta_2 + \frac{R_w}{2}(\delta_L + \delta_R)\cos\alpha\right)\right]^2 \\ + \left[\frac{d}{dt}\left(L_1\cos\theta_1 + L_{c2}\cos\theta_2 + \frac{R_w}{2}(\delta_L + \delta_R)\sin\alpha\right)\right]^2 \end{array} \right\} \tag{3.9}$$

$$T_a = 0.5M_a \left\{ \begin{array}{l} \left[\frac{d}{dt}\left(L_1\sin\theta_1 + L_a\sin\theta_2 + \frac{R_w}{2}(\delta_L + \delta_R)\cos\alpha\right)\right]^2 \\ + \left[\frac{d}{dt}\left(L_1\cos\theta_1 + L_a\cos\theta_2 + \frac{R_w}{2}(\delta_L + \delta_R)\sin\alpha\right)\right]^2 \end{array} \right\} \tag{3.10}$$

$$T_{2u} = 0.5M_{2u}\left\{\begin{array}{l} \dot{Q}^2 + \left[\frac{d}{dt}\left(L_1\sin\theta_1 + L_{2u(t)}\sin\theta_2 + \frac{R_w}{2}(\delta_L+\delta_R)\cos\alpha\right)\right]^2 \\ + \left[\frac{d}{dt}\left(L_1\cos\theta_1 + L_{2u(t)}\cos\theta_2 + \frac{R_w}{2}(\delta_L+\delta_R)\sin\alpha\right)\right]^2 \end{array}\right\} \quad (3.11)$$

$$T_{M} = 0.5M\left\{\begin{array}{l} \dot{Q}^2 + \left[\frac{d}{dt}\left(L_1\sin\theta_1 + L_{M(t)}\sin\theta_2 + \frac{R_w}{2}(\delta_L+\delta_R)\cos\alpha\right)\right]^2 \\ + \left[\frac{d}{dt}\left(L_1\cos\theta_1 + L_{M(t)}\cos\theta_2 + \frac{R_w}{2}(\delta_L+\delta_R)\sin\alpha\right)\right]^2 \end{array}\right\} \quad (3.12)$$

The total kinetic energy can be simplified and expressed as

$$\begin{aligned} T_T = {} & C_1(\dot{\delta}_L+\dot{\delta}_R)^2 + C_2\dot{\theta}_1^2 + 0.5\dot{\theta}_2^2\left(C_3 + M_{2u}(Q^2+2C_8Q+C_{10}) + M(Q^2+2C_9Q+C_{11}\right) \\ & + C_4R_w(\dot{\delta}_L+\dot{\delta}_R) + \dot{\theta}_1\dot{\theta}_2\cos(\theta_1-\theta_2)\left(C_5 + M_{2u}L_1(C_8+Q) + ML_1(C_9+Q)\right) \\ & + C_6\dot{\theta}_1(\dot{\delta}_L+\dot{\delta}_R)\cos(\theta_1+\alpha) + C_{12}(\dot{\delta}_L^2+\dot{\delta}_R^2) + 0.5C_{13}\dot{\phi}^2 + 0.5C_{19}\dot{Q}^2 \\ & + 0.5\dot{\theta}_2(\dot{\delta}_L+\dot{\delta}_R)\cos(\theta_2+\alpha)\left(C_7 + M_{2u}R_w(C_8+Q) + MR_w(C_9+Q)\right) \end{aligned} \quad (3.13)$$

The constants C_i are given in Appendix B.

Assuming the wheels remain in full contact with ground at all times, the robot will have no motion in the Z direction and therefore there will be no potential energy for the system in the Z direction.

The potential energy of various components can be expressed as:

$$V_1 = M_1g(L_{c1}\cos\theta_1 + (\delta_L+\delta_R)\sin\alpha) \quad (3.14)$$

$$V_m = M_mg(L_1\cos\theta_1 + (\delta_L+\delta_R)\sin\alpha) \quad (3.15)$$

$$V_{2l} = M_{2l}g(L_1\cos\theta_1 + L_{c2}\cos\theta_2 + (\delta_L+\delta_R)\sin\alpha) \quad (3.16)$$

$$V_a = M_ag(L_1\cos\theta_1 + L_a\cos\theta_2 + (\delta_L+\delta_R)\sin\alpha) \quad (3.17)$$

$$V_{2u} = M_{2u}g(L_1\cos\theta_1 + L_{2u(t)}\cos\theta_2 + (\delta_L + \delta_R)\sin\alpha) \tag{3.18}$$

$$V_M = Mg(L_1\cos\theta_1 + L_{M(t)}\cos\theta_2 + (\delta_L + \delta_R)\sin\alpha) \tag{3.19}$$

where $L_{2u(t)}$ and $L_{M(t)}$ are the positions of the centre of mass of upper part of the second link and the payload respectively. Both variables are time dependent, in correspondence to the displacement caused by the linear actuator, and can be expressed as:

$$L_{2u(t)} = 2L_{2l} + L_{2u} + Q \tag{3.20}$$

$$L_{M(t)} = 2L_{2l} + 2L_{2u} + Q \tag{3.21}$$

Manipulating the above equations yield the following two expressions for the total kinetic and total potential energies of the system respectively;

$$\begin{aligned} T_T = {} & C_1(\dot{\delta}_L + \dot{\delta}_R)^2 + C_2\dot{\theta}_1^2 + 0.5\dot{\theta}_2^2\left(C_3 + M_{2u}(Q^2 + 2C_8Q + C_{10}) + M(Q^2 + 2C_9Q + C_{11}\right) \\ & + C_4R_w(\dot{\delta}_L + \dot{\delta}_R) + \dot{\theta}_1\dot{\theta}_2\cos(\theta_1 - \theta_2)\left(C_5 + M_{2u}L_1(C_8 + Q) + ML_1(C_9 + Q)\right) \\ & + C_6\dot{\theta}_1(\dot{\delta}_L + \dot{\delta}_R)\cos(\theta_1 + \alpha) + C_{12}(\dot{\delta}_L^2 + \dot{\delta}_R^2) + 0.5C_{13}\dot{\phi}^2 + 0.5C_{19}\dot{Q}^2 \\ & + 0.5\dot{\theta}_2(\dot{\delta}_L + \dot{\delta}_R)\cos(\theta_2 + \alpha)\left(C_7 + M_{2u}R_w(C_8 + Q) + MR_w(C_9 + Q)\right) \end{aligned} \tag{3.22}$$

$$V_T = gC_{14}\cos\theta_1 + g\cos\theta_2(C_{17} + C_{18}Q) + gC_{16}(\delta_L + \delta_R)\sin\alpha \tag{3.23}$$

The Lagrangian equation of motion is presented as

$$\frac{dq}{dt}\left(\frac{\partial L}{\partial \dot{q}_i}\right) - \frac{\partial L}{\partial q_i} = Q_i \tag{3.24}$$

where q_i represents a particular generalized coordinate, and

$$\dot{q}_i = \frac{dq_i}{dt} \tag{3.25}$$

The overall motion of the system can be described using equation (3.24) for each generalized coordinate. The generalized coordinates describing the motion of the system may be identified as follows

$$q_i = \begin{bmatrix} \delta_{\mathrm{L}} & \delta_{\mathrm{R}} & \theta_1 & \theta_2 & \mathrm{Q} \end{bmatrix}^T \tag{3.26}$$

The associated generalized forces are expressed as

$$Q_i = \begin{bmatrix} T_{LT} & T_{RT} & T_{AV} & T_{MT} & F_{aT} \end{bmatrix}^T \tag{3.27}$$

where the generalized forces and moments are given as:

$$T_{LT} = T_L - T_{fL} \tag{3.28}$$

$$T_{RT} = T_R - T_{fR} \tag{3.29}$$

$$T_{AV} = \frac{1}{2}\left(T_{RT} + T_{LR}\right) \tag{3.30}$$

$$T_{MT} = T_M - T_{fM} - L_d F_d \tag{3.31}$$

$$F_{aT} = F_a - F_{fa} \tag{3.32}$$

3.4 Joints friction effects

Assuming a similar damping characteristics for all the vehicle joints, the frictional moments can be expressed, based on Coulomb's friction model, as follows:

$$T_{fL} = c_v \dot{\delta}_L + c_c \sin \dot{\delta}_L \tag{3.33}$$

$$T_{fR} = c_v\dot{\delta}_R + c_c \sin\dot{\delta}_R \tag{3.34}$$

$$T_{fM} = c_v\dot{\theta}_2 + c_c \sin\dot{\theta}_2 \tag{3.35}$$

$$F_{fa} = c_v\dot{Q} + c_c \sin\dot{Q} \tag{3.36}$$

Where T_{fL}, T_{fR}, are the frictional moments of the left and right wheels respectively. T_{fM}, F_{fa} are the frictional moments of the intermediate joint connecting the first and second links and the frictional force in the actuator. c_v and c_c are the viscous and Coulomb friction coefficients at the vehicle joints respectively. $\dot{\delta}_L$ and $\dot{\delta}_R$ are the rate of displacements of the left and right wheels respectively. $\dot{\theta}_2$ is the rate of angular position of the second link and $\dot{Q}$ is the velocity of the attached payload.

3.5 Lagrangian formulation

The Lagrangian function of the system, L can be expressed as the difference between the system kinetic and potential energy as follows:

$$\begin{aligned}
L = {} & C_1(\dot{\delta}_L^2 + \dot{\delta}_R^2) + C_2\dot{\theta}_1^2 + 0.5\dot{\theta}_2^2\left(C_3 + M_{2u}(Q^2 + 2C_8Q + C_{10}) + M(Q^2 + 2C_9Q + C_{11}\right) \\
& + C_4R_w(\dot{\delta}_L + \dot{\delta}_R) + \dot{\theta}_1\dot{\theta}_2\cos(\theta_1 - \theta_2)\left(C_5 + M_{2u}L_1(C_8 + Q) + ML_1(C_9 + Q)\right) \\
& + C_6\dot{\theta}_1(\dot{\delta}_L + \dot{\delta}_R)\cos(\theta_1 + \alpha) + C_{12}(\dot{\delta}_L^2 + \dot{\delta}_R^2) + 0.5C_{13}\dot{\phi}^2 + 0.5C_{19}\dot{Q}^2 + 2C_1\dot{\delta}_L\dot{\delta}_R \\
& + 0.5\dot{\theta}_2(\dot{\delta}_L + \dot{\delta}_R)\cos(\theta_2 + \alpha)\left(C_7 + M_{2u}R_w(C_8 + Q) + MR_w(C_9 + Q)\right) \\
& - gC_{14}\cos\theta_1 - g\cos\theta_2(C_{17} + C_{18}Q) - gC_{16}(\delta_L + \delta_R)\sin\alpha + 0.5C_{19}\dot{Q}^2
\end{aligned} \tag{3.37}$$

The Lagrangian equations of motion of the vehicle can be represented as:

$$\frac{d}{dt}\left(\frac{\partial L}{\partial\dot{\delta}_L}\right) - \frac{\partial L}{\partial\delta_L} = T_L - T_{fL} \tag{3.38}$$

$$\frac{d}{dt}\left(\frac{\partial L}{\partial \dot{\delta}_R}\right)-\frac{\partial L}{\partial \delta_R}=T_R-T_{fR} \tag{3.39}$$

$$\frac{d}{dt}\left(\frac{\partial L}{\partial \dot{\theta}_1}\right)-\frac{\partial L}{\partial \theta_1}=\frac{1}{2}(T_{LT}+T_{RT}) \tag{3.40}$$

$$\frac{d}{dt}\left(\frac{\partial L}{\partial \dot{\theta}_2}\right)-\frac{\partial L}{\partial \theta_2}=T_M-T_{fM}-L_dF_d \tag{3.41}$$

$$\frac{d}{dt}\left(\frac{\partial L}{\partial \dot{Q}}\right)-\frac{\partial L}{\partial Q}=F_a-F_{fa} \tag{3.42}$$

3.6 Vehicle dynamic equations

Manipulating the above expressions yields the following five highly non-linear differential equations describing the vehicle dynamics alongside the driving moments and an external disturbance force as:

$$\begin{aligned}
&2C_{27}\ddot{\delta}_L+2C_{1}\ddot{\delta}_R+C_6\ddot{\theta}_1\cos(\theta_1+\alpha)-C_6\dot{\theta}_1^2\sin(\theta_1+\alpha)\\
&+0.5(C_{25}+C_{26}Q)\left(\ddot{\theta}_2\cos(\theta_2+\alpha)-\dot{\theta}_2^2\sin(\theta_2+\alpha)\right)\\
&+0.5C_{28}\dot{Q}\dot{\theta}_2\cos(\theta_2+\alpha)+C_{16}g\sin\alpha=T_L-T_{fL}
\end{aligned} \tag{3.43}$$

$$\begin{aligned}
&2C_{27}\ddot{\delta}_R+2C_{1}\ddot{\delta}_L+C_6\ddot{\theta}_1\cos(\theta_1+\alpha)-C_6\dot{\theta}_1^2\sin(\theta_1+\alpha)\\
&+0.5(C_{25}+C_{26}Q)\left(\ddot{\theta}_2\cos(\theta_2+\alpha)-\dot{\theta}_2^2\sin(\theta_2+\alpha)\right)\\
&+0.5C_{28}\dot{Q}\dot{\theta}_2\cos(\theta_2+\alpha)+C_{16}g\sin\alpha=T_R-T_{fR}
\end{aligned} \tag{3.44}$$

$$
\begin{aligned}
&2C_2\ddot{\theta}_1+C_6(\ddot{\delta}_L+\ddot{\delta}_R)\cos(\theta_1+\alpha)+C_6(\dot{\delta}_L+\dot{\delta}_R)(\dot{\theta}_1^2-\dot{\theta}_1)\sin(\theta_1+\alpha)\\
&+\left(\dot{Q}(M_{2u}L_1+ML_1)\right)\dot{\theta}_2\cos(\theta_1-\theta_2)-\begin{pmatrix}C_5+M_{2u}L_1(C_8+Q)\\+ML_1(C_9+Q)\end{pmatrix}\dot{\theta}_2(\dot{\theta}_1-\dot{\theta}_2)\sin(\theta_1-\theta_2)\\
&+\begin{pmatrix}C_5+M_{2u}L_1(C_8+Q)\\+ML_1(C_9+Q)\end{pmatrix}\dot{\theta}_1^2\dot{\theta}_2\sin(\theta_1-\theta_2)+\begin{pmatrix}C_5+M_{2u}L_1(C_8+Q)\\+ML_1(C_9+Q)\end{pmatrix}\ddot{\theta}_2\cos(\theta_1-\theta_2)\\
&-gC_{14}\dot{\theta}_1\sin\theta_1=0.5(T_{RT}+T_{LT})
\end{aligned}
\tag{3.45}
$$

$$
\begin{aligned}
&\ddot{\theta}_2(C_{19}Q^2+C_{20}Q+C_{21})+\dot{\theta}_2(2C_{19}Q^2+C_{22})+\ddot{\theta}_1\cos(\theta_1-\theta_2)(C_{23}Q+C_{24})\\
&-\dot{\theta}_1(\dot{\theta}_1-\dot{\theta}_2)\sin(\theta_1-\theta_2)(C_{23}Q+C_{24})+C_{23}\dot{\theta}_1\cos(\theta_1-\theta_2)\\
&+0.5(\ddot{\delta}_L+\ddot{\delta}_R)\cos(\theta_2+\alpha)(C_{25}Q+C_{26})-0.5(\dot{\delta}_L+\dot{\delta}_R)\dot{\theta}_2\sin(\theta_2+\alpha)(C_{25}Q+C_{26})\\
&+0.5C_{25}(\dot{\delta}_L+\dot{\delta}_R)\cos(\theta_2+\alpha)-\dot{\theta}_1\dot{\theta}_2\sin(\theta_1-\theta_2)(C_{23}Q+C_{24})\\
&+0.5\dot{\theta}_2^2(\dot{\delta}_L+\dot{\delta}_R)\sin(\theta_2+\alpha)(C_{25}Q+C_{26})-g\dot{\theta}_2\sin\theta_2(C_{17}+C_{18}Q)=T_M-T_{fM}-L_dF_d
\end{aligned}
\tag{3.46}
$$

$$
\begin{aligned}
&C_{19}\ddot{Q}-0.5\dot{\theta}_2^2(2C_{19}Q+C_{22})-C_{23}\dot{\theta}_1\dot{\theta}_2\cos(\theta_1-\theta_2)\\
&-0.5C_{25}\dot{\theta}_2(\dot{\delta}_L+\dot{\delta}_R)\cos(\theta_2+\alpha)+gC_{18}\cos\theta_2=F_a-F_{fa}
\end{aligned}
\tag{3.47}
$$

Equations (3.43) – (3.47) present the general model of the vehicle that has a variable inclination angle α. The inclination angle will have various values to simulate the system dynamics while moving on various inclined surfaces and terrains. To simulate the system dynamics while moving on flat surfaces α should be set to zero; i.e. zero surface inclination angle.

3.7 PID control of the vehicle moving on flat and inclined surfaces

The PID control strategy adopted consists of developing a feedback control mechanism of five control loops, in order to drive the vehicle to undergo a specific planar motion in the XY plane. The input to the control loop of each wheel is the error in the displacements of each wheel measured as the difference between the desired and actual displacement of the corresponding wheel. The angular position of the intermediate body is controlled by measuring the error in positions of first and second links. In order to control the position of the attached payload, a feedback control loop is developed with the error in the payload position as an input and the actuation force as the output of the control loop.

The vehicle system is a multi-input multi-output (MIMO) system characterized by its highly nonlinear and highly coupled dynamics. The inputs to the system are the driving torques of the wheel motors; T_{LT} and T_{RT}, torque driving the motor activating second link, T_{MT} , the linear actuator force, F_{aT} , and the average of the torques of motors to stabilize the first link. The system has five outputs; the displacements of the left and right wheels; δ_L and δ_R respectively, the angular positions of the IB links, θ_1 and θ_2 , and the displacement of the payload, Q.

Three PD controllers are used to control the displacements the left and right wheels and the first link tilt angle. The control inputs are the error and the derivative of error for the three measured variables, δ_L, δ_R and θ_1 whereas the control outputs are the motor torques;

$$e_{\delta_L} = \delta_{Ld} - \delta_{Lm} \tag{3.48}$$

$$\dot{e}_{\delta_L} = \frac{d\left(e_{\delta_L}\right)}{dt} = \frac{\delta_L(k) - \delta_L(k-1)}{\Delta t} \tag{3.49}$$

$$e_{\delta_R} = \delta_{Rd} - \delta_{Rm} \tag{3.50}$$

$$\dot{e}_{\delta_R} = \frac{d\left(e_{\delta_R}\right)}{dt} = \frac{\delta_R(k) - \delta_R(k-1)}{\Delta t} \tag{3.51}$$

$$e_{\theta_1} = \theta_{1d} - \theta_{1m} \tag{3.52}$$

$$\dot{e}_{\theta_1} = \frac{d\left(e_{\theta_1}\right)}{dt} = \frac{\theta_1(k) - \theta_1(k-1)}{\Delta t} \tag{3.53}$$

Two PID controllers are used to control the second link tilt angle, θ_2, and the displacement of the payload, Q. As the type of motion considered at this stage of the study is linear, the left and right wheels input signals are identical in order to drive the vehicle in a straight line. The tilt angle error and its time derivative are defined as:

$$e_{\theta_2} = \theta_{2d} - \theta_{2m} \tag{3.54}$$

$$\dot{e}_{\theta_2} = \frac{d\left(e_{\theta_2}\right)}{dt} = \frac{\theta_2(k) - \theta_2(k-1)}{\Delta t} \tag{3.55}$$

Similarly, displacement error and its derivative are defined as:

$$e_Q = Q_d - Q_m \tag{3.56}$$

$$\dot{e}_Q = \frac{d\left(e_Q\right)}{dt} = \frac{Q(k) - Q(k-1)}{\Delta t} \tag{3.57}$$

where θ_d is the desired tilt angle, θ_m is the measured tilt angle of IB, Q_d is the desired payload displacement, and Q_m is the measured payload displacement.

For the current stage of the study, the control parameters of the system were tuned heuristically with the gains described in Table 3.2. The system is simulated with the initial conditions $\delta_L = \delta_R = 0$, $\theta_1 = \theta_1 = 0$, $Q_d = 0$.

Table 3.2. Heuristically adjusted robust PID controller gains

Feedback loop	PID controller Gains		
	K_P	K_I	K_D
Left wheel	50	NA	1
Right wheel	50	NA	1
First pendulum	10	NA	2
Second pendulum	30	15	10
Linear actuator	5	0.001	60

The desired outputs are $\delta_L = \delta_R = 0.8$ and $\theta_1 = \theta_1 = 0$, for the upright position, and the payload to follow the predefined input signal of Figure 2.3. As can be noticed from Figure 3.2 the system was capable of balancing and converging to the desired set values on a flat surface. The vehicle reached the desired linear position but with a little deviation around the set point in the time interval between 3-15 seconds. This deviation is due to payload lifting mechanism. The pendulum links were stabilised with slight negligible oscillations. The payload was successfully lifted to the desired position and has followed the predefined movement signal. Figure 3.3 shows the control effort of the PID controller. The controller exerted large amounts of torque to stabilise the system, and this can be attributed to the heuristic tuning of the control parameters. The stable response was encouraging; and using the hybrid FLC control strategy was thought to improve the response.

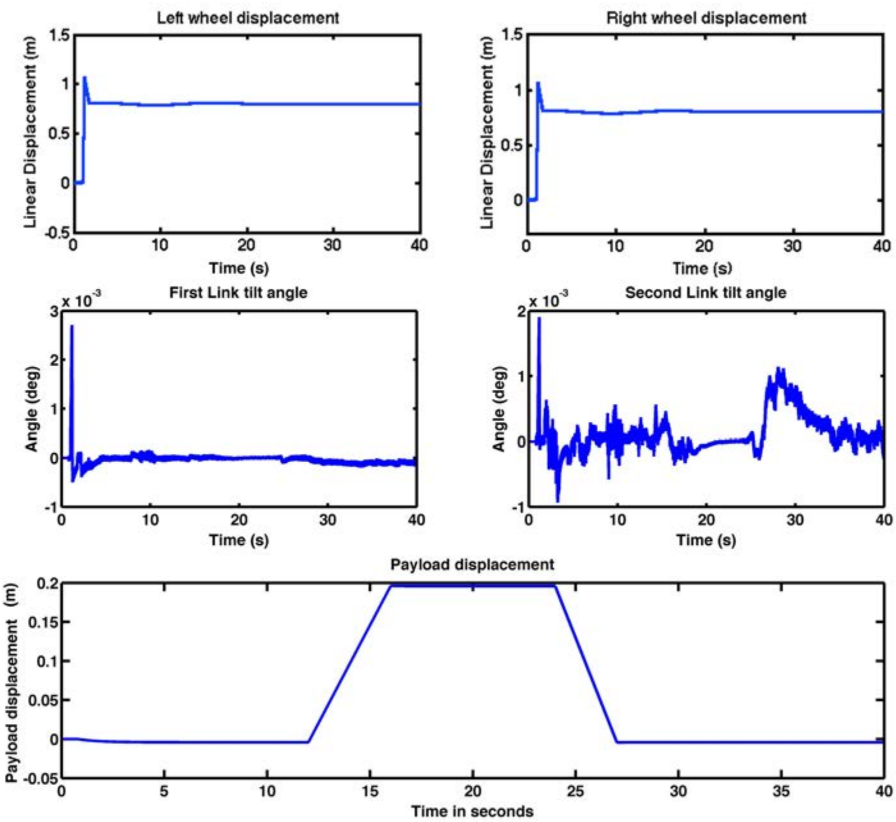

Figure 3.2: Controlled system response with PID control

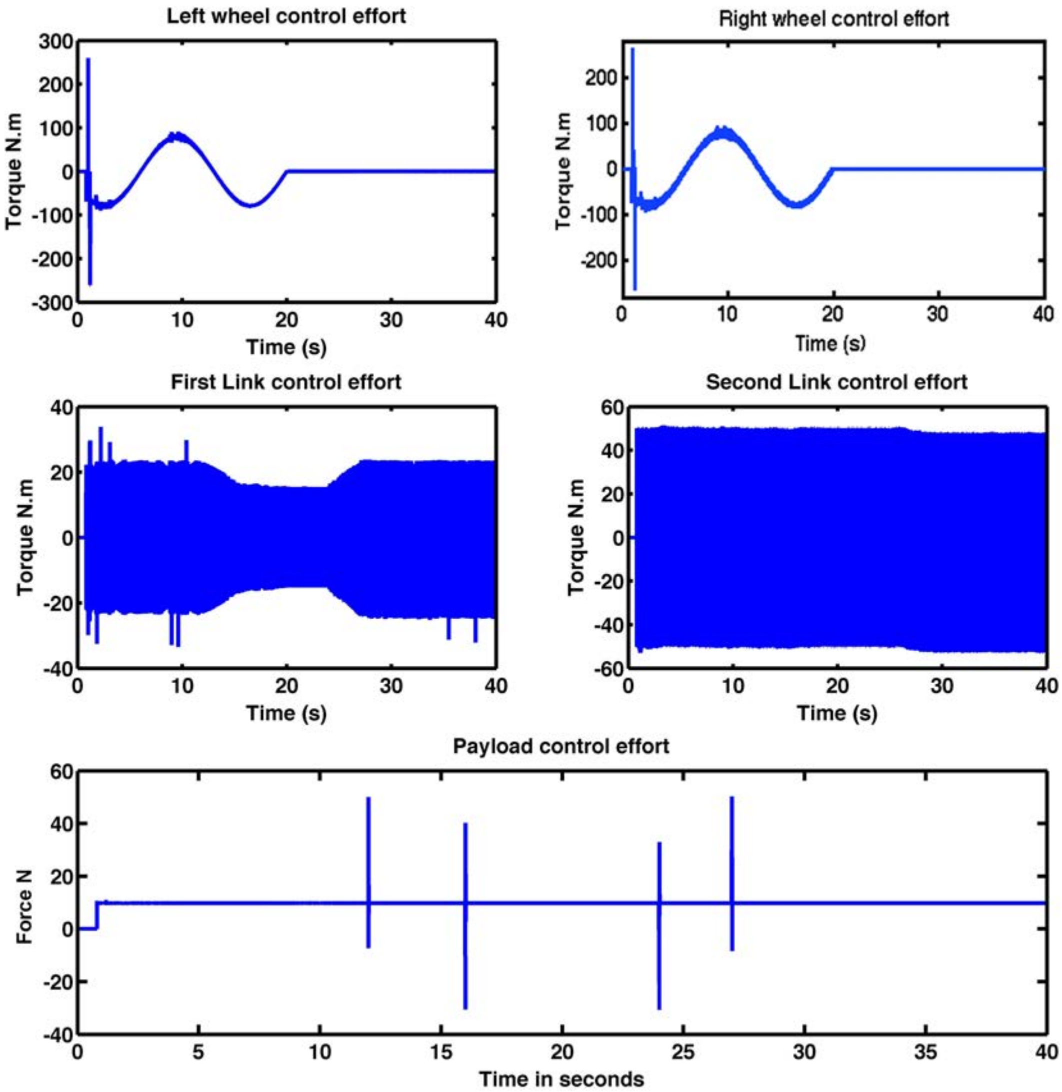

Figure 3.3: PID control effort to stabilise the system

To verify the vehicle ability to move on inclined surfaces, the system was tested to move on different surface inclination angles of $\alpha = 0^o$, 10^o and 30^o. Figures 3.4 and 3.5 present the vehicle system response with the defined surface inclination angles and the PID control effort respectively. The controller was able to stabilise the system on different slopes. The overshoots appearing at the wheel displacements are attributed to the exerted amount of torque that was directly proportional to the surface inclination angle, and this can be seen in Figure 3.5. Oscillations appearing at the first and second link were negligible in quantity. The payload lifting mechanism was not affected by the change of surface inclination angle. There are two possible explanations of this result; the first is that the payload lifting is only activated once the balancing position is achieved. While the second reason is that the payload lifting mechanism is mainly coupled with the second link tilt angle and this is noted from equation (3.47).

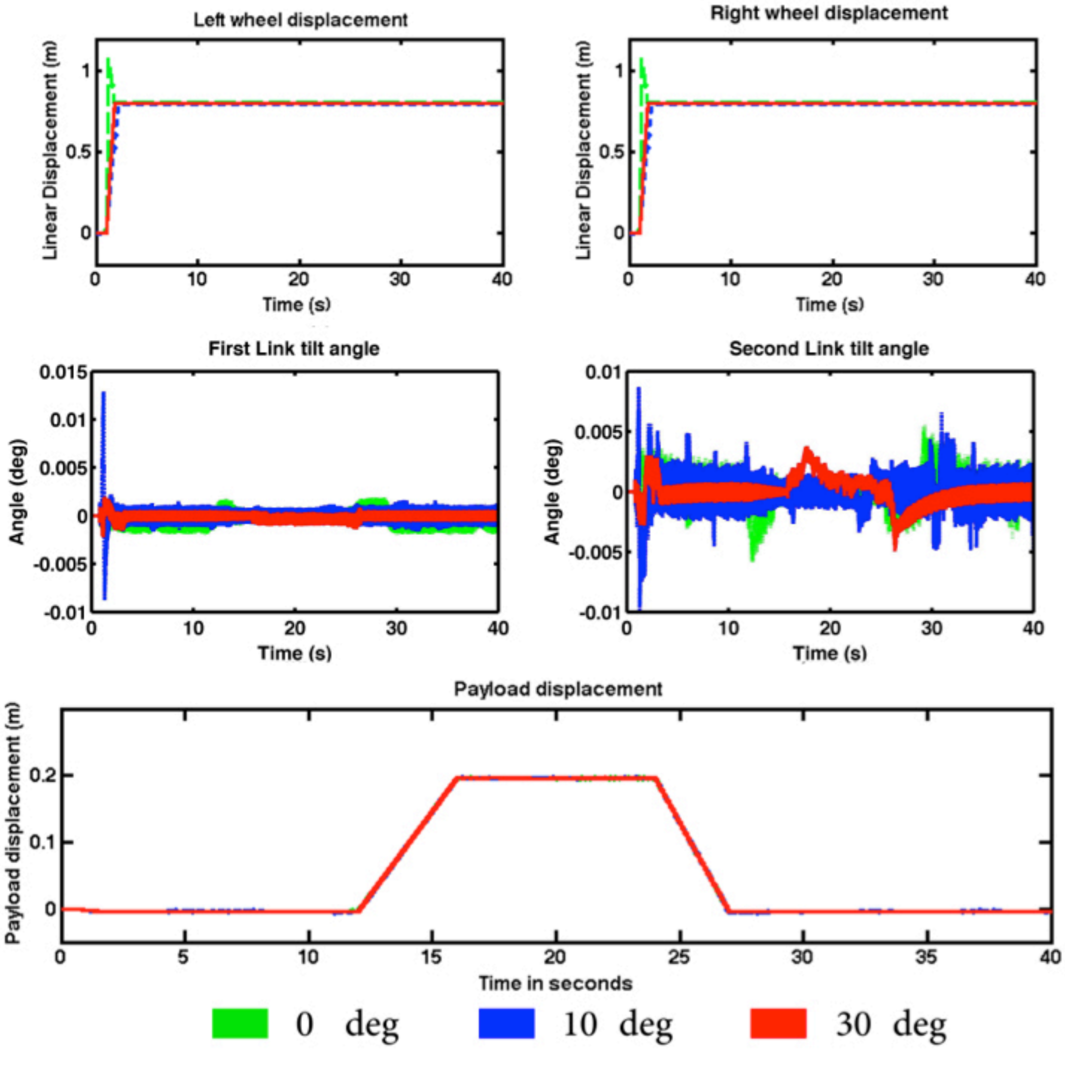

Figure 3.4: System response with PID controller on different inclination angles

Figure 3.5 and Figure 3.6 shows that an increase in surface inclination angle leads to increased amount of exerted torques to stabilise the vehicle. Considerable amount of torque exerted was noted on the vehicle links and the payload actuator. In the next section, a hybrid FLC will be incorporated into the system to reduce the excessive amount of control effort and improve the overall system response.

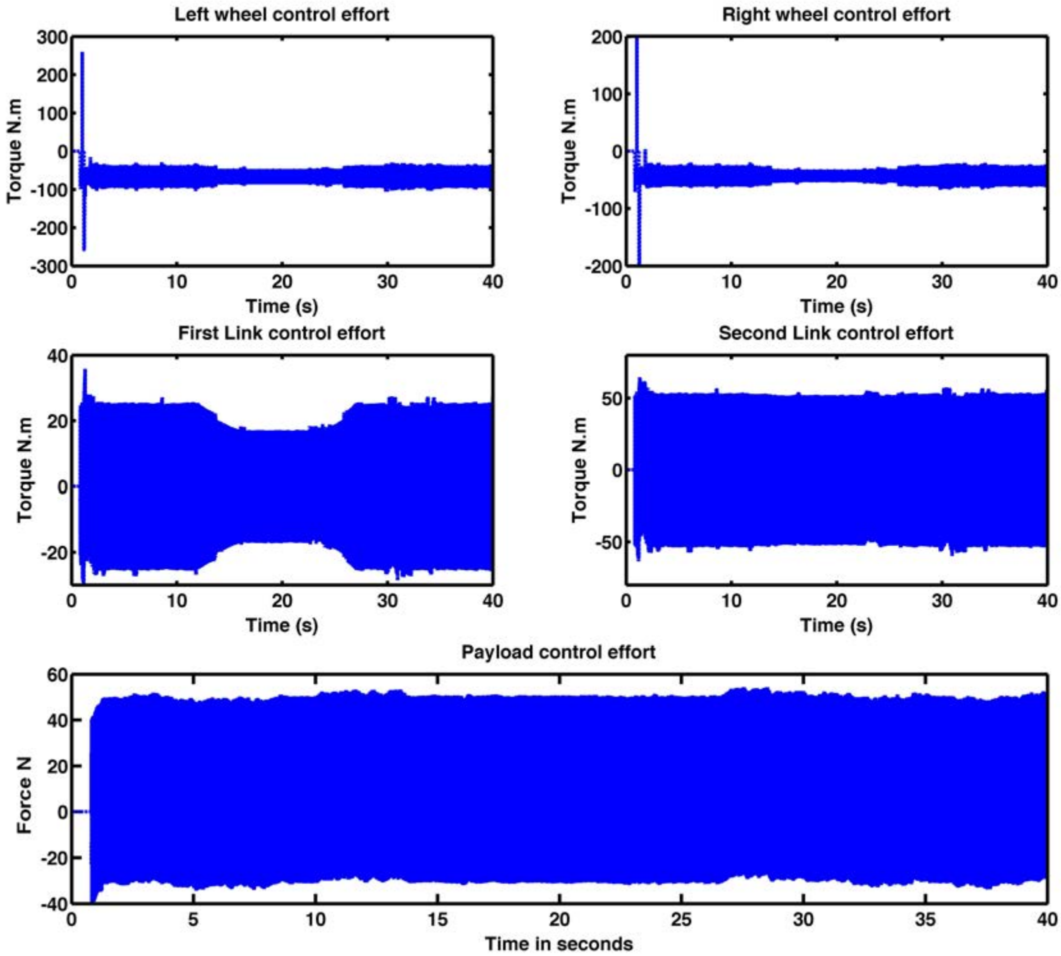

Figure 3.5: PID control effort for the vehicle on an inclined surface of 10 degrees

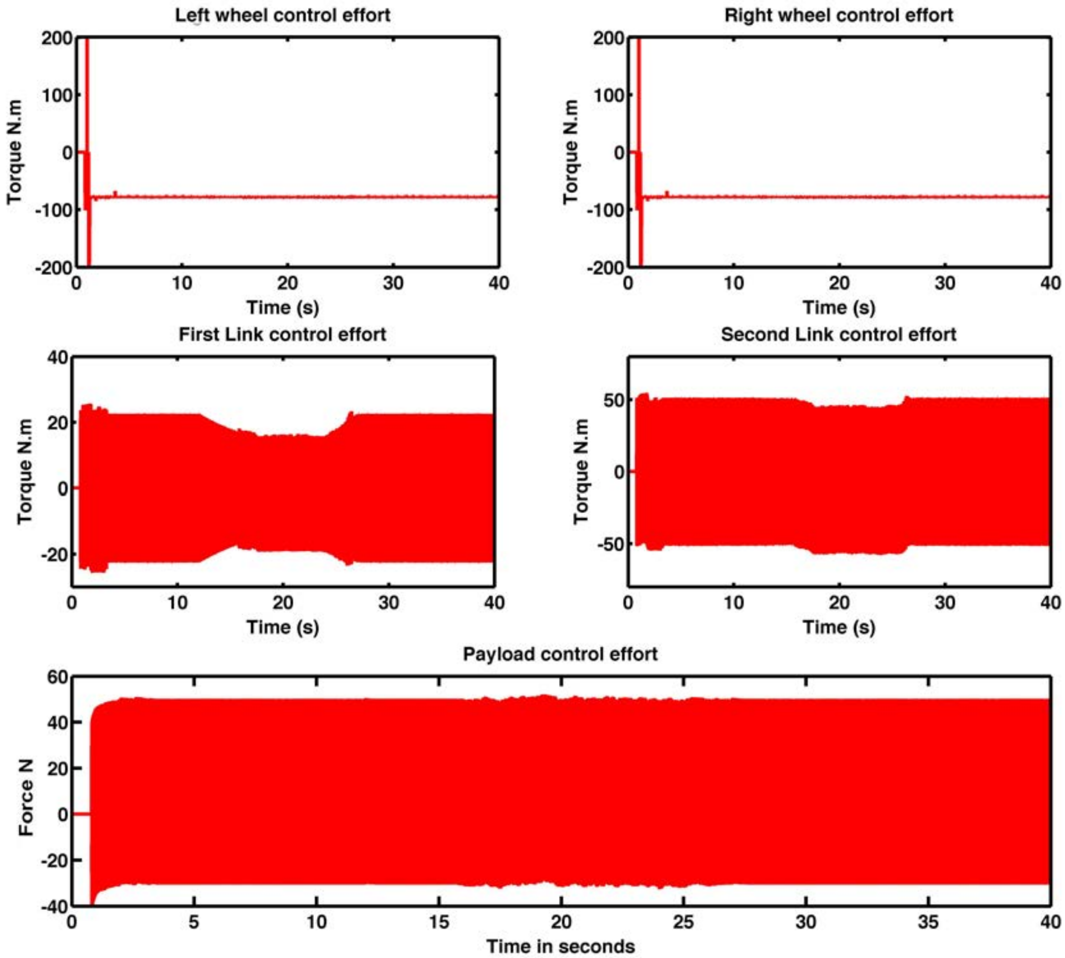

Figure 3.6: PID control effort for the vehicle on an inclined surface of 30 degrees

3.8 Hybrid fuzzy logic control of the vehicle moving on flat and inclined surfaces

The hybrid FLC, presented in chapter 2, is applied to the vehicle general model to stabilise the system and to analyse the overall behaviour of the system. The main aim is to control and stabilise the vehicle with sufficient control effort yet without using excessive amount of energy. At this stage, the hybrid FLC parameters were tuned heuristically in order to test the system initial behaviour. The hybrid FLC parameters thus obtained are described in Table 3.3.

Table 3.3. Heuristically adjusted hybrid FLC controller gains

Feedback loop	**PID controller Gains**		
	K_P	K_I	K_D
Left wheel	2	-	2
Right wheel	2	-	2
First pendulum	10	-	10
Second pendulum	150	200	100
Linear actuator	10	-	2

The response of the system with the hybrid FLC strategy is illustrated in Figure 3.7. The initial conditions are $\delta_L = \delta_R$=0 , $\theta_1 = \theta_1$=0, and α = 0 It is noted that the hybrid FLC successfully stabilised the vehicle with significant reduction in oscillations as compared to the PID controlled system. The wheel displacements reached the desired position without any deviations from the set point; in this case the set-point was 0.7 m. The first link and second link tilt angles were at the upright position without any oscillations. The payload was lifted successfully to the desired height but with an undershoot at the start. This is attributed to the manual tuning of the controller parameters. Figure 3.8 presents the hybrid FLC control effort exerted to stabilise the vehicle system on flat surface. As noted the control effort were significantly reduced compared to the PID control strategy. A significant reduction in the exerted torques can be clearly observed at the first and second link controller efforts. This is due to the smaller control parameters and scaling factors used in the control loops of the FLC controlled system. The overall response of the system with the hybrid FLC controller was obviously better than with the PID control strategy due to the aforementioned observations.

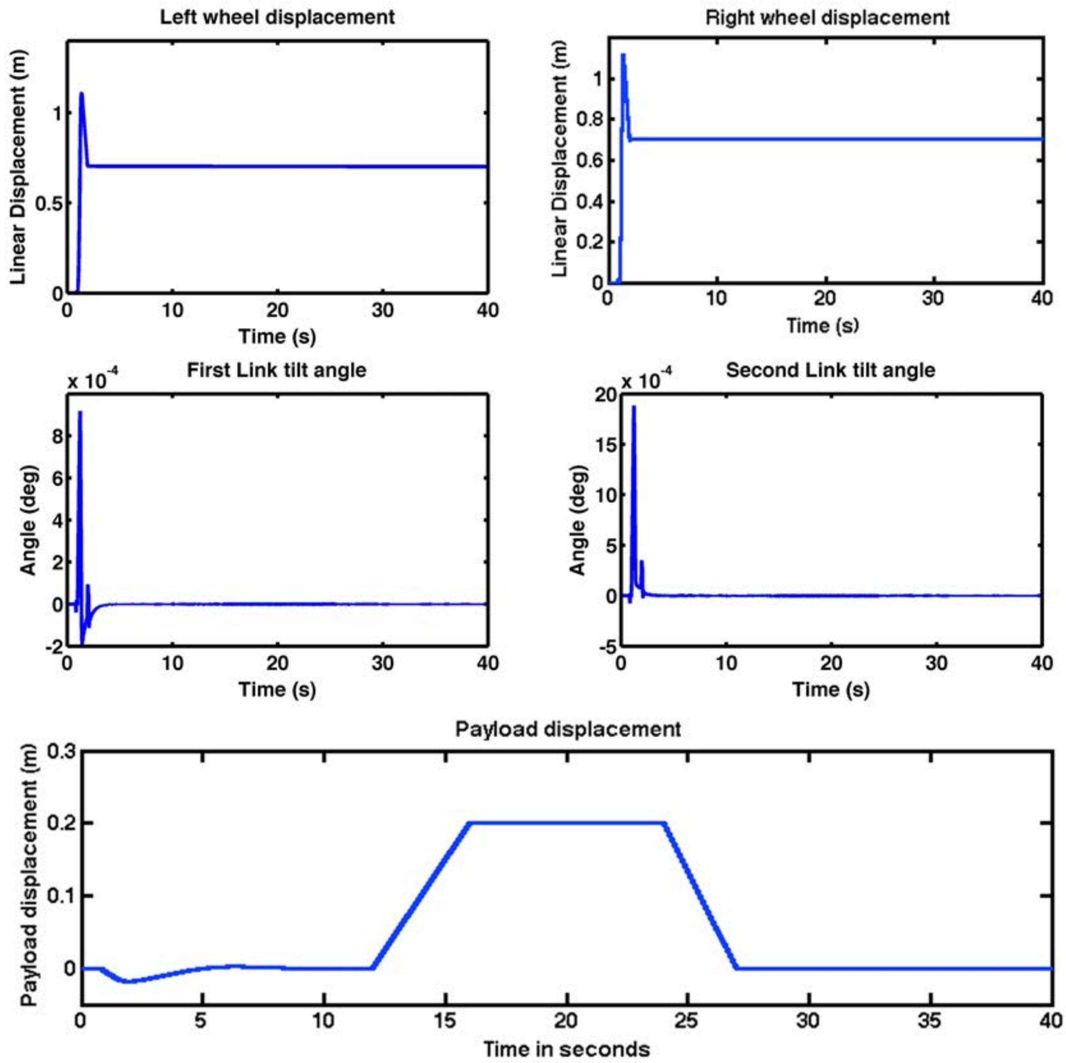

Figure 3.7: Controlled system response using hybrid FLC approach

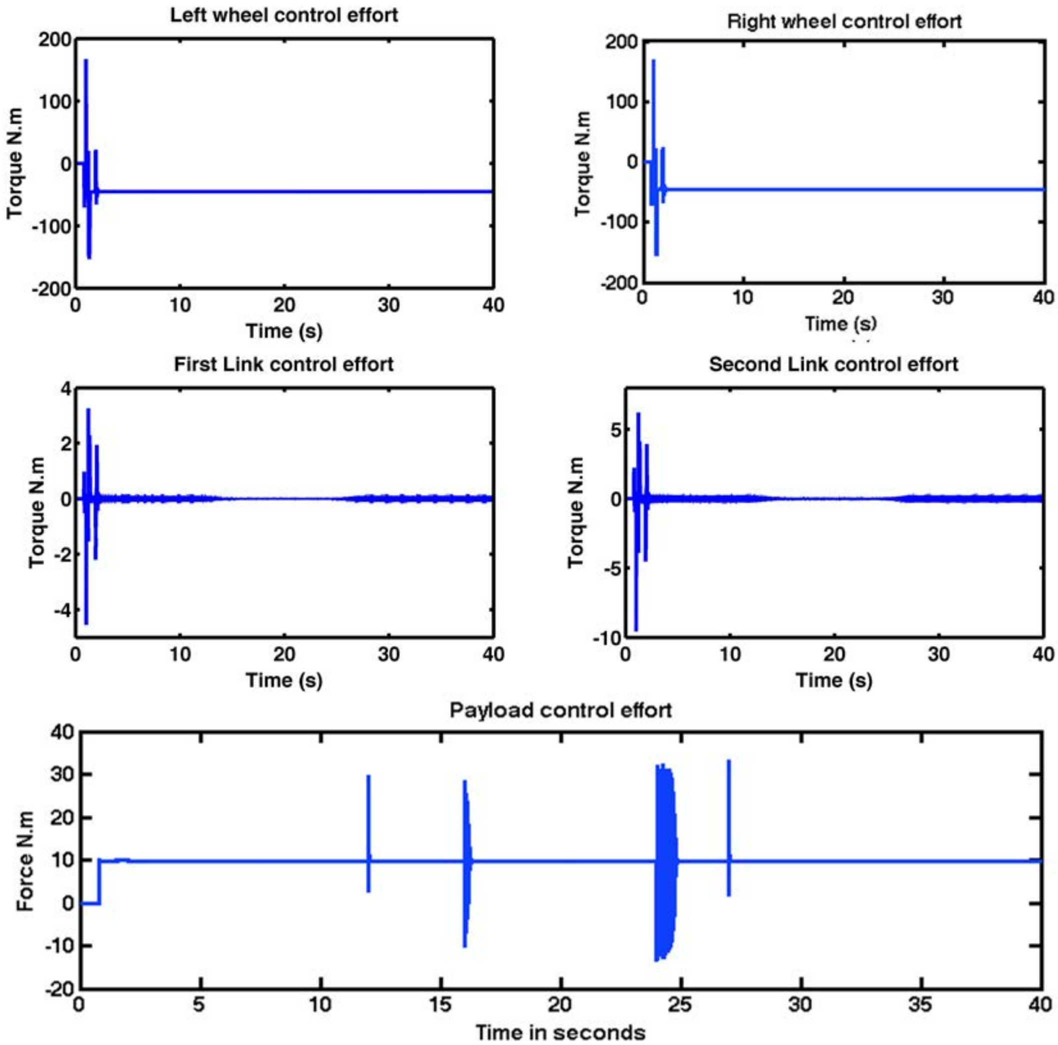

Figure 3.8: Hybrid FLC control effort to stabilise the system

To evaluate the performance of the hybrid FLC in controlling the vehicle while moving on inclined planes, the system was simulated with different inclination angles. In a similar approach as with the PID controller in sections 3.6, the surface inclination angle values used were α = 0^{o}, 10^{o} and 30^{o}. Figure 3.9 and Figure 3.10 shows the hybrid FLC controlled system response with the associated control effort in Figure 3.11. The wheel displacements were affected by the increase in the inclination angles and that is noted by the increase in response overshoots. This is due to the higher torques exerted to stabilise the IB, as shown in Figure 3.11. Physically, the larger the inclination angle, the higher the torque is needed to move the vehicle and to stabilise the links in the upright position. Similarly, the first and second links were affected by the increase in the inclination angle but with a smooth steady state value with no fluctuations. While the payload actuator movement was not affected by the change in inclination angles.

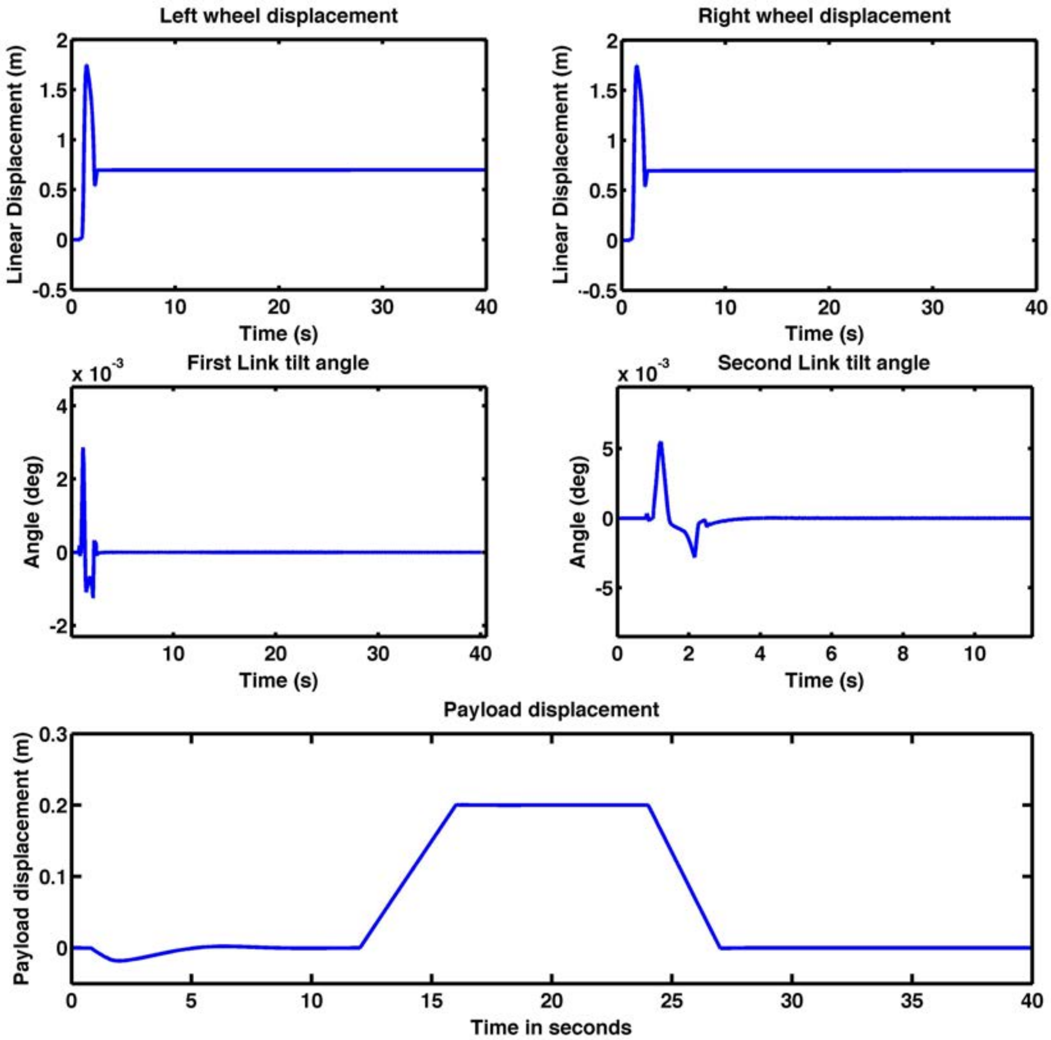

Figure 3.9: System response with hybrid FLC controller and inclined surface of 10 degrees

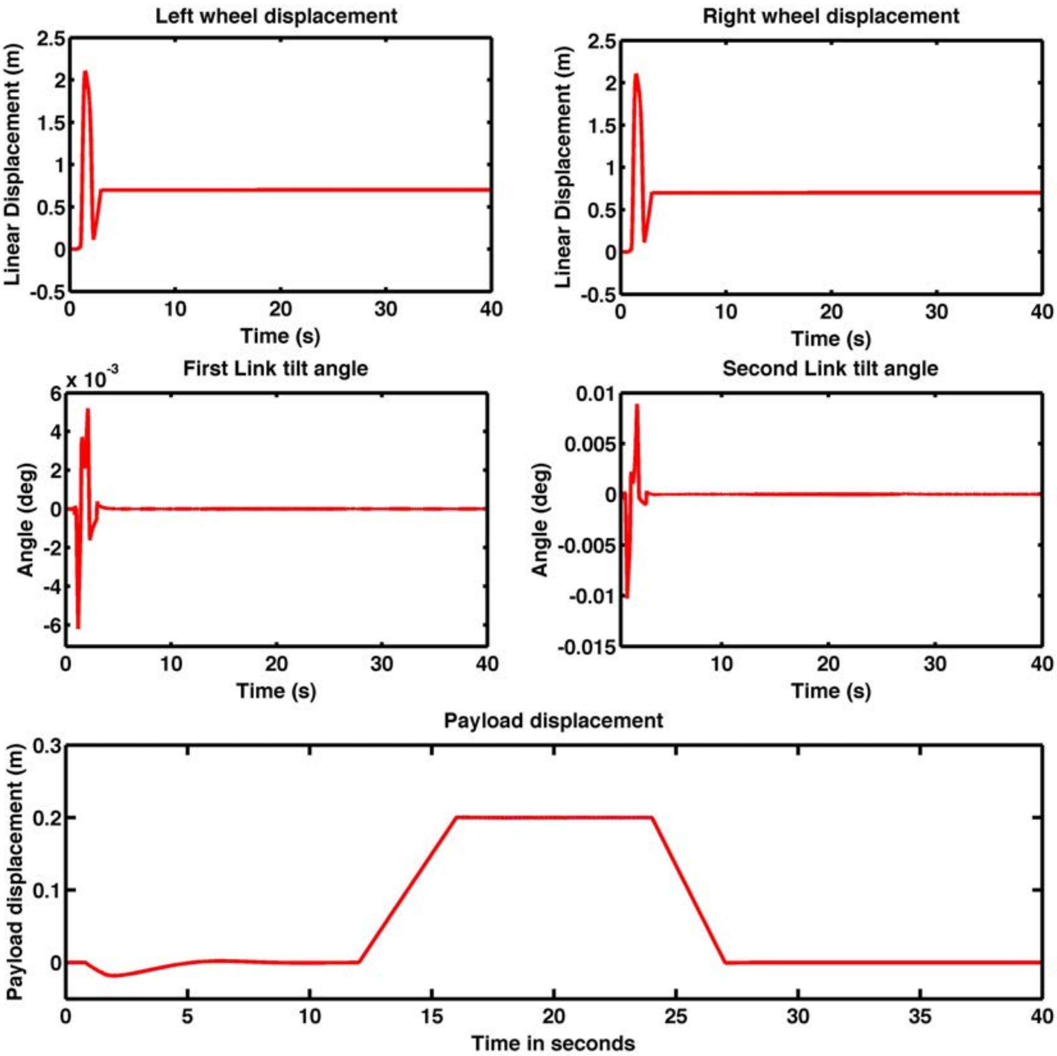

Figure 3.10: System response with hybrid FLC controller and inclined surface of 30 degrees

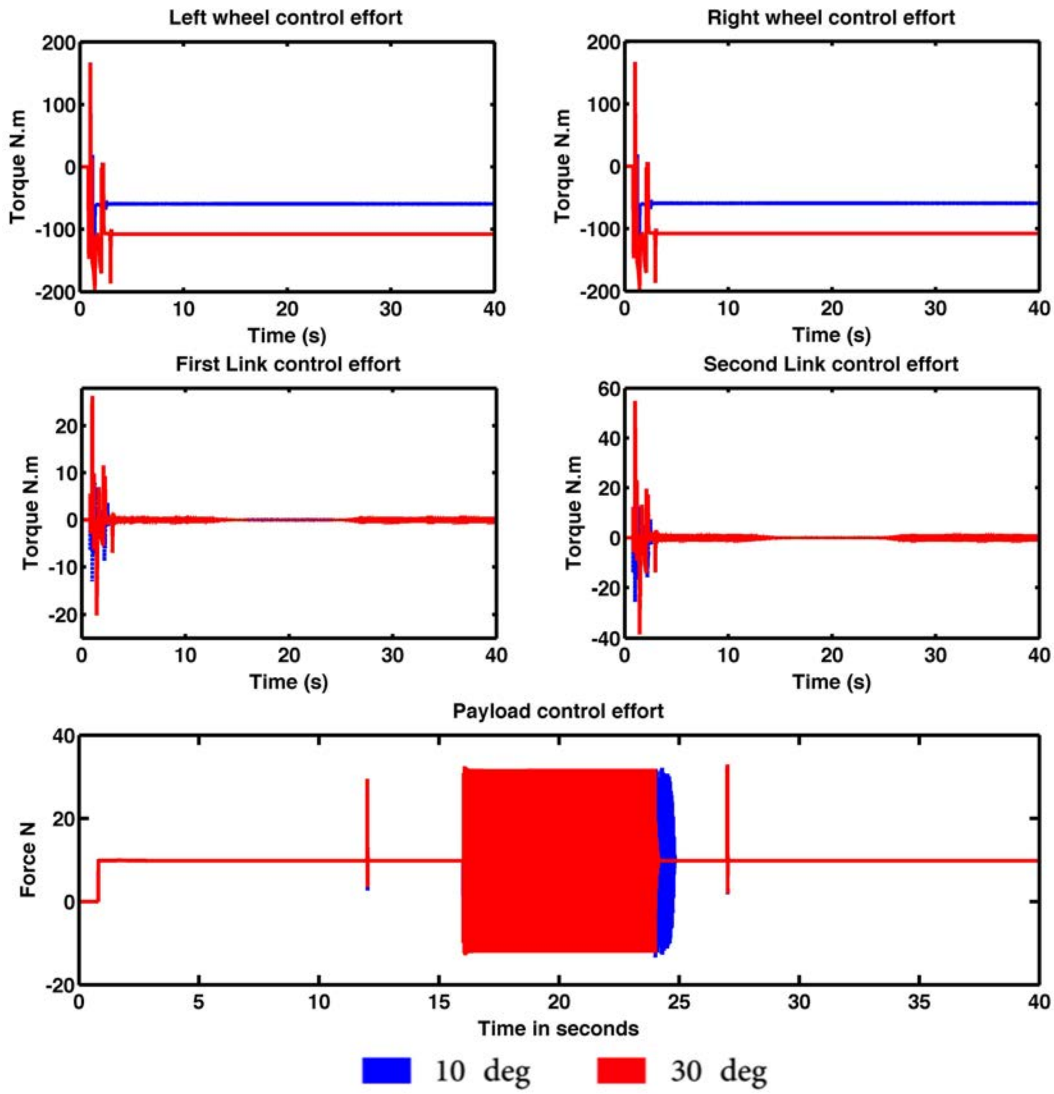

Figure 3.11: Hybrid FLC control effort for the vehicle on different inclination angles

Compared to the PID control strategy, the system response with hybrid FLC was far superior than the PID controlled system response. The improvements can be clearly observed in the elimination of the tilt angle fluctuations and the significant reduction in the control effort. Indeed, a proper tuning of the controller gains by minimising the mean squared error (MSE) would improve the system response and reduce the energy consumption of the overall system. These results encourage more investigation to simulate the vehicle model to move on complicated and irregular terrains and environments to mimic the real life movement scenarios. Different movement and various types of environments are demonstrated in the upcoming chapters of this thesis.

3.9 Summary

The general model of the vehicle that describes the vehicle dynamic behaviour in moving on different inclination angles has been derived. The Euler-Lagrange approach has been used to derive the dynamic equations of motion describing the proposed vehicle model. The model developed comprises five highly non-linear and coupled differential equations describing the vehicle model with five DOF. The general model will be adopted in this study because of its proven validity and inclusion of nonlinearities of the system. The model has been simulated using two control strategies, namely PID and hybrid FLC. The hybrid FLC control approach has proven to be effective in stabilising the system on different inclined surfaces whilst reducing the exerted control effort. The general model with hybrid FLC approach will be used in the upcoming analysis and different movement scenarios in this study.

Chapter 4
Hybrid spiral dynamic bacteria chemotaxis optimisation algorithm

4.1 Introduction

Using optimum control parameters is one of the utmost important design criteria. The optimum control gains improve the system response and reduce the energy consumption; thus leading to more efficient use of energy. In this chapter, a recently developed optimisation algorithm, named hybrid spiral dynamic bacterial chemotaxis (HSDBC) developed by (Nasir et al., 2012), is implemented to optimise the control system parameters. The HSDBC algorithm is a hybrid algorithm that combines the strengths of the original bacteria foraging algorithm (BFA) (Passino, 2002) and the Spiral Dynamic Algorithm (SDA) (Tamura and Yasuda, 2010). The HSDBC algorithm has been proven to be efficient when compared to BFA and SDA in terms of convergence speed and accuracy (Nasir et al., 2012). The HSDBC algorithm is applied for the first time in this research to a constrained optimisation problem via penalty functions and defining the boundaries of the feasibility region of the vehicle system.

In this chapter, a brief overview of the BFA and SDA algorithms is presented followed by a descriptive overview of the HSDBC algorithm. The BFA, SDA and HSDBC are integrated into the vehicle system to provide a comparative analysis and to find the optimum control parameters that minimise the mean square error (MSE) in system response and energy consumption. Simulations and analyses of the optimisation process are presented that show the efficiency of the optimised system.

4.2 Bacteria foraging optimisation algorithm

Bacterial foraging algorithm is a biologically inspired optimisation algorithm developed by (Passino, 2000; Passino, 2002). BFA optimisation is inspired by the foraging strategy of Escherichia Coli (E. Coli) bacteria that lives in human intestine. The optimisation process mimics the way that bacteria search for areas with high nutrient and avoid areas with toxins. The E. Coli uses a series of movements that enables it to swim and search for nutrients. Each E. Coli bacterium has a body and flagella that allows swimming and change in direction by tumbling.

As reported by Passino (2002), the bacteria swim continuously in the medium to search for high nutrient areas. If the area is noxious, the bacterium releases a repellent chemical substance and tumbles to get away from the noxious area. In neutral areas, where there are neither nutrients nor noxious substances, the bacterium continues tumbling more frequently to change the direction and search for better nutrient-rich areas. If the area has high nutrients, the bacterium continues swimming in the same direction and releases an attractant for other bacteria in the medium. The bacteria have an exponential growth rate that has motivated researchers to model it as an optimisation method. The bacteria with high fitness reproduce and bacteria with low fitness are eliminated in order to reach the high-nutrient mediums quickly and accurately.

These processes were modelled via a series of continuous processes defined as chemotaxis, swarming, reproduction, and elimination and dispersal events. Table 4.1 presents the nomenclature of the parameters that will be used in the optimisation pseudo code in the order they appear.

Table 4.1 BFA optimisation nomenclature

Parameter	Description
p	The dimension of the search space
S	Total number of bacteria in the population. S must be even.
Nc	Number of chemotactic steps of the bacterium lifetime between reproduction steps
Ns	Number of swims of bacterium in the same direction
Nre	Number of reproduction steps
p_{ed}	Probability of bacterium to be eliminated or dispersed
i=1,2,3,…S	Index of bacterium
j=1,2,3,…Nc	Index of chemotaxis
k=1,2,3,…Nre	Index of reproduction steps
l=1,2,3,…Ned	Index of elimination and dispersal events
m_s*=1,2,3,…Ns*	Index of the number of swims
J	The cost function value
C	Step size of tumble of bacterium

The BFA optimisation pseudo code developed by Passino (2002) is as follows:

1. Elimination and dispersal loop: for $l = 1,2,3,...,N_{ed}$ do $l = l+1$
2. Reproduction loop: for $k = 1,2,3,...,N_{re}$ do $k = k+1$
3. Chemotaxis loop: for $j = 1,2,3,...,N_c$ do $j = j+1$
    - **a.** For $i = 1,2,3,...,S$, take a chemotactic step for bacterium i as follows
    - **b.** Compute the nutrient media (cost function) value $J(i,j,k,l)$ as $J(i,j,k,l) = J(i,j,k,l) + J_{cc}(\theta^i(j,k,l),P(j,k,l))$ (i.e., add on the cell-to-cell attractant effect to the nutrient concentration). If there is no swarming effect then $J_{cc}(\theta^i(j,k,l),P(j,k,l))$ =0
    - **c.** Put $J_{last} = J(i,j,k,l)$ to save this value since a better cost via a run may be found.
    - **d.** Tumble: generate a random vector $\Delta(i) \in \Re^p$ with each element $\Delta_{m_p}(i), m_p = 1,2,3,...,\rho$ a random number in the range [-1,1]
    - **e.** Move: Let $\theta^i(j+1,k,l) = \theta^i(j,k,l) + C(i)\dfrac{\Delta(i)}{\sqrt{\Delta^T(i)\Delta(i)}}$ be the result in a step of size C(i) in the direction of the tumble of bacterium i
    - **f.** Compute the nutrient media (cost function) value $J(i,j+1,k,l)$, and calculate $J(i,j+1,k,l)$ = $J(i,j+1,k,l)$ + $J_{cc}(\theta^i(j+1,k,l),P(j+1,k,l))$. If

there is no swarming effect then $J_{cc}(\theta^i(j+1,k,l),P(j+1,k,l))=0$

g. Swim (note that we use an approximation since we decide behavior of each cell as if the bacteria numbered {1,2,…,*i*} have moved and {*i*+1,*i*+2, *i*+3, …,S} have not; this is much simpler to simulate than simultaneous decisions about swimming and tumbling by all bacteria at the same time):

i. Let $m_s = 0$ (counter for swim length)

ii. While $m_s < N_s$ (if have not climbed down too long)

1. Count $m_s = m_s + 1$

2. If $J(i,j+1,k,l) < J_{last}$ (if doing better), then $J_{last} = J(i,j+1,k,l)$ and calculate $\theta^i(j+1,k,l) = \theta^i(j,k,l) + C(i)\frac{\Delta(i)}{\sqrt{\Delta^T(i)\Delta(i)}}$ this results in a step of size C(i) in the direction of the tumble for bacterium *i*. Use this $\theta^i(j+1,k,l)$ to compute the new $J(i,j+1,k,l)$ as in step f above.

3. Else let $m = N_s$ (the end of the while statement)

h. Go to the next bacterium $(i+1)$ if $i \neq S$ (i.e. go to step b above) to process the next bacterium.

4. If $j < N_c$ go to step 3.

5. Reproduction:

a. For the given k and l, for each $i = 1,2,3,...,S$, let $J^i_{health} = \sum_{j=1}^{Nc+1} J(i,j,k,l)$ be the health of bacterium *i* (a measure of how many nutrients it got over its lifetime and how successful it was at avoiding noxious substances). Sort bacteria and chemotactic parameters C(i) in an ascending order since that higher cost means a lower health.

b. The S_r bacteria with the highest J_{health} values die and the other S_r bacteria with the best value splot (and the copies that were made are replaced at the same location as their parent)

6. If $k < N_{re}$ go to step 2.

7. Elimination-dispersal: for $i = 1,2,3,...,S$, eliminate and disperse each bacterium which has probability value less than p_{ed}. If one bacterium is eliminated then it is dispersed to random location of nutrient media. This mechanism makes computation simple and keeps the number of bacteria in the population constant

For m=1:S

If $p_{ed} > rand$ (generate random number for each bacterium and if the generated number is smaller than p_{ed} then eliminate/disperse the bacterium)

Generate new random positions for bacteria

Else

Bacteria keep their current position (not dispersed)

End

end

8. If $l < N_{ed}$ then go to step 1; otherwise end

4.3 Spiral dynamics optimisation algorithm

Spiral dynamic algorithm is a metaheuristic optimisation algorithm inspired by the spiral phenomena in nature, such as whirling current, developed by Tamura and Yasuda (2011). It is relatively new optimisation algorithm and was reported first for two dimensional search spaces (Tamura and Yasuda, 2010). Later, it was derived into a general model for n-dimension problems (Tamura and Yasuda, 2011). The common feature of logarithmic spirals motivated the authors in developing the algorithm, which they believed could make an effective search strategy. The algorithm was tested and compared with other proven search strategies, such as Particle Swarm Optimisation (PSO), and showed either a better or equal performance in terms of accuracy and speed of convergence (Tamura and Yasuda, 2011).

The algorithm is based on spiral search trajectories. One of the strong features of the algorithm is in the diversification and intensification at the early and later phases of the search trajectory. Diversification is to search for better solutions by searching in a wider area of the search space, while intensification is to search for better solutions by searching intensively around a good solution. Table 4.2 presents a description of parameters used in the SDA optimisation pseudo code.

Table 4.2. SDA optimisation nomenclature

Parameter	Description
θ	Rotation angle, $0 \le \theta \le 2\pi$
$k_{\max}$	Maximum iteration number.
r	Convergence rate of distance between a point and the origin, $0 \le r \le 1$
$R_{i,j}$	Rotation matrix between $x_i - x_j$ planes
m	Dimension of the search space

The rotation matrix for the n-dimension SDA algorithm is defined as

$$R^{n}{}_{i,j}(\theta_{i,j}) = \begin{array}{cc} & \begin{matrix} & & & i & & & & j & & & \end{matrix} \\ \begin{matrix} \\ \\ \\ i \\ \\ \\ \\ j \\ \\ \\ \\ \end{matrix} & \begin{bmatrix} 1 & & & & & & & & & & \\ & \ddots & & & & & & & & & \\ & & 1 & & & & & & & & \\ & & & \cos\theta_{i,j} & & \cdots & & -\sin\theta_{i,j} & & & \\ & & & & 1 & & & & & & \\ & & & \vdots & & \ddots & & \vdots & & & \\ & & & & & & 1 & & & & \\ & & & \sin\theta_{i,j} & & \cdots & & \cos\theta_{i,j} & & & \\ & & & & & & & & 1 & & \\ & & & & & & & & & \ddots & \\ & & & & & & & & & & 1 \end{bmatrix} \end{array}$$

The n-dimension spiral dynamic model is expressed using the rotational matrix as:

$$x_i(k+1) = S_n(r\ ,\theta)x_i(k) - (S_n(r,\theta) - I_n)x^*$$

where

$$S_n(r\ ,\theta)x(k) = \prod_{i=1}^{n-1}(\prod_{j=1}^{i} R^n_{n-i,n+1-j}(\theta_{n-i,n+1-j}))$$

The n-dimension SDA optimisation pseudo code reported by Tamura and Yasuda (2011) is as follows:

Step 0: Preparation Select the number of search points $m \geq 2$, parameters $0 \leq \theta < 2\pi$, $0 < r < 1$ of $S_n(r,\theta)$, and maximum number of iterations $k_{\max}$ Set $k = 0$.

Step 1: Initialization

Set initial points $x_i(0) \in R^n$, $i = 1,2,...m$ in the feasible region at random and centre x^* as $x^* = x_{i_g}(0)$, $i_g = \arg\min_i f(x_i(0))$, $i = 1,2,...,m$.

Step 2: Updating x_i

$$x_i(k+1) = S_n(r,\theta)x_i(k) - (S_n(r,\theta) - I_n)x^*$$

$$i = 1,2,...,m.$$

Step 3: Updating x^*

$x^* = x_{i_g}(k+1)$,

$i_g = \arg\min_i f(x_i(k+1))$, $i = 1,2,...,m$.

Step 4: Checking termination criterion

If $k = k_{\max}$ then terminate. Otherwise set $k = k+1$, and return to step 2.

4.4 Hybrid spiral dynamic bacteria chemotaxis optimisation algorithm

The HSDBC algorithm for global optimisation was developed by Nasir et al. (2012). The HSDBC algorithm is a hybridisation between the Spiral Dynamics Algorithm (SDA) developed by Tamura et al. (2011) and the Bacterial Foraging Algorithm (BFA) algorithm developed by Passino et al. (2002). The BFA algorithm has faster convergence speed to feasible solutions in the defined search space but suffers from oscillations toward the end of the search operation. The SDA algorithm has a faster computation time and a better accuracy than the BFA algorithm. Furthermore, the SDA algorithm has better stability, due to the spiral steps, when searching toward the optimum point. The HSDBC algorithm combines the strengths of BFA and SDA into a faster, stable and accurate global optimisation algorithm. This is achieved by incorporating the BFA chemotaxis part into the SDA and thus reducing the computational time and retaining the strength and performance of the SDA. Table 4.3 shows description of variables used in HSDBC algorithm.

Table 4.3: Nomenclature associated with HSDBC algorithm

Parameter	Description
θ_{tumble}	Bacteria angular displacement on $x_i - x_j$ plane around the origin for tumbling.
θ_{swim}	Bacteria angular displacement on $x_i - x_j$ plane around the origin for swimming.
r_{tumble}	Spiral radius from bacteria tumble.
r_{swim}	Spiral radius for bacteria swim.
m	Number of search points.
$k_{\max}$	Maximum iteration number.
N_{sw}	Maximum number of swim.
$x_i(k)$	Bacteria position.
R^n	n x n matrix.

The HSDBC optimisation pseudo code is as follows:

Step 0: Preparation

Select the number of search points (bacteria) $m \geq 2$, parameters $0 \leq \theta_{tumble}, \theta_{swim} < 2\pi, 0 < r_{tumble}, r_{swim} < 1$ of $S_n(r,\theta)$, maximum iteration number, $k_{\max}$ and maximum number of swim, N_s for bacteria chemotaxis. Set $k = 0, s = 0$.

Step 1: Initialization

Set initial points $x_i(0) \in R^n, i = 1,2,...m$ in the feasible region at random and center x^* as

$x^* = x_{i_g}(0)$, $i_g = \arg\min_i f(x_i(0))$, $i = 1,2,...,m$.

Step 2: Applying bacteria chemotaxis

i. Bacteria tumble

(a)Update x_i

$$x_i(k+1) = S_n(r_{tumble}, \theta_{tumble})x_i(k) - (S_n(r_{tumble}, \theta_{swim}) - I_n)x^*$$

$i = 1,2,...,m$.

ii. Bacteria swim

(a) Check number swim for bacteria i.

If $s < N_s$, then check fitness,

Otherwise set $i = i+1$, and return to step (i).

(b) Check fitness

1. If $f(x_i(k+1)) < f(x_i(k)$, then go to step (c) to update x_i,

Otherwise set $s = N_s$, and return to step (i).

(c) Update x_i

$$x_i(k+1) = S_n(r_{swim}, \theta_{swim})x_i(k) - (S_n(r_{swim}, \theta_{swim}) - I_n)x^*$$

$i = 1,2,...,m$.

Step 3: Updating x^*

$x^* = x_{i_g}(k+1)$,

$i_g = \arg\min_i f(x_i(k+1))$, $i = 1,2,...,m$.

Step 4: Checking termination criterion

If $k = k_{\max}$ then terminate. Otherwise set $k = k+1$, and return to step 2.

Figure 4.1 illustrates a flowchart of the HSDBC optimisation algorithm reported by Nasir et al. (2012).

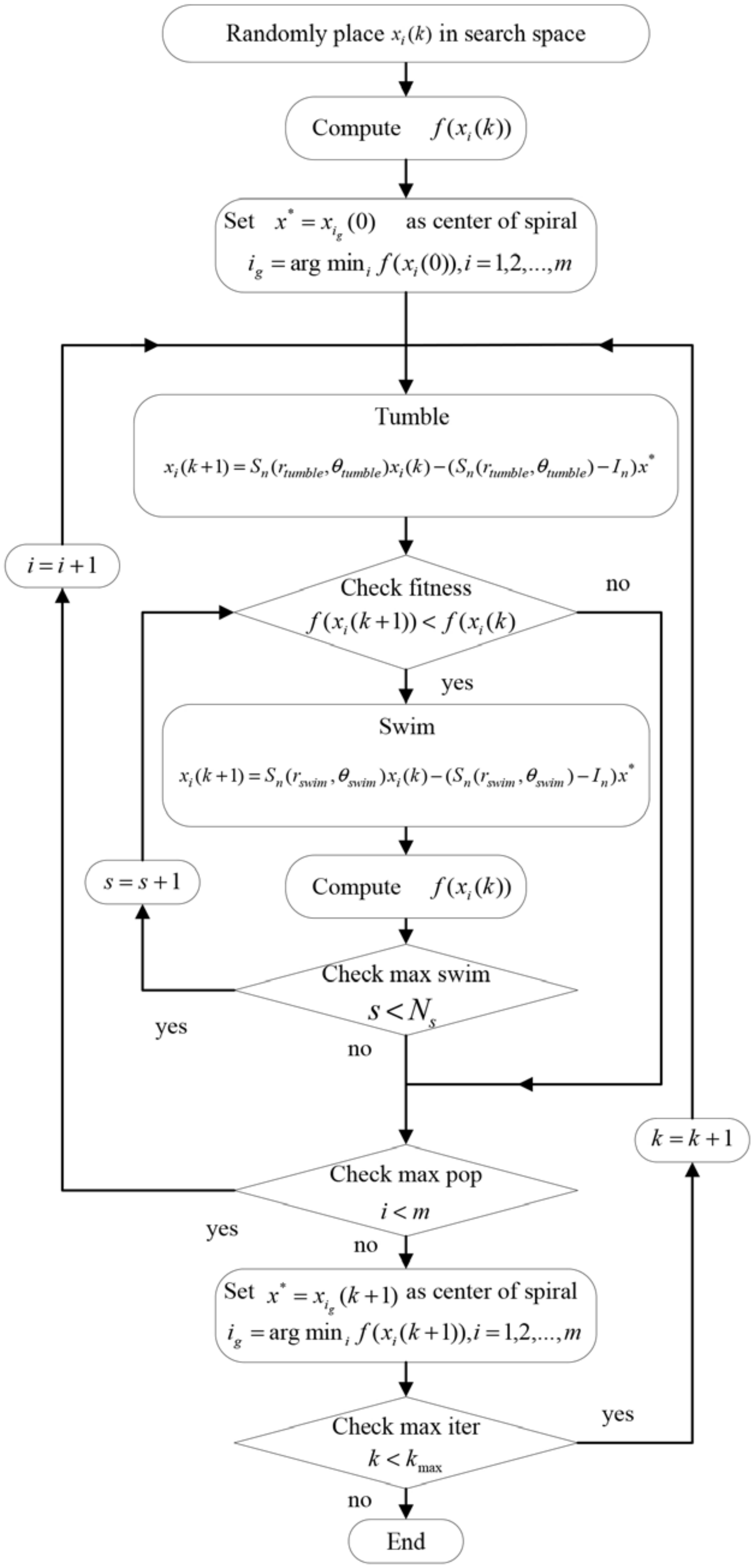

Figure 4.1: Flowchart of the HSDBC algorithm (Nasir et al.,2012)

In Figure 4.2, the control system block diagram of the vehicle is illustrated. The system consists of five hybrid PD+I FLC controllers, each with 3 parameters, with a total of 15 parameters.

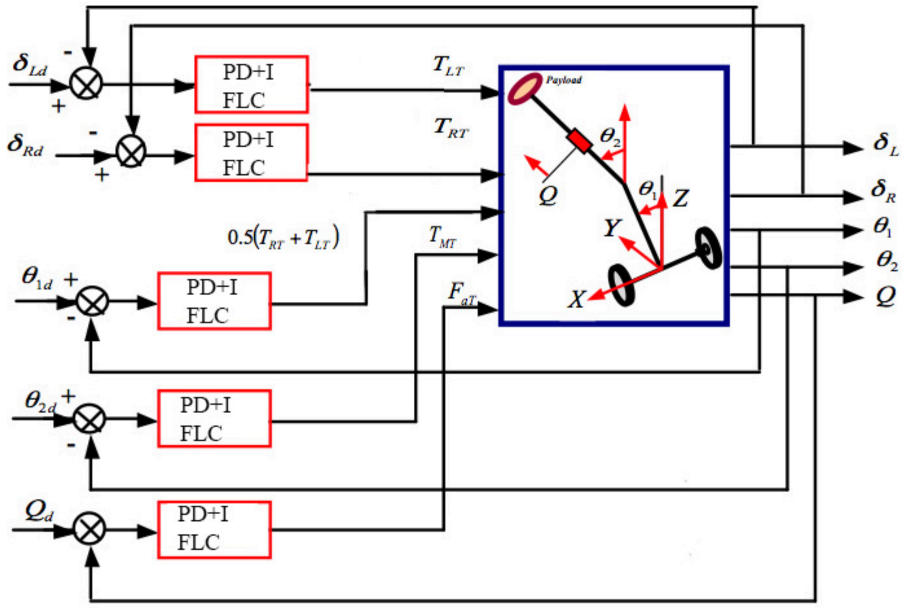

Figure 4.2: Block diagram of the vehicle control system

Three optimisation algorithms namely BFA,SDA and HSDBC will be applied to the system to analyse its behaviour and to find the optimal solution within a shortest time.

The performance index of the system is chosen as the minimum mean squared error (MSE) of system response. The MSE is calculated for each control loop in the system as follows:

$$MSE\ 1 = \min\left\{\frac{1}{N}\sum_{i=1}^{N}(\delta_{Ld}-\delta_{Lm})^2\right\} \tag{4.1}$$

$$MSE\ 2 = \min\left\{\frac{1}{N}\sum_{i=1}^{N}(\delta_{Rd}-\delta_{Rm})^2\right\} \tag{4.2}$$

$$MSE\ 3 = \min\left\{\frac{1}{N}\sum_{i=1}^{N}(\theta_{1d} - \theta_{1m})^2\right\} \tag{4.3}$$

$$MSE\ 4 = \min\left\{\frac{1}{N}\sum_{i=1}^{N}(\theta_{2d} - \theta_{2m})^2\right\} \tag{4.4}$$

$$MSE\ 5 = \min\left\{\frac{1}{N}\sum_{i=1}^{N}(Q_{d} - Q_{m})^2\right\} \tag{4.5}$$

The objective function is chosen as the summation of the MSE of the system that can be expressed as the summation of equations (4.1) – (4.5)

$$J = MSE_1 + MSE_2 + MSE_3 + MSE_4 + MSE_5 \tag{4.6}$$

Hence; minimizing the objective function J will result in finding the optimum control parameters with the minimum mean square error of the overall system response

In order to restrict the optimisation algorithms to search within the feasibility region of the system, which is the stability region of the vehicle, system constraints must be defined to ensure stability. The following section formulates the constrained optimisation problem.

4.5 HSDBC constrained optimisation

With the complexity of the model, slight changes in the control gains results in oscillations in the system response and may lead the vehicle into instability. Constrained optimisation is used to avoid the occurrence of this issue while searching for optimum parameters. The optimization process will be constrained within the stability region of the system. This is achieved by defining a feasible interval for each control parameter; shown in Table 4.4, that assures the stability of the system. These boundaries were defined by trial and error and examination of the system maximum stability limits.

Table 4.4: Boundary limits of the controller gain parameters

Boundaries	Loop 1			Loop 2			Loop 3			Loop 4			Loop 5		
	Kp	**Kd**	**Ki**	**Kp**	**Kd**	**Ki**	**Kp**	**Kd**	**Ki**	**Kp**	**Kd**	**Ki**	**Kp**	**Kd**	**Ki**
Lower	1.5	0.5	0.9	5	2.5	1.5	8	7.5	0	8	5	0	30	10	1
Upper	2.4	1	1.4	6.5	4	2	12	9	0.5	10	8	0.5	50	20	10

Many techniques exist to solve constrained optimisation problems these include penalty methods and Lagrange multipliers (Snyman, 2005). Penalty methods are used to convert the constrained optimisation problem into an unconstrained problem by adding a penalty function P(x) to the objective function when the constraint is violated. The cost function of the system can be rewritten as:

$$J(x) = \begin{cases} J(x) & x \in feasible \;\; region \\ J(x) + P(x) & x \notin feasible \;\; region \end{cases}$$

Where J(x) represents the cost function and P(x) represents the penalty function. The penalty function is added to the cost function to result in a very high cost whenever a constraint is violated. Thus; eliminating the solution from the feasible solutions when selecting the minimum cost value in a minimisation problem. A proper selection of P(x) is important to guarantee a feasible solution to the constrained optimisation problem.

In the work, the penalty function is defined as ten times the cost function of the unfeasible region and zero otherwise. This can be expressed as:

$$P(x) = \begin{cases} 0 & x \in feasible \;\; region \\ 10\,.\,J(x) & x \notin feasible \;\; region \end{cases}$$

4.6 Simulations and results

The simulation scenario presented in this section allows comparison of the performance of the HSDBC with other similar optimization algorithms and finding the most accurate and efficient control parameters of the system. Tables (4.5) – (4.7) provide the simulation parameters used for BFA, SDA and HSDBC algorithms respectively.

Table 4.5: BFA parameters

P	**S**	**Nc**	**Ns**	**Nre**	**Ned**	**Ped**	**Sr**
15	20	14	6	2	2	0.25	S/2

Table 4.6: SDA parameters

P	**R**	**Theta**	**Initial points**	**Iterations**
15	0.95	$\pi / 4$	10	150

Table 4.7: HSDBC parameters

P	**R**	**Rzw**	**Ns**	**Theta**	**Initial points**	**Iterations**
15	0.95	0.55	2	$\pi / 4$	10	150

Using the optimisation algorithms, the optimized control parameters shown in Table 4.8 were obtained. Table 4.9 shows the corresponding minimum cost function calculated by each optimization algorithm. It is noted that the HSDBC algorithm found the minimum cost function value of 0.3682

The system is simulated with the payload actuator lifted to 0.2 m and on an inclined plane of 5 degrees as shown in Figure 4.3 to demonstrate the reduction in the exerted control effort. Figure 4.4 presents the system response based on the optimized control parameters obtained by the three algorithms in comparison to the manually tuned control parameters. The convergence plot of the cost function for each of the optimisation algorithms is illustrated in Figure 4.5.

Table 4.8: Optimized controller gains

	Parameter	BFA	SD	HSDBC
Loop 1	Kp_1	2.0729	2.3452	2.1566
	Kd_1	0.8572	0.8714	0.8095
	Ki_1	1.3925	1.2778	1.2026
Loop 2	Kp_2	6.0155	5.1504	5.1530
	Kd_2	2.8185	3.1264	2.6917
	Ki_2	1.6390	1.9794	1.8754
Loop 3	Kp_3	8.7514	11.3330	11.4514
	Kd_3	8.1889	8.3229	8.9946
	Ki_3	0.2449	0.2731	0.3771
Loop 4	Kp_4	8.9718	9.8522	9.9903
	Kd_4	5.1315	6.7829	6.6239
	Ki_4	0.0071	0.0532	0.0410
Loop 5	Kp_5	49.9646	36.5230	36.6753
	Kd_5	13.6834	14.2519	14.3583
	Ki_5	4.0408	5.3567	5.4203

Table 4.9**:** minimum cost function of the system calculated by the algorithms

Minimum Cost function value	BFA	SDA	HSDBC
J	0.3684	0.3685	0.3682

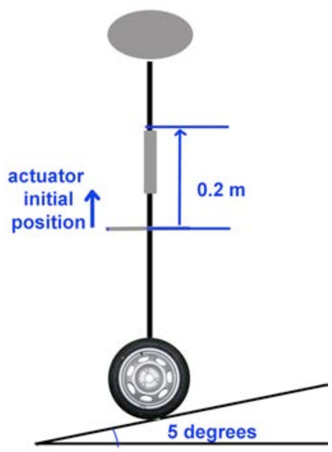

Figure 4.3 Schematic diagram of the vehicle on an inclined plane

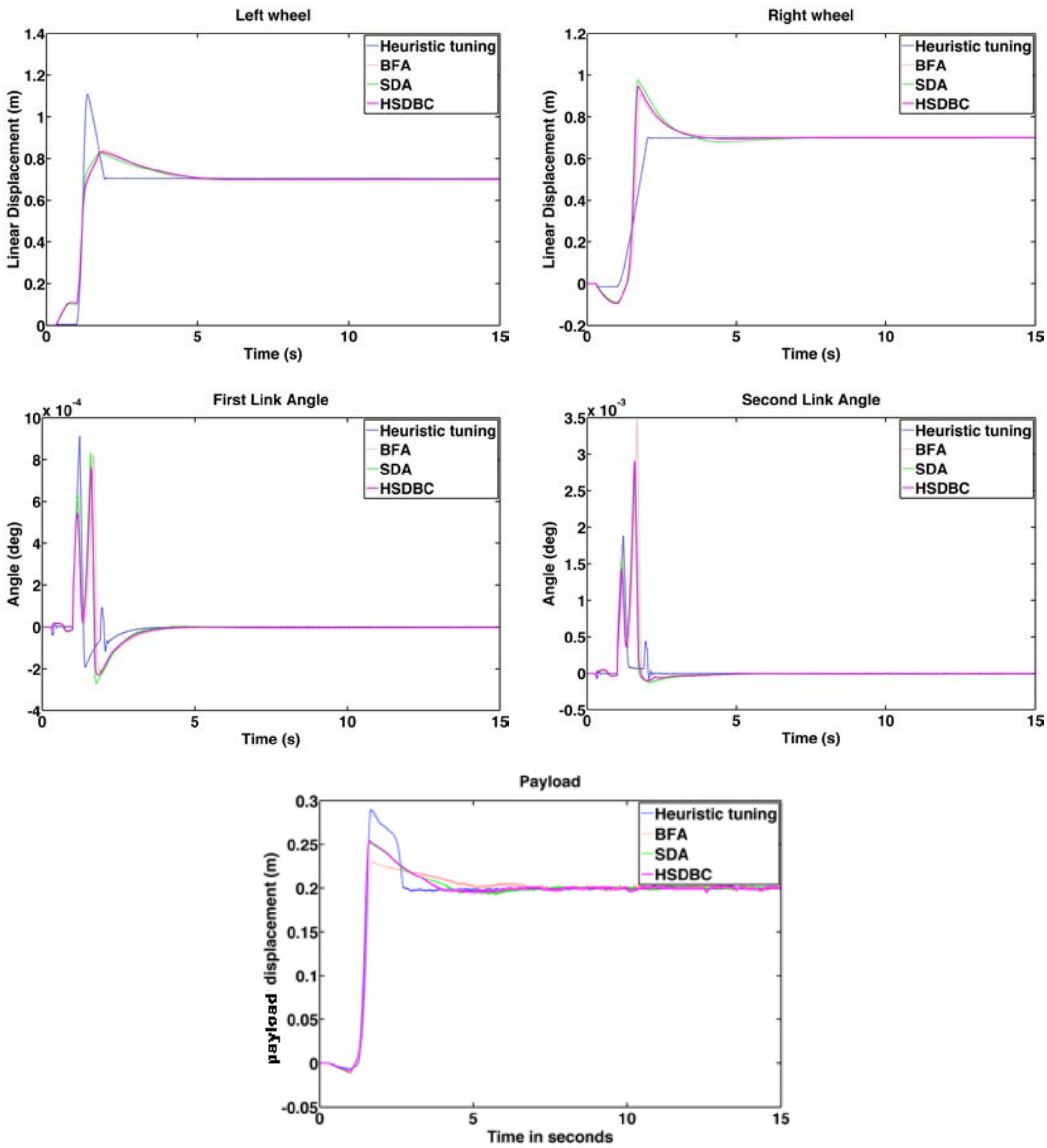

Figure 4.4: Vehicle system response with optimised sets of control parameters found by BFA,SDA and HSDBC

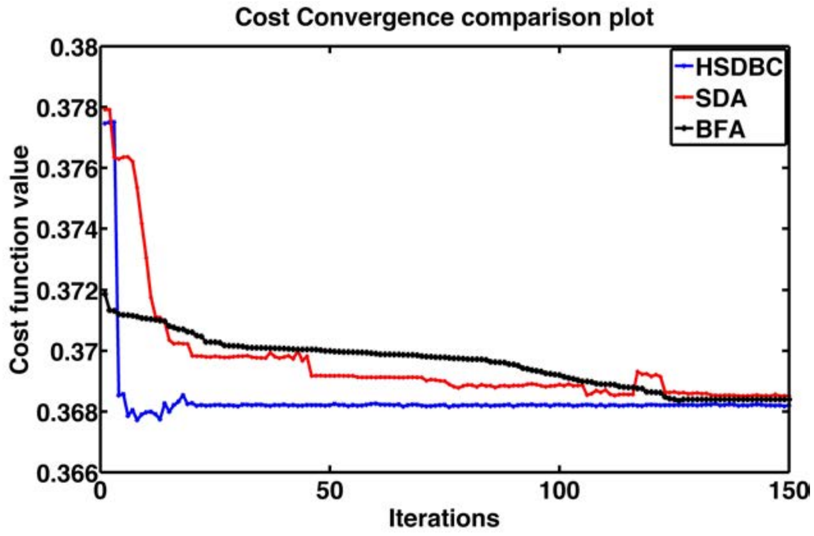

Figure 4.5: Cost function convergence plot for BFA, SDA and HSDBC algorithms

It can be noted that BFA, SDA and HSDBC performed similar in respect of system response by finding stable solutions, lowering the overshoots and improved steady-state error. However, HSDBC algorithm had a superior performance in minimizing the percentage overshoot and the settling time for the linear displacement of the left and right wheel and the tilt angles of the two links. Furthermore, HSDBC-optimized controller parameters clearly improved the settling time of the payload actuator displacement as depicted.

Referring to Figure 4.5, the HSDBC algorithm cost function converged to the minimum value within approximately 25 iterations. While, the BFA and SDA algorithms needed more iterations to settle into their best-found minimum values. HSDBC successfully found the minimum cost function and proved its speed in convergence. Figure 4.6 shows the exerted control effort. The control effort were minimised by the implementation of HSDBC algorithm for the left and right wheels, and the payload linear actuator. While on the first and second link tilt angles the reduction was almost similar among the optimisation algorithms. In general, the

HSDBC-optimised parameters resulted in a better system response and better, or almost equal, exerted control effort. The HSDBC optimised parameters will be used as the primary control parameters for the system in further simulation scenarios in this study.

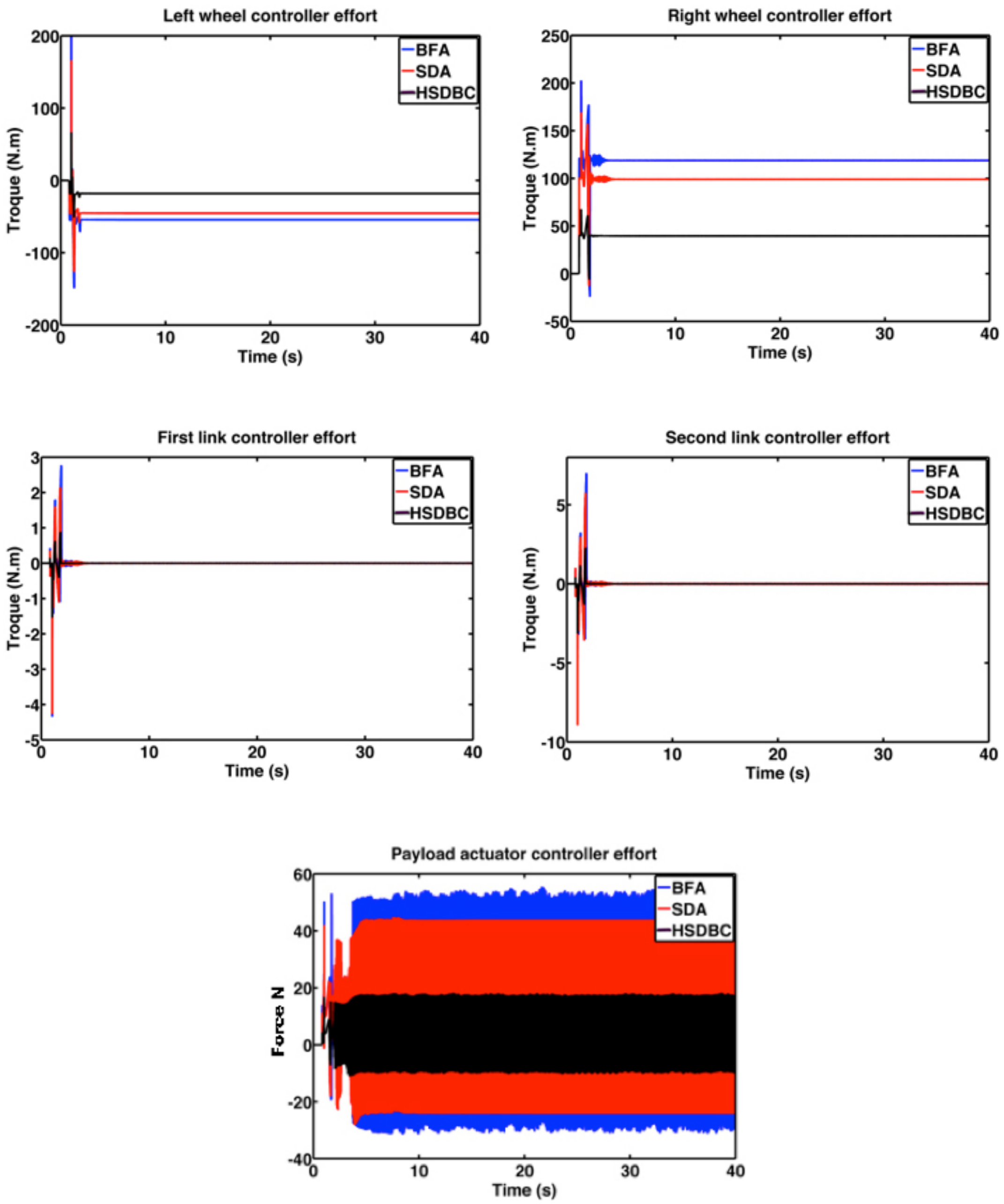

Figure 4.6: Control effort of the system with different optimised controllers

4.7 Summary

Optimisation of the vehicle control system parameters has been presented in this chapter. Various optimisation algorithms were applied to the control system including BFA, SDA and HSDBC algorithms. The system was simulated with each algorithm and results were obtained for comparative assessment of the cost function values and speed of convergence. The optimised sets of parameters obtained by each algorithm were implemented in the system to study the system performance. The HSDBC algorithm was proven to be efficient in finding the parameters that result in the minimum mean squared error of the system. Moreover, the HSDBC has resulted in a good reduction of the exerted control effort of the system.

Chapter 5

Control robustness and disturbance rejection analysis

5.1 Introduction

This chapter critically examines the robustness of the hybrid FLC approach and the ability to cope with various disturbances. Different disturbance forces with various amplitudes and durations are applied to the pendulum links of the vehicle while monitoring the system response and the exerted control effort. With such rigorous analysis, the controller robustness can be validated and demonstrated to ensure the ability of the vehicle to cope with different environments and movement scenarios.

While the main objective of controlling the vehicle is to stabilise it, the vehicle intermediate body is the most critical component of the system. This is because it has the payload, first and second pendulum links that are not stable by nature and are very sensitive to disturbances. The controller must guarantee stability of the system at different environments that may have frictional elements or even with directly applied disturbances to the vehicle. The study of directly applied disturbance forces is presented in this chapter. While in later chapters, further real-life inspired movement scenarios are presented to prove the robustness of the controller.

5.2 Robustness analysis approach

The robustness analysis will be divided into two main parts. The first part is concerned with applying disturbance forces of different amplitudes to each pendulum link. While in the second part, the system will be perturbed with disturbance forces of different durations applied to each pendulum link. The disturbance forces applied are simulated pulse signals of various amplitudes and durations. Forces will be applied at the centre of each of pendulum link. At each simulation, the response of the system will be presented along with the associated control effort for each system component. Furthermore, the system response characteristics are presented using data analysis chart of 100% stacked lines type. The recorded numerical values of the system characteristics for each simulation are provided in Appendix C.

5.3 Disturbances with varying amplitudes

A predefined train of pulses is applied as disturbing forces on the vehicle components. The pulse characteristics are presented in Table 5.1.

Table 5.1: Disturbance force characteristics with various amplitudes

Pulse amplitude	40 N / 80 N / 160 N / 300 N
Phase delay	10 seconds
Period	25 seconds
Pulse duration	0.5 second

5.3.1 Disturbances with different amplitudes applied on the left wheel

The response of the system undergoing a disturbance force applied on the left wheel is presented in Figures 5.1-5.3 and the associated numerical values are provided in Table C1.1. The disturbances produced positive peaks at the displacement of the left wheel that would skid the cart from the desired path. This explains the oscillations appearing at the tilt angle of the first link and the fluctuations at the displacement of the right wheel. The larger the applied disturbance the larger the peak amplitude in the response. A maximum peak increase of approximately 300% over the set point was noted at the maximum applied disturbance. The settling time had a slight increase of 4.3% at the maximum disturbance. While the rise time had insignificant increase of

0.2% at maximum disturbance. The controller stabilised the system within approximately 3 seconds. The tilt angle of the second link and the displacement of the payload actuator remained unaffected by this disturbance.

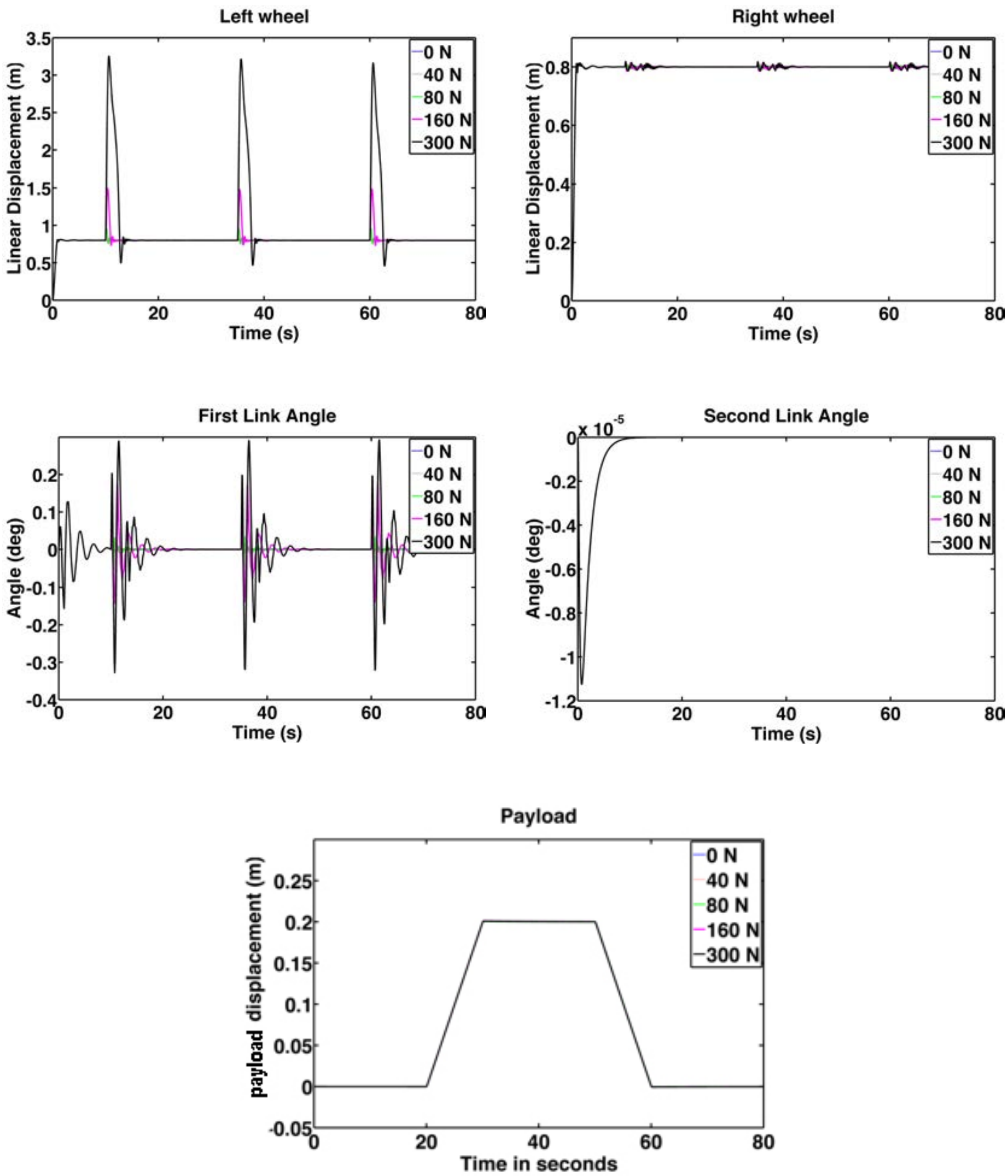

Figure 5.1: System performance with disturbances applied on the left wheel

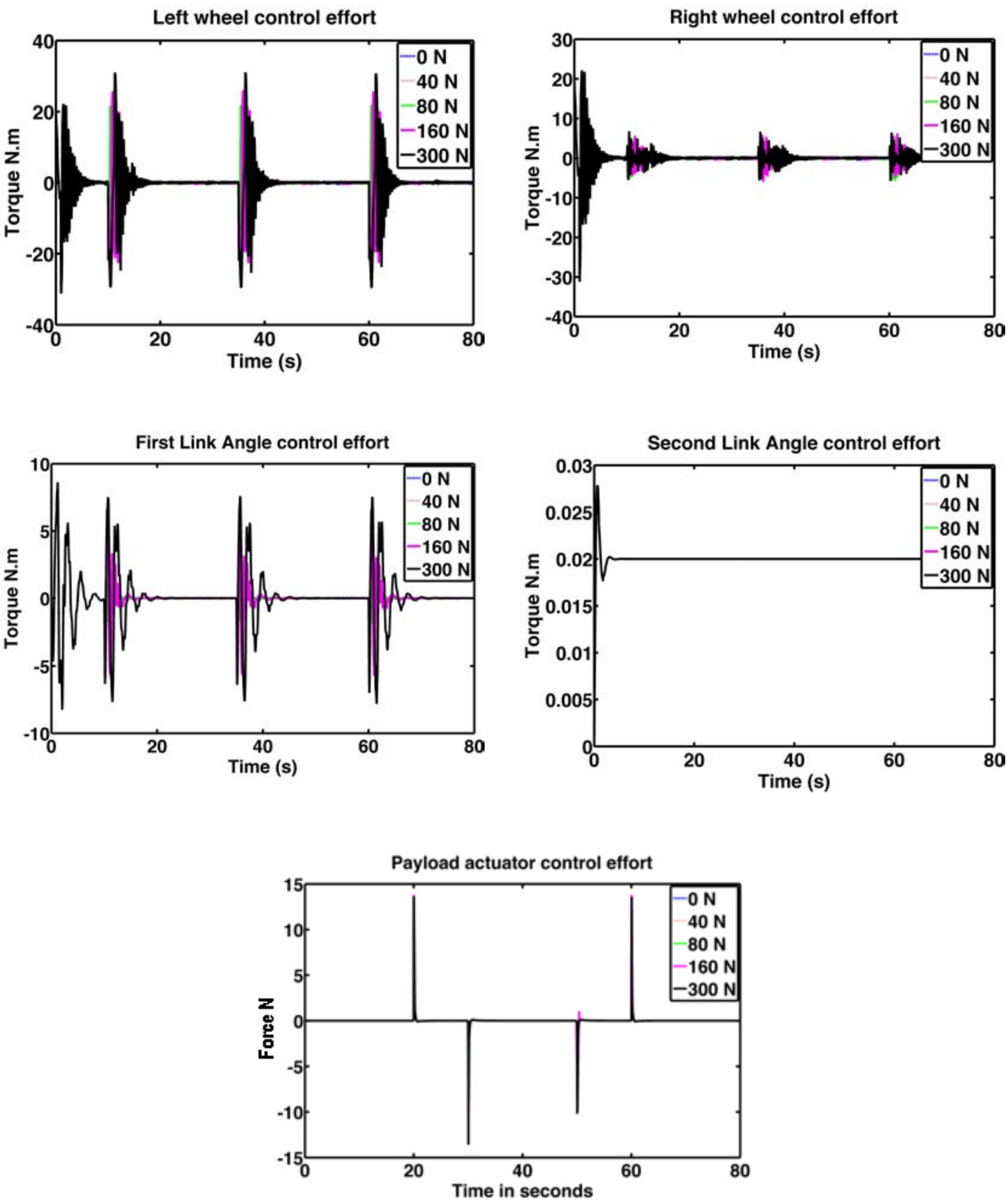

Figure 5.2: Control effort with disturbance applied on the left wheel

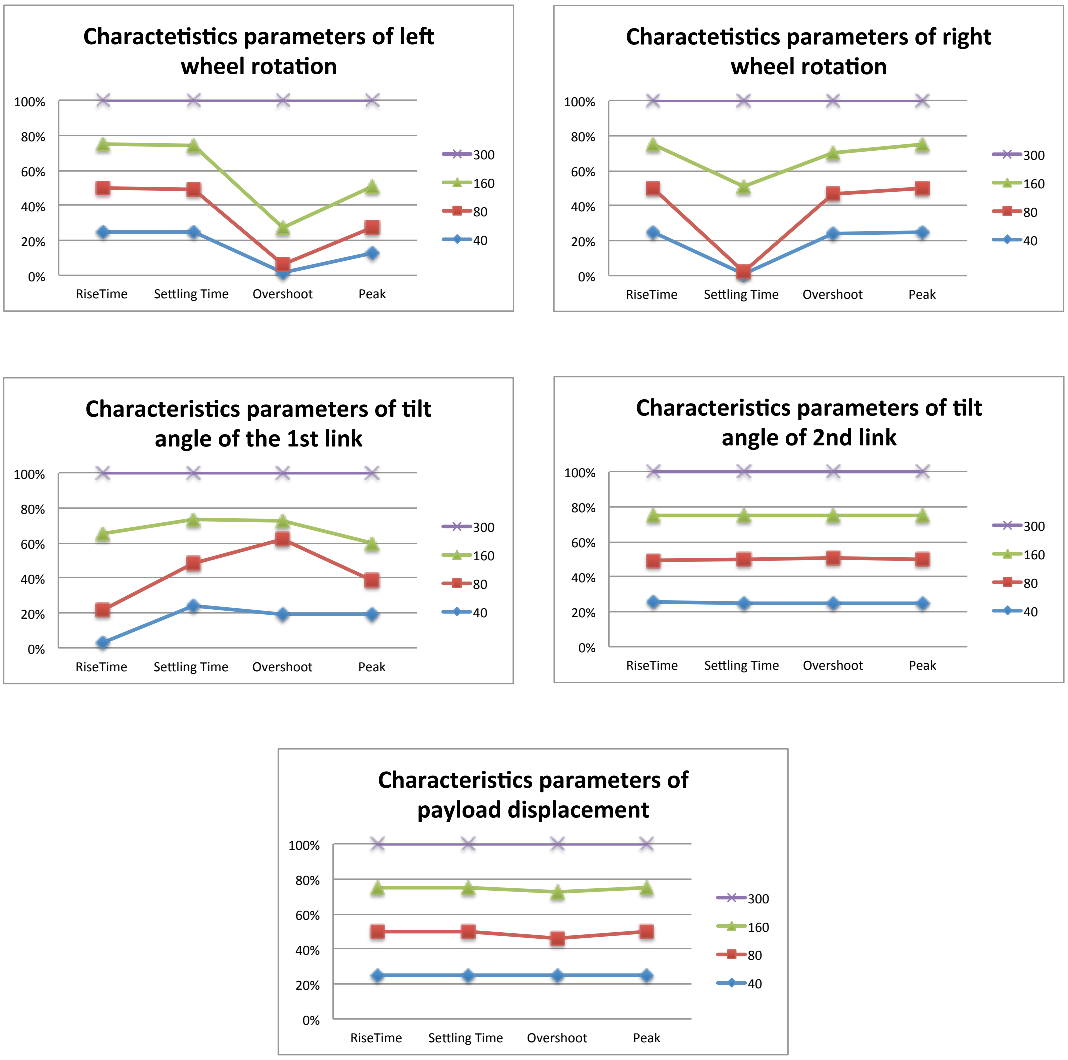

Figure 5.3: Graphical analysis of system performance characteristics
with disturbances applied on the left wheel

5.3.2 Disturbances with different amplitudes applied on the right wheel

As it was assumed, at this stage of research, that the vehicle was constrained to move on a straight line, the inputs to both wheel motors were exactly the same. As a result of this assumption, the response of the system undergoing disturbances applied on the right wheel motor was exactly similar to the response of the left wheel motor. This explains the consistency in the system response to the disturbances applied on both wheels. Figures 5.4-5.6 and Table C1.2 present the system response and the corresponding numerical values respectively.

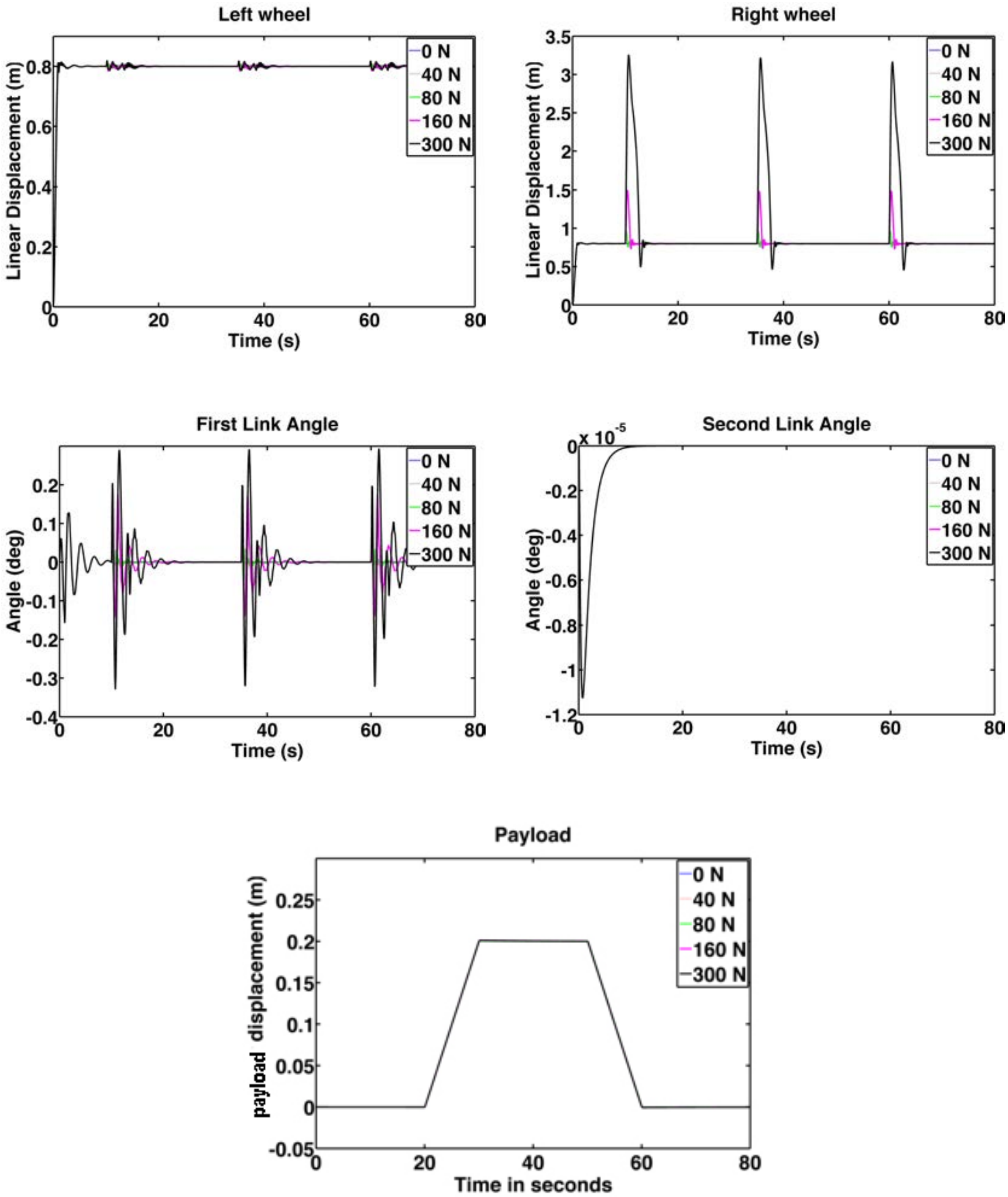

Figure 5.4: System performance with disturbances applied on the right wheel

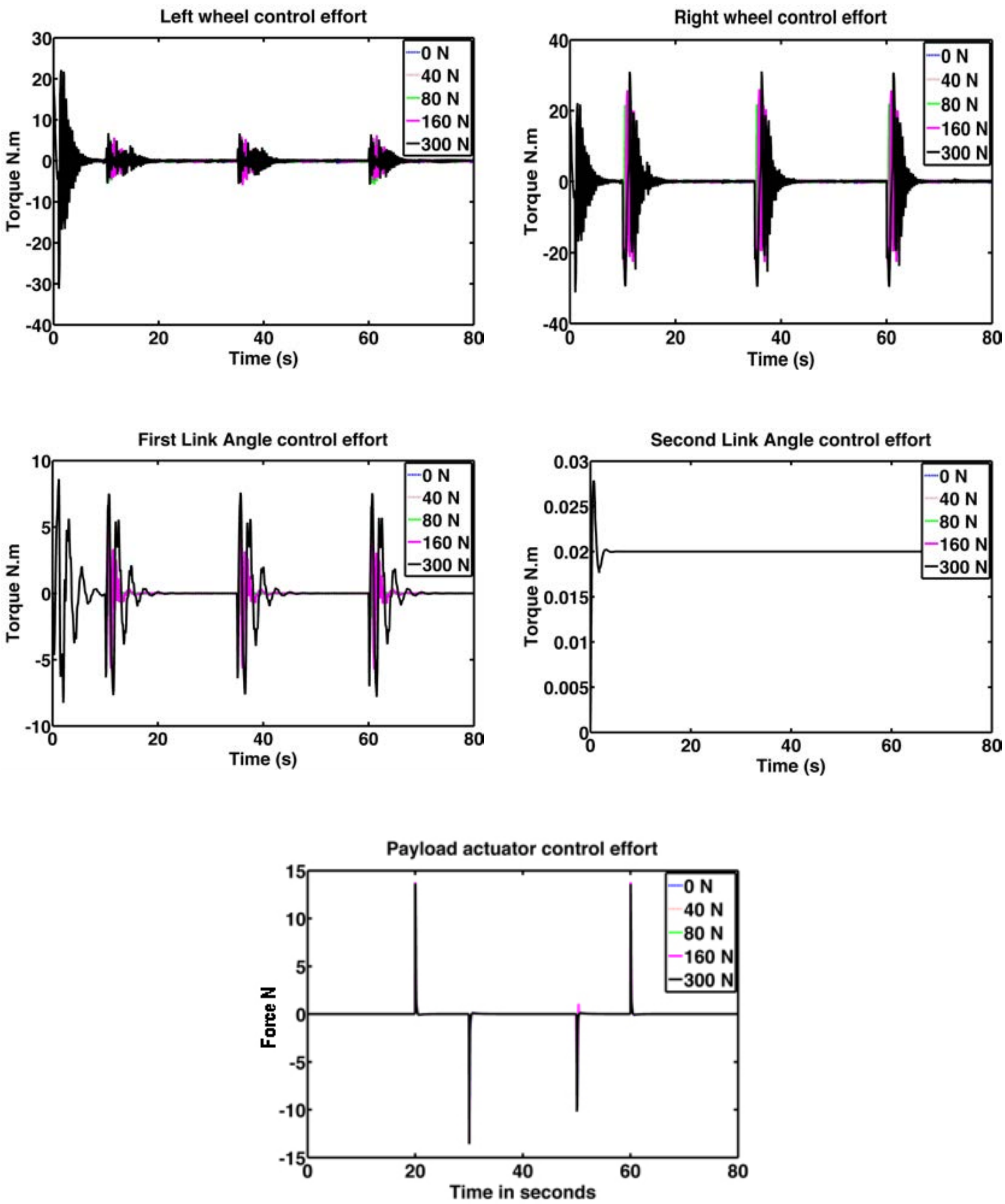

Figure 5.5: Control effort with disturbance applied on the right wheel

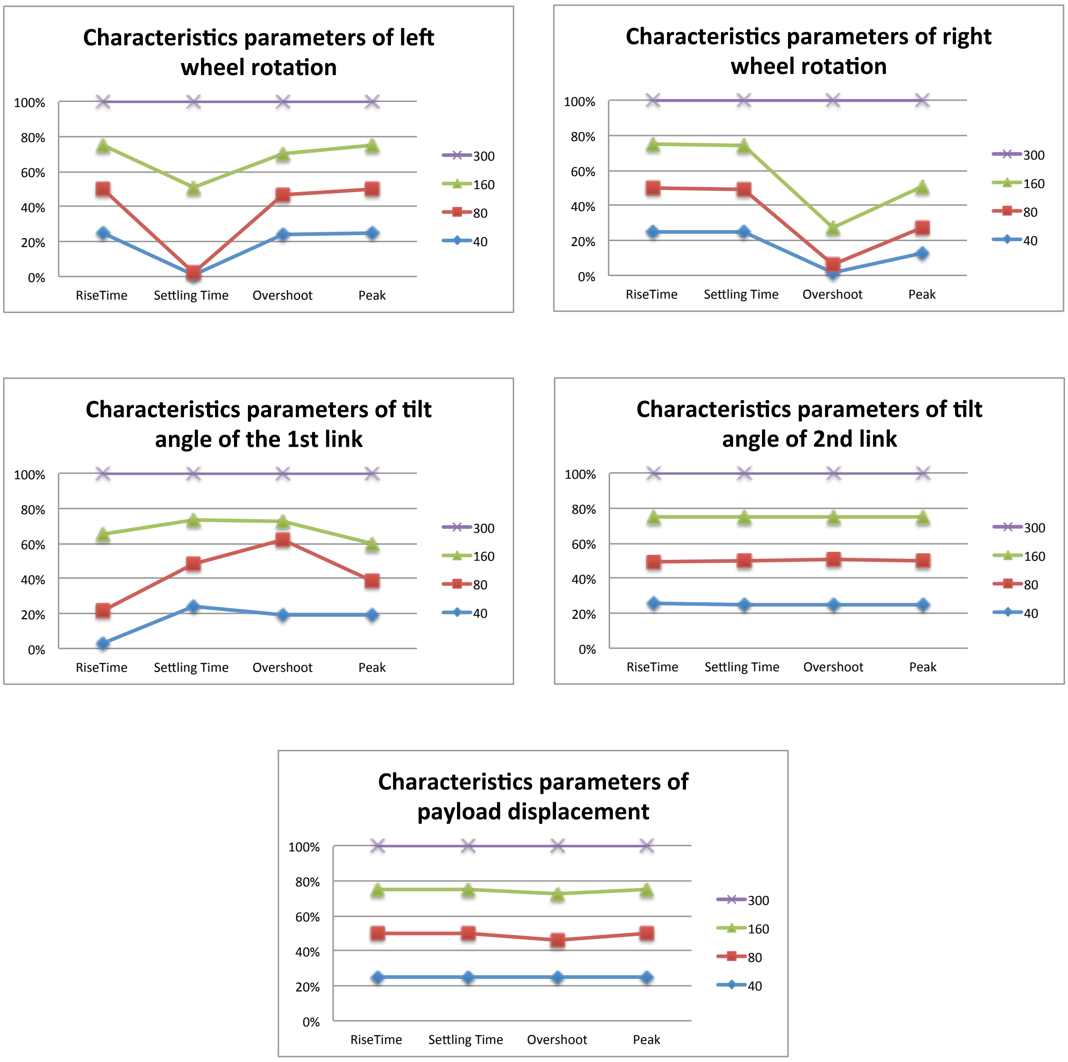

Figure 5.6: Graphical analysis of system performance characteristics
with disturbances applied on the right wheel

5.3.3 Disturbances with different amplitudes applied on the first link

Figures 5.7-5.9 and the numerical results in Table C1.3 represent the system response with disturbances applied at the centre of the first link. Overshoots can be noted in the tilt angle of the first link with a maximum peak amplitude increase of 331% at the maximum disturbance. The average settling time was approximately 5 seconds. The settling time increased by 3% of the initial value with each increase in the disturbance amplitude. Negative peaks appearing at displacements of both wheel motors explains the opposing movement of the cart to overcome the disturbances and to stabilise the first link at the upright position. The tilt angle of the second link and the displacement of the payload actuator were not affected by this disturbance.

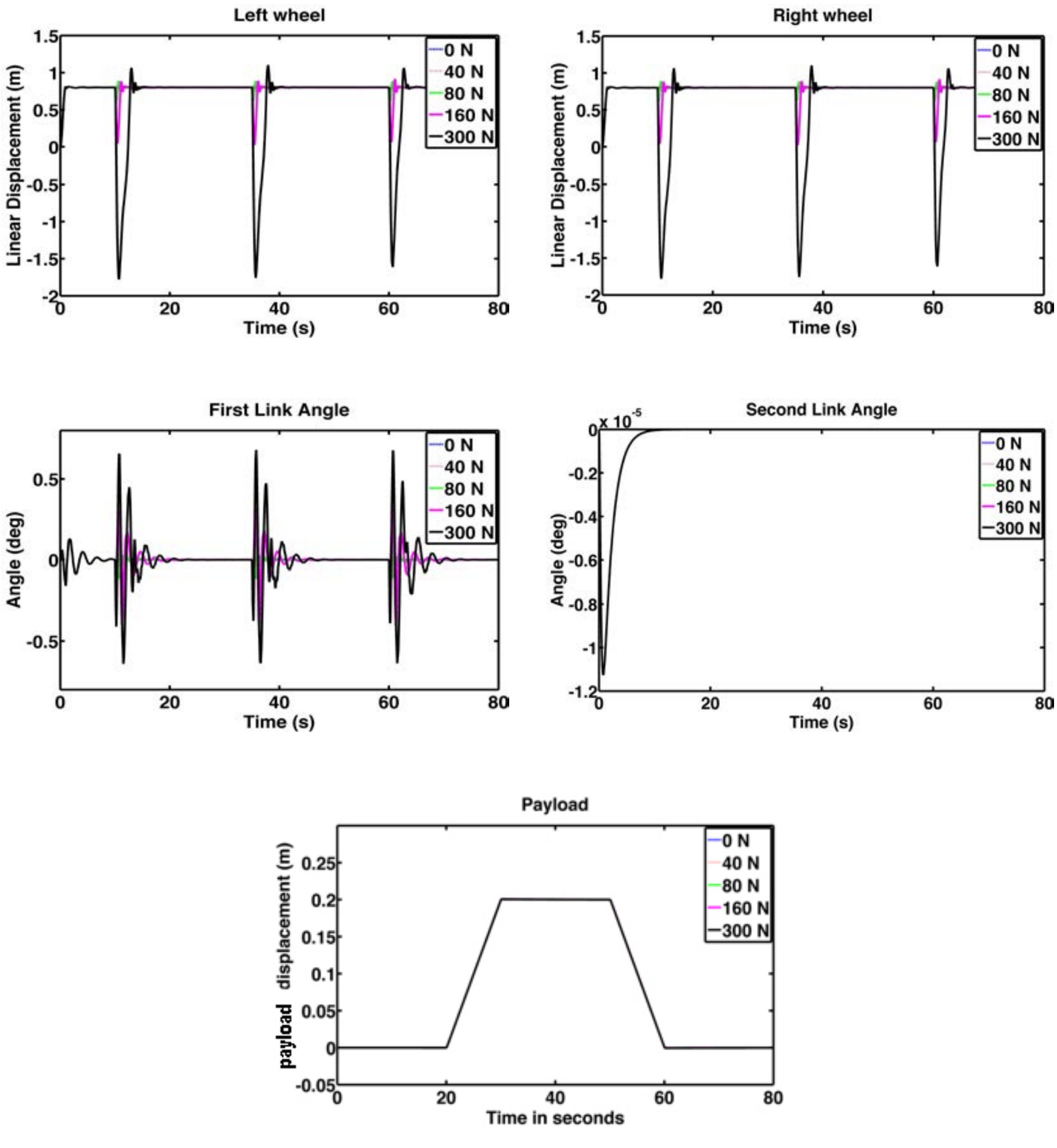

Figure 5.7: System performance with disturbances applied at the centre of first link

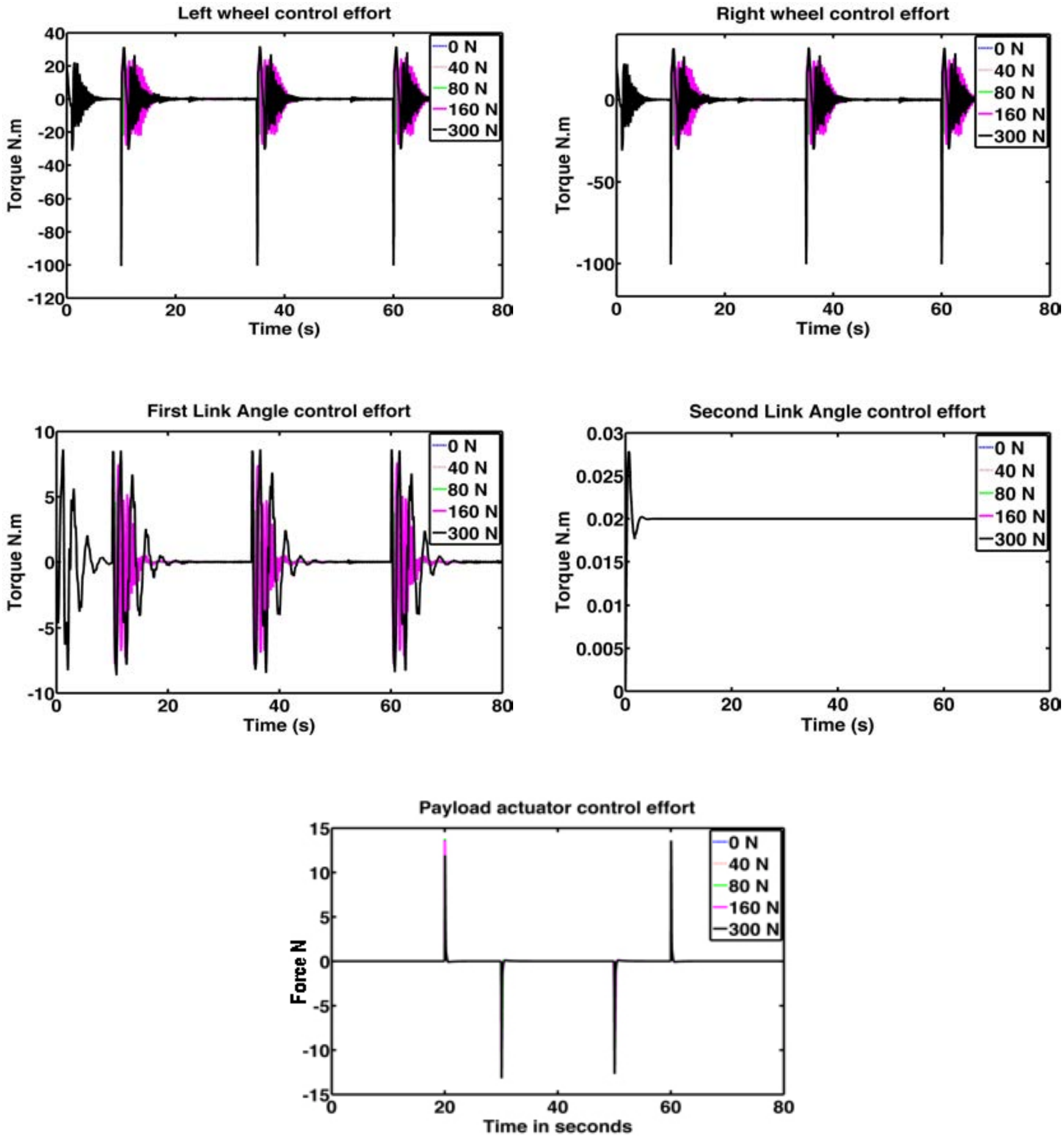

Figure 5.8: Control effort with disturbance applied at the centre of first link

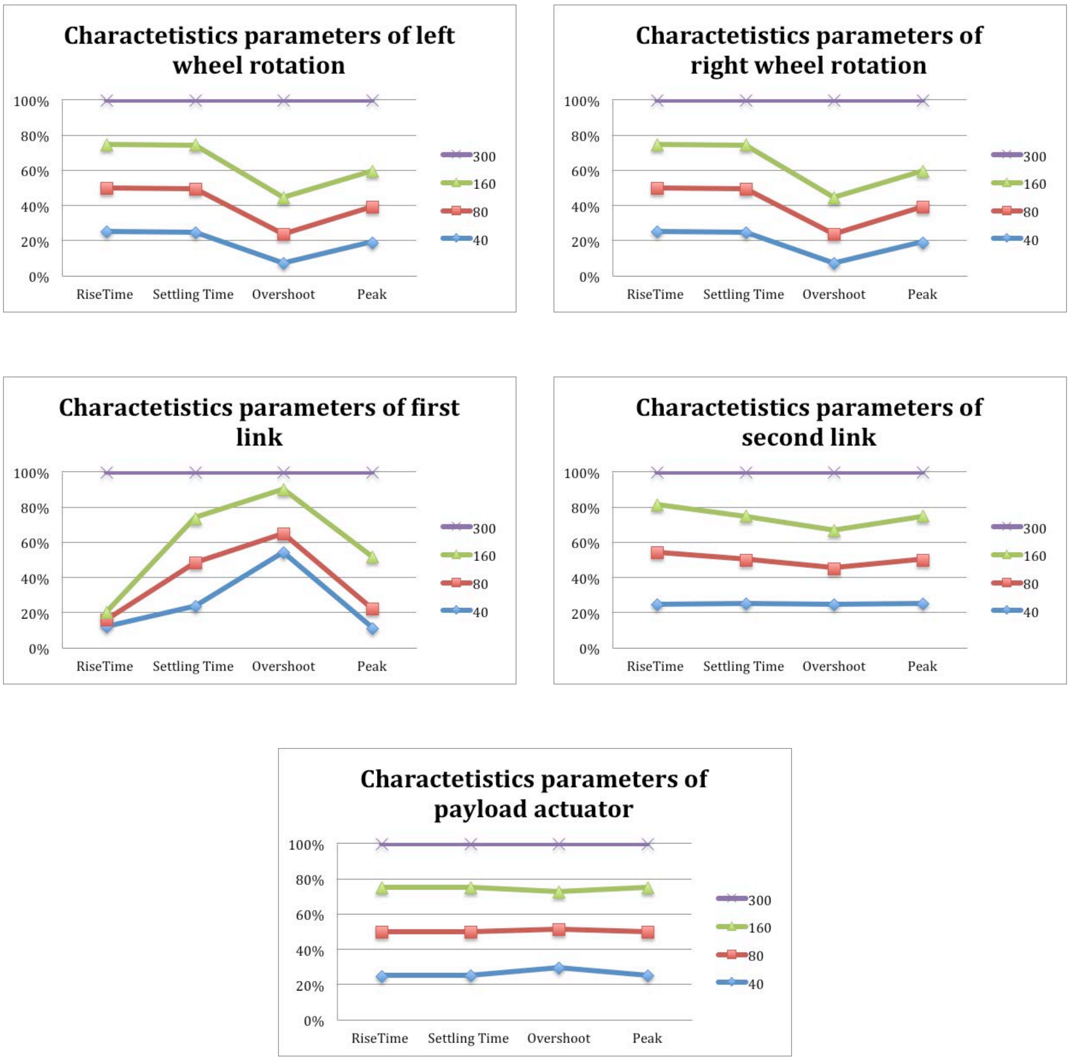

Figure 5.9: Graphical analysis of system performance characteristics with disturbances applied at centre of first link

5.3.4 Disturbances with different amplitudes applied on the second link

Referring to Figures 5.10-5.12 and Table C1.4, the effect of applying disturbances to the centre of the second link can be noted. Disturbances resulted in oscillations in the tilt angle of the second link. The tilt angle converged to the set point within 5 seconds at the maximum applied disturbance force while the rise time remained unchanged. With every increment in amplitude of disturbance force, the peak value increased by an average of 50%. The displacements of both wheels, the tilt angle of the first link and the displacement of the payload actuator remained unaffected by this disturbance.

This is due to the high damping effects caused by the joints of the vehicle and the motor linking the pendulum links and payload actuator motor.

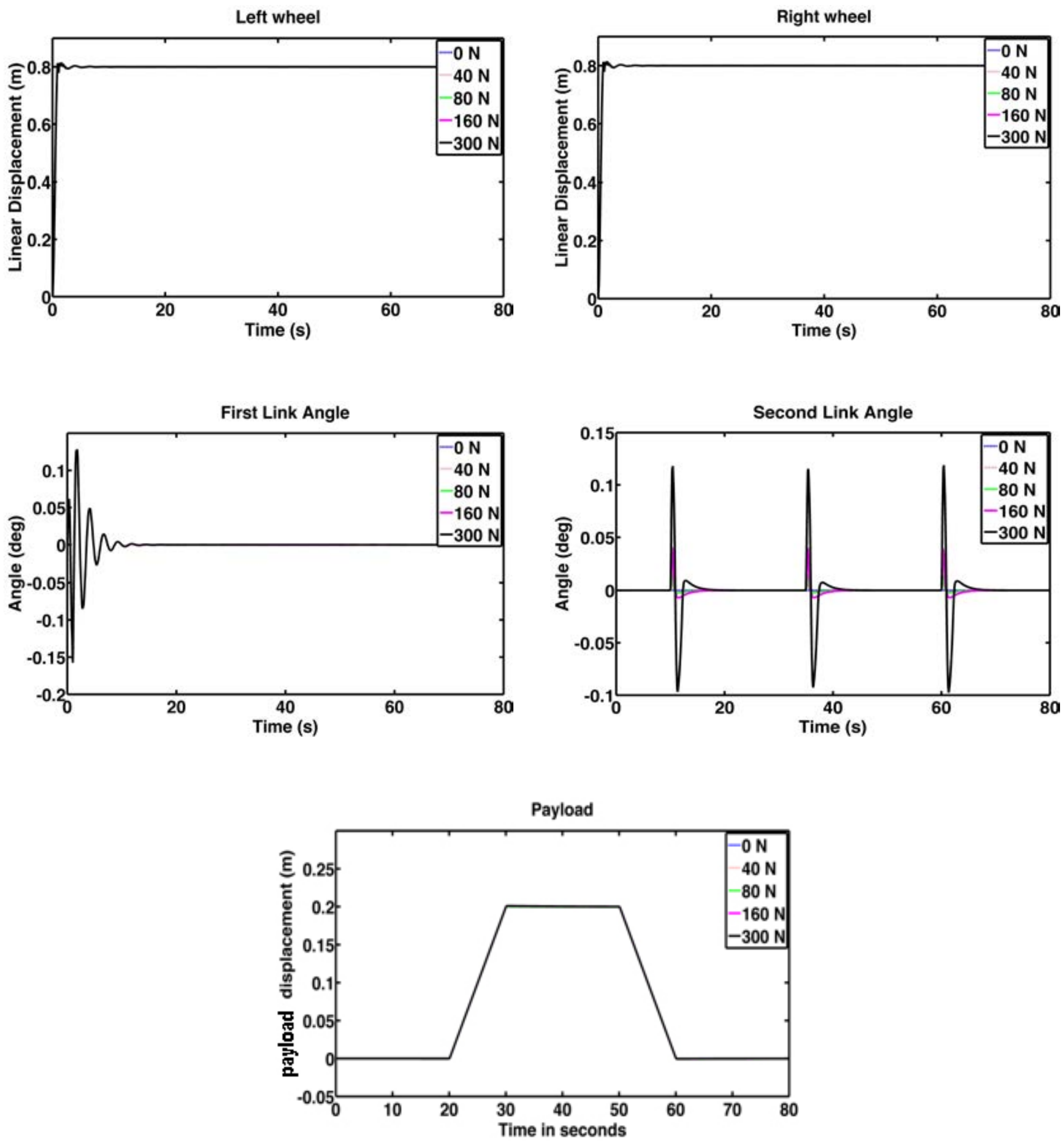

Figure 5.10: System performance with disturbances applied at the centre of second link

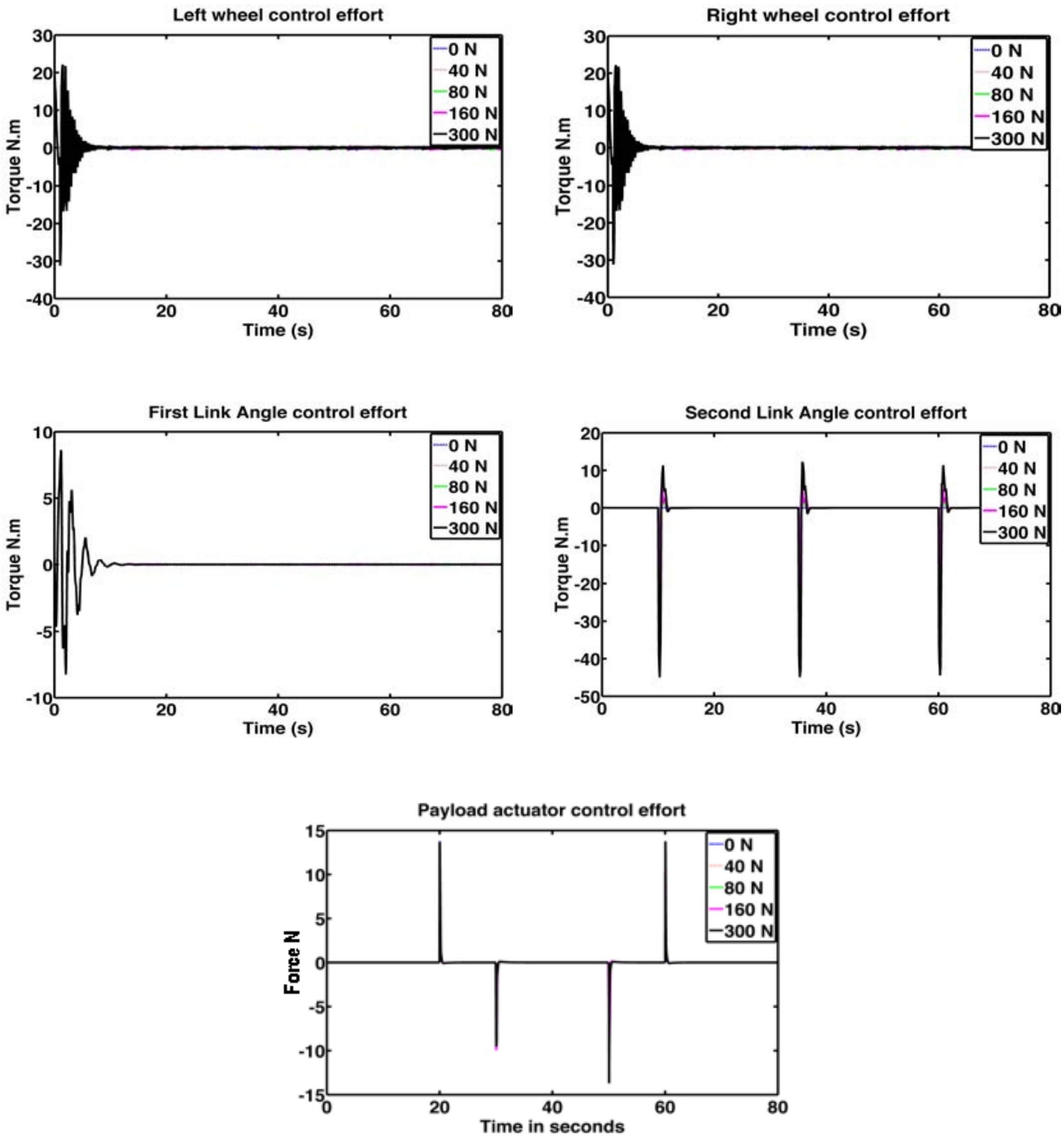

Figure 5.11: Control effort with disturbance applied at the centre of second link

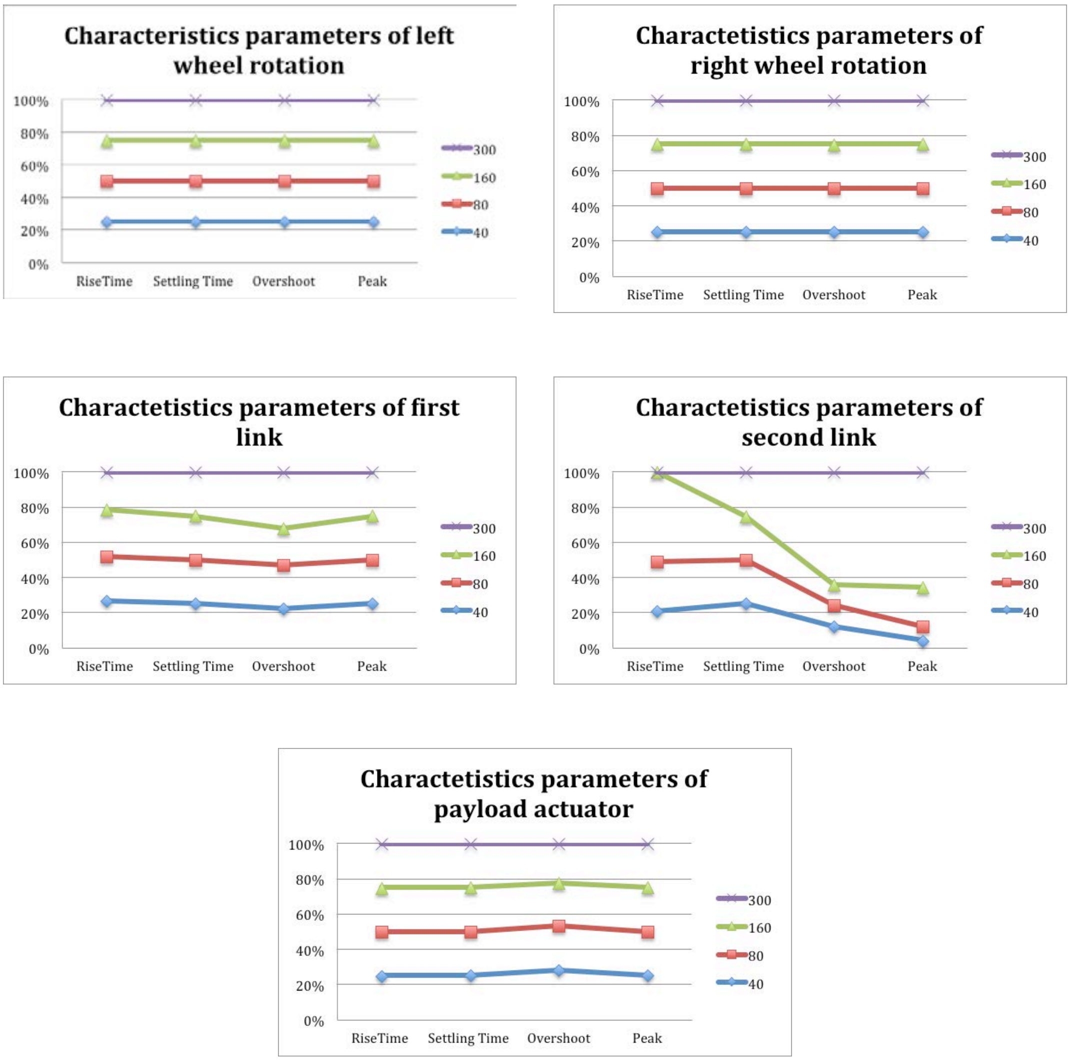

Figure 5.12: Graphical analysis of system performance characteristics
with disturbances applied on the second link

5.3.5 Disturbances with different amplitudes applied on the payload

Figures 5.13-5.15 and the numerical values presented in Table C1.5 show the effect of the disturbance force applied on the payload on the system response. The disturbance clearly affected the payload movement by causing notable positive peaks at the payload displacement. Peak amplitudes increased by increase of the disturbance force amplitude with a maximum increase of 42% over the set point at the maximum disturbance. The signal converged to the set point within an average settling time of 4 seconds approximately. Moreover, the displacement of the left and right wheels, the tilt angles of the first and second links remained unaffected by this disturbance.

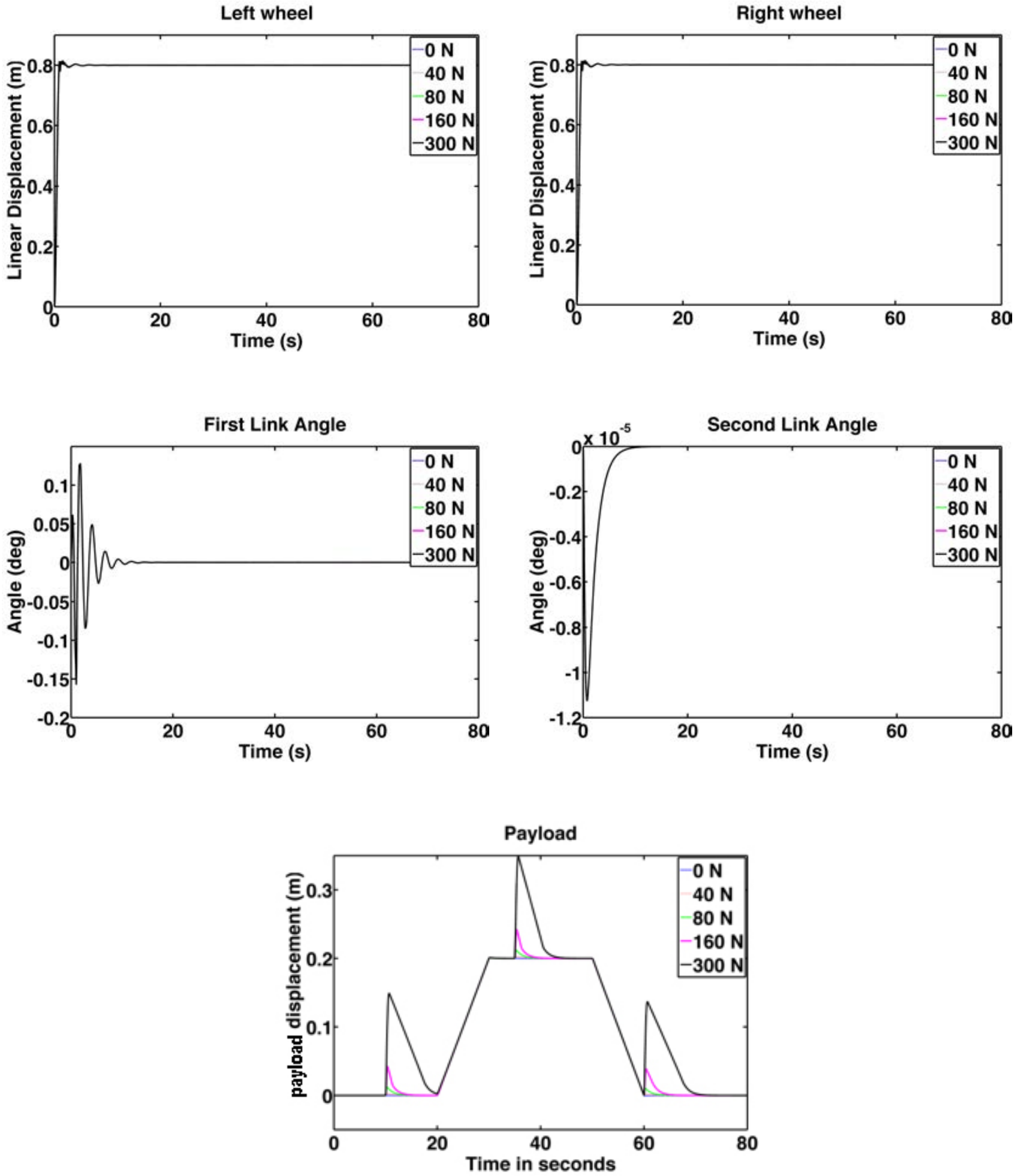

Figure 5.13: System performance with disturbances applied on the payload

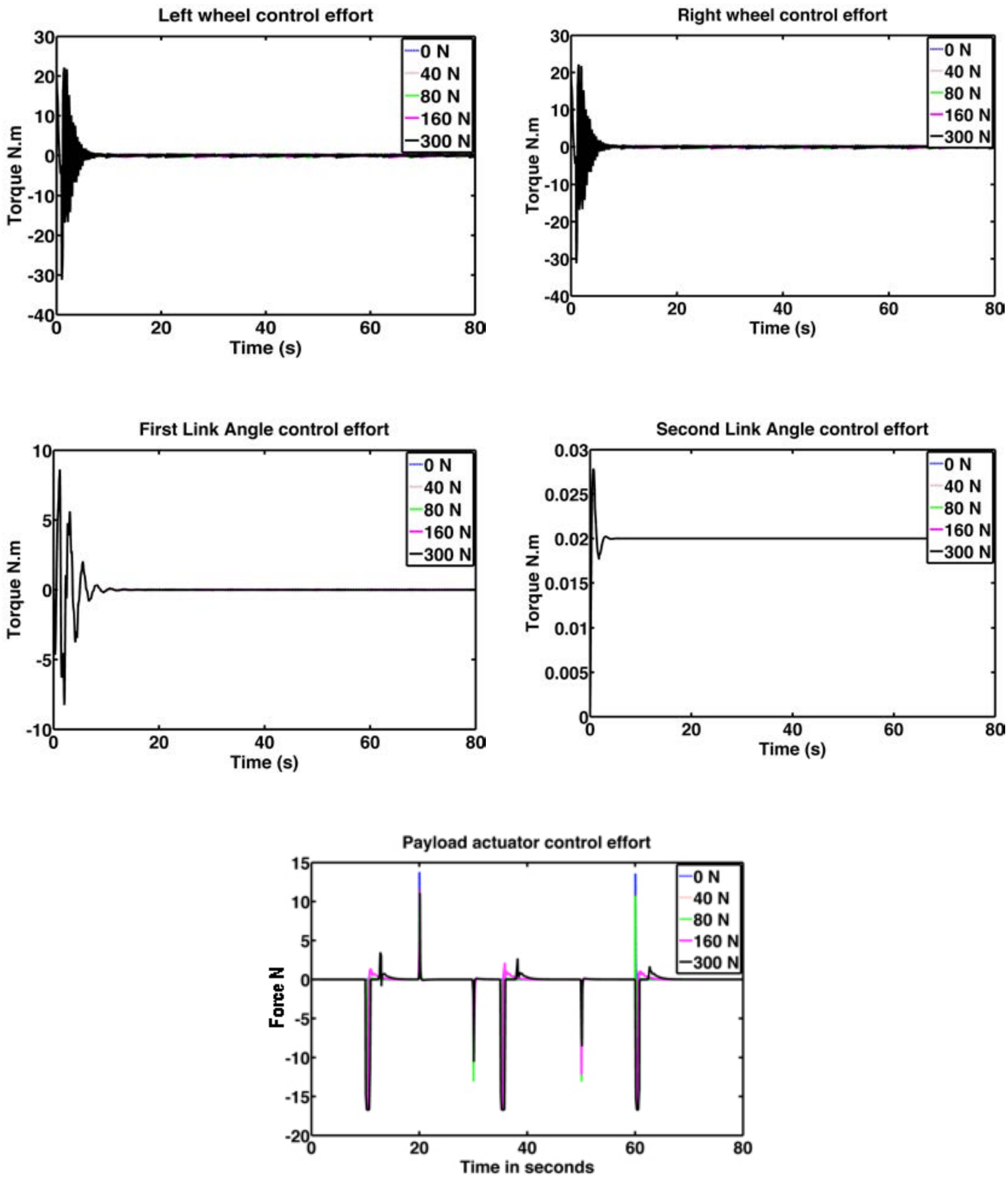

Figure 5.14: Control effort with disturbance applied on the payload

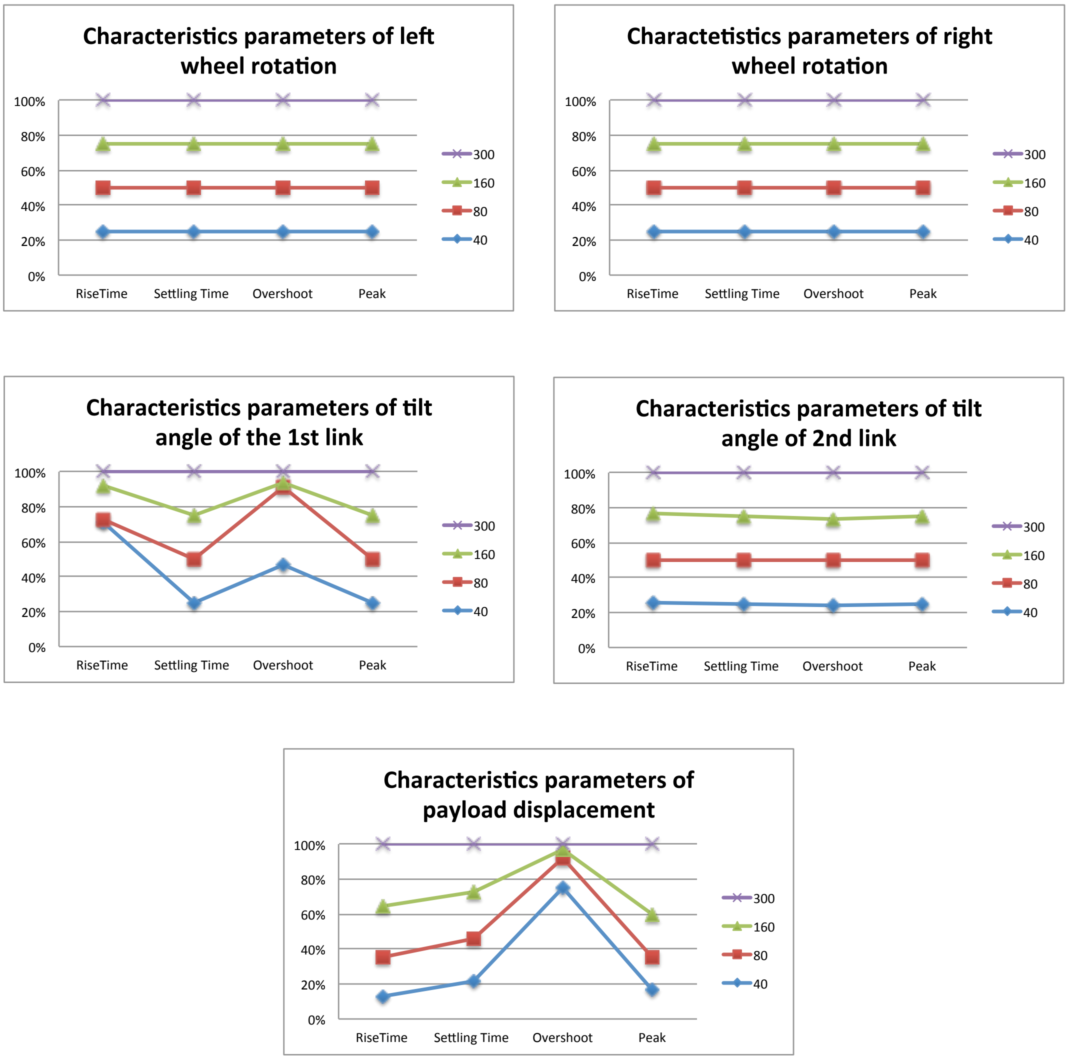

Figure 5.15: Graphical analysis of system performance characteristics
with disturbances applied on the payload

5.4 Disturbances with varying durations

Disturbance forces with varying durations were applied to the vehicle components to analyse the system behaviour and control robustness. The disturbance forces characteristics used are summarised in Table 5.2.

Table 5.2: Disturbance force characteristics with varying duration

Pulse amplitude	80 N
Pulse duration	1.25 sec / 2.5 sec / 7.5 sec / 12.5 sec
Phase delay	10 seconds
Period	25 seconds

5.4.1 Disturbances with different durations applied on the left wheel

The effects of applying disturbance forces on the left wheel motor are presented in Figures 5.16-5.18 and the associated numerical values in Table C2.1. It is noted that displacement of the left wheel was affected by variation of duration of the disturbance force. The longer the duration of the applied disturbance the larger the overshoots observed in the system response. The overshoots resulted in fluctuations in the displacement of the right wheel. Hence, longer durations of the applied disturbances could cause the cart to drift away from the defined path. Another implication of this force can be noted in the oscillations appearing in the tilt angle of the first link. The settling time increases by an approximate factor of 2.5 each time the disturbance duration was increased while the rise-time remained constant at a value of 0.57 seconds. The controller was able to stabilise the system at the set point within an average time of 8 seconds approximately. The tilt angle of the second link and the displacement of the payload actuator remained unaffected by this disturbance.

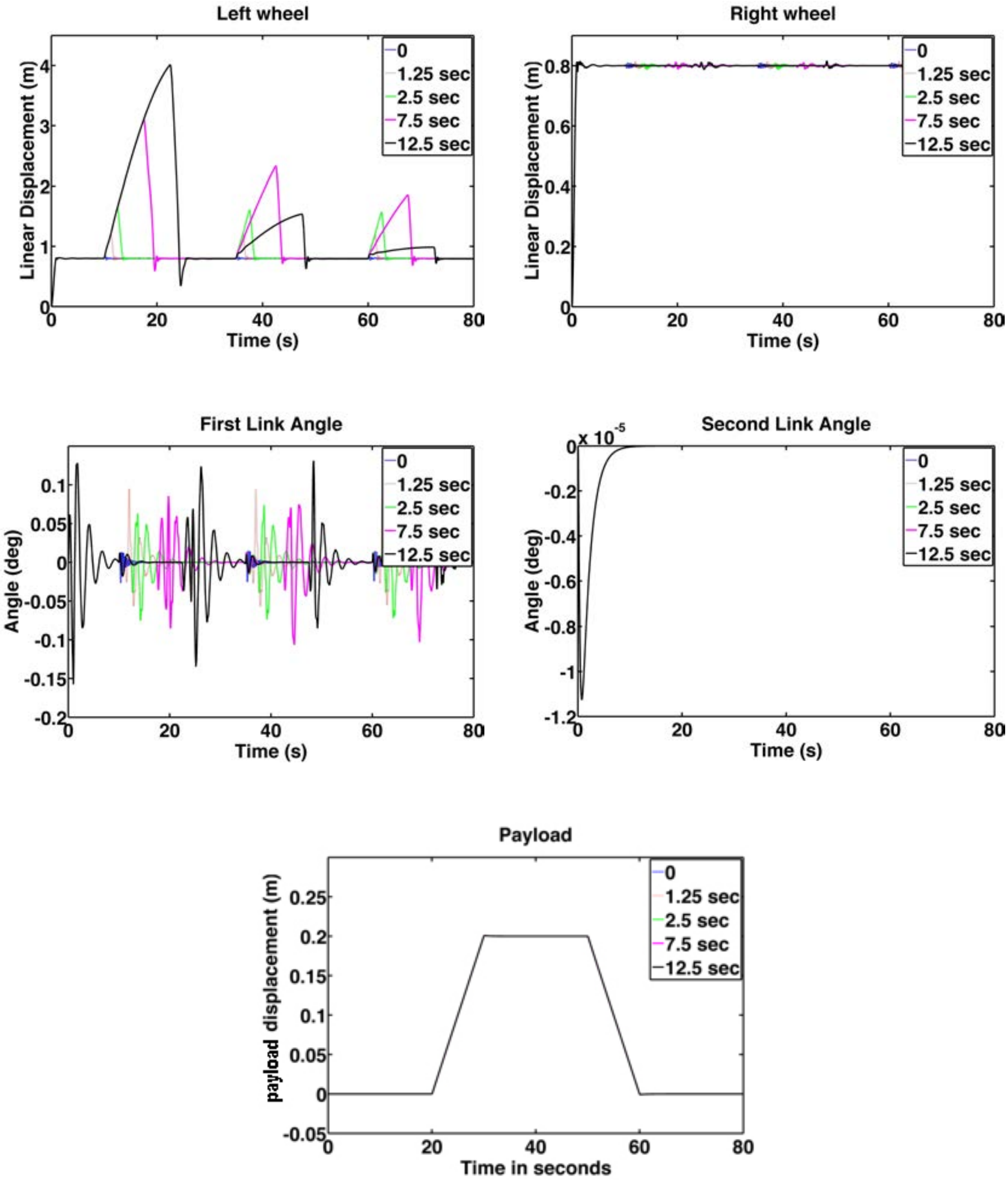

Figure 5.16: System performance with disturbances applied on the left wheel

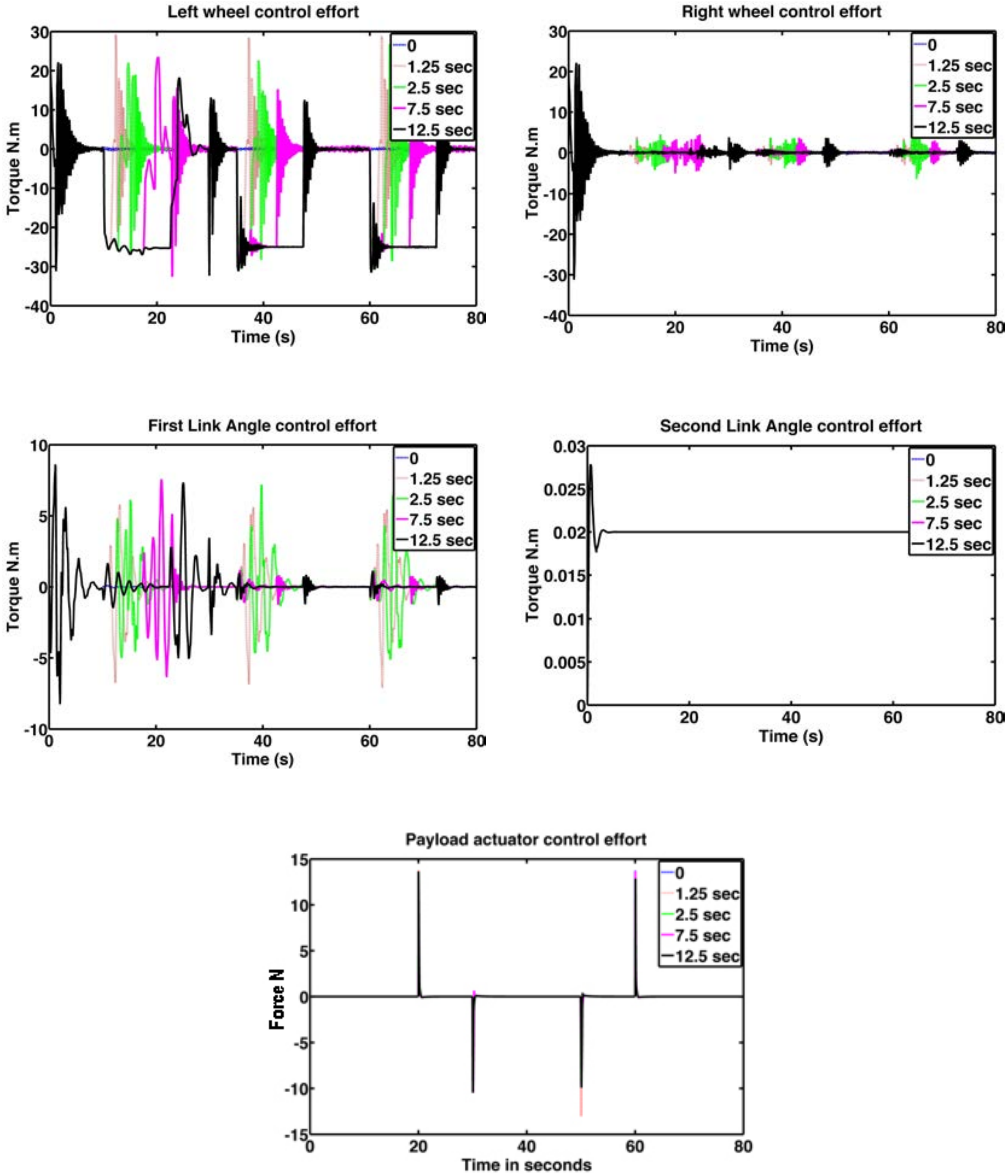

Figure 5.17: Control effort with disturbance applied on the left wheel

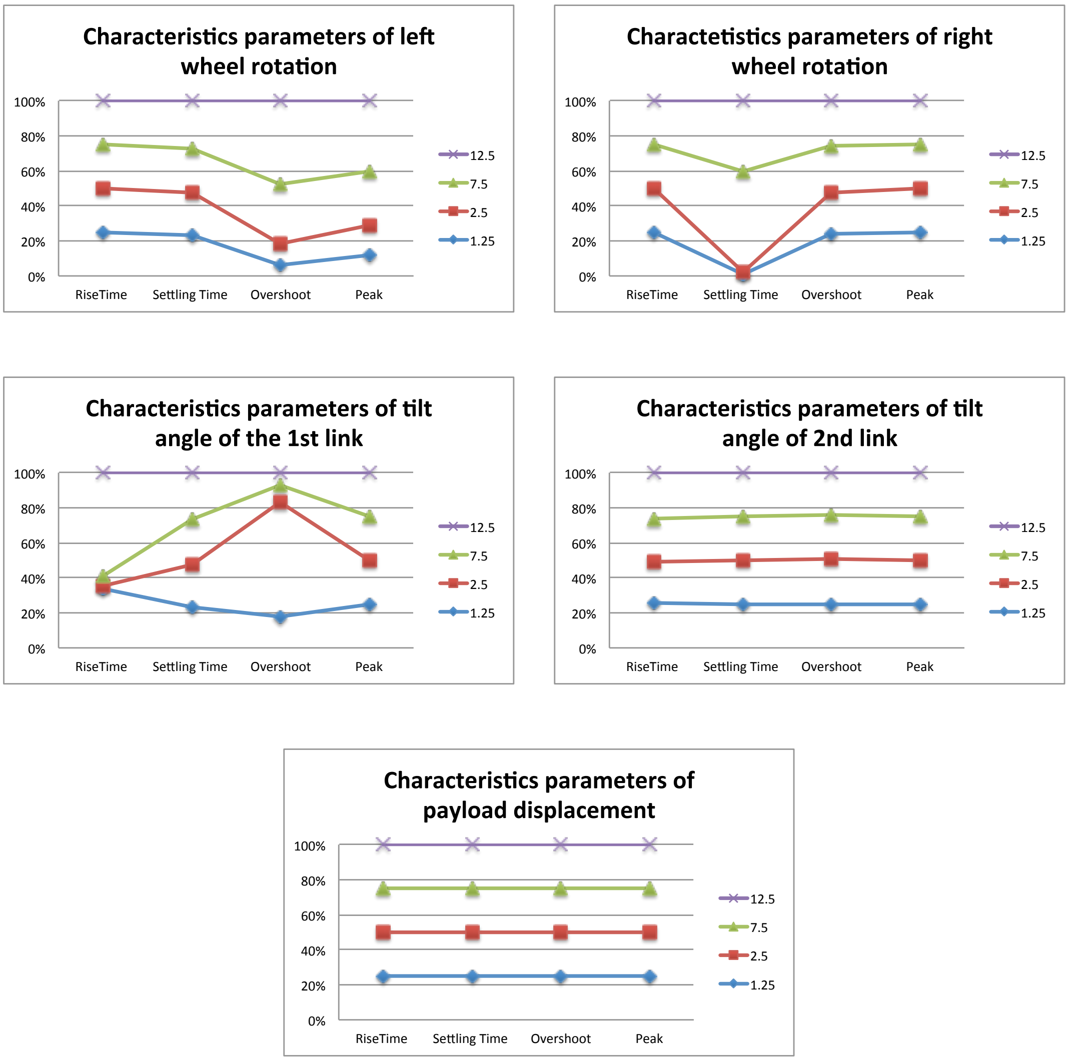

Figure 5.18: Graphical analysis of system performance characteristics
with disturbances applied on the left wheel

5.4.2 Disturbances with different durations applied on the right wheel

Figures 5.19-5.21 and the associated numerical results in Table C2.2 show effects of disturbances applied on the right wheel motor. With the aforementioned reasons in section 5.3.1 applying the disturbance force on the right wheel resulted in exactly similar response of the system as applying the force on the left wheel.

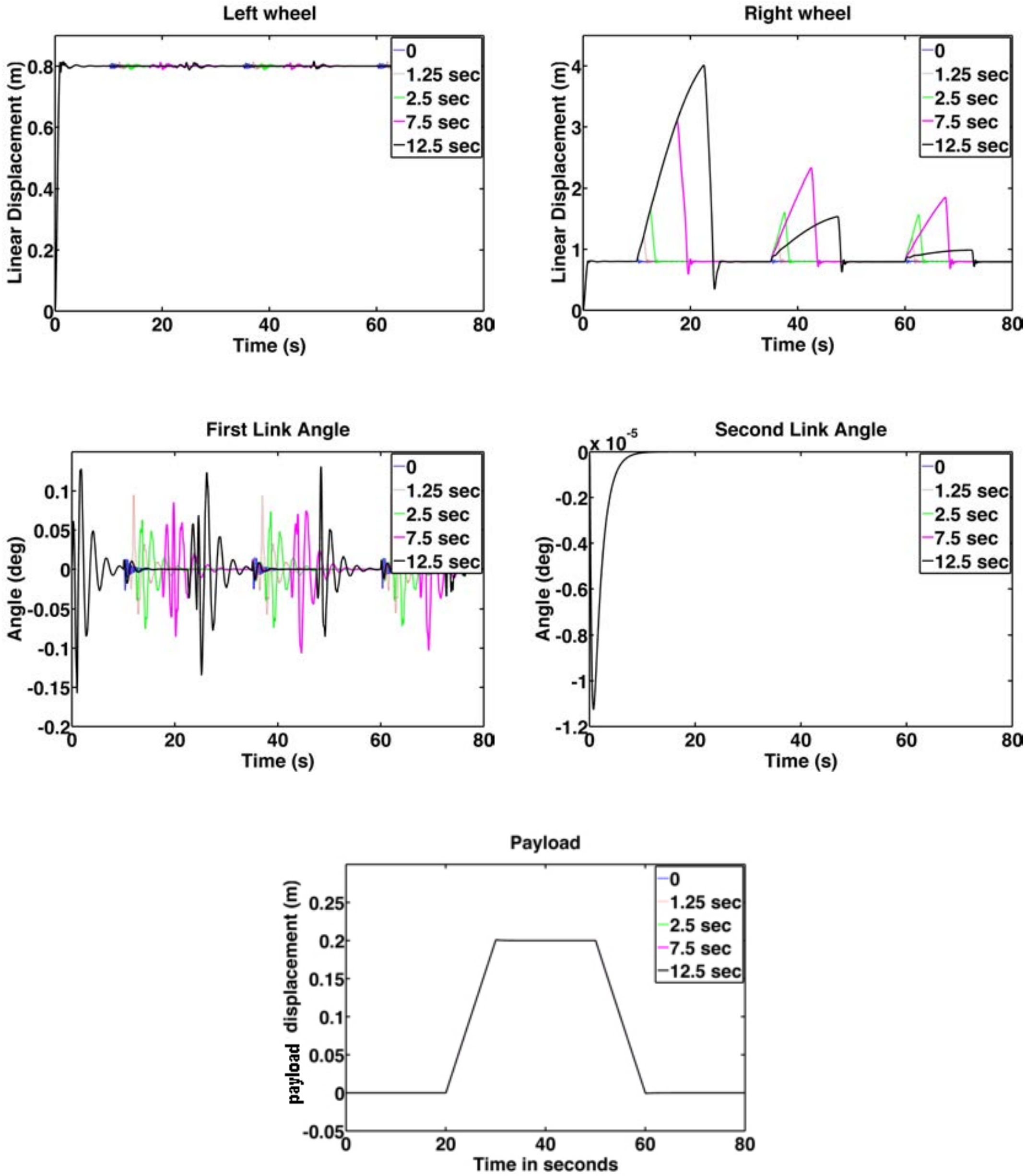

Figure 5.19: System performance with disturbances applied on the right wheel

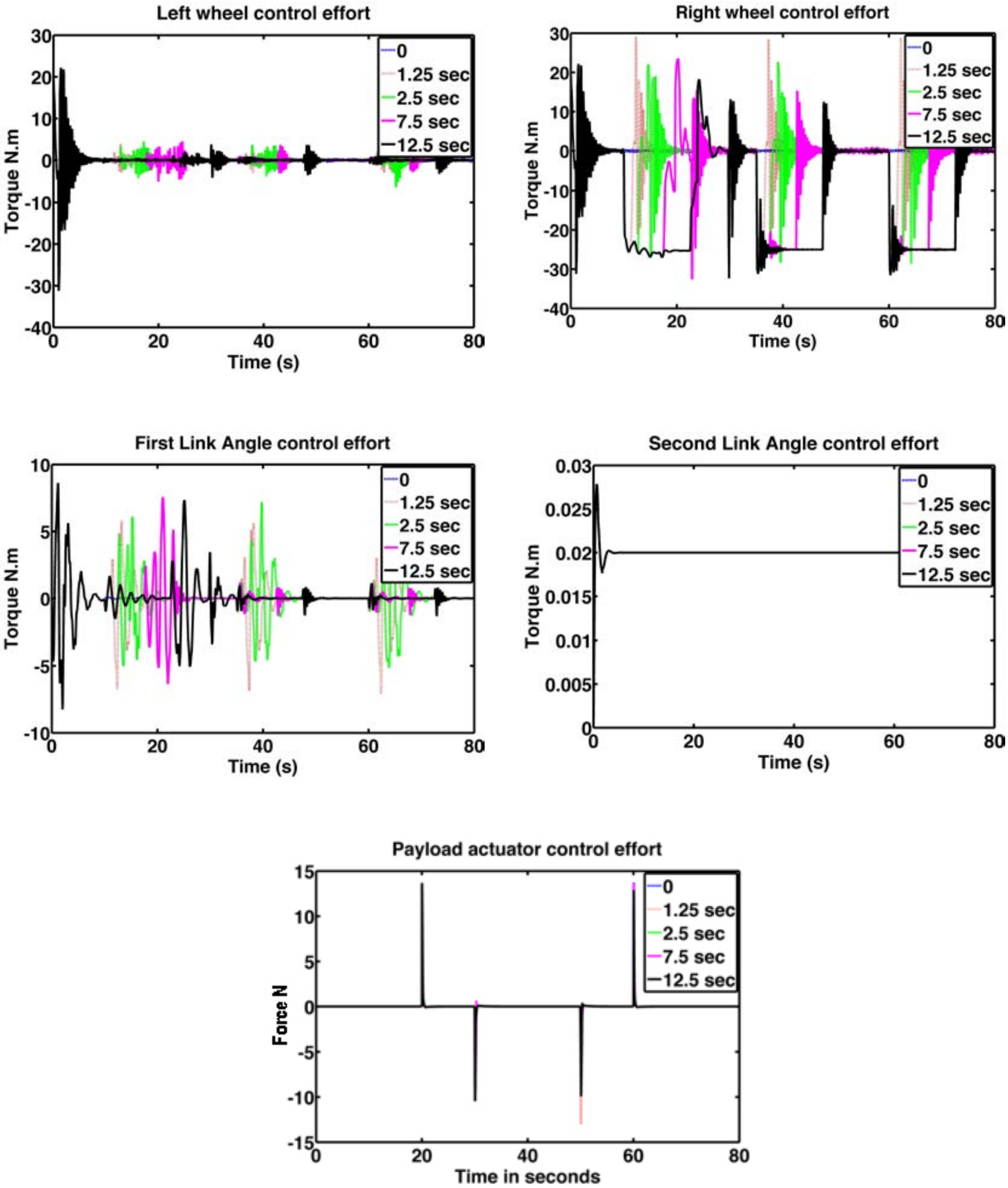

Figure 5.20: Control effort with disturbance applied on the right wheel

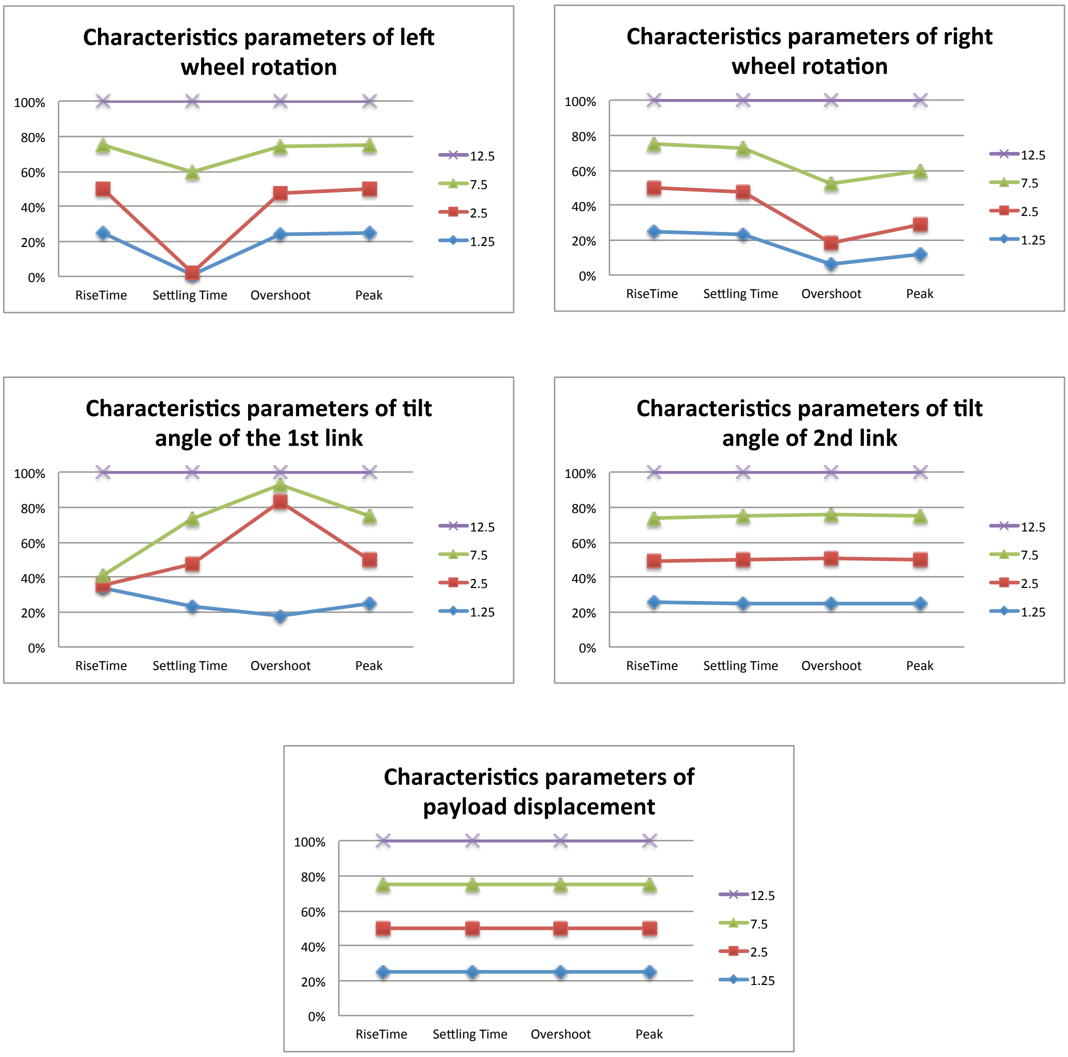

Figure 5.21: Graphical analysis of system performance characteristics
with disturbances applied on the right wheel

5.4.3 Disturbances with different durations applied on the first link

Figures 5.22-5.24 and Table C2.3 represent the response of the system to the disturbance forces applied to the centre of the first link. As noted, oscillations appeared in the tilt angle of the first link with varied amplitudes. The longer the applied disturbance duration the larger the amplitudes of oscillations noted. The settling-time increased by an average of 6% while the rise-time fluctuated by increasing and decreasing depending on the duration of the applied disturbance. The right and left wheel displacements were affected by this disturbance and fluctuations were noted. The tilt angle of the second link and the payload actuator displacement were not affected by this disturbance.

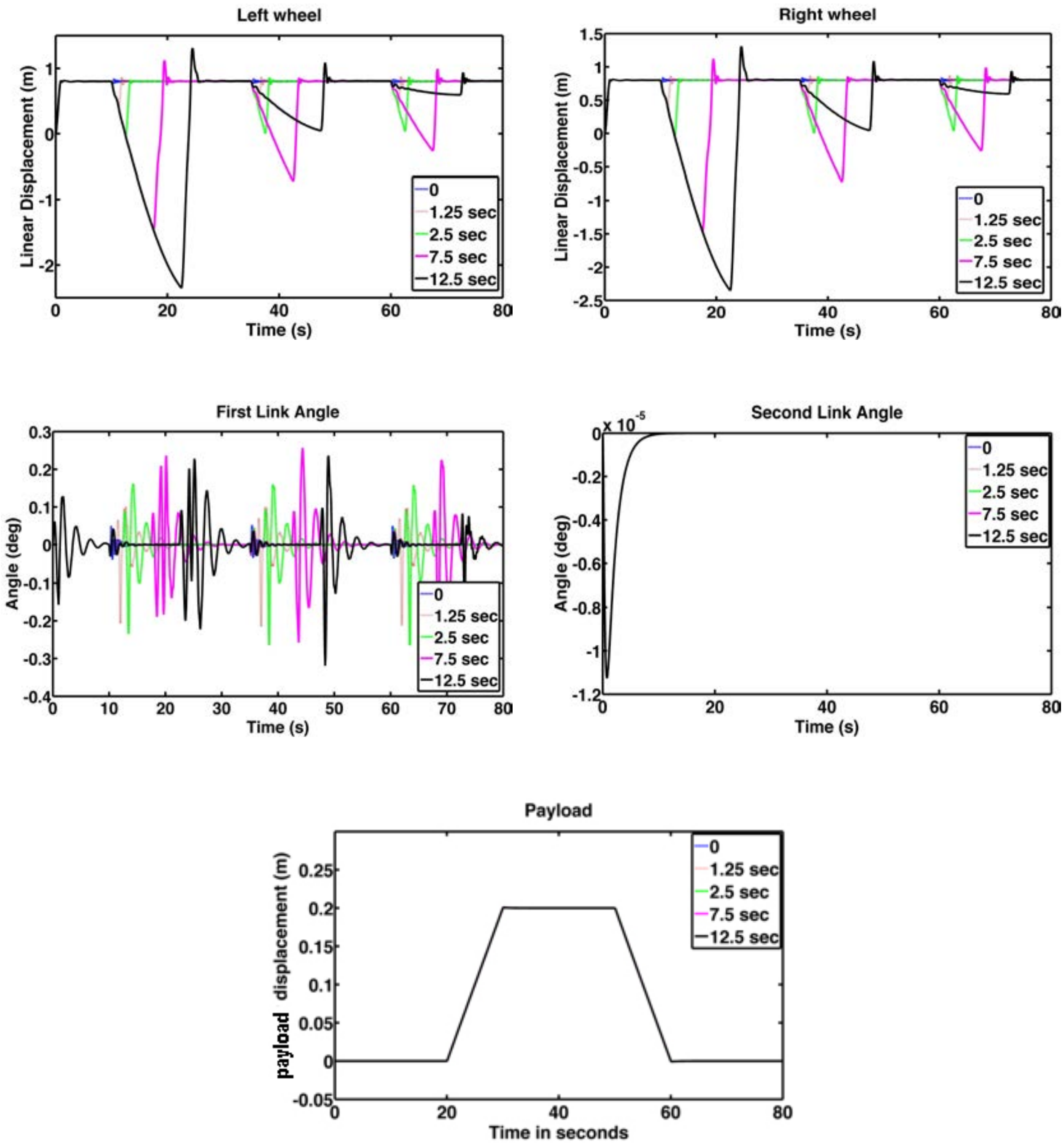

Figure 5.22: System performance with disturbances applied at the centre of the first link

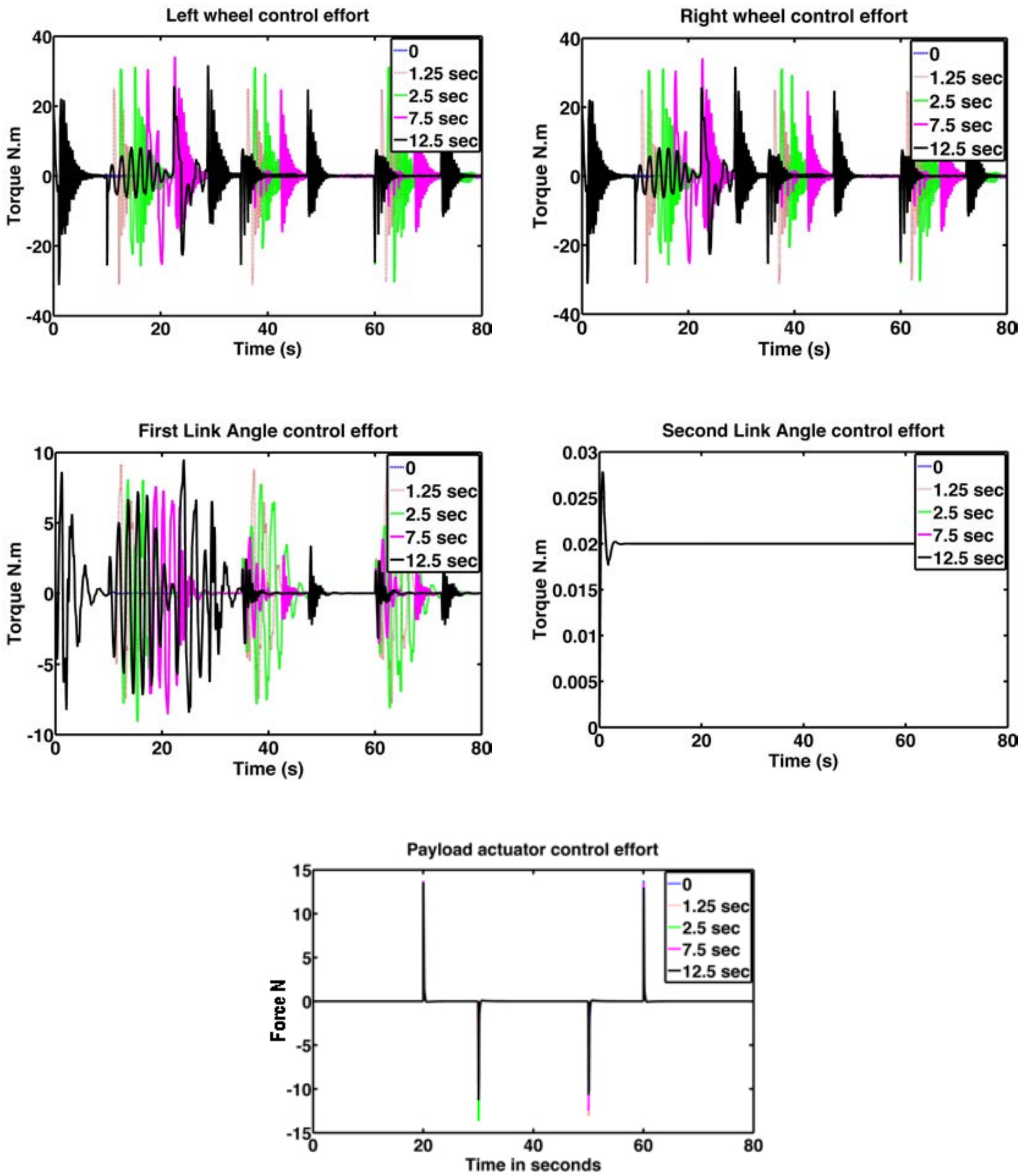

Figure 5.23: Control effort with disturbance applied at the centre of the first link

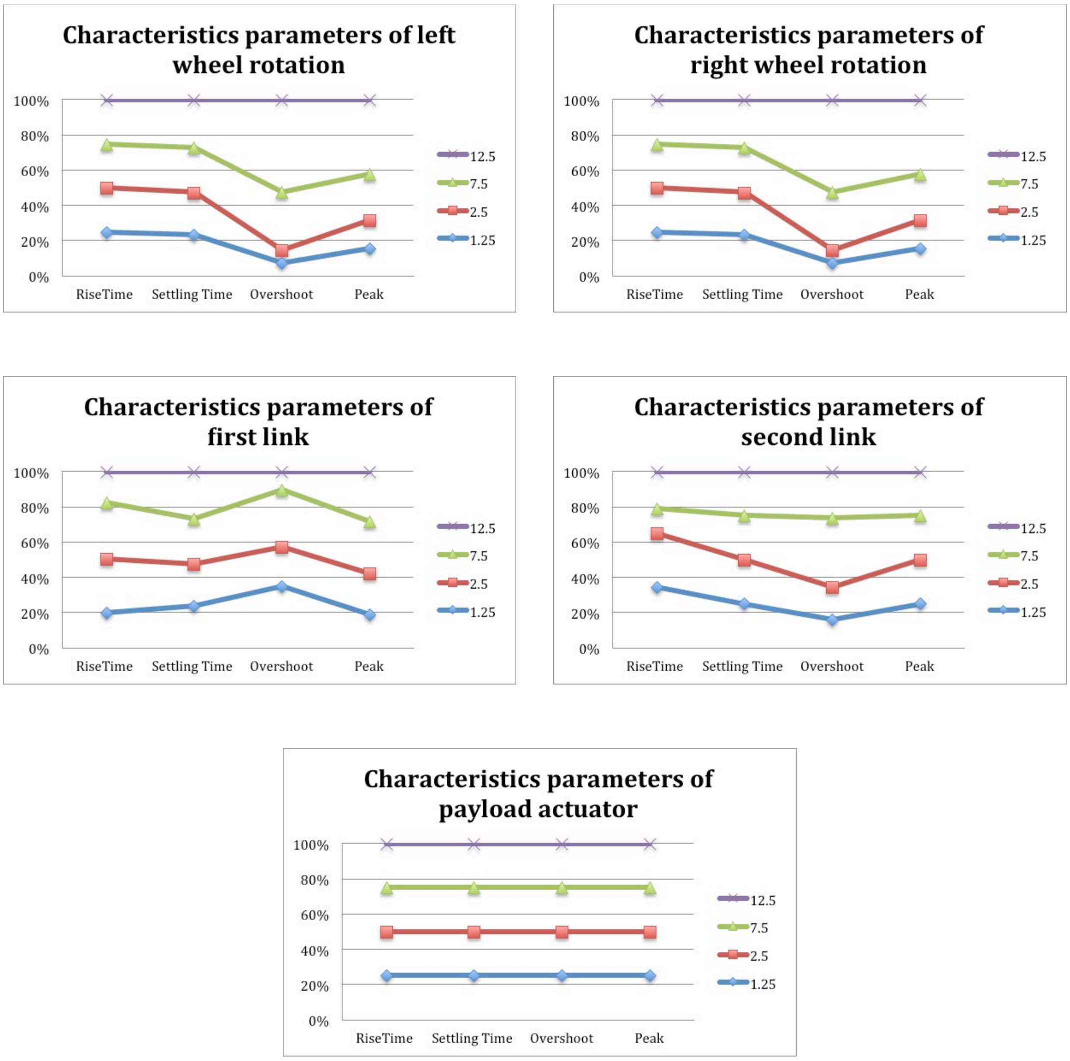

Figure 5.24: Graphical analysis of system performance characteristics with disturbances applied at the centre of the first link

5.4.4 Disturbances with different durations applied on the second link

Figures 5.25-5.27 and Table C2.4 present the response of the system for disturbances applied at the centre of the second link. The disturbances resulted in an oscillatory response in the tilt angle of the second link; at disturbance durations up to 7.5 seconds, the controller was able to control the tilt angle of the second link and stabilise the system within an approximate average time of 7 seconds. Settling-time increased by an average of 7% each time. Finally, The right and left wheel displacements, tilt angle of first link and the payload actuator displacement were not affected by this disturbance.

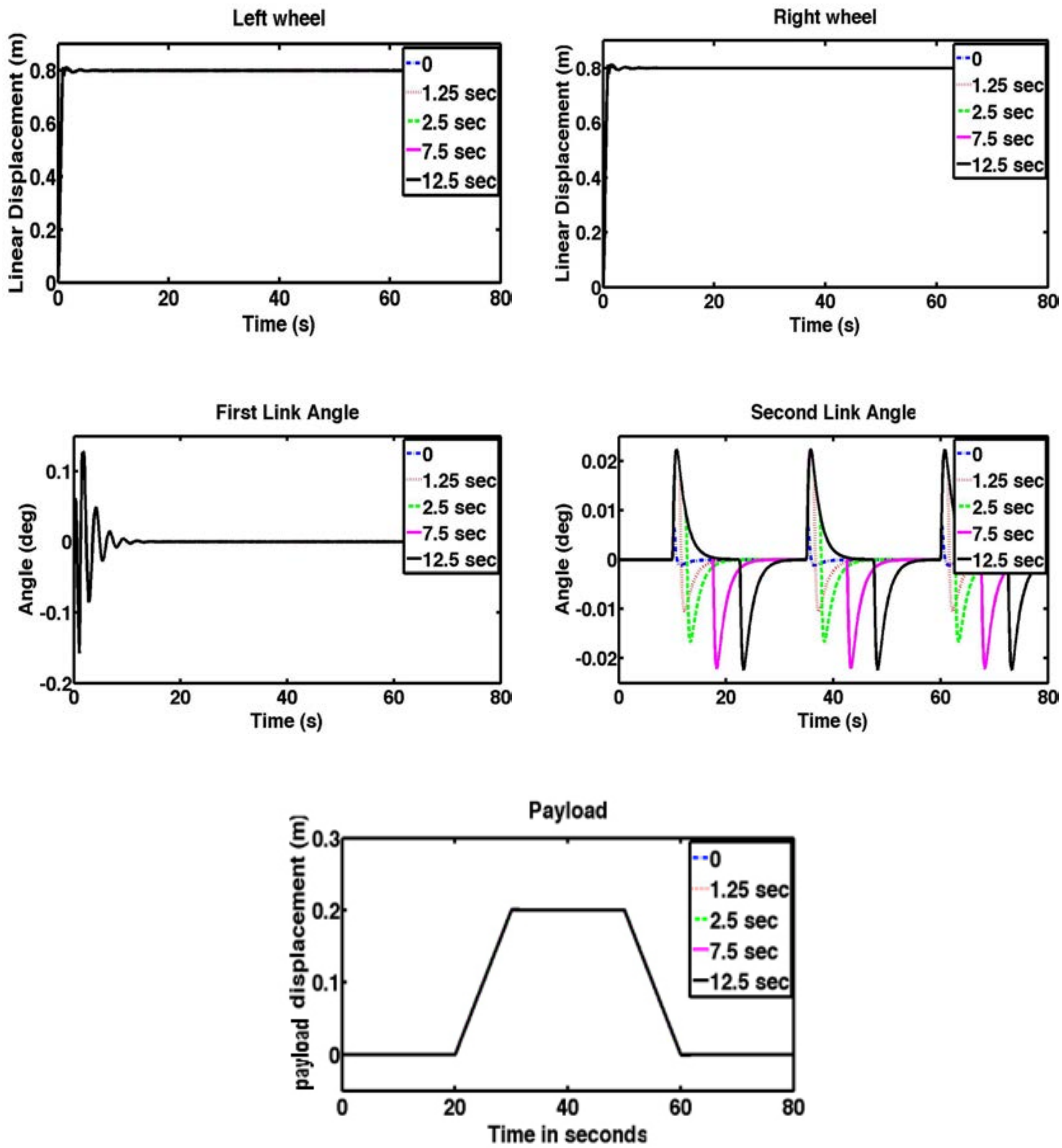

Figure 5.25: System performance with disturbances applied at the centre of the second link

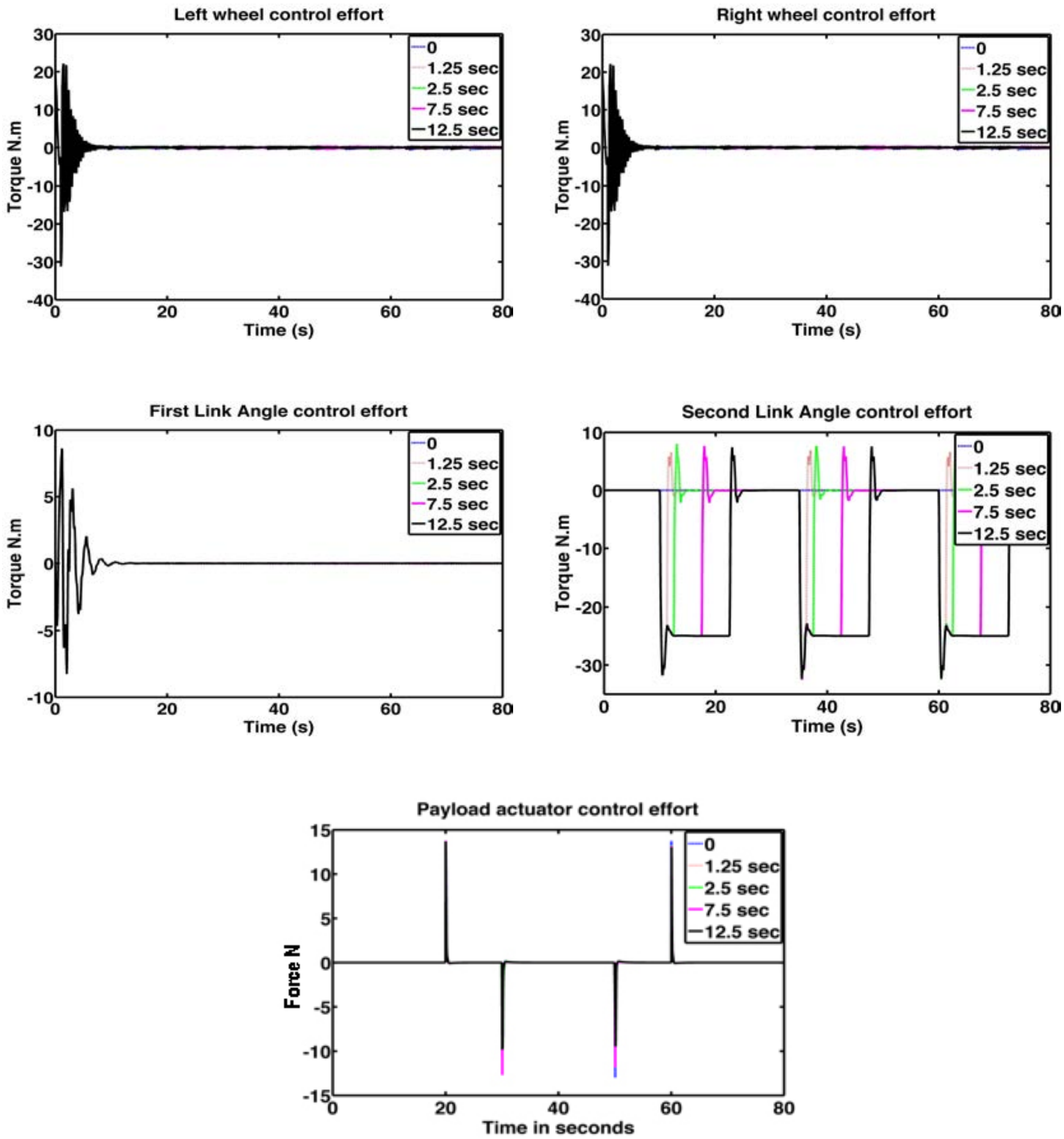

Figure 5.26: Control effort with disturbance applied at the centre of the second link

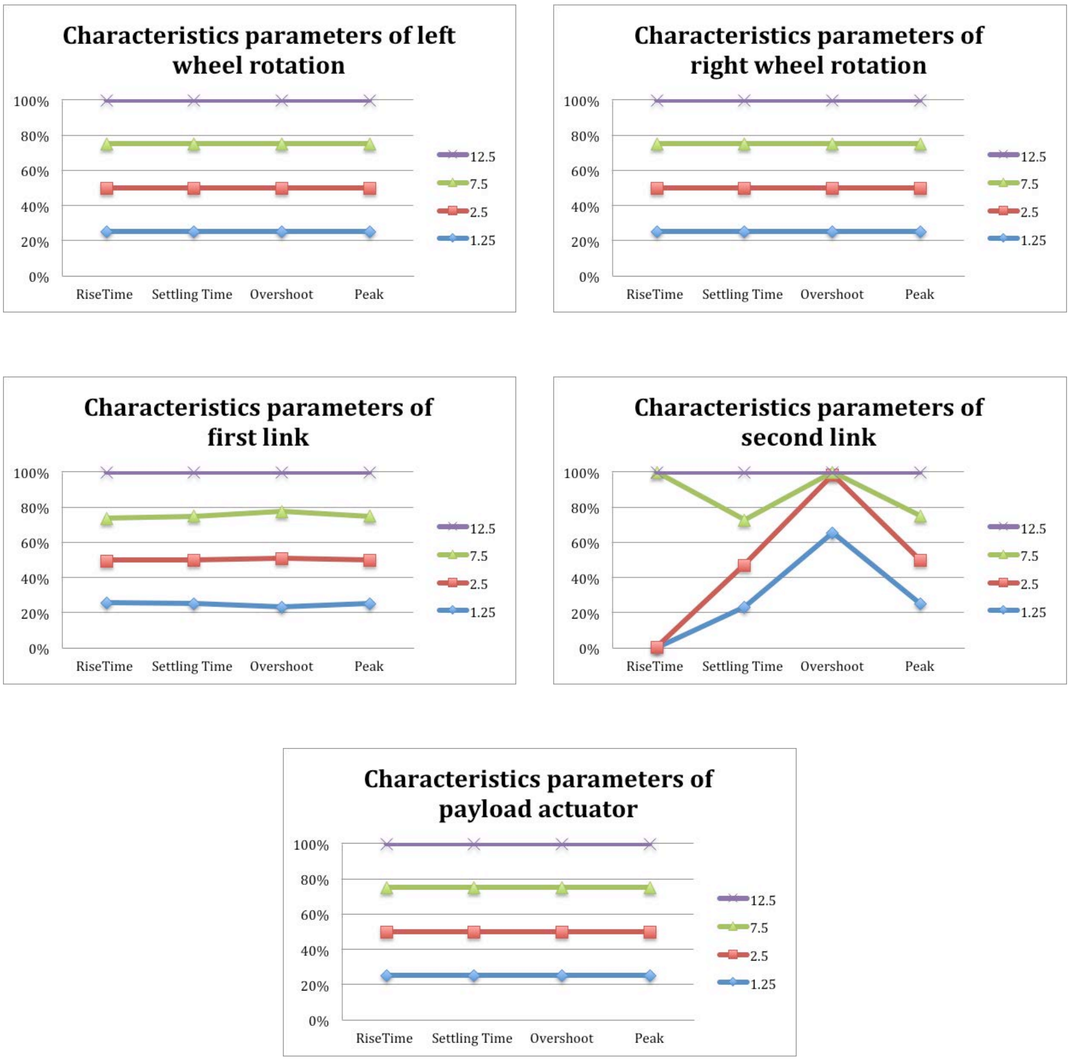

Figure 5.27: Graphical analysis of system performance characteristics
with disturbances applied at the centre of the second link

5.4.5 Disturbances with different durations applied on the payload

The effect of applying the disturbance force on the payload can be noted in Figures 5.28-5.30 and the associated numerical values in Table C2.5. Clearly the payload actuator was greatly affected; overshoots appearing at the time of applying the disturbance force were observed. For disturbance durations less than 7.5, the controller successfully stabilised the system with an average settling time of 4 seconds. On the other hand, the controller failed to control the payload with disturbance durations larger than 7.5. This was due to insufficient time between two consecutive disturbance forces, which was defined as 10 seconds at this stage.

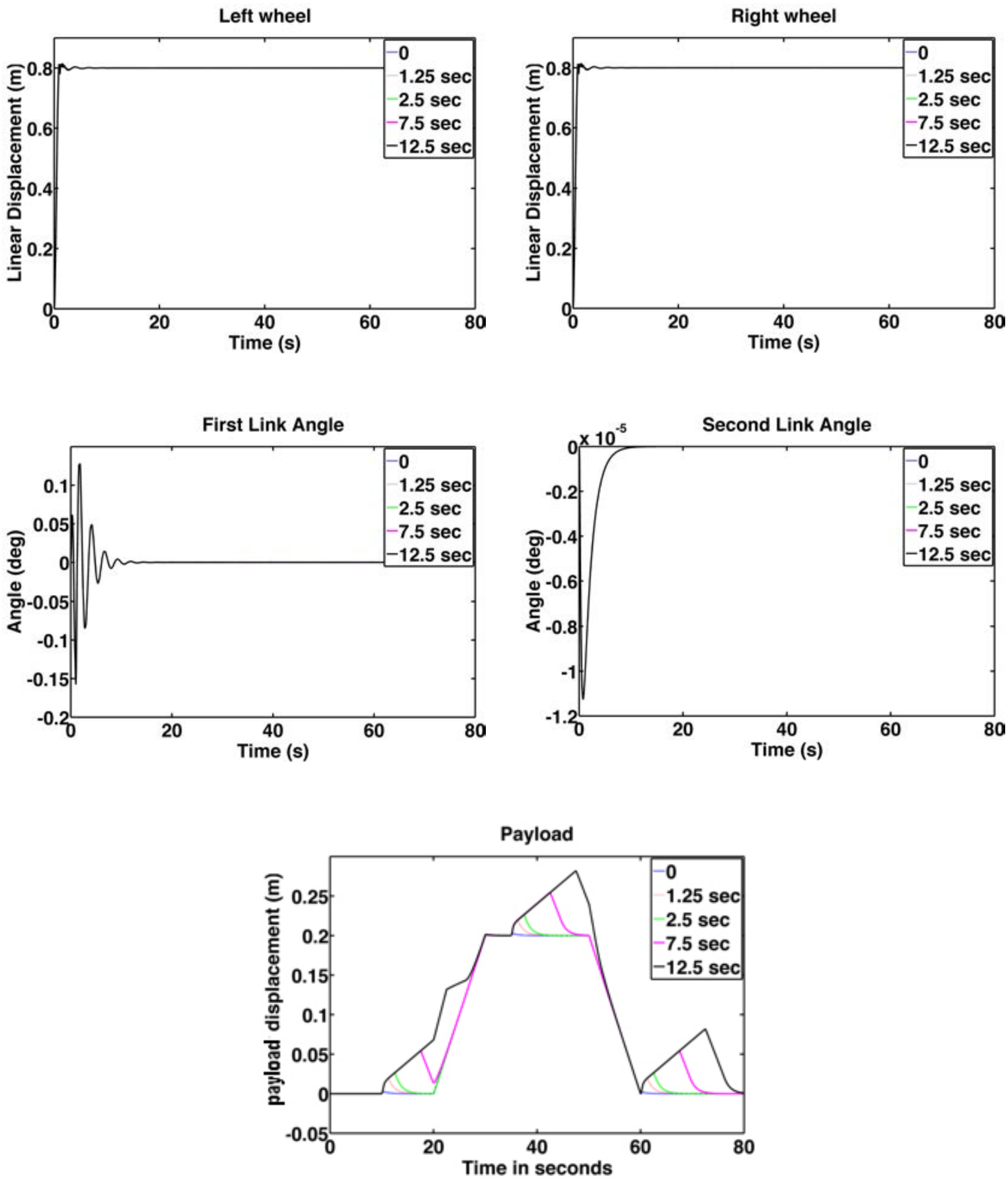

Figure 5.28: System performance with disturbances applied on the payload

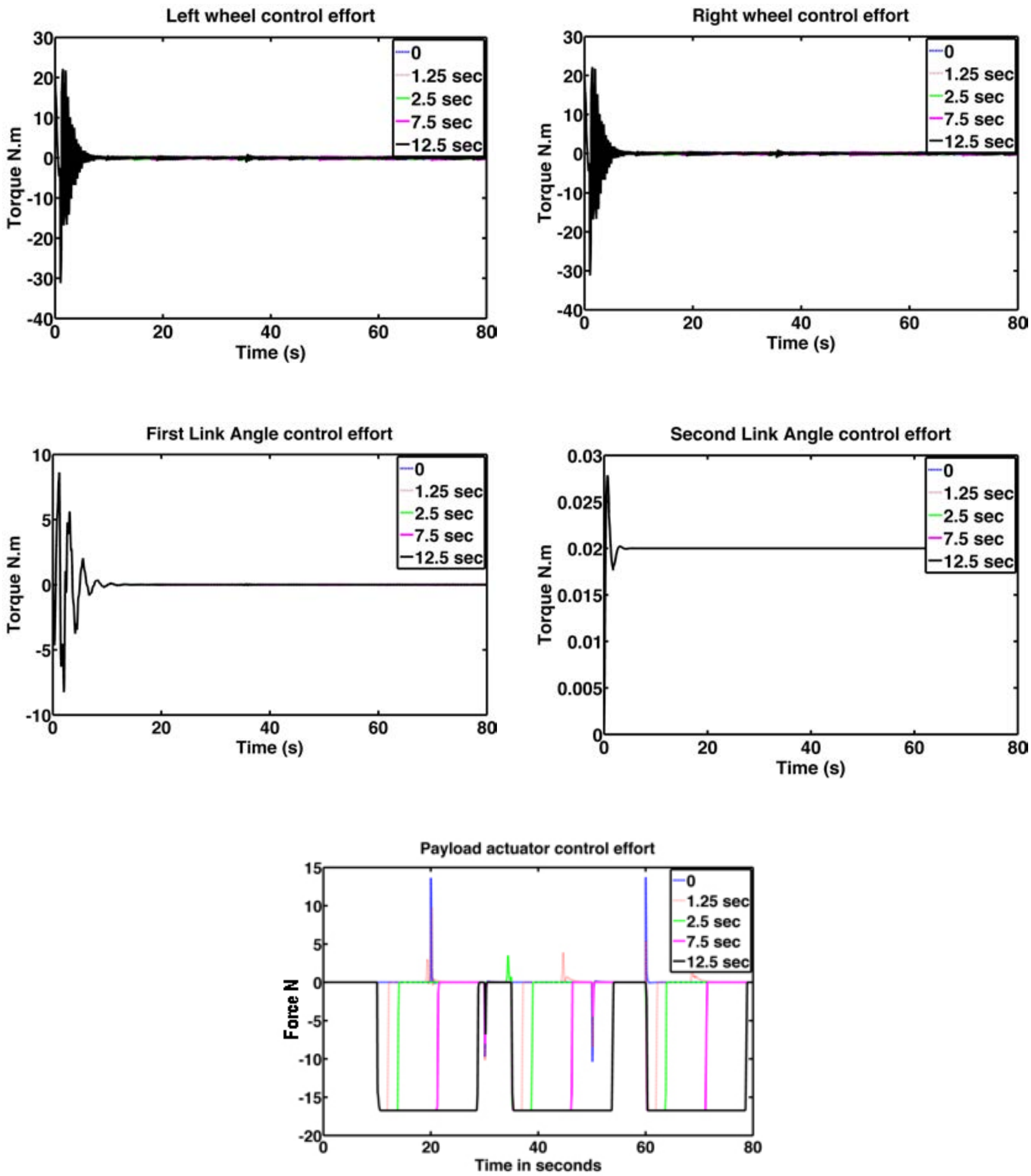

Figure 5.29: Control effort with disturbance applied on the payload

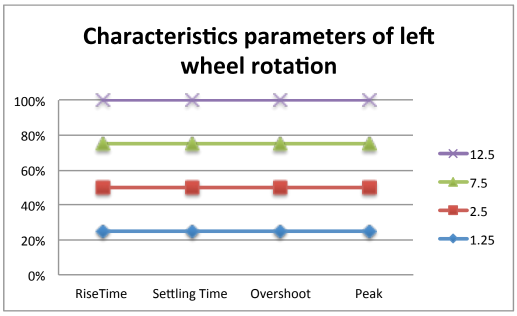

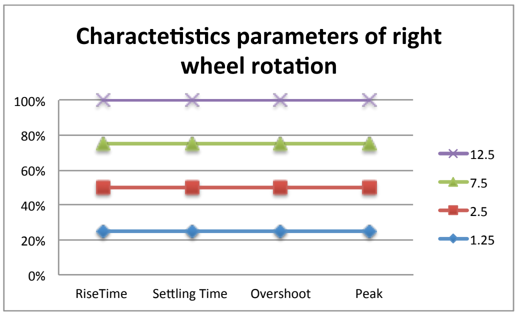

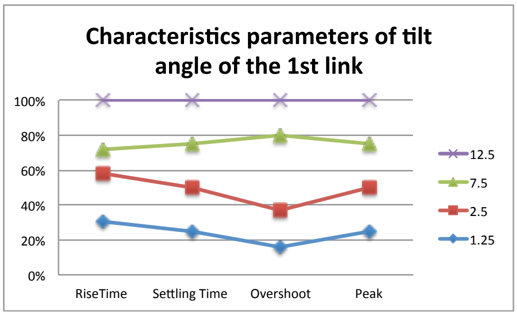

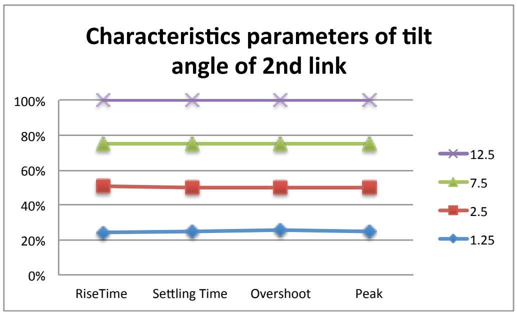

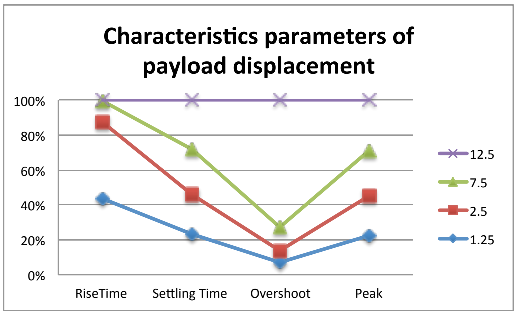

Figure 5.30: Graphical analysis of system performance characteristics with disturbances applied on the payload

5.5 Summary

The purpose of this chapter was to assess the robustness of the hybrid FLC strategy. Disturbance forces of varying amplitudes and durations were applied to the vehicle components to investigate the hybrid FLC control robustness. The result of this investigation showed that the controller is able to stabilise the vehicle and cope with various disturbances with high degree of robustness. Furthermore, it showed the limitation of the controller in stabilising the payload with applied disturbance duration of 7.5 seconds and above. One of the weaknesses of this robustness analysis approach is that the disturbance force is applied on one component at a time. A more comprehensive analysis approach is needed to study the vehicle behaviour. In subsequent chapters, more realistic movement and steering scenarios in different environments will be carried out to demonstrate the control system robustness.

Chapter 6
Vehicle Steering and manoeuvring in different environments

6.1 Introduction

One of the main objectives of this research is to develop a vehicle that is able to manoeuvre on irregular surfaces and environments. It is of utmost importance for the developed vehicle to have steering ability in order to achieve this objective. In this chapter, a steering mechanism is developed for the vehicle and tested on different simulated indoor and outdoor environments. The vehicle is tested to drive on both indoor flat and outdoor irregular surfaces with different friction profiles. These simulations are carried out to mimic real life movements and steering scenarios. Thus ensuring the robustness of the controller and to prove the efficiency of the developed vehicle to adapt to different environments.

6.2 Differential steering

Differential steering is a steering mechanism that is commonly used in robotics (Bekey, 2005; Özgüner, 2011; Siegwart, 2004). This is explained by its simple structure and ease of implementation. Differential steering requires two independent motors with variable speed to drive and steer the vehicle. Movements and turns can be achieved by manipulating the speed of each motor to achieve a certain steering scenario. Thus for a straight line drive, the motors would require two equal inputs in the same direction. For a left or right turn, only one motor is required to operate and rotate the vehicle to the desired yaw angle. While for a curvilinear motion, the motors require two different rotational speeds and the vehicle moves inward toward the slower wheel. The yaw angle of the vehicle is measured from the vertical z-axis as illustrated in Figure 6.1

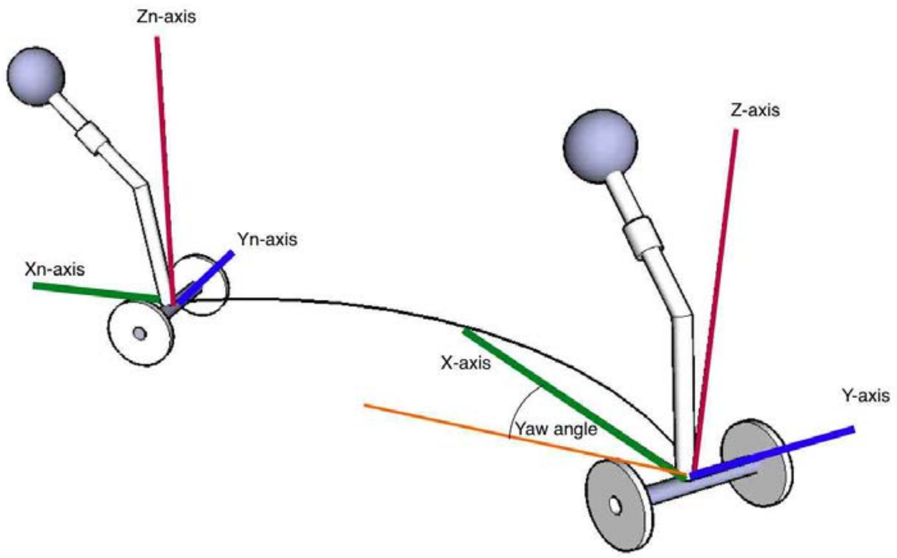

Figure 6.1: vehicle steering in a curvilinear motion

6.3 Robot navigation and position tracking

It is essential to be able to measure the position and yaw angle of the vehicle to define the trajectory of the vehicle. Odometry is a method used for tracking a robot position and defining its heading angle (Borenstein, 1996). Tracking the position and defining the heading angle is simply achieved by reading the incremental motion information over the time of motion. To locate the robot position, instantaneous travel distances for each wheel must be determined. Let s_R and s_L be the travel distances for the right and left wheels respectively. Then the total vehicle travel distance can be written as:

$$\overline{s} = \frac{(s_R + s_L)}{2} \tag{6.1}$$

Hence, the yaw or heading angle of the vehicle is defined as:

$$\phi = \frac{(s_R - s_L)}{b} + \phi_o \tag{6.2}$$

Where b is the wheelbase length of the vehicle and ϕ_o is the current heading angle of the vehicle. By calculating the total travel distance vector and the yaw angle of the vehicle, the x and y coordinates of the vehicle are the horizontal and vertical components of the distance vector and can be written as:

$$x = \overline{s}\cos(\phi) + x_o \tag{6.3}$$

$$y = \overline{s}\sin(\phi) + y_o \tag{6.4}$$

where x_o and y_o are the current coordinates of the vehicle.

To verify the calculation of the vehicle position and heading angle, the vehicle is commanded to move on a straight line for 1.5 meters. The movement simulation scenario will be as follows:

1- Allow the vehicle to balance and lift the payload to 0.2 metres within 20 seconds timeframe.
2- Travel 1.5 metres forward

Figure 6.2 illustrates responses of the vehicle components controlled with the hybrid FLC while Figure 6.3 presents the vehicle coordinates, yaw angle and travel trajectory. It can be seen that the vehicle has successfully travelled the required distance without loosing the balance of the first and second links. Some negligible fluctuations at the tilt angles of the links appeared when the vehicle started to drive forward, and this is expected. The same phenomenon was observed at the yaw angle and the y coordinate of the vehicle. The trajectory of the vehicle was not affected by these fluctuations.

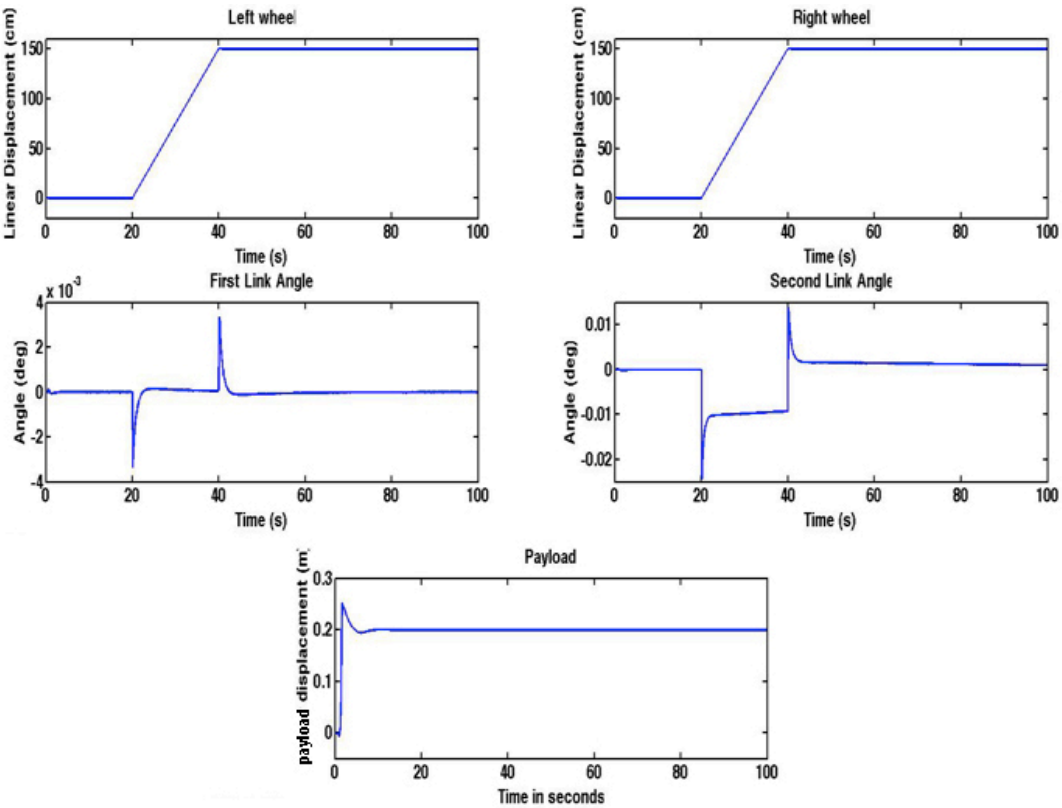

Figure 6.2: Vehicle response for straight line movement

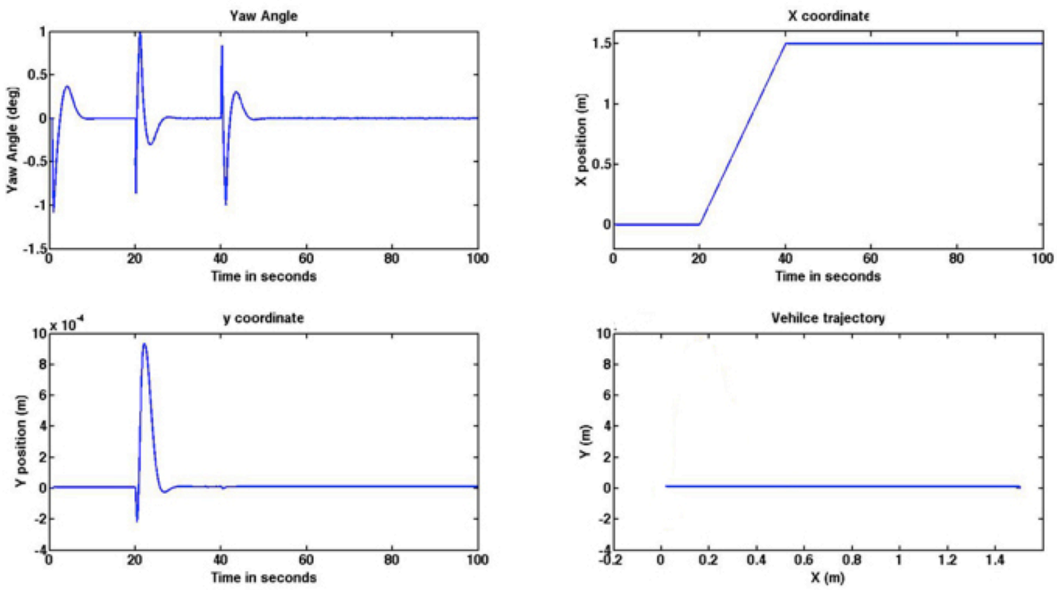

Figure 6.3: Vehicle position, yaw angle and trajectory

6.4 Indoor steering

The ability to steer and manoeuvre in confined and narrow spaces is one of the advantages of the developed vehicle. With the designed steering strategy presented in the previous section, it is important to study the vehicle behaviour in different indoor and outdoor environments. Simulations that imitate real life steering scenarios are needed. In this section, a case study of the vehicle steering in a super market is presented. This example should highlight the vehicle's ability to steer in confined and restricted areas consisting of straight lines and turns.

However, this scenario has some limitations. One of the limitations is that the surface is assumed to be almost frictionless. Moreover, the surface is assumed to be flat with angle of zero degrees inclination. These limitations need to be investigated further by more challenging real-life situations to analyse the vehicle response and robustness of the controller in controlling the vehicle components. Such analyses are presented in upcoming sections of this chapter. The supermarket 3D schematic and top view plan are illustrated in Figures 6.4 and 6.5 respectively. The supermarket has a narrow entrance and limited spaces between shelves. A simple movement scenario is illustrated in Figure 6.6.

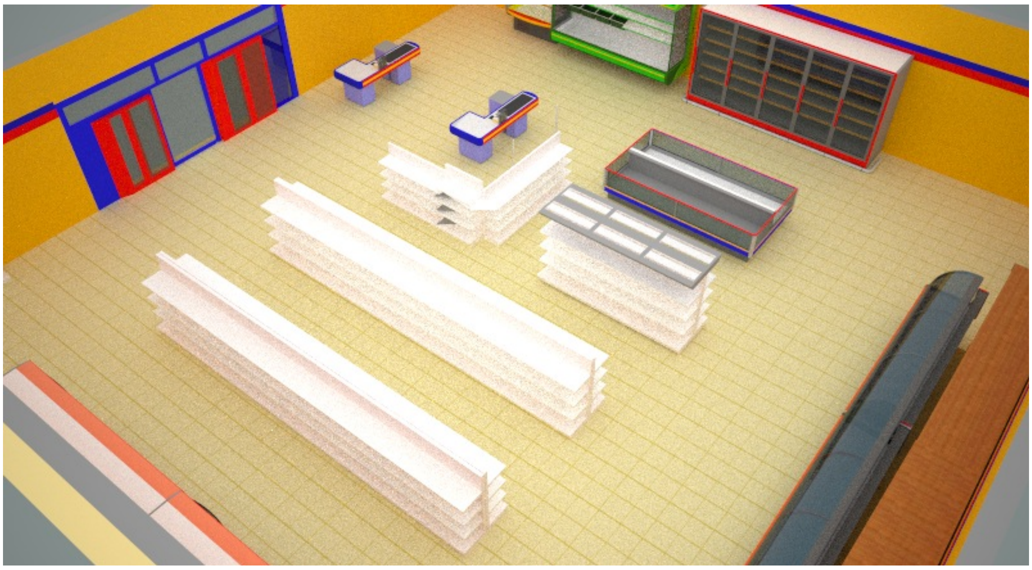

Figure 6.4: Schematic diagram of a mini market

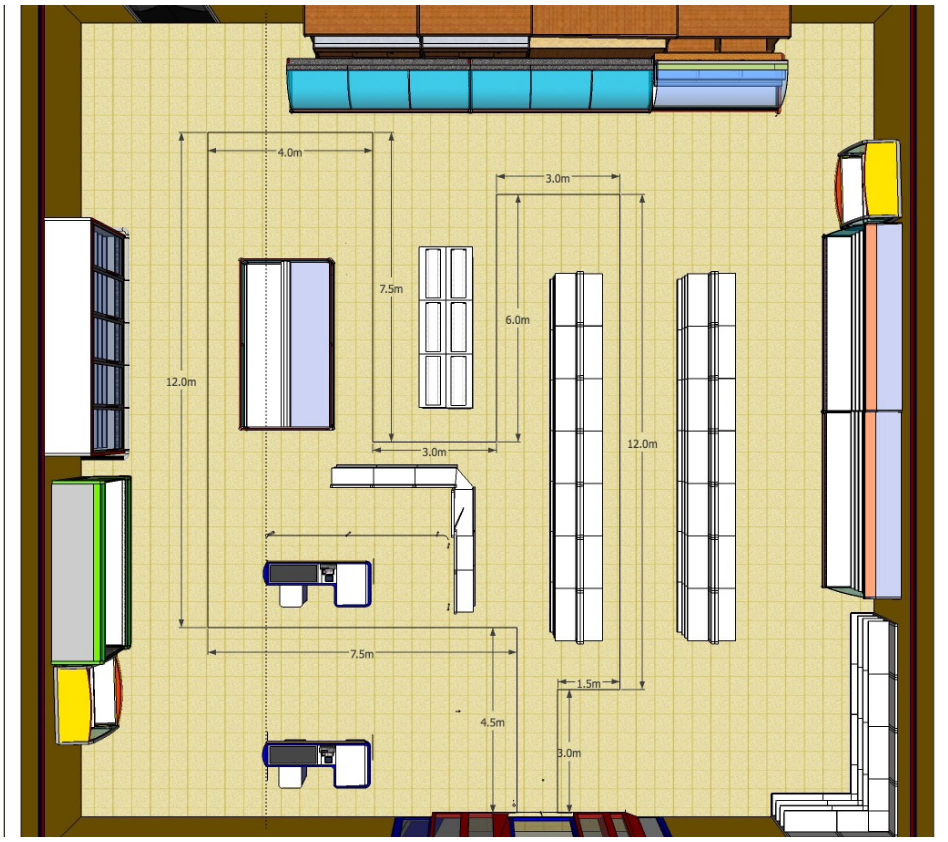

Figure 6.5: Plan top view of a mini market

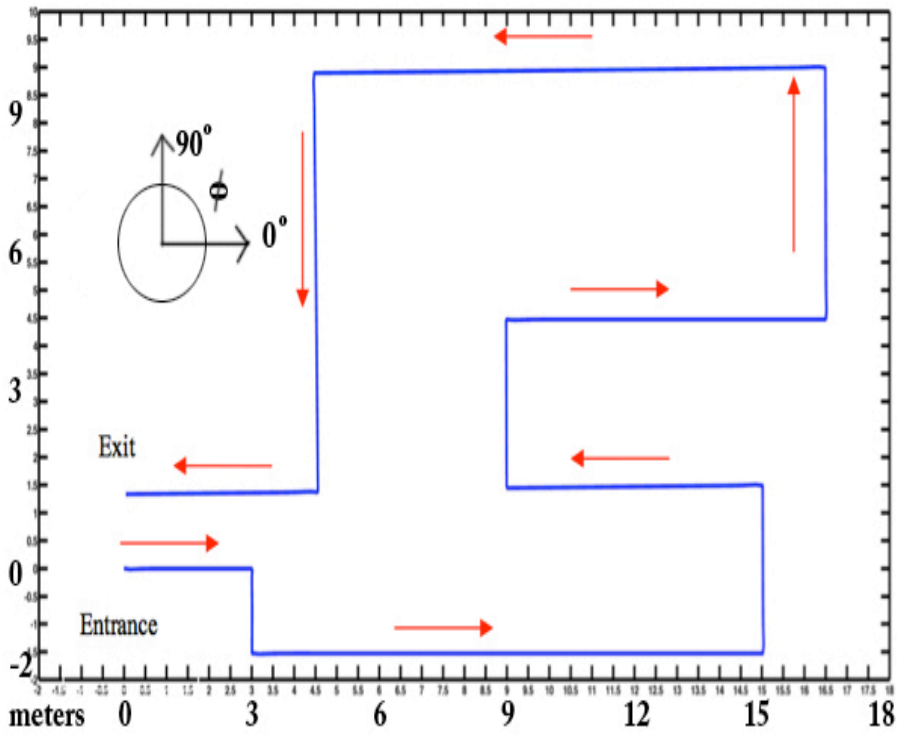

Figure 6.6: Detailed trajectory of the vehicle motion

Referring to Figure 6.7, it can be clearly observed that the vehicle was able to track the planned steering movement with the exact yaw angle at turn points. In Figure 6.8, it can be noted that the controller successfully preserved the balance of vehicle components while undergoing the planned movement scenario with a total travel distance of 64 meters. Small fluctuations appearing at the first and second link response can be observed. These fluctuations were due to the sudden sharp turns at the turn points of the trajectory. As a consequence; the exerted control effort and angular velocities were affected in the same manner. The payload response was not affected by these fluctuations and remained stable. Figure 6.9 illustrates the velocity of each component of the vehicle. While Figure 6.10 presents the control effort exerted to stabilise the vehicle system.

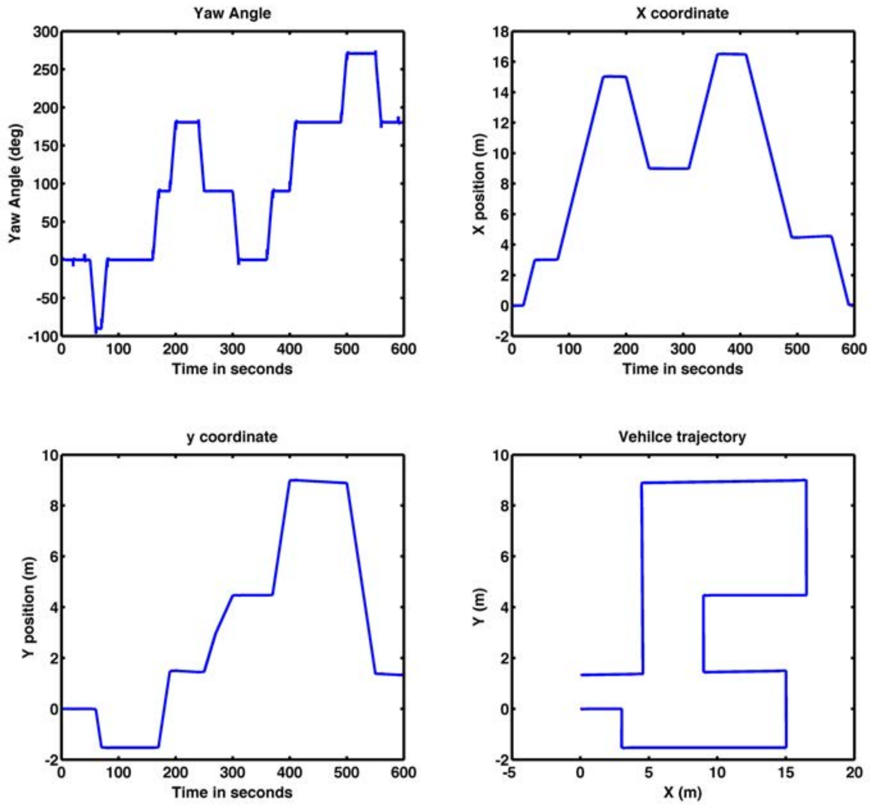

Figure 6.7: Steering motion of the vehicle in a supermarket

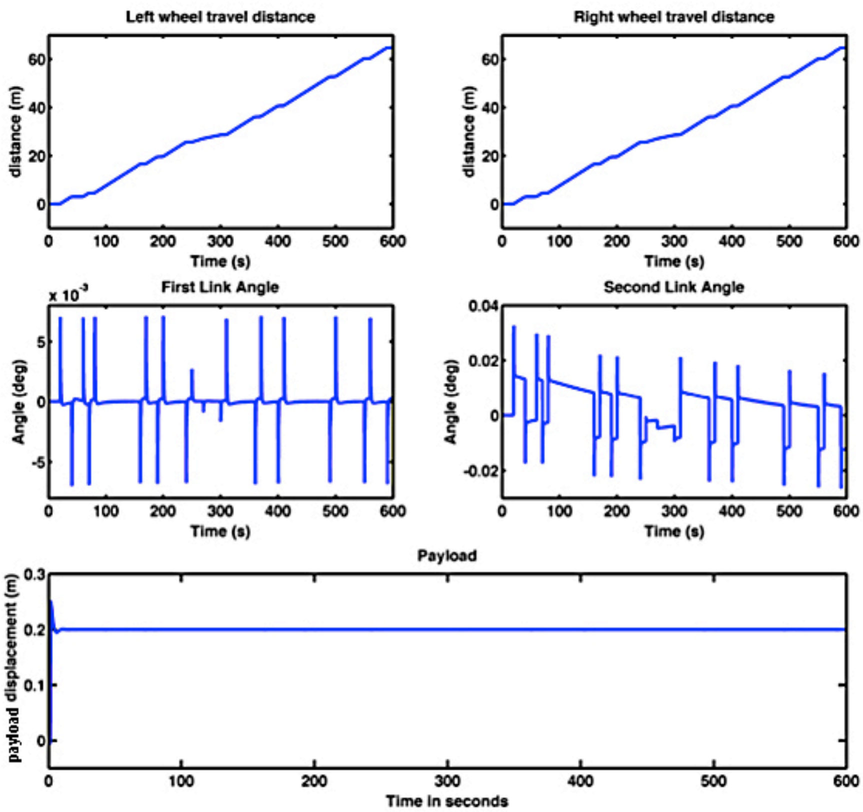

Figure 6.8: Displacements of the vehicle main components in a supermarket

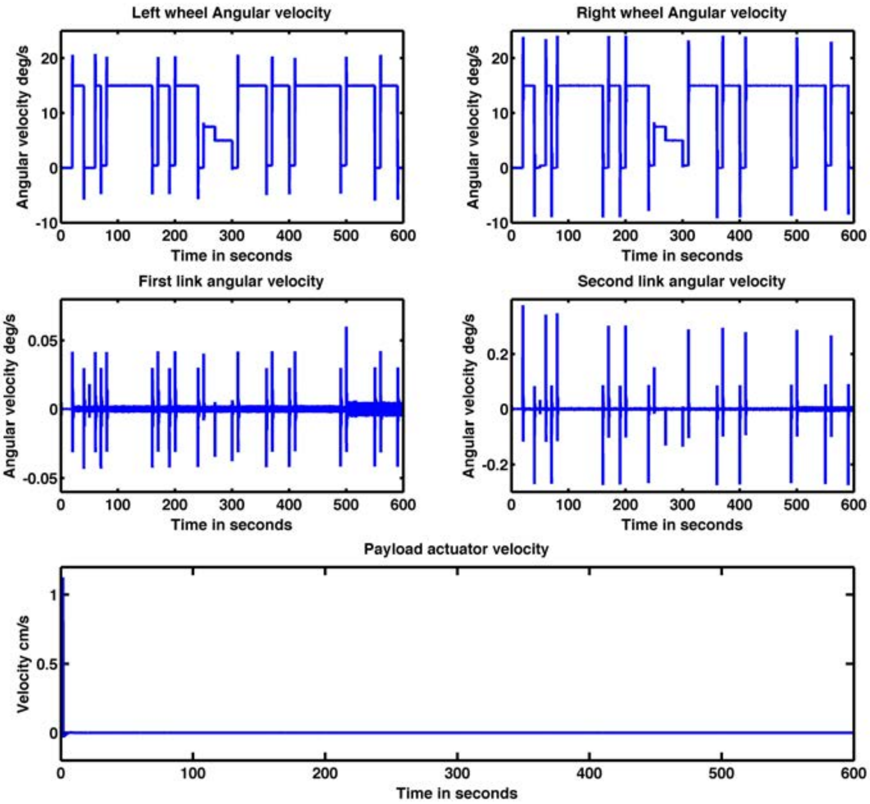

Figure 6.9: Velocities of the vehicle main components in a supermarket

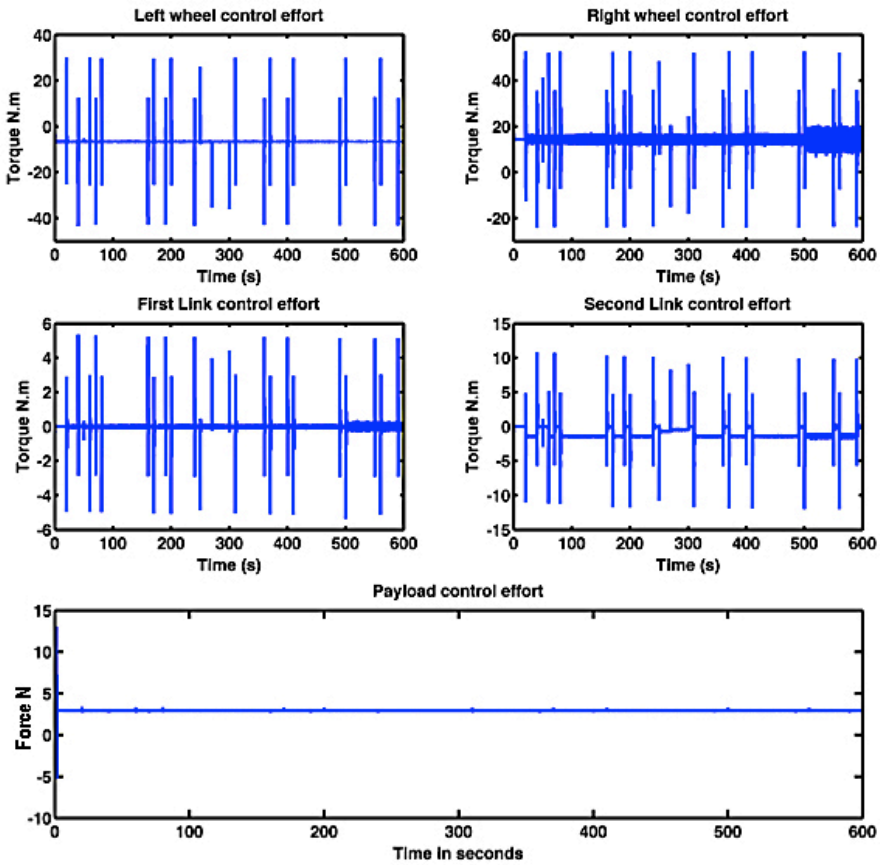

Figure 6.10: Control effort exerted by the vehicle actuators in a supermarket

6.5 Modelling environments with different friction and terrain profiles

To simulate the vehicle in outdoor environments and test its ability to steer on different friction profiles, environment modelling must be integrated into the simulation blocks. The aim is to be able to model various terrains and environment friction profiles that are close to real life environments. Environment modelling is based on study of soil mechanics and was reported in literature, specifically in locomotion systems, by many researchers to enable them to study the foot-ground interaction forces (Bekker, 1969; Hunt and Crossley, 1975; Manko, 1992; Silva et al, 2005; Suvinen et al., 2003). Silva et al. (2005) have used a modified spring-damper dashpot system to simulate different types of grounds to study the foot-ground interaction for locomotion systems. They have presented the modification by changing the parameters of damping and stiffness *B* and *K* respectively for both horizontal and vertical deflection forces. The contact of the foot and ground can be described by the nonlinear equations:

$$f_{i\eta F} = -K_{\eta F}(\eta_{iF} - \eta_{iF0}) - B^{`}_{\eta F}[-(y_{iF} - y_{iF0})]^{v_n}(\dot{\eta}_{iF} - \dot{\eta}_{iF0}) \tag{6.5}$$

$$-B^{`}_{\eta F}(-\Delta_{iyFMax})^{v_\eta} = -B_{nF} \tag{6.6}$$

where

$K_{\eta F}$ = Linear stiffness factor

$B^{`}_{\eta F}$ = Nonlinear damping factor

η = Directions in x and y

x_{if0}, y_{if0} = Coordinates of the wheel-ground touchdown

v_η = A parameter dependent on ground characteristics with $0.9 < v_\eta < 1.0$

Δ_{iyFMax} = Maximum penetration depth of wheel into ground

The linear damping and stiffness parameter values for different ground profiles, extracted from soil mechanics and Young's modulus of elasticity of different soil types reported by Suvinen et al., 2003 are presented in Table 6.1.

Table 6.1 linear damping and stiffness parameter values for different ground profiles

Soil type	K_{xF} (Nm^{-1})	B_{xF} (Nsm^{-1})	K_{yF} (Nm^{-1})	B_{xF} (Nsm^{-1})
Concrete	2604304130	153097	3410398265	175196
Gravel	17362028	12500	22735988	14305
Sand	6944811	7906	9094395	9047
Clay	260430	1531	341040	1752
Peat	43405	625	56840	715

Integrating the damping and stiffness factors of Table 6.1 into equations 6.5-6.6 would result in different environment blocks describing the interaction between the different soil types with the vehicle wheels. The environment block was built in the Matlab Simulink and was incorporated into the main vehicle model. In the next sections, the vehicle will be simulated to drive on various environments to prove the steering ability and demonstrate the efficiency of the vehicle. First, the vehicle will be simulated to drive on flat surfaces of different environments. Followed by simulations on inclined surfaces of different environments and finally a case study of Golf course will be presented combining irregular terrains with diverse environments.

6.6 Steering outdoor on flat surfaces of different environments

The developed model is tested in this section while performing various steering exercises on different outdoor terrains. The vehicle is simulated to move on a flat and frictionless surface with random trajectory to be used as a reference to compare with other environments. Moreover, this reference will assist in analysing the performance of the vehicle, when compared to, moving on terrains that have rough surfaces and disturbance profiles. Two soil types, peat and gravel, are chosen as environment profiles in this section to investigate the stability of the vehicle on two contrastive profiles. Other soil types will be used later in the golf course case study.

Simulation results are investigated in terms of the performance of the system including the yaw steering angle, the control effort exerted by the vehicle actuators and the disturbance forces exerted by each type of the suggested terrain.

Figures 6.11 and 6.12 represent the vehicle reference trajectory and the vehicle response respectively. In the reference trajectory, the stabilization of the system is the main concern; the yaw angle is kept fixed for the first 20 seconds, then a dynamic change of the yaw angle is considered as shown in Figure 6.11.

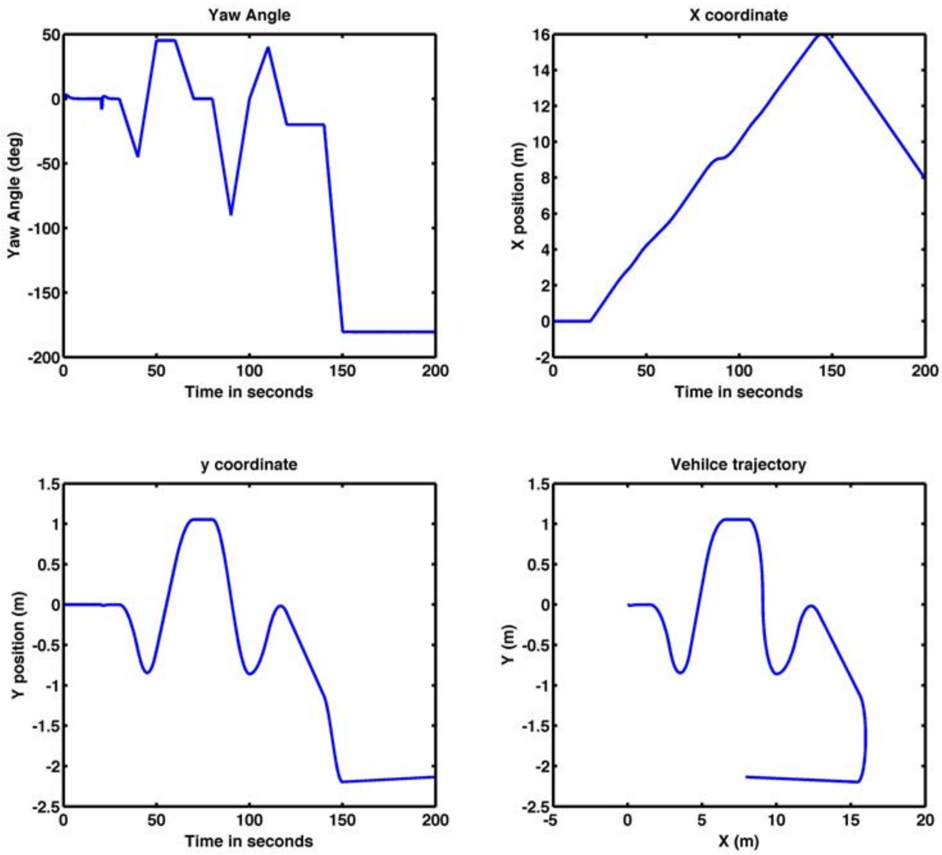

Figure 6.11: Steering motion of the vehicle on flat frictionless reference trajectory

The displacements and velocities of vehicle components are presented in Figures 6.12 and 6.13. The vehicle was set to move a total distance of around 25 meters for the entire reference trajectory. It is clear that the developed control algorithm has demonstrated high degree of robustness in terms of its ability to compensate for the repetitive sudden changes of the yaw angle. This is clearly shown in Figure 6.14 where all control components are identified for the entire course. As can be noticed from the same figure; the control effort exerted by the linear actuator was not affected by the change in the yaw angle while manoeuvring on a non-frictional flat surface. In the next two sections; the vehicle will be tested while manoeuvring on two types of floors; Peat and Gravel.

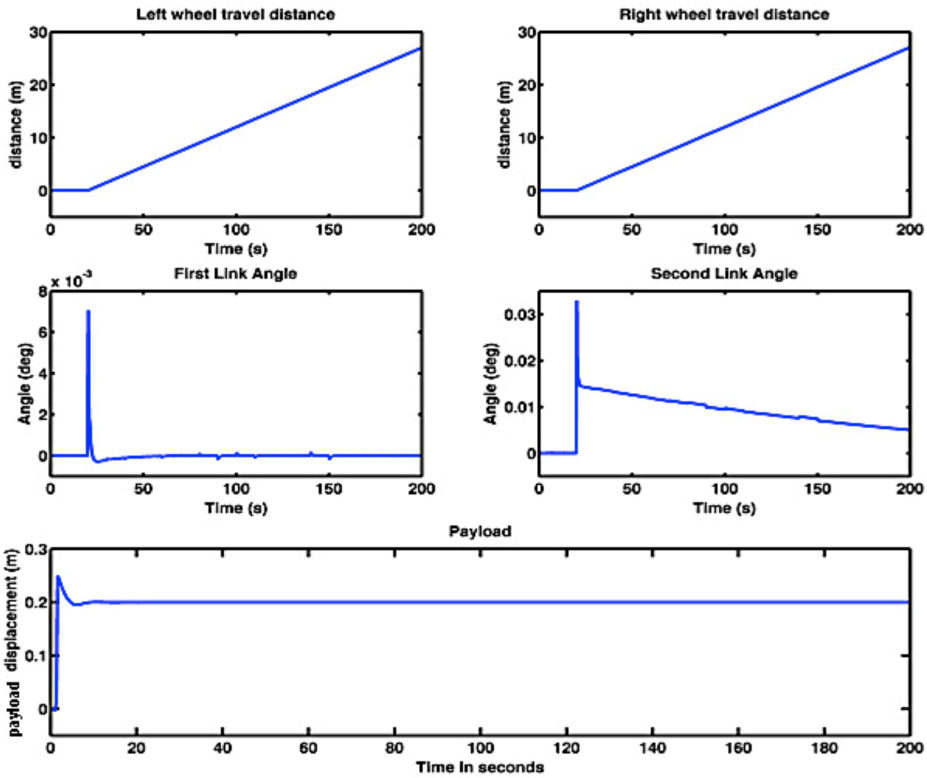

Figure 6.12: Displacements of the vehicle main components on flat frictionless surface

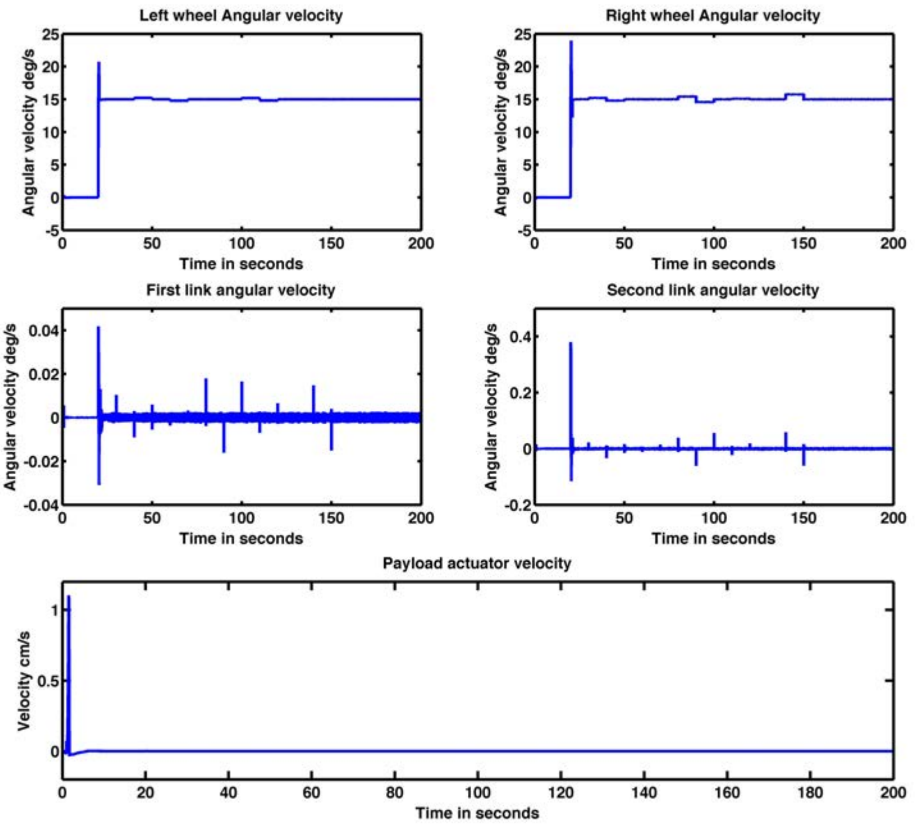

Figure 6.13: Velocities of the vehicle main components on flat frictionless surface

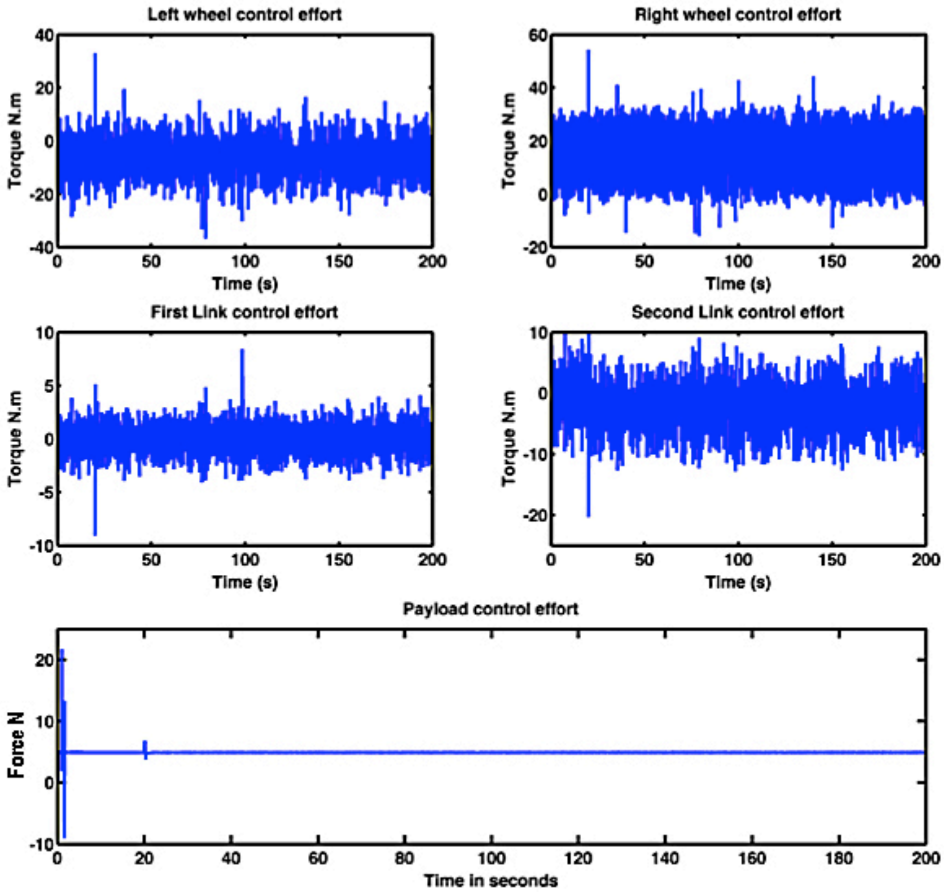

Figure 6.14: Control effort exerted by the vehicle actuators on flat frictionless surface

6.6.1 Flat peat ground

Using the environment block developed in Simulink, a peat ground was modelled with the ground profile shown in Figure 6.15. The ground profile illustrates the horizontal and vertical interaction forces between the wheels of the vehicle and the ground. The ground profile is of high frequency that describes continuous distributed friction. The peat ground profile was integrated into the vehicle system to simulate the steering scenario. The vehicle was commanded to track the reference trajectory described in section 6.6 on peat ground. Figures 6.16 and 6.17 show the trajectory tracking and the vehicle component response respectively. As noted, the vehicle successfully tracked the reference trajectory very well. In Figure 6.17, very small oscillations are noted at the link tilt angles and payload actuator displacement. These oscillations were expected due to the irregularity of the ground. However, these have not affected the overall balance of the vehicle.

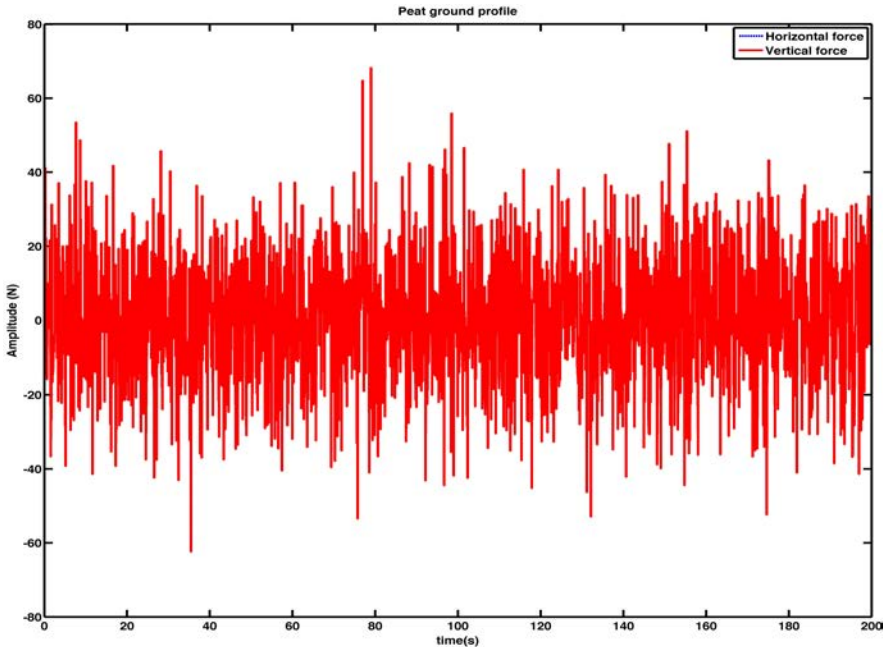

Figure 6.15: Ground profile of a peat ground

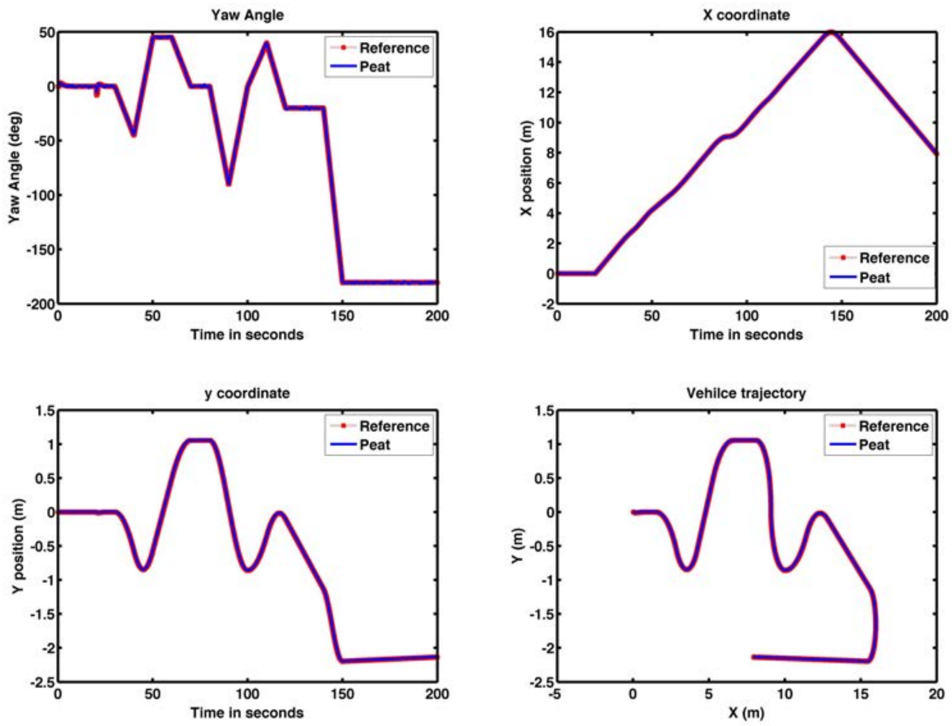

Figure 6.16: Steering motion of the vehicle on flat peat ground

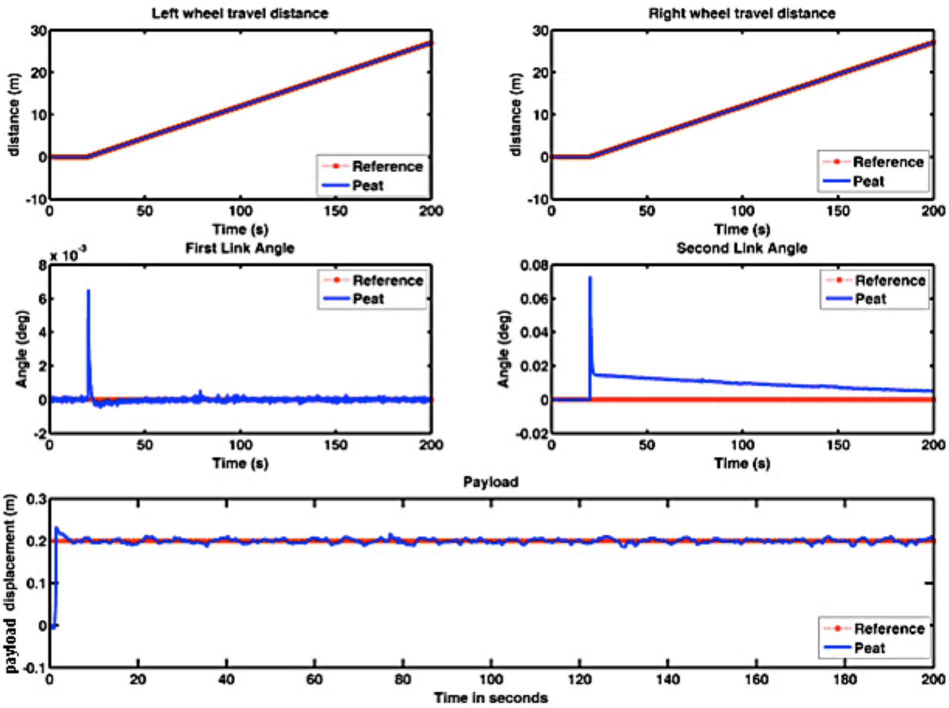

Figure 6.17: Displacements of the vehicle main components on flat peat ground

Figures 6.18 and 6.19 show the velocities and control effort of the vehicle components respectively. Continuous control effort with high frequency is noted to react to the ground frictional interaction and maintain the balance of the vehicle. Velocities of the vehicle components were affected accordingly with control effort. The overall system was stable with good performance in tracking the reference trajectory signal and in terms of the vehicle component response.

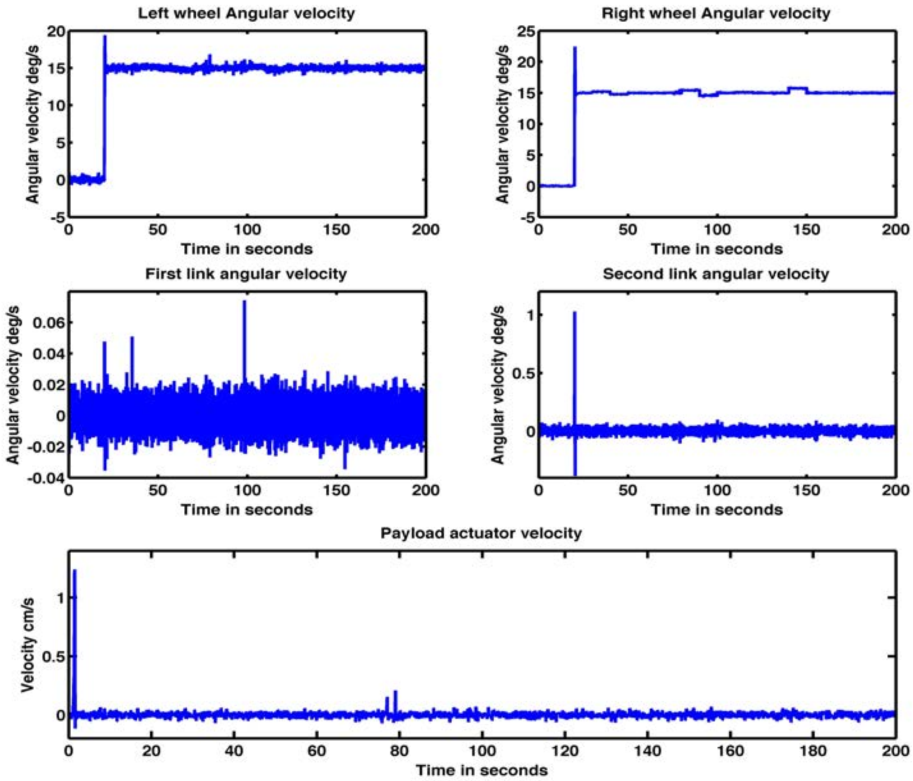

Figure 6.18: Displacements of the vehicle main components on flat peat ground

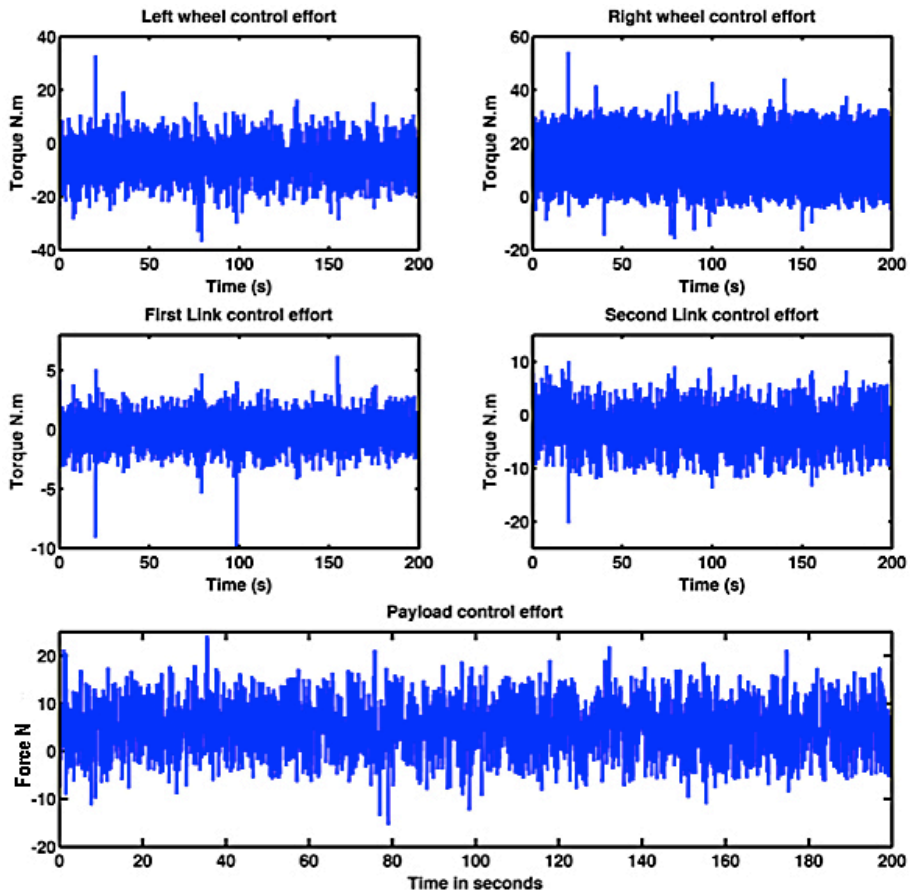

Figure 6.19: Control effort exerted by the vehicle actuators on flat peat ground

6.6.2 Flat gravel surface

In a similar approach as above, the vehicle was simulated to move on a flat gravel ground. The gravel soil is harder than peat and has a higher frictional force profile, as shown in Figure 6.20.

The trajectories on gravel and component responses are presented in Figures 6.21 and 6.22 respectively. As noted, the vehicle was able to steer successfully and follow the reference trajectory with some negligible oscillations mainly at the yaw angle. Although the overall system performance was similar to the performance of the vehicle on peat ground, differences are observed in the amount of control effort and vehicle component velocities. These differences can be highlighted by the minor increase in velocities and control effort in Figures 6.23 and 6.24. The payload required more control effort to be stabilised on gravel than on peat. This can be explained by the fact that gravel has a harder surface that causes vibrations on the vehicle more than the peat, as noted in the vehicle component responses.

With the current promising performance of the vehicle on two grounds of contrastive nature, it is encouraging to test the vehicle in a more complex steering scenario. In order to analyse the performance in a rigorous manner and to be able to understand the behaviour of the vehicle on different grounds, the vehicle will be tested on inclined slopes of peat and gravel with different grades of inclination. More complex steering simulations will be performed on the vehicle and presented later in this chapter.

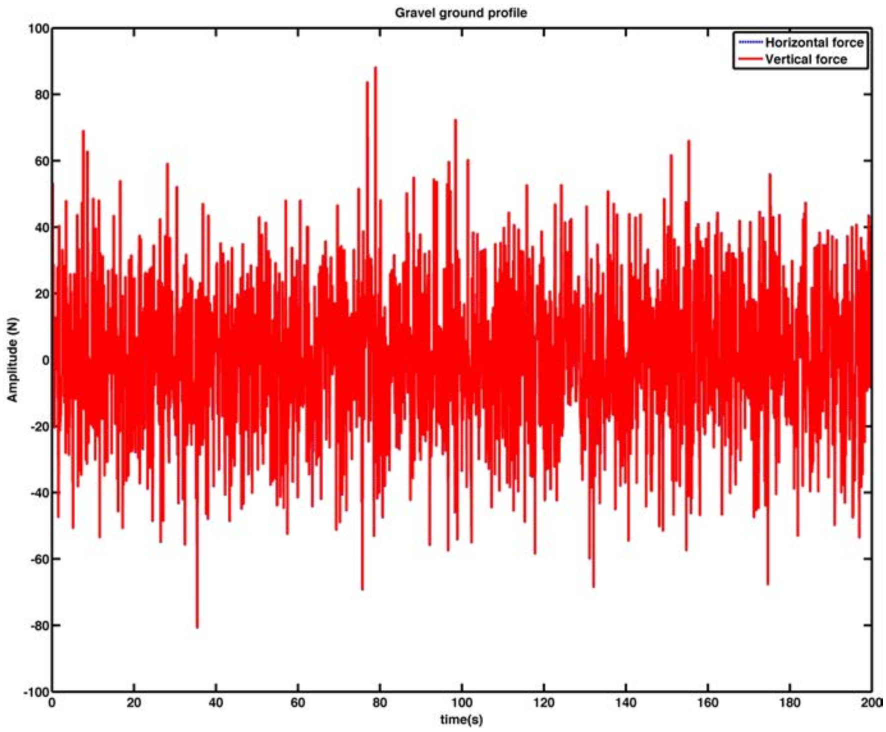

Figure 6.20: Ground profile of a gravel ground

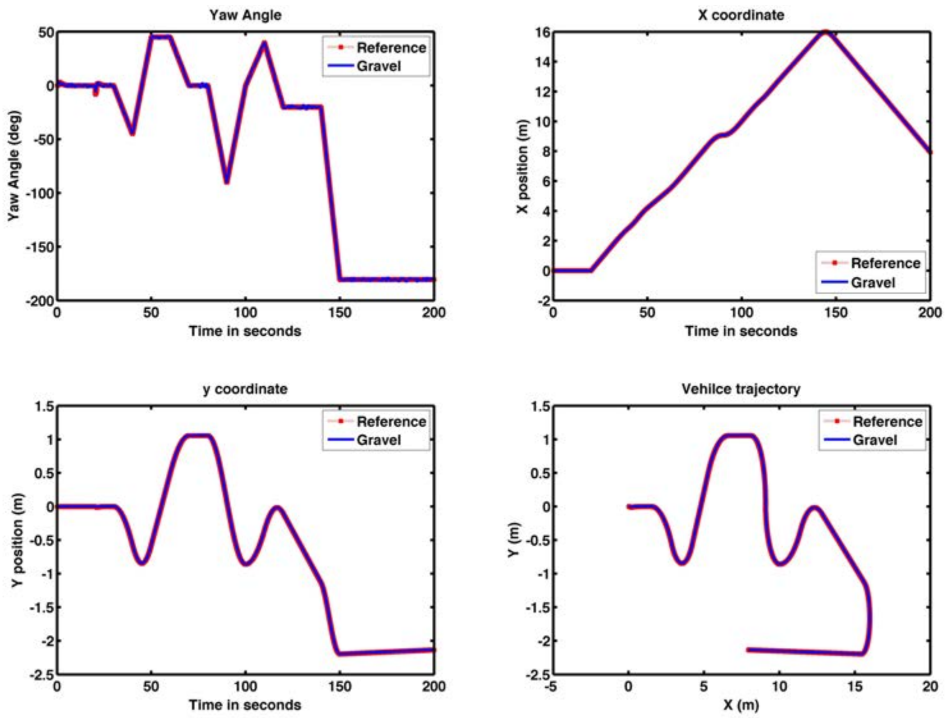

Figure 6.21: Steering motion of the vehicle on gravel ground

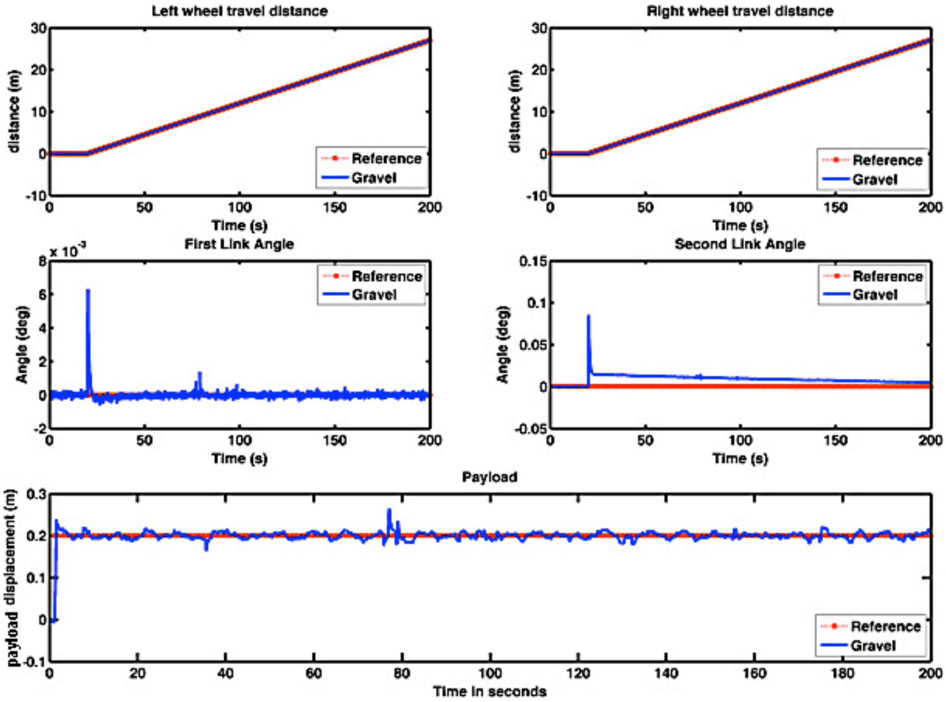

Figure 6.22: Displacements of the vehicle main components on gravel ground

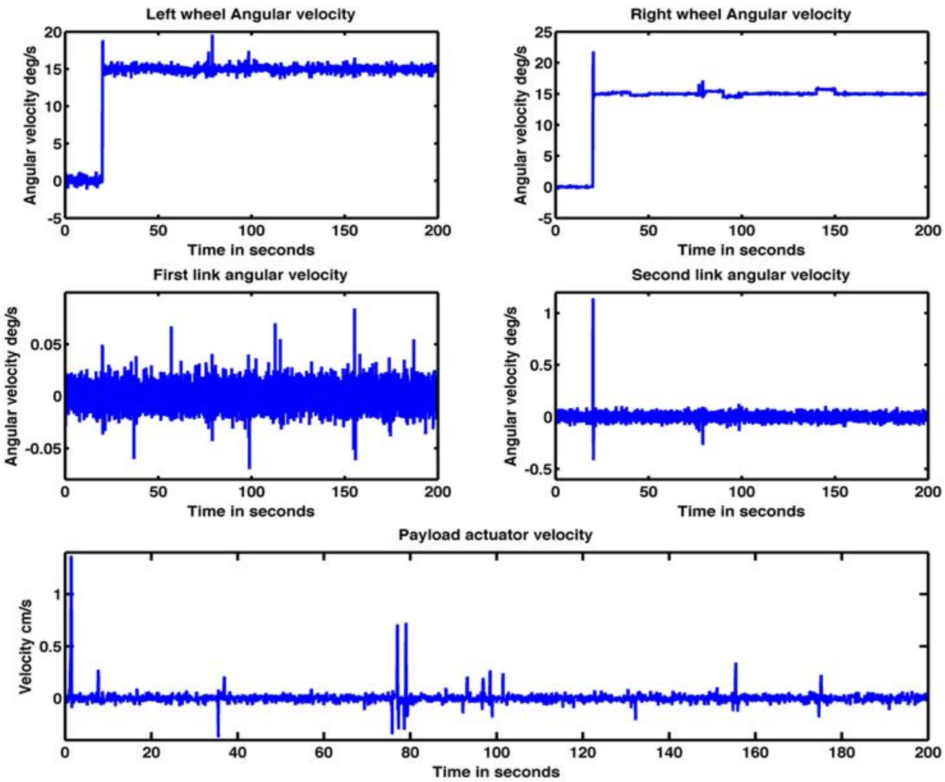

Figure 6.23: Velocities of the vehicle main components on gravel ground

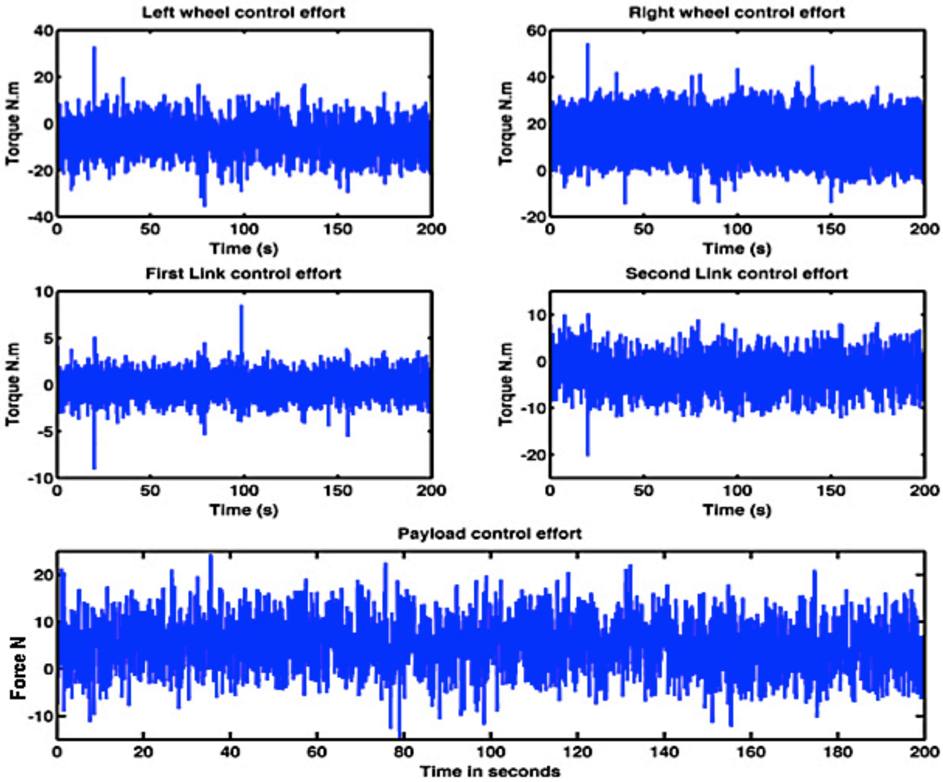

Figure 6.24: Control effort exerted by the vehicle actuators on gravel ground

6.7 Steering on an inclined surface

This section investigates the dynamic performance of the vehicle in manoeuvring on inclined surfaces with different slopes. In highway and civil engineering, sloped roads are defined as gradients. Pathak and Gite (2009) define the gradient as "the rise or fall given to the road pavement in it's longitudinal section". Gradients or grades of the roads are expressed as percentages rather than degrees. Figure 6.25 defines the grades and equivalent slopes in degrees. In this section, two grade values are considered in the simulation of the vehicle. For each grade, peat and gravel environments will be simulated accordingly to have a comparative overview with the vehicle performance on flat surfaces of similar ground profiles. Grades of 20% and 50% are chosen to have contrastive tests. Higher-grade values and dynamic change in grades will be considered later in this chapter.

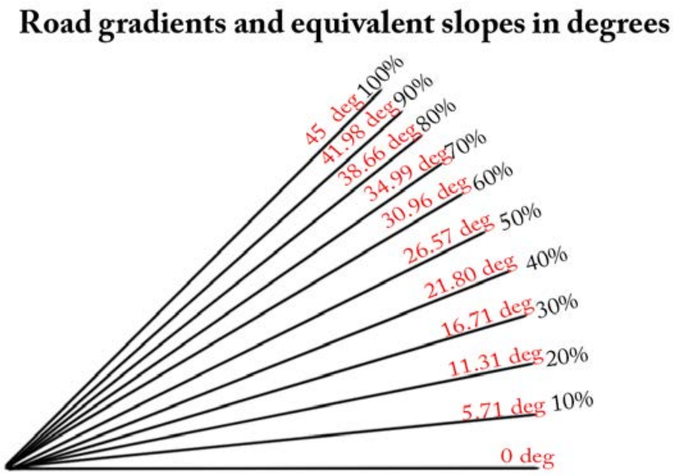

Figure 6.25: Standard grades of inclined surfaces

6.7.1 Inclined surfaces of 20% grade (11.31 deg)

6.7.1.1 Peat Inclined surface of 20% grade

The vehicle model was simulated on a peat ground with a gradient of 20%. The vehicle response on inclined surfaces will be compared against the vehicle response on flat surface to measure the affect of the surface inclination. Figure 6.26 presents the vehicle trajectory and coordinates and Figure 6.27 presents the vehicle components responses. As noted, the vehicle was able to follow the trajectory while preserving the balance of the links and payload. Velocities of the vehicle components are shown in Figure 6.28. Large velocities were observed when compared to the velocities of the vehicle steering on flat peat ground. As a result, the control effort were increased significantly as clearly noted in Figure 6.29. This increase can be explained by the fact that the vehicle must exert more effort to drive on an inclined surface.

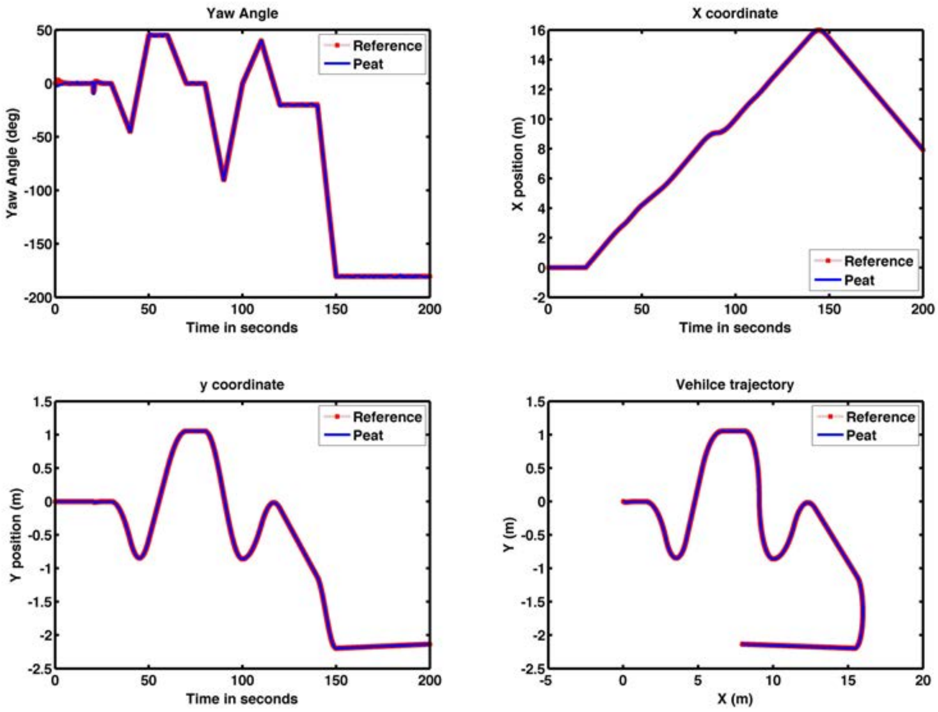

Figure 6.26: Steering motion of the vehicle on peat ground of 20% grade

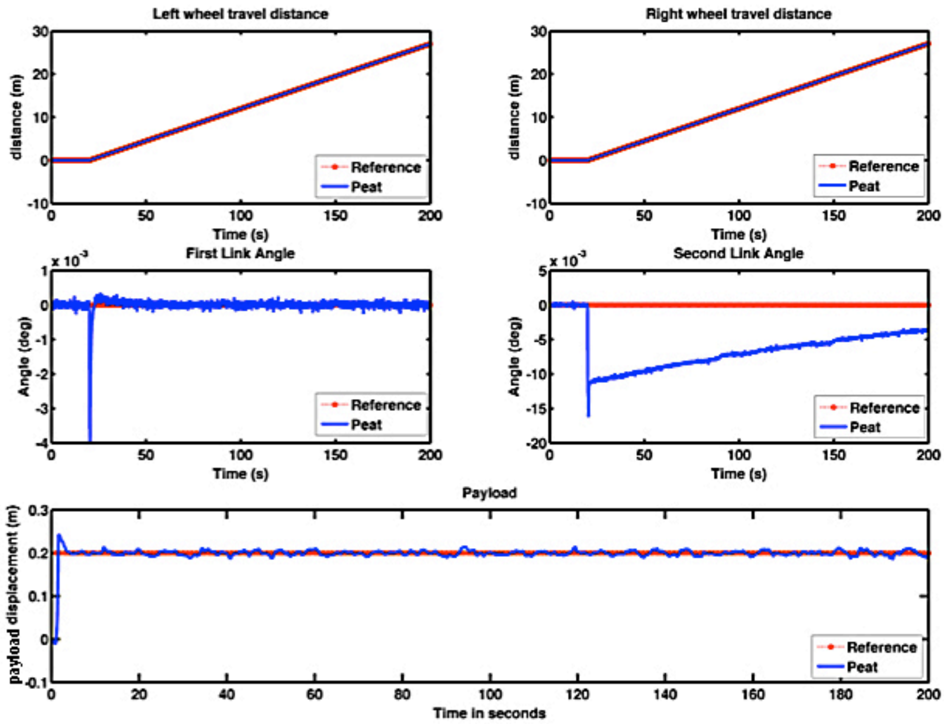

Figure 6.27: Displacement of the vehicle main components on peat ground of 20% grade

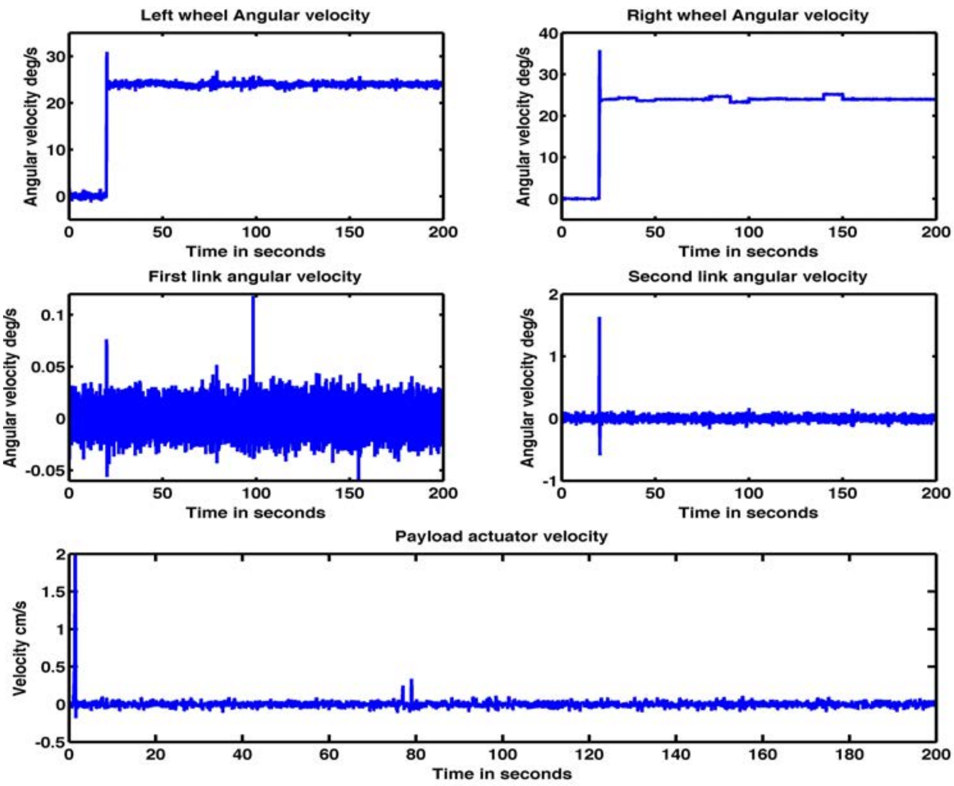

Figure 6.28: Velocities of the vehicle main components on peat ground of 20% grade

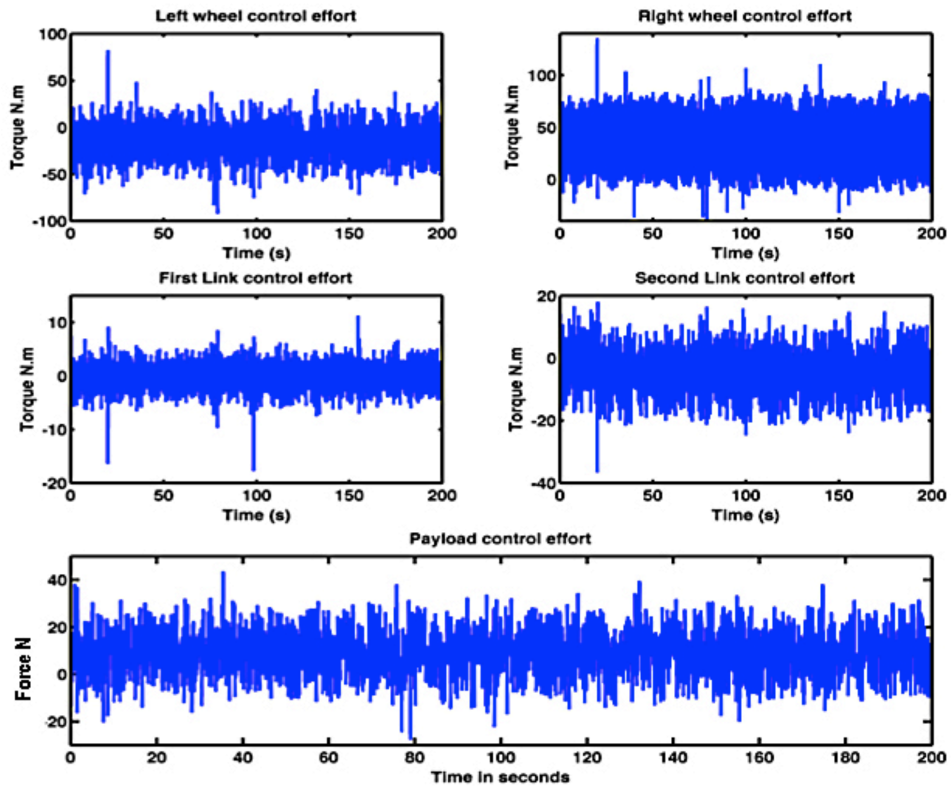

Figure 6.29: Control effort exerted by the vehicle actuators on peat ground of 20% grade

6.7.1.2 Gravel Inclined surface of 20% grade

The simulation of steering scenario on a gravel ground of 20% is presented in this section. Figures 6.30 and 6.31 illustrate the vehicle trajectory and response respectively. Compared to the response of the vehicle on flat gravel ground, a negligible increase in the oscillations at the vehicle response was noted without affecting the vehicle trajectory and balance. On the contrary, a significant increase was noted at the velocities and control effort exerted as observed in Figures 6.32 and 6.33 respectively.

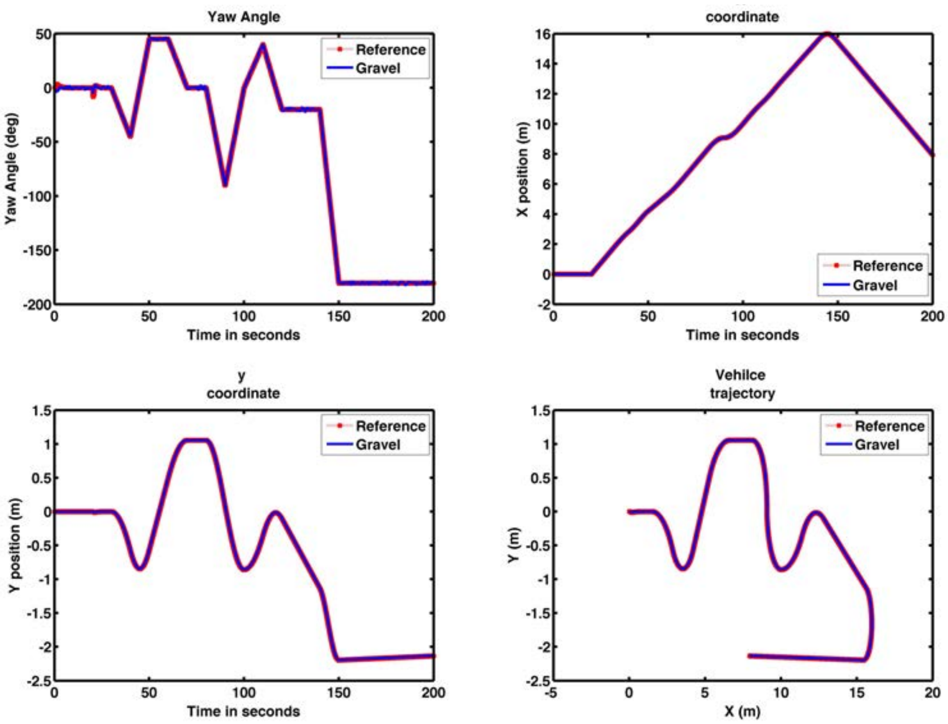

Figure 6.30: Steering motion of the vehicle on gravel ground of 20% grade

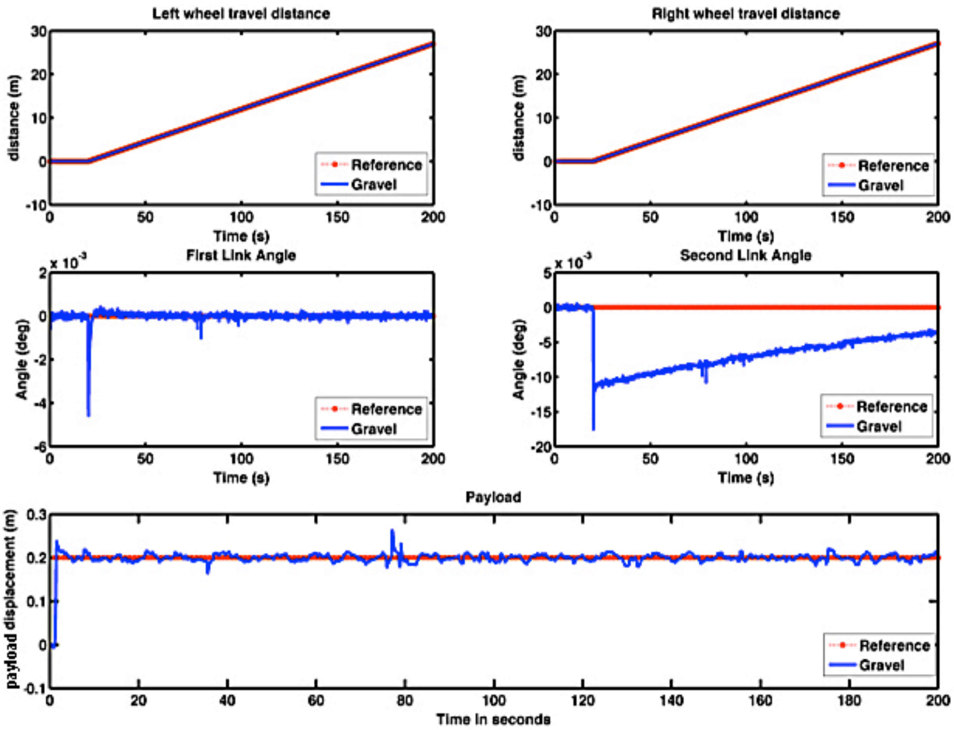

Figure 6.31: Displacements of the vehicle main components on gravel ground of 20% grade

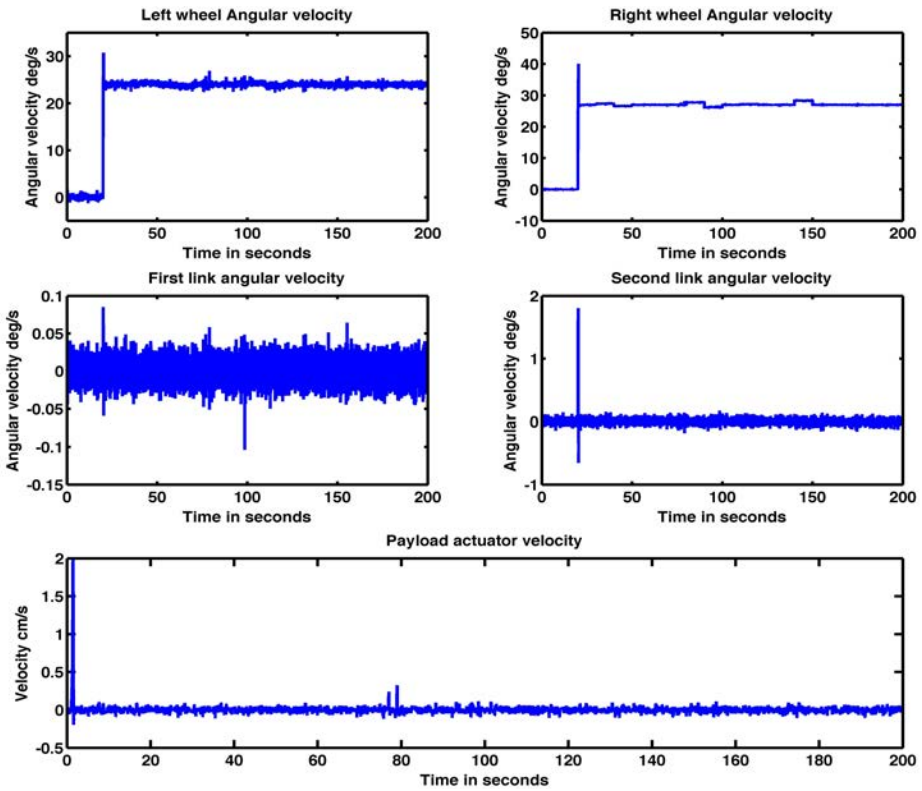

Figure 6.32: Velocities of the vehicle main components on gravel ground of 20% grade

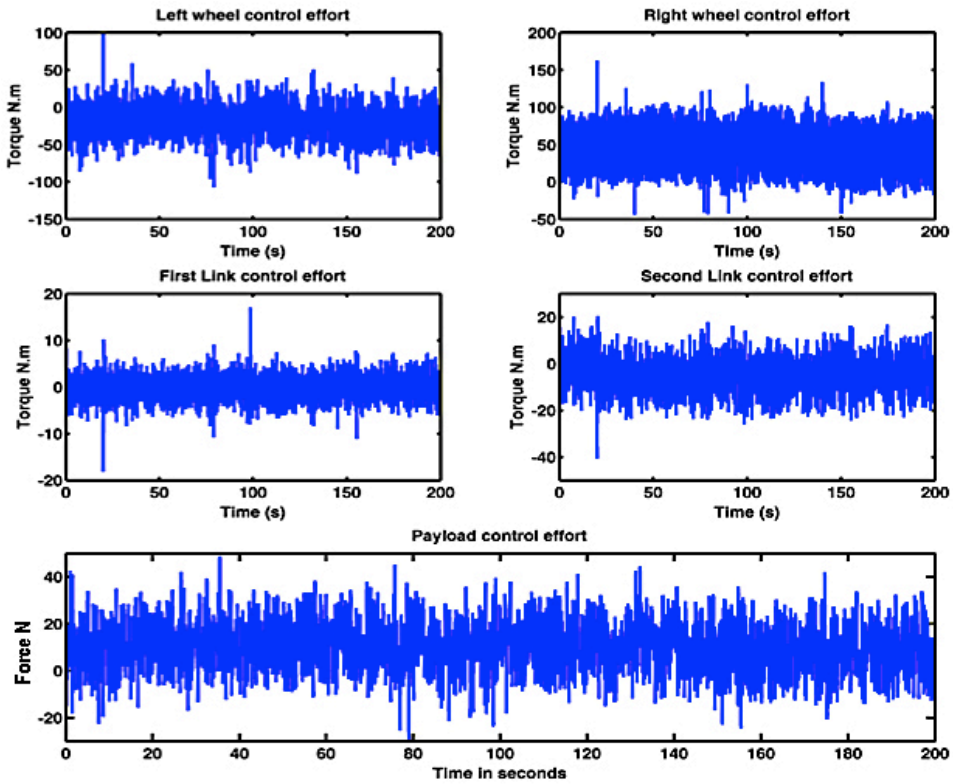

Figure 6.33: Control effort exerted by the vehicle actuators on gravel ground of 20% grade

6.7.2 Inclined surfaces of 50% grade (26.57 deg)

6.7.2.1 Peat inclined surface of 50% grade

Further steering exercise is considered in this section where the vehicle is subjected to manoeuvring on an inclined surface with peat ground of 26.57 degrees inclination angle. The vehicle trajectory and response were almost unaffected. This can be noted in Figures 6.34 and 6.35. Moreover, as noted in Figure 6.36 the increase in velocities of vehicle components was not significant. On the other hand, as noted in Figure 6.37 a noticeable increase in the control effort was seen. The overall system was stable with a high degree of robustness.

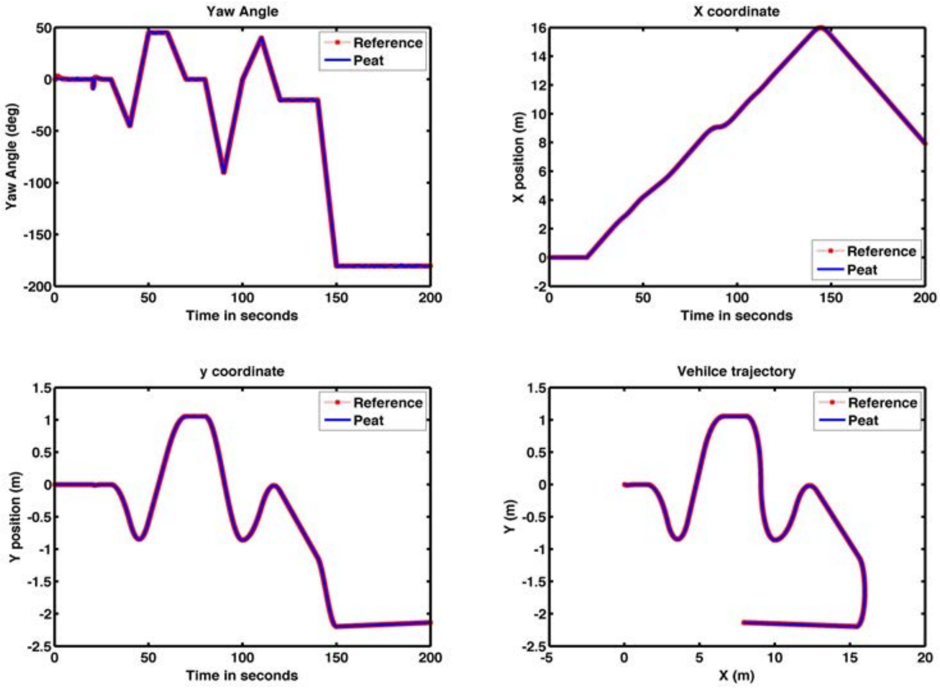

Figure 6.34: Steering motion of the vehicle on peat ground of 50% grade

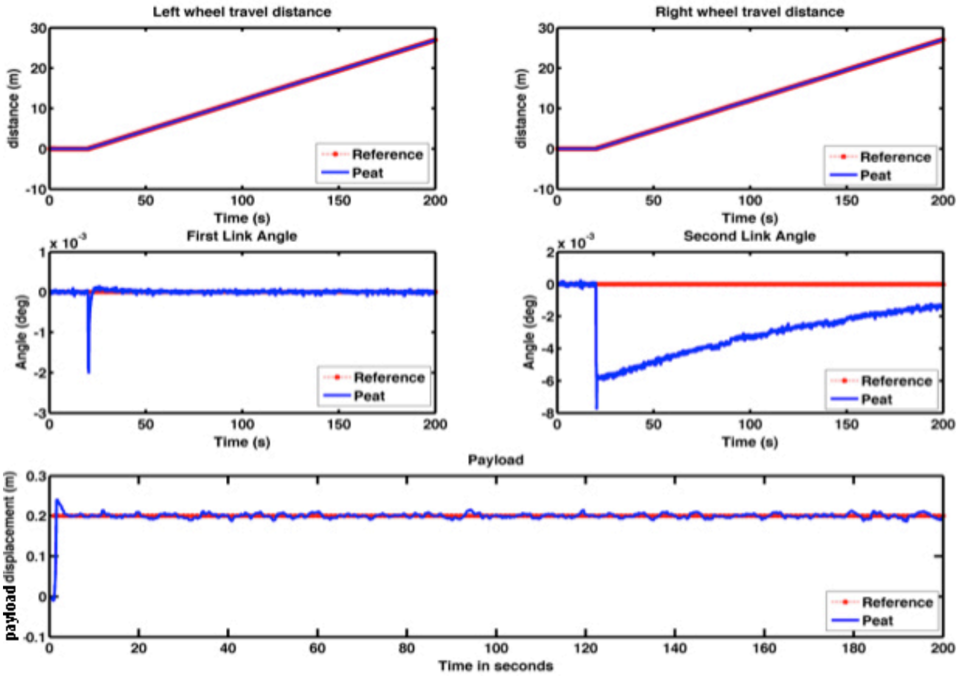

Figure 6.35: Displacements of the vehicle main components on peat ground of 50% grade

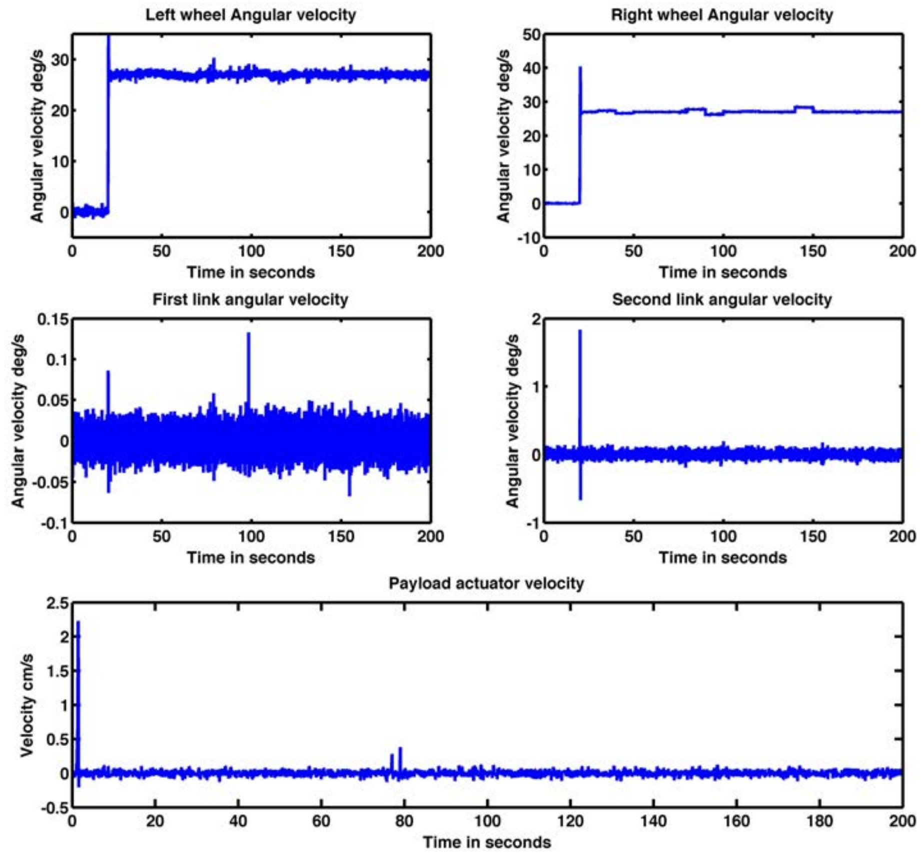

Figure 6.36: Velocities of the vehicle main components on peat ground of 50% grade

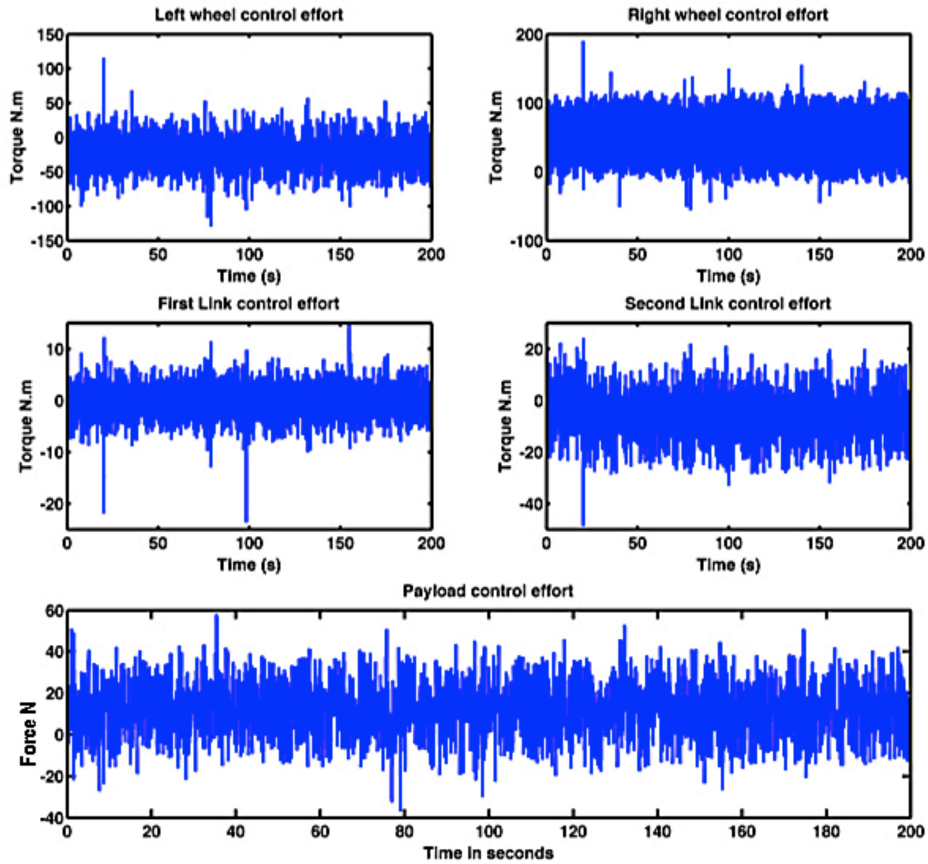

Figure 6.37: Control effort exerted by the vehicle actuators on peat ground of 50% grade

6.7.2.2 Gravel Inclined surface of 50% grade

The gravel inclined ground with 50% grade was simulated to study the vehicle response. By referring to Figures 6.38 and 6.39, it is clear that the vehicle was still able to steer successfully and follow the reference trajectory. When compared to the response of the vehicle to gravel inclined ground of 20% grade, response oscillations increased slightly with the increase of surface gradient. Furthermore, there was considerable increase in velocities and control effort, as noted in Figures 6.40 and 6.41. Such increase is expected and verify that the controller exert more effort to stabilise the vehicle with additional torques.

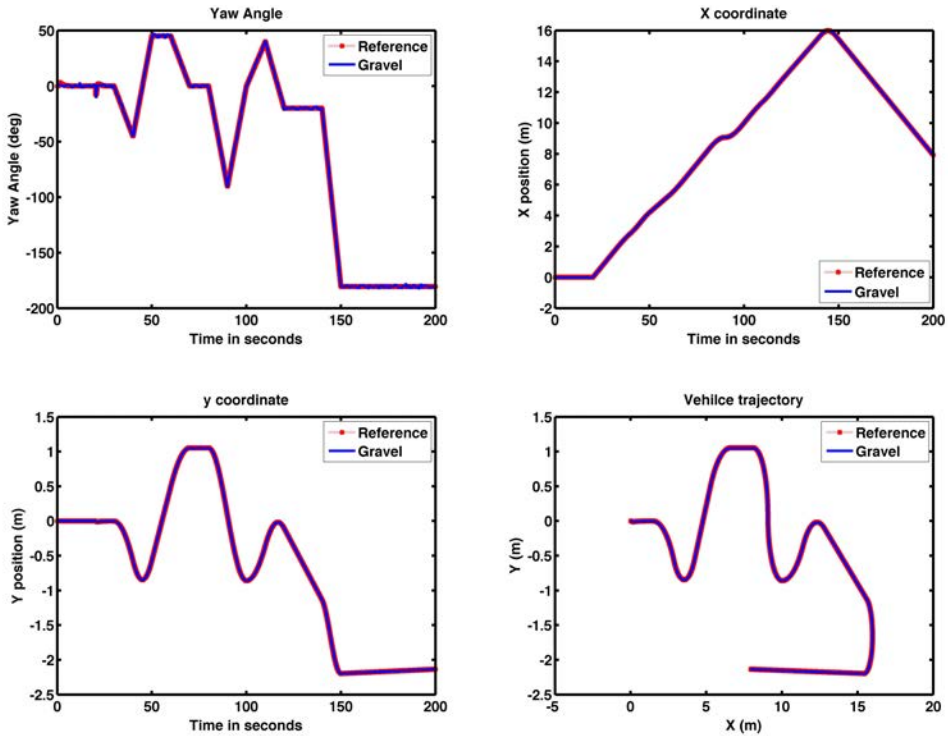

Figure 6.38: Steering motion of the vehicle on gravel ground of 50% grade

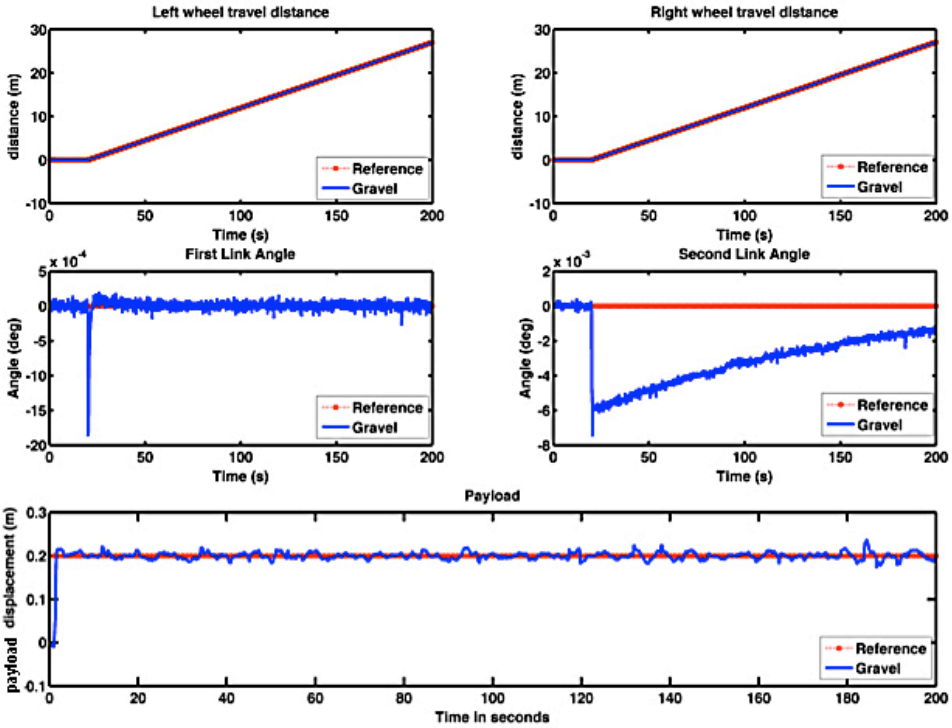

Figure 6.39: Displacements of the vehicle main components on gravel ground of 50% grade

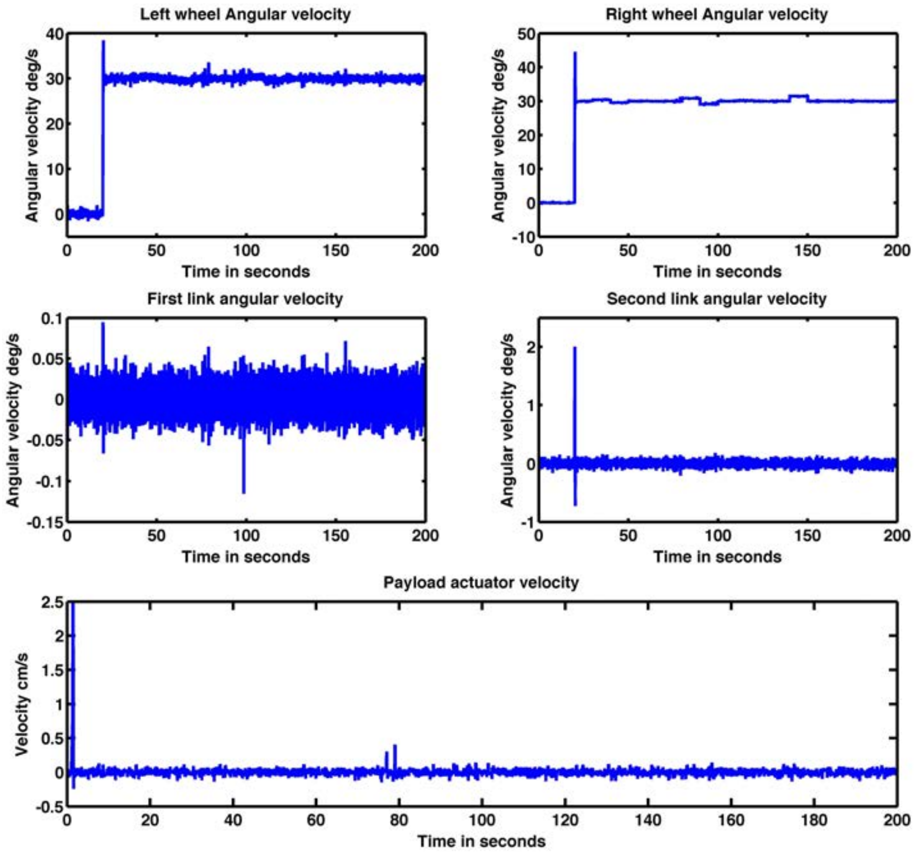

Figure 6.40: Velocities of the vehicle main components on gravel ground of 50% grade

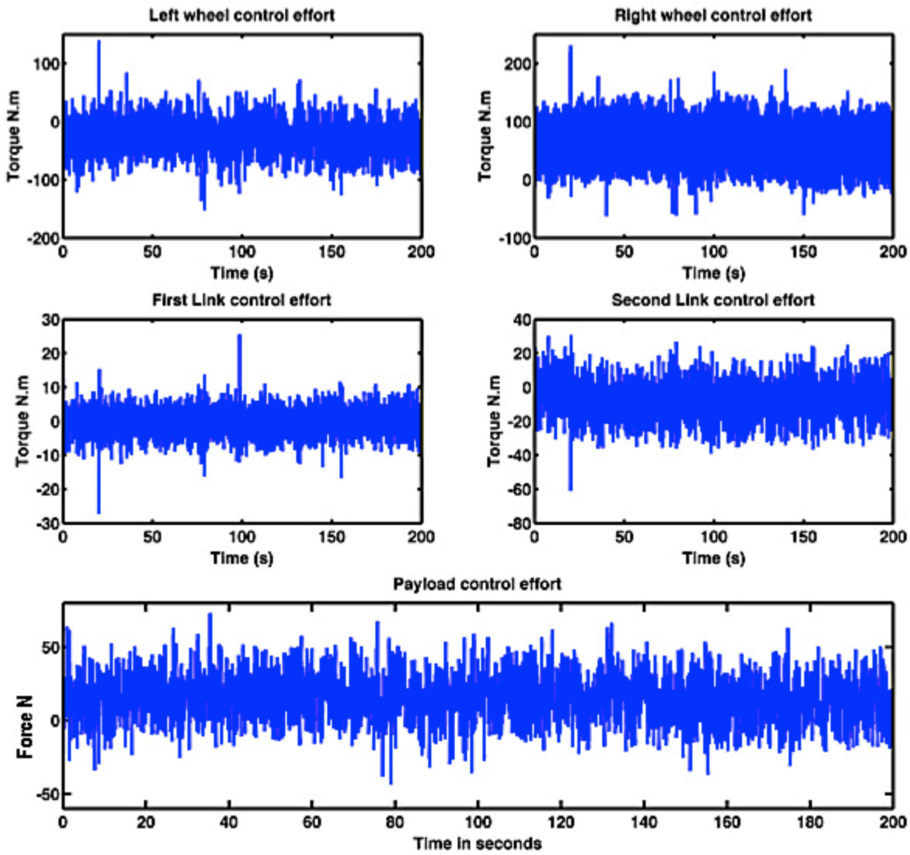

Figure 6.41: Control effort exerted by the vehicle actuators on gravel ground of 50% grade

6.8 Golf course steering scenario

With the results presented in sections 6.7.1 and 6.7.2, the vehicle demonstrated a very good degree of robustness on steering in different environments. In these tests, the vehicle was assumed to move on either flat or inclined surfaces of different environments. With such promising results the author was encouraged to simulate the vehicle in a more dynamic environment that has various grounds and variable inclination angles. A golf course is an environment that suits this need. A simple golf course consists of fairways, rough ways, out of bound areas and a road for cars and golf carts. A sample 3D illustration of a proposed environment is presented in Figure 6.42. This environment is composed of soil types presented earlier in section 6.5. It combines hard and soft ground profiles such as the gravel, asphalt or concrete, peat, sand and clay. A predefined steering trajectory is shown as a reference. Simulating the vehicle in such an environment would highlight the control efficiency of the system to deal with rapid dynamic changes in ground types and road gradients.

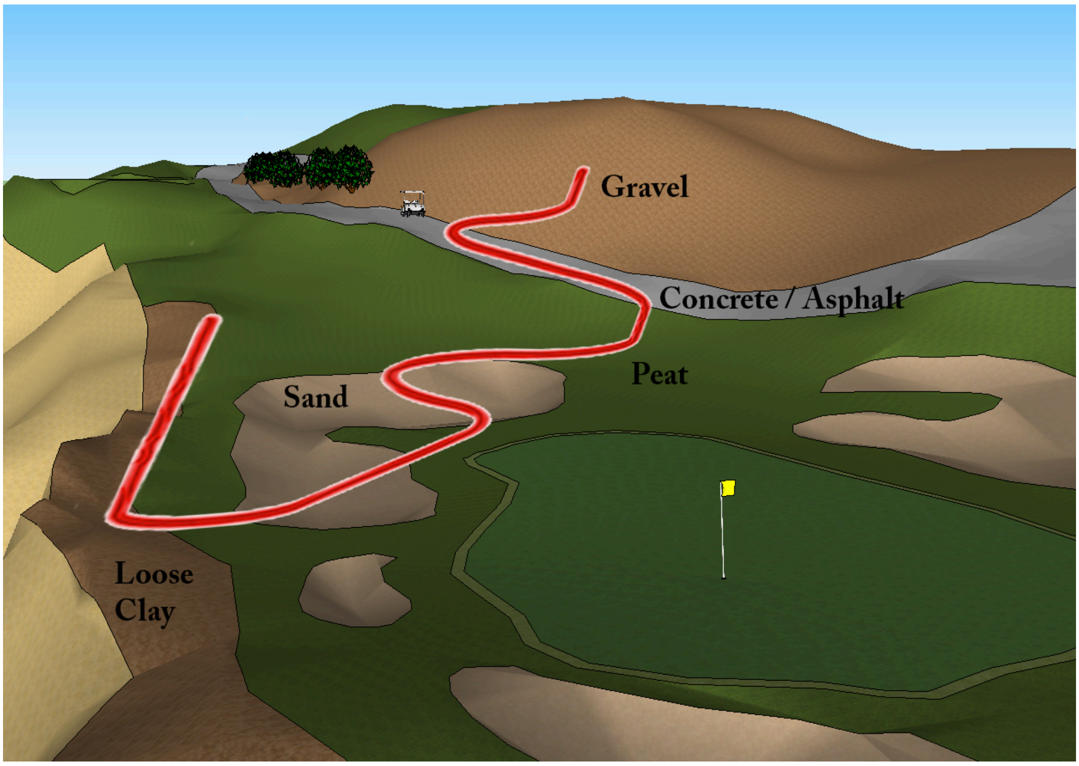

Figure 6.42: Golf course and predefined vehicle steering path

A dynamic road gradient signal is used to simulate the irregularity of the terrains. The sample dynamic inclination angle is presented in Figure 6.43. Moreover, ground profiles distribution intervals are illustrated on Figure 6.44. It can be noted that the inclination angle has both rapid and gradual changes in value. This was premeditated to test the robustness at extreme situations.

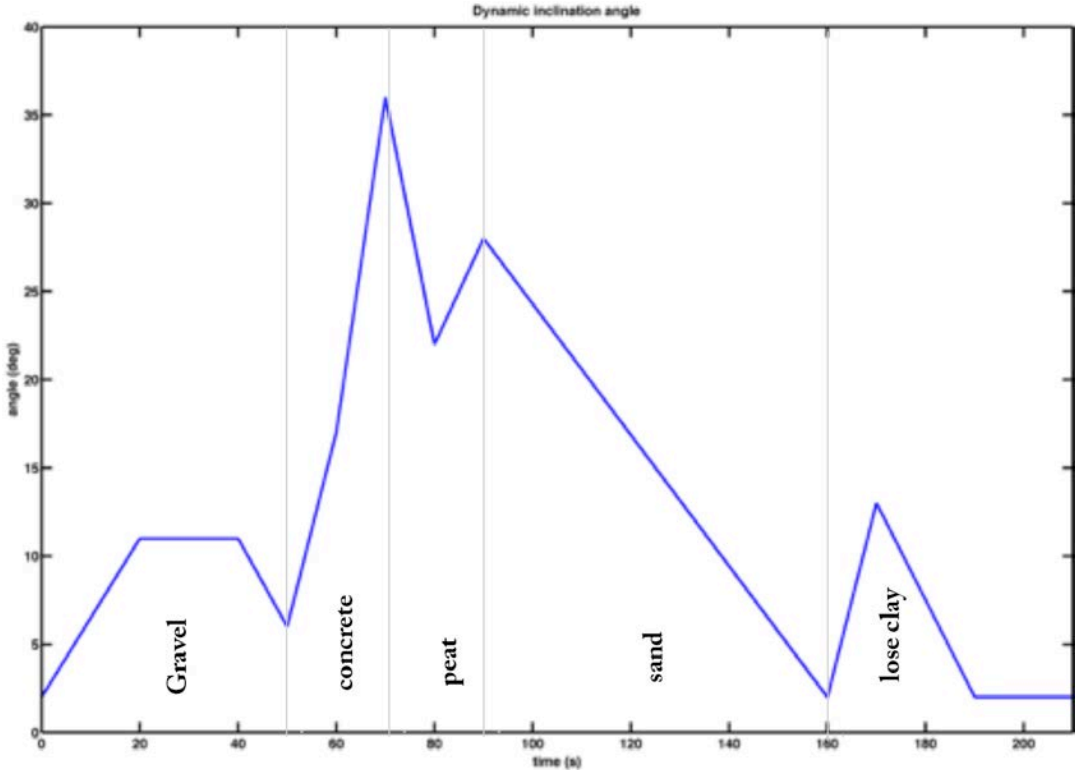

Figure 6.43: Dynamic inclination angle

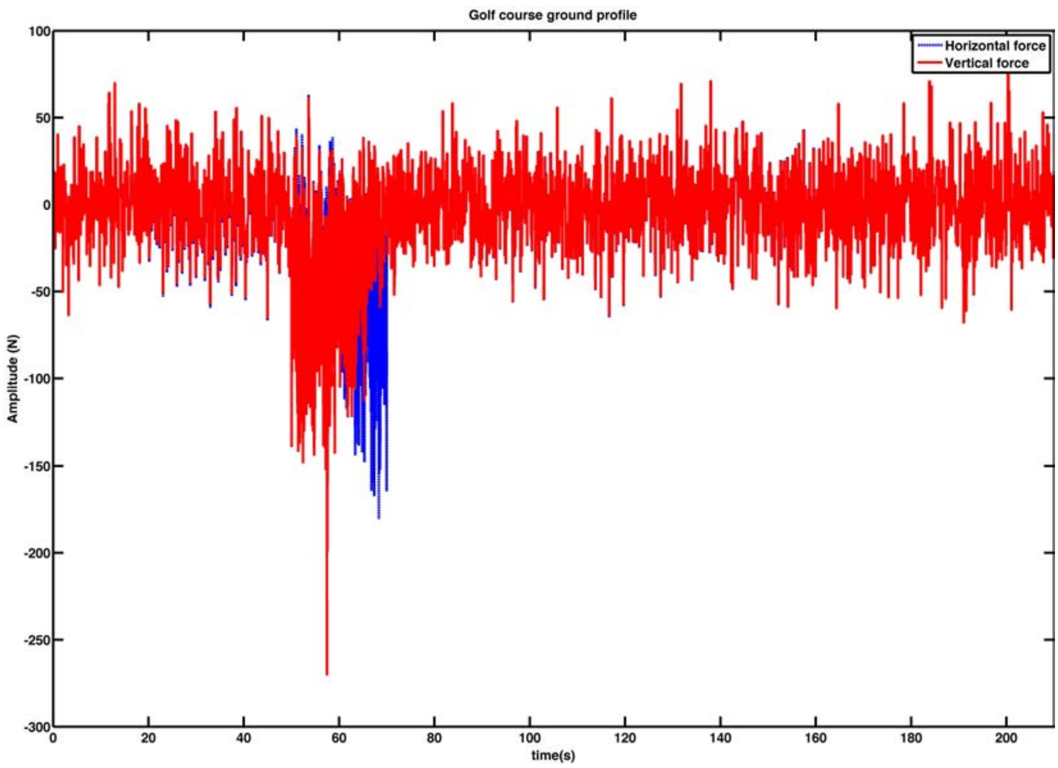

Figure 6.44: Ground profile of the golf course

The vehicle trajectory after steering on the golf course is presented in Figure 6.45. It is noted that the dynamic angle and ground profiles affected the yaw angle and coordinates of the vehicle. However, the vehicle was able to complete the trajectory without loosing its stability and overall balance as demonstrated in the vehicle responses in Figure 6.46. Oscillations noted in at the tilt angle were still limited within a small range. These oscillations were due to the rapid changes in the ground profiles. The payload was affected slightly and the overall response proved the efficiency of the hybrid FLC controller. Figure 6.47 shows the velocities of the vehicle components, and as noted the angular velocities of the links increased significantly. In Figure 6.48, a significant increase in control effort can be observed. This is due to the terrain irregularity and dynamic ground profile that needs more effort to be exerted in order to maintain the stability of the system.

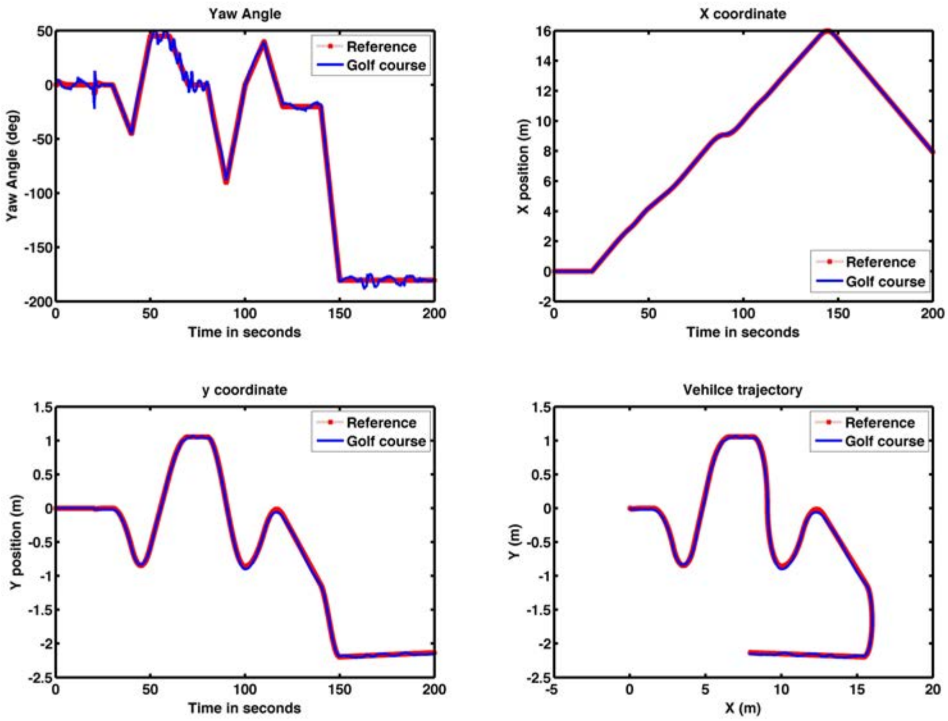

Figure 6.45: Steering motion of the vehicle on golf course

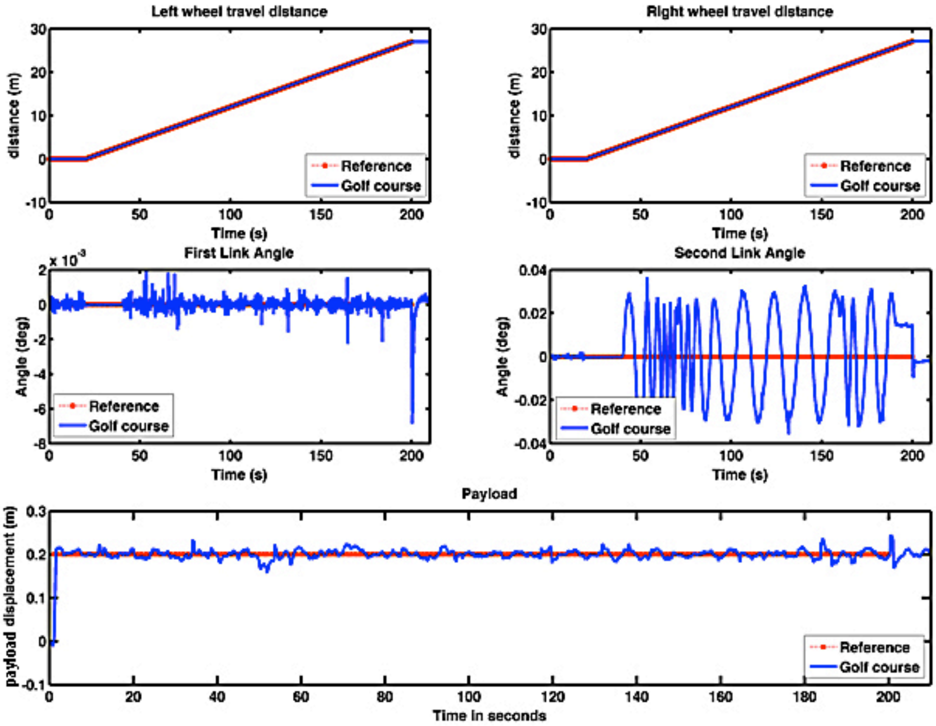

Figure 6.46: Displacements of the vehicle main components at the golf course

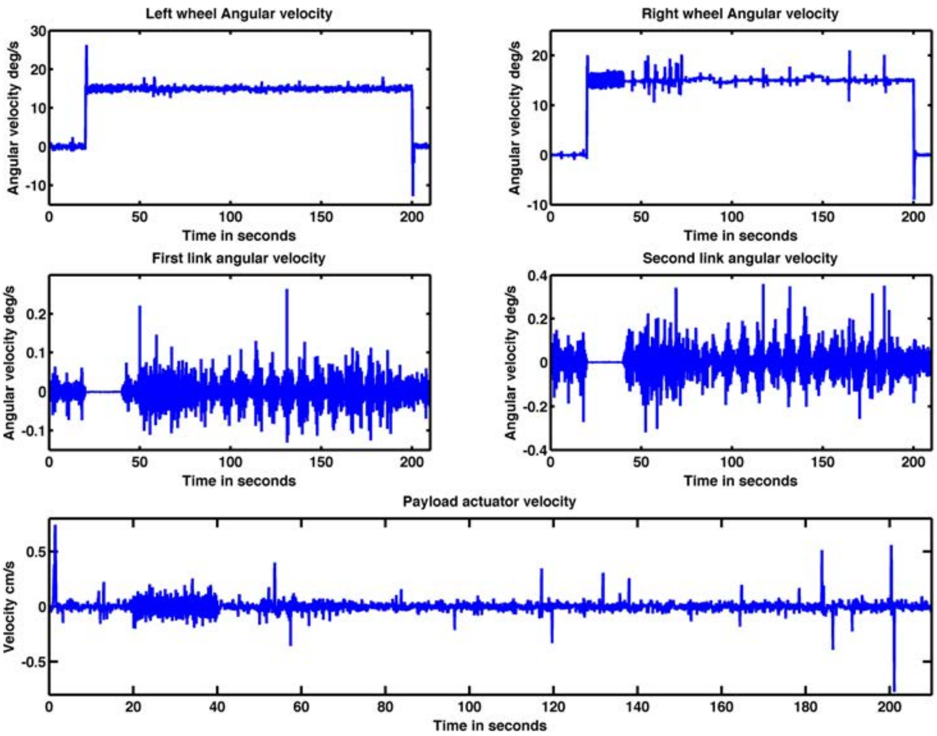

Figure 6.47: Velocities of the vehicle main components at the golf course

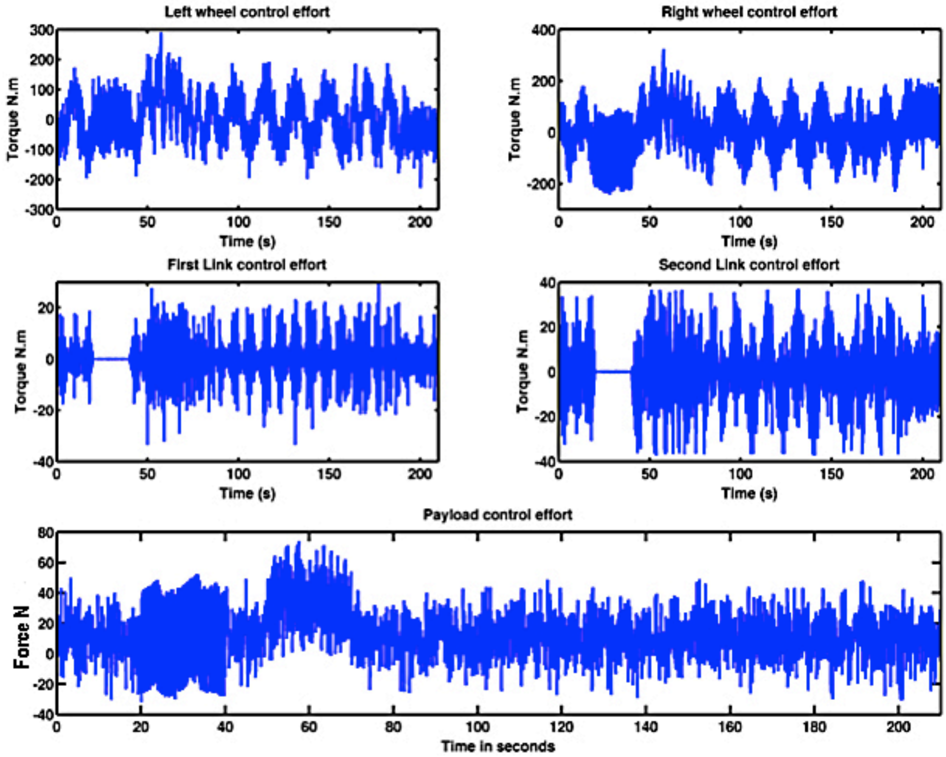

Figure 6.48: Control effort exerted by the vehicle actuators at the golf course

The system overall was stable and the vehicle was able to drive on the dynamic ground profile of the presented golf course with a high degree of robustness.

6.9 Summary

This chapter has presented the steering capability of the developed two-wheeled robotic vehicle. A steering strategy based on differential driving method has been implemented in the vehicle model. The vehicle has successfully been able to steer on predefined trajectories. Further simulations were carried on to study the impact of different degrees of complexity in the steering environments. This was interpreted in simulating different ground profiles of different environments at indoor and outdoor spaces. Adding to the complexity of this nonlinear system; investigation of the impact of different types of terrains has been addressed. Various types of surfaces have been modelled in this study including Peat, Gravel and a Golf course. In order to verify the system and capabilities of the control approach to cope with such variations; the vehicle dynamic performance has been studied based on different types of surfaces with various degrees of inclination. It has been demonstrated that the control approach has been able to cope with random disruption caused by complex and continuous uncertainties in keeping the vehicle stable in the upright position

Chapter 7: Conclusion and future work

7.1 Summary and concluding remarks

The aim of this study has been to design a new structure of two-wheeled robotic vehicle with 5 DOF and a movable payload that is capable of moving on different environments and terrains. Furthermore, to design a suitable control system that is simple yet efficient to cope with the different environments whilst manoeuvring the vehicle.

The design is based on the double inverted pendulum on cart system with novel modifications to add the capability of lifting up a payload to an extended height and moving on irregular terrains and inclined surfaces. The movable payload allows the vehicle to serve as a basis for designs of balancing wheelchairs and contributes to serve new mobility solution applications. A model of the proposed structure of the vehicle has been described and derived mathematically using the Euler-Lagrange approach in a set of nonlinear differential equations. The vehicle has firstly been modelled on a flat ground to study its dynamic behaviour and to verify the model. A PID control strategy was proposed to control the vehicle. The PID control system was proved to be feasible in the linear region of the system when the interactions and Coriolis effects are negligible. A hybrid FLC system was developed to control the vehicle and to overcome uncertainties and disturbances.

The model was then improved to include the effect of the inclination of the surface and to study its impact on the vehicle response. The vehicle was tested on various inclined surfaces successfully. The hybrid FLC improved the system overall response while exerting smaller amounts of control effort, when compared to the PID control strategy. The vehicle ability to move on various inclinations was demonstrated and proved via simulation results. Thus the objective of the design has been achieved and demonstrated.

Rigorous investigations were carried out to find the optimal control parameters for the presented hybrid FLC strategy. Different optimisation algorithms were implemented and the system response was analysed. The HSDBC optimisation algorithm performed the best in finding optimal gain parameters for the optimal system response. Furthermore, the optimal control parameters reduced the exerted efforts to a significant extent.

Further investigations on the control system robustness and vehicle ability to work in a perturbed environment were demonstrated by studying the impact of applied disturbances on the vehicle. Disturbances of varying amplitudes and durations were applied on the vehicle and system responses were analysed. The vehicle was able to cope with the disturbances with a high degree of robustness. Thus demonstrating the efficiency of vehicle design and control strategy.

One of major aims of this study has been to develop a steering strategy that is applicable to different environments and operating conditions found in real life. The separated driving motors of the vehicle enabled the implementation of differential steering mechanism into the vehicle system. Initially, the vehicle steering ability on flat and inclined surfaces was demonstrated with promising results. These results were extended to a further challenging steering scenario. The vehicle was tested to manoeuvre and steer in both indoor and outdoor areas. Simulations on both flat and inclined surface manoeuvring scenarios were presented which confirmed the vehicle’s ability to track the predefined trajectory.

Environmental frictions were taken into consideration in developing the steering mechanism. Different grounds were modelled using a foot-ground interaction force model. The modelling of different environments and ground friction elements has provided a resemblance to the real life outdoor steering scenarios. Hard and soft grounds were modelled and a virtual outdoor steering on a golf course was simulated. The vehicle demonstrated a high degree of robustness in working on grounds with dynamic inclination angles and uncertainties of ground frictions.

This research has presented the development of a new structure of two-wheeled robotic vehicle with extended abilities that work in various operating conditions and environments. Modelling of the vehicle dynamics has been presented along with the design of a hybrid FLC control system. Simulations have been carried out highlighting the vehicle's ability and high degree of robustness in working on different grounds. Thus fulfilling the design objectives set at the beginning of the research. The vehicle design, with its presented capabilities, has the potential to be used as a basis for new mobility solutions and applications such as balancing wheelchairs.

7.2 Suggestions for future work

The study has succeeded in fulfilling the specified objectives. The results and simulations presented give an insight into further investigations and studies. This section highlights a number of suggestions worth investigating that may enhance the system performance or add extra capabilities for more advanced applications.

- In the vehicle model, a mass of an average human of 70 kg was used to represent the payload. It would be interesting to assess the effect of varying the mass of the payload while steering in challenging environments. More broadly, a research to find the maximum mass that can be carried on the vehicle would be beneficial.

- Scalability of the vehicle structure would add more capabilities to the vehicle model, in terms of flexibility, to suit different applications. It is recommended to explore the scaling of each vehicle component and establish the boundary limits for scaling the structure without affecting the system performance.
- By studying the scalability of the vehicle, it would be interesting to find the optimal structure design criteria that lead to equal or better performance to the current performance while reducing the energy consumption. A study of the lower parts and vehicle driving system can be utilised to achieve these analyses.
- More investigations on different steering scenarios can be carried out by incorporating obstacles in the path of the vehicle and analysing the extreme points, in terms of the maximum inclination angle and maximum frictional forces, that allow safe operation for the vehicle without collapsing.
- A more advanced investigation is to add a step or stair-climbing feature to the vehicle. A possible solution is to utilise a third auxiliary wheel for use in climbing situations only.
- A recommended research is in the situations where the vehicle is moving on a sloppy surface such as muddy and wet surfaces is needed to analyse the vehicle performance and explore its limitations in working on different surfaces.

- Studying the aforementioned suggestions would be beneficial toward developing and implementation of an experimental prototype of the vehicle. Thus providing a validation and comparative study with the simulations presented in this research.
- Adding further DOF could add more flexibility to the structure and broaden application designs. As an example, further DOF can be added to extend a supportive extra link to allow a sit-to-stand position for the user.
- The vehicle could serve as a basis to design an exoskeleton for elder and disabled people to be able to stand and walk on irregular terrains and surfaces.

References

Ahmad, S. (2010). *Modelling and Fuzzy Control of Two-Wheeled Wheelchairs*. Unpublished doctoral dissertation. The University of Sheffield, Sheffield, United Kingdom

Ahmad, S., Tokhi, M. O., & Toha, S. F. (2009). Genetic algorithm optimisation for fuzzy control of wheelchair lifting and balancing. *EMS'09. Third UKSim European Symposium on Computer Modeling and Simulation, 2009*. (pp. 97–101).

Amir, D., & Chefranov, A. G. (2010). An effective hybrid swing-up and stabilization controller for the inverted pendulum-cart system. *IEEE International Conference on Automation Quality and Testing Robotics (AQTR 2010)* (Vol. 1, pp. 1–6).

Angeli, D. (2001). Almost global stabilization of the inverted pendulum via continuous state feedback. *Automatica*, *37*(7), 1103–1108.

Anybots Co. (2013). Anybots virtual presence systems, (15^{th} May 2013),[Available from] http://www.anybots.com

Aoi, S., & Tsuchiya, K. (2005). Locomotion control of a biped robot using nonlinear oscillators. *Autonomous Robots*, *19*(3), 219–232.

Asa, E., Benjanarasuth, T., Ngamwiwit, J., & Komine, N. (2008). Hybrid controller for swinging up and stabilizing the inverted pendulum on cart. *International Conference on Control, Automation and Systems ICCAS 2008*. (pp. 2504–2507).

Ashrafiuon, H., & Whitman, A. M. (2010). Closed-loop response analysis of an inverted pendulum. *American Control Conference (ACC), 2010* (pp. 646–651).

Askari, M., Mohamed, H. A. F., Moghavvemi, M., & Yang, S. S. (2009). Model predictive control of an inverted pendulum. *International Conference for Technical Postgraduates (TECHPOS)*. (pp. 1–4).

Åström, K. J., & Furuta, K. (2000). Swinging up a pendulum by energy control. *Automatica*, *36*(2), 287–295

Azizan, H., Jafarinasab, M., Behbahani, S., & Danesh, M. (2010). Fuzzy control based on LMI approach and fuzzy interpretation of the rider input for two wheeled balancing human transporter. *8th IEEE International Conference on Control and Automation (ICCA)*. (pp. 192–197).

Balan, R., Maties, V., Hancu, O., & Stan, S. (2005). A predictive control approach for the inverse pendulum on a cart problem. *IEEE International Conference Mechatronics and Automation*. (Vol. 4, pp. 2026–2031).

Ban, X., Gao, X. Z., & Huang, X. (2004). Design of a hybrid fuzzy-PD controller for inverted pendulum. *IEEE International Conference on Systems, Man and Cybernetics*. (Vol. 3, pp. 2286–2291).

Bekey, G. A. (2005). *Autonomous robots: from biological inspiration to implementation and control*. The MIT Press.

Bekker, M. G. (1969). *Introduction to terrain-vehicle systems*. University of Michigan Press Ann Arbor, MI.

Benjanarasuth, T., & Nundrakwang, S. (2008). Hybrid controller for rotational inverted pendulum systems. *SICE Annual Conference, 2008* (pp. 1889–1894).

Blackwell, T., Casner, D., & Wiley, S. (2012). Remotely controlled self-balancing robot including kinematic image stabilization. Google Patents.

Bogdanov, A. (2004). Optimal control of a double inverted pendulum on a cart. *Oregon Health and Science University, Tech. Rep. CSE-04-006, OGI School of Science and Engineering, Beaverton, OR.*

Boone, G. N., & Hodgins, J. K. (1997). Slipping and tripping reflexes for bipedal robots. *Autonomous robots*, *4*(3), 259–271.

Borenstein, J., Everett, H. R., & Feng, L. (1996). Where am I? Sensors and methods for mobile robot positioning. *University of Michigan*, *119*, 120.

Bugeja, M. (2003). Non-linear swing-up and stabilizing control of an inverted pendulum system. *The IEEE Region 8 EUROCON 2003 Computer as a Tool*. (Vol. 2, pp. 437–441).

Chalupa, P., & Bobál, V. (2008). Modelling and predictive control of inverted pendulum. *22nd European Conference on Modelling and Simulation* (pp. 531–537).

Chen, W., Li, Q., & Gu, R. (2010). Chaos optimization neural network control for the stability of double inverted pendulum. *2nd International Conference on Industrial Mechatronics and Automation ICIMA,* (Vol. 2, pp. 491–494).

Cheng-jun, D., Ping, D., Ming-lu, Z., & Yan-fang, Z. (2009). Double inverted pendulum system control strategy based on fuzzy genetic algorithm. *IEEE International Conference on Automation and Logistics ICAL'09, (*pp. 1318–1323).

Chew, C.-M., Pratt, J., & Pratt, G. (1999). Blind walking of a planar bipedal robot on sloped terrain. *Proceedings of 1999 IEEE International Conference on Robotics and Automation,* (Vol. 1, pp. 381–386).

Chiu, C. (2010). The Design and Implementation of a Wheeled Inverted Pendulum Using an Adaptive Output Recurrent Cerebellar Model Articulation Controller. *IEEE Transactions on Industrial Electronics*, *57*(5), 1814–1822

Chung, C. C., & Hauser, J. (1995). Nonlinear control of a swinging pendulum. *Automatica*, *31*(6), 851–862.

Doi, K. (2012). U.S. Patent No. 8,165,771. Washington, DC: U.S. Patent and Trademark Office.

Doi, K. (2013). U.S. Patent No. 8,442,753. Washington, DC: U.S. Patent and Trademark Office.

Fiacchini, M., Viguria, A., Cano, R., Prieto, A., Rubio, F. R., Aracil, J., & Canudas-de-Wit, C. (2006). Design and experimentation of a personal pendulum vehicle. *Proceedings of the Seventh Portuguese Conference of Automatic Control*.

Furuta, K., Kajiwara, H., & Kosuge, K. (1980). Digital control of a double inverted pendulum on an inclined rail. *International Journal of control*, *32*(5), 907–924.

Goher, K., Ahmad, S., & Tokhi, O. M. (2010). A new configuration of two wheeled vehicles: Towards a more workspace and motion flexibility. *4th Annual IEEE Systems Conference*. pp. 524–528.

Ha, K.-J., & Kim, H.-M. (1997). A genetic approach to the attitude control of an inverted pendulum system. *Proceedings of the 9th IEEE International Conference on Tools with Artificial Intelligence, 1997*. (pp. 268–269).

Han, Y., & Liu, Y. (2010). One rod inverted pendulum controller design based on self-adaptive fuzzy PID with fuzzy. *8th World Congress on Intelligent Control and Automation (WCICA),* pp. 4891–4894.

Han, Y., & Liu, Y. (2010). One rod inverted pendulum controller design based on self-adaptive fuzzy PID with fuzzy. *8th World Congress on Intelligent Control and Automation WCICA,* (pp. 4891–4894).

Hasegawa, Y., Arakawa, T., & Fukuda, T. (2000). Trajectory generation for biped locomotion robot. *Mechatronics*, *10*(1), 67–89.

Honda motor company (2001). ASIMO the world most advanced humanoid robot. *Honda.com*. Retrieved January 20th, 2010, from http://asimo.honda.com

Hong, Y.-D., Lee, B.-J., & Kim, J.-H. (2011). Command state-based modifiable walking pattern generation on an inclined plane in pitch and roll directions for humanoid robots. *IEEE/ASME Transactions on Mechatronics, 16*(4), 783–789.

Huang, W., Chew, C.-M., Zheng, Y., & Hong, G.-S. (2008). Pattern generation for bipedal walking on slopes and stairs. *IEEE-RAS International Conference on Humanoid Robots Humanoids 2008,* (pp. 205–210).

Hunt, K. H., & Crossley, F. R. E. (1975). Coefficient of restitution interpreted as damping in vibroimpact. *ASME Journal of Applied Mechanics,* 440-445

Independence technology LLC (2001). Independence IBot mobility system. iBotnow.com, Retrieved February 2nd, 2010, http://www.ibotnow.com/index.html.

Jung, S., & Kim, S. S. (2008). Control experiment of a wheel-driven mobile inverted pendulum using neural network. *, IEEE Transactions on Control Systems Technology*, *16*(2), 297–303.

Kajita, S., & Tani, K. (1991). Study of dynamic biped locomotion on rugged terrain-derivation and application of the linear inverted pendulum mode. *. Proceedings of the 1991 IEEE International Conference on Robotics and Automation,* (pp. 1405–1411).

Kajita, S., Kanehiro, F., Kaneko, K., Fujiwara, K., Harada, K., Yokoi, K., & Hirukawa, H. (2003). Biped walking pattern generation by using preview control of zero-moment point. *Proceedings of IEEE International Conference on Robotics and Automation ICRA'03,* (Vol. 2, pp. 1620–1626).

Kiankhah, E., Teshnelab, M., & Shoorehdeli, M. A. (2009). Feedback-error-learning for stability of Double Inverted Pendulum. *. IEEE International Conference on Systems, Man and Cybernetics, SMC* (pp. 4496–4501).

Kim, J.-Y., Park, I.-W., & Oh, J.-H. (2007). Walking control algorithm of biped humanoid robot on uneven and inclined floor. *Journal of Intelligent and Robotic Systems*, *48*(4), 457–484.

Kim, Y.-D., Park, I.-W., Yoo, J.-K., & Kim, J.-H. (2008). Stabilization control for humanoid robot to walk on inclined plane. *8th IEEE-RAS International Conference on Humanoid Robots,* (pp. 28–33).

Kim, Y.-D., Park, I.-W., Yoo, J.-K., & Kim, J.-H. (2008). Stabilization control for humanoid robot to walk on inclined plane. *8th IEEE-RAS International Conference on Humanoid Robots, Humanoids,* (pp. 28–33).

Kouda, N., Matsui, N., & Nishimura, H. (2002). Control for swing-up of an inverted pendulum using qubit neural network. *Proceedings of the 41st SICE Annual Conference SICE,* (Vol. 2, pp. 765–770).

Lee, H., Lee, J., & Lee, J. (2009). Hill climbing algorithm of an inverted pendulum. *2009 IEEE International Symposium on Computational Intelligence in Robotics and Automation - (CIRA)*, (2), 574–579.

Li, J., Gao, X., Huang, Q., & Matsumoto, O. (2008). Controller design of a two-wheeled inverted pendulum mobile robot. *IEEE International Conference on Mechatronics and Automation ICMA 2008,* (pp. 7–12).

Li, J., Gao, X., Huang, Q., Du, Q., & Duan, X. (2007). Mechanical design and dynamic modeling of a two-wheeled inverted pendulum mobile robot. *IEEE International Conference on Automation and Logistics,* (pp. 1614–1619).

Lin, Z., Saberi, A., Gutmann, M., & Shamash, Y. A. (1996). Linear controller for an inverted pendulum having restricted travel: a high-and-low gain approach. *Automatica*, *32*(6), 933–937.

Lingyan, H., Guoping, L., Xiaoping, L., & Hua, Z. (2009). The Computer Simulation and Real-Time Stabilization Control for the Inverted Pendulum System Based on LQR. *2009 Fifth International Conference on Natural Computation*, (c), pp. 438–442.

Liu, G., Li, M., Guo, W., & Cai, H. (2012). Control of a biped walking with dynamic balance. *IEEE International Conference on Mechatronics and Automation (ICMA),* (pp. 261–267).

Liu, Y., Chen, Z., Xue, D., & Xu, X. (2009). Real-time controlling of inverted pendulum by fuzzy logic. *IEEE International Conference on Automation and Logistics ICAL'09*. (pp. 1180–1183).

Lu, C.-N., Tsai, C.-C., Tsai, M.-C., Ling, K. V, & Yao, W.-S. (2007). Application of model predictive control to parallel-type double inverted pendulum driven by a linear motor. *33rd Annual Conference of the IEEE* Industrial *Electronics Society IECON 2007*. (pp. 2904–2909).

Luo, Z., Shi, Z., Hu, P., Hao, L., & Liu, H. (2010). Error analysis of a inverted pendulum on an inclined rail. *2nd International Conference on Advanced Computer Control (ICACC),* (Vol. 3, pp. 52–55).

Manko, D. J. (1992). A General Model Of Legged Locomotion On Natural Terrain (The Springer International Series In Engineering And Computer Sc.

Miki, N., Horiguchi, M., Tachibana, T., Sakakibara, F., Doi, K., Fukuda, T., & Matsuno, T. (2011). U.S. Patent No. 8,016,060. Washington, DC: U.S. Patent and Trademark Office.

Mills, A., Wills, A., & Ninness, B. (2009). Nonlinear model predictive control of an inverted pendulum. *American Control Conference, 2009. ACC'09*. (pp. 2335–2340).

Muskinja, N., & Tovornik, B. (2006). Swinging up and stabilization of a real inverted pendulum. *IEEE Transactions on Industrial Electronics, 53*(2), 631–639.

Nakayama, S., Deng, M., Bi, S., & Yanou, A. (2010). Genetic algorithm with a robust solution searching scheme based controller parameters selection of a cart-type inverted pendulum. *The 2010 International Conference on Modelling, Identification and Control (ICMIC),* (pp. 568–573).

Nasir, A. N. K., Tokhi, M. O., Ghani, N. M., & Ahmad, M. A. (2012). A novel hybrid spiral dynamics bacterial chemotaxis algorithm for global optimization with application to controller design. *2012 UKACC International Conference on Control (CONTROL),* (pp. 753–758).

Noh, J. S., Lee, G. H., Choi, H. J., & Jung, S. (2009). Robust control of a mobile inverted pendulum robot using a RBF neural network controller. *IEEE International Conference on Robotics and Biomimetics*, 1932–1937.

Nundrakwang, S., Benjanarasuth, T., Ngamwiwit, J., & Komine, N. (2005). Hybrid controller for swinging up inverted pendulum system. *Fifth International Conference on Information, Communications and Signal Processing,* (pp. 488–492).

Ono, T., Murakami, T., & Ohnishi, K. (1998). An approach to biped robot control according to surface condition of ground. *5th International Workshop on Advanced Motion Control AMC'98-Coimbra,* (pp. 129–134).

Özgüner, Ü., Acarman, T., & Redmill, K. A. (2011). *Autonomous ground vehicles*. Artech House.

Panya, S., Benjanarasuth, T., Nundrakwang, S., Ngamwiwit, J., & Komine, N. (2008). Hybrid controller for inverted pendulum system. *International Symposium on Communications and Information Technologies ISCIT 2008,* (pp. 385–388).

Passino, K. M. (2002). Biomimicry of bacterial foraging for distributed optimization and control. *Control Systems, IEEE*, *22*(3), 52–67.

Phatak, D R & Gite, H. K. (2009). *Highway Engineering: Degree Course in Civil Engineering*. Shivaji Nagar: Nirali Prakashan

Pratt, J., Chew, C.-M., Torres, A., Dilworth, P., & Pratt, G. (2001). Virtual model control: An intuitive approach for bipedal locomotion. *The International Journal of Robotics Research*, *20*(2), 129–143.

Qiang, S., Zhou, Q., Gao, X. Z., & Yu, S. (2008). ANFIS controller for double inverted pendulum. *6th IEEE International Conference on Industrial Informatics INDIN,* (pp. 475–480).

Salation, A. W., & Zheng, Y. F. (1997). Reinforcement learning for a biped robot to climb sloping surfaces. *Journal of Robotic Systems*, *14*(4), 283–296.

Segway Inc. (2001). Segway-simply moving. *Segway.com*. Retrieved January 23rd, 2010, from http://www.segway.com/.

Seven, U., Akbas, T., Fidan, K. C., Yilmaz, M., & Erbatur, K. (2011). Humanoid robot walking control on inclined planes. *IEEE International Conference on Mechatronics (ICM),* (pp. 875–880).

Shih, C.-L., & Chiou, C.-J. (1998). The motion control of a statically stable biped robot on an uneven floor. *IEEE Transactions on Systems, Man, and Cybernetics, Part B: Cybernetics, 28*(2), 244–249.

Shimizu, Y., & Shimada, A. (2010). Direct tilt angle control on inverted pendulum mobile robots. *11th IEEE International Workshop on Advanced Motion Control,* (pp. 234–239).

Shirokura, S., Murakami, H., & Takenaka, T. (2013). U.S. Patent No. 20,130,133,968. Washington, DC: U.S. Patent and Trademark Office.

Siegwart, R., & Nourbakhsh, I. R. (2004). *Intro to Autonomous Mobile Robots*. MIT press.

Silva, M. F., Machado, J. A. T., & Lopes, A. M. (2005). Modelling and simulation of artificial locomotion systems. *Robotica*, *23*(5), 595–606.

Snyman, J. A. (2005). *Practical mathematical optimization: an introduction to basic optimization theory and classical and new gradient-based algorithms* (Vol. 97). Springer Science+ Business Media.

Solihin, M. I., Akmeliawati, W., & Akmeliawati, R. (2009). Self-erecting inverted pendulum employing PSO for stabilizing and tracking controller. *5th International Colloquium on Signal Processing & Its Applications CSPA,* (pp. 63–68).

Solowheel Co. (2011). A gyro-stabilized electric unicycle, (1st June 2012),[Available from] http://www.solowheel.com

Sugahara, Y., Mikuriya, Y., Hashimoto, K., Hosobata, T., Sunazuka, H., Kawase, M., Lim, H., et al. (2005). Walking control method of biped locomotors on inclined plane. *Proceedings of the IEEE International Conference on Robotics and Automation ICRA,* (pp. 1977–1982).

Suvinen, A., Saarilahti, M., & Tokola, T. (2003). Terrain mobility model and determination of optimal off-road route. *Proceedings of the 9th Scandinavian Research Conference on Geographical Information Science*, (pp. 251–259).

Taga, G., Yamaguchi, Y., & Shimizu, H. (1991). Self-organized control of bipedal locomotion by neural oscillators in unpredictable environment. *Biological cybernetics*, *65*(3), 147–159.

Takahashi, Y., & Ogawa, S. (2000). Step climbing using power assist wheel chair robot with inverse pendulum control. *Robotics and Automation,* 1360–1365.

Takahashi, Y., & Tsubouchi, O. (2005). Modern control approach for robotic wheelchair with inverse pendulum control. *Proceedings. 5th International Conference on Intelligent Systems Design and Applications ISDA 2005,* (pp. 364–369).

Takahashi, Y., Ishikawa, N., & Hagiwara, T. (2001). Inverse pendulum controlled two wheel drive system. *Proceedings of the 40th SICE Annual Conference International Session Papers* (pp. 112–115).

Takahashi, Y., Ishikawa, N., & Hagiwara, T. (2003). Soft raising and lowering of front wheels for inverse pendulum control wheel chair robot. *Proceedings of IEEE/RSJ International Conference on Intelligent Robots and Systems IROS,* (Vol. 4, pp. 3618–3623).

Takahashi, Y., Ogawa, S., & Machida, S. (1999). Front wheel raising and inverse pendulum control of power assist wheel chair robot. *Proceedings of the 25th Annual Conference of the IEEE Industrial Electronics Society IECON'99* ,(Vol. 2, pp. 668–673).

Takahashi, Y., Takagaki, T., Kishi, J., & Ishii, Y. (2001). Back and forward moving scheme of front wheel raising for inverse pendulum control wheel chair robot. *Proceedings* of *IEEE International Conference on Robotics and Automation, 2001. ICRA,* (Vol. 4, pp. 3189–3194).

Tamura, K., & Yasuda, K. (2011). Primary study of spiral dynamics inspired optimization. *IEEJ Transactions on Electrical and Electronic Engineering*, *6*(S1), S98–S100.

Tamura, K., & Yasuda, K. (2011). Spiral Dynamics Inspired Optimization. *JACIII*, *15*(8), 1116–1122.

Tatikonda, R. C., Battula, V. P., & Kumar, V. (2010). Control of inverted pendulum using adaptive neuro fuzzy inference structure (ANFIS). *Proceedings of IEEE International Symposium on Circuits and Systems ISCAS 2010,* (pp. 1348–1351).

Tinkir, M., Onen, U., Kalyoncu, M., & Botsali, F. M. (2010). PID and interval type-2 fuzzy logic control of double inverted pendulum system. *The 2nd International Conference on Computer and Automation Engineering (ICCAE),* (Vol. 1, pp. 117–121).

Vundavilli, P. R., & Pratihar, D. K. (2009). Soft computing-based gait planners for a dynamically balanced biped robot negotiating sloping surfaces. *Applied Soft Computing*, *9*(1), 191–208.

Vundavilli, P. R., & Pratihar, D. K. (2011). Balanced gait generations of a two-legged robot on sloping surface. *Sadhana*, *36*(4), 525–550.

Wang, D., & Fan, F. (2009). Parameters Tuning of Fuzzy Controller for Rotated Pendulum Based on Improved Particle Swarm Optimization. *International Conference on Computational Intelligence and Software Engineering CiSE 2009* (pp. 1–5).

Wang, H. O., Tanaka, K., & Griffin, M. F. (1996). An approach to fuzzy control of nonlinear systems: stability and design issues. *IEEE Transactions on Fuzzy Systems*, *4*(1), 14–23.

Wang, L., Zheng, S., Wang, X., & Fan, L. (2010). Fuzzy control of a double inverted pendulum based on information fusion. *International Conference on Intelligent Control and Information Processing (ICICIP),* (pp. 327–331).

Wang, S., Hu, P., & Lin, L. (2006). Study on State Feedback Fuzzy-predictive Control System of TS Fuzzy Model. *First International Conference on Innovative Computing, Information and Control ICICIC'06*. (Vol. 2, pp. 179–182).

Wang, W. (2010). Adaptive neuro sliding mode control for inverted pendulum. *2nd IEEE International Conference on Computer Engineering and Technology* (pp. V1–135–V1–138).

Wang, Z.-Y., Dai, Y.-P., Li, Y.-W., & Yao, Y. (2010). Application of adaptive critic design on angle bracket inverted pendulum control. *International Conference on Machine Learning and Cybernetics (ICMLC),* (Vol. 5, pp. 2198–2203).

Wei, Q., Qiang, H., Qiaoli, H., Yixin, Z., Lin, X. (2008). Optimization of sliding mode controller for double inverted pendulum based on genetic algorithm. *2nd International Symposium on Systems and Control in Aerospace and Astronautics ISSCAA,* (pp. 1–5).

Wongsathan, C., & Sirima, C. (2009). Application of GA to design LQR controller for an Inverted Pendulum System. . *IEEE International Conference on Robotics and Biomimetic ROBIO 2008,* (pp. 951–954).

Wu, W. (2010). Adaptive neuro sliding mode control for inverted pendulum. *2nd International Conference on Computer Engineering and Technology ICCET,* (Vol. 1, pp. V1–135).

Xiong, X., & Wan, Z. (2010). The simulation of double inverted pendulum control based on particle swarm optimization LQR algorithm. *IEEE International Conference on Software Engineering and Service Sciences (ICSESS),* (pp. 253–256).

Xu, Z.-H., Jin, D.-M., & Li, Z.-J. (2002). Using learning samples to construct fuzzy logic systems with the application to inverted pendulum control. *Proceedings of International Conference on Machine Learning and Cybernetics,* (Vol. 2, pp. 1085–1088).

Yang, L., Chew, C.-M., Zielinska, T., & Poo, A.-N. (2007). A uniform biped gait generator with offline optimization and online adjustable parameters. *Robotica*, *25*(5), 549–566.

Yang, L., Zhang, Y., & Chen, Z. (2010). Bilinear control for the triple inverted pendulum based on model bias separation. *The 2nd International Conference on Computer and Automation Engineering (ICCAE),* (Vol. 5, pp. 436–440).

Yi, J., Yubazaki, N., & Hirota, K. (1999). Upswing and stabilization control of inverted pendulum and cart system by the SIRMs dynamically connected fuzzy inference model. *Proceedings of the IEEE International Fuzzy Systems Conference FUZZ-IEEE'99,* (Vol. 1, pp. 400–405).

Yi, J., Yubazaki, N., & Hirota, K. (1999). Upswing and stabilization control of inverted pendulum and cart system by the SIRMs dynamically connected fuzzy inference model. *Proceedings of IEEE International conference* on *Fuzzy Systems FUZZ-IEEE'99,* (Vol. 1, pp. 400–405).

Zhang, S.-Y., An, R., Shao, S.-M., & Li, D. (2010). A new fuzzy controller for stabilization of double inverted pendulum system. *International Conference On Computer and Communication Technologies in Agriculture Engineering (CCTAE),* (Vol. 1, pp. 300–303).

Zheng, Y. F., & Shen, J. (1990). Gait synthesis for the SD-2 biped robot to climb sloping surface. *IEEE Transactions on Robotics and Automation*, *6*(1), 86–96.

Zheng, Y. F., & Shen, J. (1990). Gait synthesis for the SD-2 biped robot to climb sloping surface. *IEEE Transactions on Robotics and Automation,* , *6*(1), 86–96.

Zheng, Y. F., Shen, J., & Sias Jr, F. R. (1988). A motion control scheme for a biped robot to climb sloping surfaces. *Proceedings of 1988 IEEE International Conference on Robotics and Automation,* (pp. 814–816).
Zheng, Y. F., Shen, J., & Sias Jr, F. R. (1988). A motion control scheme for a biped robot to climb sloping surfaces. *Proceedings of 1988 IEEE International Conference on Robotics and Automation,* (pp. 814–816).
Zhong, W., & Rock, H. (2001). Energy and passivity based control of the double inverted pendulum on a cart. *Control Applications, 2001.(CCA'01). Proceedings of the 2001 IEEE International Conference on* (pp. 896–901).

Zhou, C., Yue, P. K., Ni, J., & Chan, S.-B. (2004). Dynamically stable gait planning for a humanoid robot to climb sloping surface. *IEEE Conference on Robotics, Automation and Mechatronics,* (Vol. 1, pp. 341–346).

APPENDIX A

Flat ground mathematical model constants

$$
\begin{aligned}
C_1 &= 2L_{2l} + L_{2u} \\
C_2 &= 2L_{2l} + 2L_{2u} \\
C_3 &= L_1(M_1 + 2(M_m + M_{2l} + M + M_a + M_{2u})) \\
C_4 &= L_{2l}(M_{2l} + 2M_a) \\
C_5 &= M_{2u}C_1 + MC_2 \\
C_6 &= C_8 = M_{2u} + M \\
C_7 &= M_1 + M_m + M + M_{2l} + M_{2u} + M_a \\
C_8 &= M_{2u} + M \\
C_9 &= M_1 + 2M_m + 2(M_{2l} + M_{2u} + M_a + M) \\
C_{10} &= L_{2l}(M_{2l} + 2M_a) + M_{2u}C_1 + MC_2 \\
C_{11} &= L_{2l}^2(M_{2l} + 4M_a) + M_{2u}C_1^2 + MC_2^2 \\
C_{12} &= 2M_{2u}C_1 + 2MC_2 \\
C_{13} &= L_1(M_1 + 2M_m) + 2L_1(M_{2l} + M_{2u} + M_a + M) \\
C_{14} &= L_{2l}M_{2l} + 2L_{2l}M_a + M_{2u}C_1 + MC_2 \\
C_{15} &= C_4 + C_5 \\
C_{16} &= 2J_w + J_{IB} \\
C_{17} &= M_w R_w^2 + J_w \\
C_{18} &= 2L_1^2(M_{2l} + M_{2u} + M_a + M) + \frac{1}{2}(M_1 L_1^2 + J_1) + \frac{1}{2}(4M_1 L_1^2 + J_m) \\
C_{19} &= J_{2l} + J_{2u} + J_a + J_M \\
C_{20} &= C_{11} + C_{19} \\
C_{21} &= \frac{1}{2}R_w^2 C_7 + C_{17} \\
C_{22} &= \frac{1}{4}R_w^2 C_7
\end{aligned}
$$

APPENDIX B

General mathematical model constants

$$C_1 = 0.125R_w(M_m + M_1 + M_{2l} + M_a + M_{2u} + M)$$
$$C_2 = 0.5(M_m L_1^2 + M_1 L_{c1}^2 + M_{2l} L_1^2 + M_a L_1^2 + M_{2u} L_1^2 + M L_1^2)$$
$$C_3 = M_{2l} L_{c2}^2 + M_a L_a^2$$
$$C_4 = 0.5M_m(\cos\alpha + \sin\alpha) + 0.5M_1(\cos\alpha + \sin\alpha)$$
$$C_5 = M_{2l} L_1 L_{c2} + M_a L_1 L_a$$
$$C_6 = 0.5R_w(M_{2l} L_1 + M_a L_1 + M_{2u} L_1 + M L_1)$$
$$C_7 = R_w(M_{2l} L_{c1} + M_a L_a)$$
$$C_8 = 2L_{c2} + L_{2u}$$
$$C_9 = 2L_{c2} + 2L_{2u}$$
$$C_{10} = 4L_{c2}^2 + L_{2u}^2 + 4L_{2u} L_{c2}$$
$$C_{11} = 4L_{c2}^2 + 4L_{2u}^2 + 8L_{2u} L_{c2}$$
$$C_{12} = M_w R_w^2 + J_w$$
$$C_{13} = 2J_w + J_{IB}$$
$$C_{14} = M_1 L_{c1} + M_m L_1 + M_{2l} L_1 + M_a L_1 + M_{2u} L_1 + M L_1$$
$$C_{15} = M_{2l} L_{c2} + M_a L_a$$
$$C_{16} = M_1 + M_m + M_{2l} + M_a + M_{2u} + M$$
$$C_{17} = C_{15} + M_{2u} C_8 + M C_9$$
$$C_{18} = C_8 + C_9$$
$$C_{19} = M_{2u} + M$$
$$C_{20} = 2C_8 M_{2u} + 2C_9 M$$
$$C_{21} = C_3 + M_{2u} C_{10} + M C_{11}$$
$$C_{22} = 2M_{2u} C_8 + 2M C_9$$
$$C_{23} = M_{2u} L_1 + M L_1$$
$$C_{24} = C_5 + M_{2u} L_1 C_8 + M L_1 C_9$$
$$C_{25} = M_{2u} R_w + M R_w$$
$$C_{26} = C_7 + M_{2u} R_w C_8 + M R_w C_9$$
$$C_{27} = C_1 + C_{12}$$
$$C_{28} = R_w(M_{2u} + M)$$
$$L_{2u(t)} = C_8 + Q$$
$$L_{2u(t)}^2 = Q^2 + 2C_8 Q + C_{10}$$
$$L_{M(t)} = C_9 + Q$$
$$L_{M(t)}^2 = Q^2 + 2C_9 Q + C_{11}$$

APPENDIX C

System characteristics with disturbances of variable amplitudes and durations

C1. Disturbance forces with variable amplitudes

C1.1 Disturbances with variable amplitudes applied at the left wheel

	Amplitude (N)	40	80	160	300
Left wheel response	*Rise Time*	*0.5727*	*0.5729*	*0.5733*	*0.5714*
	Settling Time	*60.6088*	*61.1594*	*61.915*	*63.193*
	Overshoot	*6.5362*	*19.6834*	*87.0229*	*308.2581*
	Peak	*0.8521*	*0.9575*	*1.497*	*3.2599*

Right wheel response	*Rise Time*	*0.5727*	*0.5729*	*0.5735*	*0.5735*
	Settling Time	*1.1059*	*1.1072*	*60.4499*	*60.2494*
	Overshoot	*1.9568*	*1.9272*	*1.9352*	*2.4506*
	Peak	*0.8154*	*0.8154*	*0.8162*	*0.8202*

First link response	*Rise Time*	*4.73E-04*	*0.0034*	*0.0081*	*0.0063*
	Settling Time	*62.8821*	*64.3378*	*67.688*	*69.7325*
	Overshoot	*6.34E+04*	*1.42E+05*	*3.45E+04*	*9.17E+04*
	Peak	*0.1575*	*0.1575*	*0.1775*	*0.3292*

Second link response	*Rise Time*	*4.08E-12*	*3.86E-12*	*4.13E-12*	*4.00E-12*
	Settling Time	*7.3369*	*7.3369*	*7.3369*	*7.3369*
	Overshoot	*1.25E+17*	*1.32E+17*	*1.23E+17*	*1.27E+17*
	Peak	*1.13E-05*	*1.13E-05*	*1.13E-05*	*1.13E-05*

Payload response	*Rise Time*	*57.6894*	*57.9872*	*57.5905*	*57.4793*
	Settling Time	*59.8376*	*59.8425*	*59.836*	*59.8339*
	Overshoot	*180.7592*	*150.2452*	*189.2017*	*197.9529*
	Peak	*0.2009*	*0.2007*	*0.2011*	*0.201*

C1.2 Disturbances with variable amplitudes applied at the right wheel

	Amplitude (N)	40	80	160	300
Left wheel response	*Rise Time*	*0.5727*	*0.5729*	*0.5735*	*0.5735*
	Settling Time	*1.1059*	*1.1072*	*60.4499*	*60.2494*
	Overshoot	*1.9568*	*1.9272*	*1.9352*	*2.4506*
	Peak	*0.8154*	*0.8154*	*0.8162*	*0.8202*
Right wheel response	*Rise Time*	*0.5727*	*0.5729*	*0.5733*	*0.5714*
	Settling Time	*60.6088*	*61.1594*	*61.915*	*63.193*
	Overshoot	*6.5362*	*19.6834*	*87.0229*	*308.2581*
	Peak	*0.8521*	*0.9575*	*1.497*	*3.2599*
First link response	*Rise Time*	*4.73E-04*	*0.0034*	*0.0081*	*0.0063*
	Settling Time	*62.8821*	*64.3378*	*67.688*	*69.7325*
	Overshoot	*6.34E+04*	*1.42E+05*	*3.45E+04*	*9.17E+04*
	Peak	*0.1575*	*0.1575*	*0.1775*	*0.3292*
Second link response	*Rise Time*	*4.08E-12*	*3.86E-12*	*4.13E-12*	*4.00E-12*
	Settling Time	*7.3369*	*7.3369*	*7.3369*	*7.3369*
	Overshoot	*1.25E+17*	*1.32E+17*	*1.23E+17*	*1.27E+17*
	Peak	*1.13E-05*	*1.13E-05*	*1.13E-05*	*1.13E-05*
Payload response	*Rise Time*	*57.6894*	*57.9872*	*57.5905*	*57.4793*
	Settling Time	*59.8376*	*59.8425*	*59.836*	*59.8339*
	Overshoot	*180.7592*	*150.2452*	*189.2017*	*197.9529*
	Peak	*0.2009*	*0.2007*	*0.2011*	*0.201*

C1.3 Disturbances with variable amplitudes applied at the first link

	Amplitude (N)	40	80	160	300
Left wheel response	*Rise Time*	*0.5729*	*0.5724*	*0.5733*	*0.5763*
	Settling Time	*61.1606*	*61.8852*	*62.0046*	*63.0598*
	Overshoot	*4.7969*	*11.2642*	*13.9751*	*37.221*
	Peak	*0.8384*	*0.8895*	*0.9123*	*1.779*
Right wheel response	*Rise Time*	*0.5729*	*0.5724*	*0.5733*	*0.5763*
	Settling Time	*61.1606*	*61.8852*	*62.0046*	*63.0598*
	Overshoot	*4.7969*	*11.2642*	*13.9751*	*37.221*
	Peak	*0.8384*	*0.8895*	*0.9123*	*1.779*
First link response	*Rise Time*	*0.0025*	*7.83E-04*	*8.81E-04*	*0.0165*
	Settling Time	*63.3373*	*65.7227*	*67.6565*	*69.6229*
	Overshoot	*1.92E+05*	*3.82E+04*	*8.88E+04*	*3.49E+04*
	Peak	*0.1575*	*0.1575*	*0.4109*	*0.6796*
Second link response	*Rise Time*	*4.30E-12*	*5.11E-12*	*4.78E-12*	*3.20E-12*
	Settling Time	*7.3369*	*7.3369*	*7.3369*	*7.3369*
	Overshoot	*1.18E+17*	*9.95E+16*	*1.06E+17*	*1.59E+17*
	Peak	*1.13E-05*	*1.13E-05*	*1.13E-05*	*1.13E-05*
Payload response	*Rise Time*	*57.5093*	*58.0107*	*58.0622*	*57.6846*
	Settling Time	*59.836*	*59.8427*	*59.8435*	*59.8373*
	Overshoot	*195.822*	*147.4646*	*141.7439*	*181.253*
	Peak	*0.2008*	*0.2006*	*0.2006*	*0.2005*

C1.4 Disturbances with variable amplitudes applied at the second link

	Amplitude (N)	40	80	160	300
Left wheel response	*Rise Time*	*0.5732*	*0.5732*	*0.5732*	*0.5731*
	Settling Time	*1.1088*	*1.1088*	*1.1089*	*1.1087*
	Overshoot	*1.8913*	*1.8915*	*1.8889*	*1.8949*
	Peak	*0.8154*	*0.8154*	*0.8154*	*0.8154*

Right wheel response	*Rise Time*	*0.5732*	*0.5732*	*0.5732*	*0.5731*
	Settling Time	*1.1088*	*1.1088*	*1.1089*	*1.1087*
	Overshoot	*1.8913*	*1.8915*	*1.8889*	*1.8949*
	Peak	*0.8154*	*0.8154*	*0.8154*	*0.8154*

First link response	*Rise Time*	*0.0046*	*0.0044*	*0.0047*	*0.0037*
	Settling Time	*9.5716*	*9.5729*	*9.5708*	*9.5754*
	Overshoot	*9.00E+04*	*1.01E+05*	*8.43E+04*	*1.31E+05*
	Peak	*0.1575*	*0.1575*	*0.1575*	*0.1575*

Second link response	*Rise Time*	*0.0051*	*0.007*	*0.0127*	*1.95E-06*
	Settling Time	*65.1872*	*65.1791*	*65.2894*	*65.369*
	Overshoot	*8.68E+06*	*8.75E+06*	*8.56E+06*	*4.64E+07*
	Peak	*0.0071*	*0.0143*	*0.0405*	*0.1189*

Payload response	*Rise Time*	*57.5193*	*57.7071*	*57.8267*	*57.9201*
	Settling Time	*59.8348*	*59.8378*	*59.8389*	*59.8403*
	Overshoot	*194.7114*	*179.0764*	*167.6804*	*157.8499*
	Peak	*0.2007*	*0.2005*	*0.201*	*0.2009*

C1.5 Disturbances with variable amplitudes applied at the payload

	Amplitude (N)	40	80	160	300
Left wheel response	*Rise Time*	*0.5731*	*0.5731*	*0.5729*	*0.573*
	Settling Time	*1.1082*	*1.1081*	*1.1074*	*1.1079*
	Overshoot	*1.9043*	*1.907*	*1.9239*	*1.9123*
	Peak	*0.8154*	*0.8154*	*0.8154*	*0.8154*
Right wheel response	*Rise Time*	*0.5731*	*0.5731*	*0.5729*	*0.573*
	Settling Time	*1.1082*	*1.1081*	*1.1074*	*1.1079*
	Overshoot	*1.9043*	*1.907*	*1.9239*	*1.9123*
	Peak	*0.8154*	*0.8154*	*0.8154*	*0.8154*
First link response	*Rise Time*	*8.66E-04*	*1.30E-05*	*2.41E-04*	*9.72E-05*
	Settling Time	*9.5834*	*9.5844*	*9.5947*	*9.5882*
	Overshoot	*2.43E+06*	*2.32E+06*	*1.24E+05*	*3.09E+05*
	Peak	*0.1575*	*0.1575*	*0.1575*	*0.1575*
Second link response	*Rise Time*	*4.64E-12*	*4.27E-12*	*4.89E-12*	*4.15E-12*
	Settling Time	*7.3369*	*7.3369*	*7.3369*	*7.3369*
	Overshoot	*1.09E+17*	*1.19E+17*	*1.04E+17*	*1.22E+17*
	Peak	*1.13E-05*	*1.13E-05*	*1.13E-05*	*1.13E-05*
Payload response	*Rise Time*	*0.0424*	*0.073*	*0.0947*	*0.1172*
	Settling Time	*61.1213*	*72.0501*	*76.8591*	*78.3136*
	Overshoot	*2.12E+04*	*4.82E+03*	*1.51E+03*	*757.7745*
	Peak	*0.2076*	*0.2293*	*0.3079*	*0.4982*

C2. Disturbance forces with variable durations

C2.1 Disturbances with variable durations applied at the left wheel

	Duration (sec)	1.25	2.5	7.5	12.5
Left wheel response	*Rise Time*	*0.5729*	*0.5722*	*0.568*	*0.5659*
	Settling Time	*62.6111*	*64.1465*	*68.5594*	*72.9489*
	Overshoot	*50.9678*	*105.3085*	*290.2296*	*406.5962*
	Peak	*1.2078*	*1.641*	*3.1024*	*4.0168*

Right wheel response	*Rise Time*	*0.5731*	*0.573*	*0.5725*	*0.5725*
	Settling Time	*1.1086*	*1.1078*	*68.5304*	*48.3497*
	Overshoot	*1.8956*	*1.9143*	*2.1371*	*2.0771*
	Peak	*0.8154*	*0.8154*	*0.8168*	*0.8162*

First link response	*Rise Time*	*0.0057*	*1.68E-04*	*0.001*	*0.0099*
	Settling Time	*68.3065*	*70.7959*	*75.9585*	*78.9861*
	Overshoot	*4.89E+04*	*1.78E+05*	*2.87E+04*	*1.86E+04*
	Peak	*0.1575*	*0.1575*	*0.1575*	*0.1575*

Second link response	*Rise Time*	*4.11E-12*	*3.79E-12*	*4.00E-12*	*4.24E-12*
	Settling Time	*7.3369*	*7.3369*	*7.3369*	*7.3369*
	Overshoot	*1.24E+17*	*1.34E+17*	*1.27E+17*	*1.20E+17*
	Peak	*1.13E-05*	*1.13E-05*	*1.13E-05*	*1.13E-05*

Payload response	*Rise Time*	*2.5905*	*2.5905*	*2.5905*	*2.5905*
	Settling Time	*59.7991*	*59.7993*	*59.7992*	*59.7993*
	Overshoot	*1.00E+04*	*9.96E+03*	*1.00E+04*	*1.01E+04*
	Peak	*0.2009*	*0.2008*	*0.2008*	*0.2008*

C2.2 Disturbances with variable durations applied at the right wheel

	Duration (sec)	1.25	2.5	7.5	12.5
Left wheel response	*Rise Time*	*0.5731*	*0.573*	*0.5725*	*0.5725*
	Settling Time	*1.1086*	*1.1078*	*68.5304*	*48.3497*
	Overshoot	*1.8956*	*1.9143*	*2.1371*	*2.0771*
	Peak	*0.8154*	*0.8154*	*0.8168*	*0.8162*

Right wheel response	*Rise Time*	*0.5729*	*0.5722*	*0.568*	*0.5659*
	Settling Time	*62.6111*	*64.1465*	*68.5594*	*72.9489*
	Overshoot	*50.9678*	*105.3085*	*290.2296*	*406.5962*
	Peak	*1.2078*	*1.641*	*3.1024*	*4.0168*

First link response	*Rise Time*	*0.0057*	*1.68E-04*	*0.001*	*0.0099*
	Settling Time	*68.3065*	*70.7959*	*75.9585*	*78.9861*
	Overshoot	*4.89E+04*	*1.78E+05*	*2.87E+04*	*1.86E+04*
	Peak	*0.1575*	*0.1575*	*0.1575*	*0.1575*

Second link response	*Rise Time*	*4.11E-12*	*3.79E-12*	*4.00E-12*	*4.24E-12*
	Settling Time	*7.3369*	*7.3369*	*7.3369*	*7.3369*
	Overshoot	*1.24E+17*	*1.34E+17*	*1.27E+17*	*1.20E+17*
	Peak	*1.13E-05*	*1.13E-05*	*1.13E-05*	*1.13E-05*

Payload response	*Rise Time*	*2.5905*	*2.5905*	*2.5905*	*2.5905*
	Settling Time	*59.7991*	*59.7993*	*59.7992*	*59.7993*
	Overshoot	*1.00E+04*	*9.96E+03*	*1.00E+04*	*1.01E+04*
	Peak	*0.2009*	*0.2008*	*0.2008*	*0.2008*

C2.3 Disturbances with variable durations applied at the first link

	Duration (sec)	1.25	2.5	7.5	12.5
Left wheel response	*Rise Time*	*0.5738*	*0.5744*	*0.5781*	*0.5797*
	Settling Time	*62.7182*	*64.0972*	*69.0154*	*73.0527*
	Overshoot	*8.6093*	*8.4509*	*39.3535*	*62.2706*
	Peak	*0.8699*	*0.8693*	*1.4595*	*2.3529*
Right wheel response	*Rise Time*	*0.5738*	*0.5744*	*0.5781*	*0.5797*
	Settling Time	*62.7182*	*64.0972*	*69.0154*	*73.0527*
	Overshoot	*8.6093*	*8.4509*	*39.3535*	*62.2706*
	Peak	*0.8699*	*0.8693*	*1.4595*	*2.3529*
First link response	*Rise Time*	*0.0067*	*0.0102*	*0.0107*	*0.0059*
	Settling Time	*69.5075*	*70.9055*	*75.8925*	*79.2934*
	Overshoot	*3.49E+04*	*2.21E+04*	*3.28E+04*	*1.01E+04*
	Peak	*0.2155*	*0.2643*	*0.3388*	*0.3189*
Second link response	*Rise Time*	*3.79E-12*	*3.34E-12*	*1.54E-12*	*2.30E-12*
	Settling Time	*7.3369*	*7.3369*	*7.3369*	*7.3369*
	Overshoot	*1.34E+17*	*1.52E+17*	*3.29E+17*	*2.21E+17*
	Peak	*1.13E-05*	*1.13E-05*	*1.13E-05*	*1.13E-05*
Payload response	*Rise Time*	*2.5905*	*2.5905*	*2.5905*	*2.5908*
	Settling Time	*59.7991*	*59.7993*	*59.7992*	*59.7993*
	Overshoot	*9.96E+03*	*9.97E+03*	*9.99E+03*	*9.99E+03*
	Peak	*0.2009*	*0.2008*	*0.2008*	*0.2007*

C2.4 Disturbances with variable durations applied at the second link

	Duration (sec)	1.25	2.5	7.5	12.5
Left wheel response	*Rise Time*	*0.5732*	*0.5732*	*0.5732*	*0.5732*
	Settling Time	*1.1091*	*1.109*	*1.109*	*1.1091*
	Overshoot	*1.8844*	*1.8874*	*1.8878*	*1.8844*
	Peak	*0.8154*	*0.8154*	*0.8154*	*0.8154*
Right wheel response	*Rise Time*	*0.5732*	*0.5732*	*0.5732*	*0.5732*
	Settling Time	*1.1091*	*1.109*	*1.109*	*1.1091*
	Overshoot	*1.8844*	*1.8874*	*1.8878*	*1.8844*
	Peak	*0.8154*	*0.8154*	*0.8154*	*0.8154*
First link response	*Rise Time*	*0.0056*	*0.0052*	*0.0053*	*0.0057*
	Settling Time	*9.5622*	*9.5657*	*9.5653*	*9.5614*
	Overshoot	*5.08E+04*	*6.08E+04*	*5.93E+04*	*4.91E+04*
	Peak	*0.1575*	*0.1575*	*0.1575*	*0.1575*
Second link response	*Rise Time*	*0.0207*	*0.0379*	*17.4107*	*0.027*
	Settling Time	*67.6204*	*69.4697*	*74.7729*	*78.7991*
	Overshoot	*5.34E+06*	*2.67E+06*	*1.24E+05*	*5.38E+03*
	Peak	*0.0223*	*0.0223*	*0.0223*	*0.0223*
Payload response	*Rise Time*	*2.5905*	*2.5905*	*2.5905*	*2.5905*
	Settling Time	*59.7992*	*59.7992*	*59.7994*	*59.799*
	Overshoot	*9.98E+03*	*9.97E+03*	*9.97E+03*	*9.97E+03*
	Peak	*0.2008*	*0.2008*	*0.2006*	*0.201*

C2.5 Disturbances with variable durations applied at the payload

	Duration (sec)	1.25	2.5	7.5	12.5
Left wheel response	*Rise Time*	*0.573*	*0.5729*	*0.5728*	*0.5729*
	Settling Time	*1.1075*	*1.1073*	*1.1069*	*1.1075*
	Overshoot	*1.92*	*1.9254*	*1.9347*	*1.9218*
	Peak	*0.8154*	*0.8154*	*0.8154*	*0.8154*
Right wheel response	*Rise Time*	*0.573*	*0.5729*	*0.5728*	*0.5729*
	Settling Time	*1.1075*	*1.1073*	*1.1069*	*1.1075*
	Overshoot	*1.92*	*1.9254*	*1.9347*	*1.9218*
	Peak	*0.8154*	*0.8154*	*0.8154*	*0.8154*
First link response	*Rise Time*	*0.0046*	*0.0042*	*0.0021*	*0.0043*
	Settling Time	*9.5713*	*9.5744*	*9.5793*	*9.5739*
	Overshoot	*8.83E+04*	*1.17E+05*	*2.42E+05*	*1.11E+05*
	Peak	*0.1575*	*0.1575*	*0.1575*	*0.1575*
Second link response	*Rise Time*	*3.95E-12*	*4.24E-12*	*3.99E-12*	*4.07E-12*
	Settling Time	*7.3369*	*7.3369*	*7.3369*	*7.3369*
	Overshoot	*1.29E+17*	*1.20E+17*	*1.27E+17*	*1.25E+17*
	Peak	*1.13E-05*	*1.13E-05*	*1.13E-05*	*1.13E-05*
Payload response	*Rise Time*	*2.5858*	*2.5718*	*0.706*	*0.044*
	Settling Time	*63.0518*	*64.6813*	*71.1958*	*77.5414*
	Overshoot	*3.35E+03*	*3.21E+03*	*6.31E+03*	*3.47E+04*
	Peak	*0.2194*	*0.2264*	*0.2544*	*0.2819*